Rovibrational excitation in collisions involving diatomic molecules

D. J. Baker

ROVIBRATIONAL EXCITATION IN COLLISIONS INVOLVING DIATOMIC MOLECULES

by

D. J. BAKER, B.Sc. (Bristol)

A thesis submitted to the University of Durham for the Degree of Doctor of Philosophy

December, 1984.

'The writing of many books is endless, and excessive devotion to books is wearying to the body'.

Ecclesiastes 12,12.

ABSTRACT

The applicability of asymptotic series expansions of the type introduced by Gailitis (1976) in heavy particle scattering calculations is examined. The convergence of the solutions, with respect to the value of the scattering coordinate is found to be greatly improved in a model problem of the rovibrational excitation of H_2 by H^+.

The results of infinite order sudden (IOS) and breathing sphere (BS) calculations of cross sections for the rovibrational excitation of $^{12}C^{16}O$ by para-H_2 ($j_1 = 0$ only) are presented. Comparisons are made with existing theoretical and experimental results. Allowing for remaining uncertainties in the interaction potential of Poulsen (1982), our results are in reasonable accord with the experimental results of Andrews and Simpson (1976) for the vibrational relaxation of CO ($v_2 = 1$) by ortho-H_2.

IOS calculations of the vibrational deactivation of $^{12}C^{16}O$ ($v_2 = 1$) by H_2 ($j_1 = 0$ or 2) which simultaneously undergoes the rotational transitions $\Delta j_1 = 0, 2$, or 4 are presented. Of major interest is the near-resonance process

$$CO(v_2=1) + H_2(j_1=2) \longrightarrow CO(v_2=0) + H_2(j_1=6) + 87.03\ cm^{-1}.$$

Comparison is made with both recent quantum mechanical and semi-classical calculations of this process, and with experiment. The near-resonance process is insufficient to account for the experimentally determined difference

between the rates of the deactivation of CO ($v_2 = 1$) by para- and ortho- H_2 (Andrews and Simpson (1976)).

IOS calculations of the vibrational deactivation of CO ($v_2 = 1$) by HD ($j_1 = 0$ or 1) are presented and discussed. The agreement with the experimental results (Andrews and Simpson (1976)) is acceptable in the temperature range $140 \lesssim T \lesssim 240$ K.

ACKNOWLEDGEMENTS

I am indebted to Dr. D.R. Flower for his excellent supervision of this research. I am extremely grateful for his guidance, assistance, and encouragement throughout the course of this work. Also I would like to thank Professor B.H. Bransden for accepting me as a graduate student at Durham.

I am grateful to all those who have given me help and advice during this research, in particular Drs. D. Dewangan, D. Kirkpatrick, C. Newby, and R. Shingal. I wish to thank my colleague, G. Danby, for numerous stimulating discussions.

I would like to thank the SERC for the provision of a studentship, and of the grants which made possible the use of the Cray-1 computer.

Finally, I am very grateful to Ms. M. Chipchase for her efficient and patient typing of the manuscript, and wish to express my gratitude to Dr. C. Newby for his assistance in proof reading the typed manuscript.

CONTENTS

CHAPTER I

INTRODUCTION

1. Molecular Processes in the Interstellar Medium

In recent years it has been determined that the interstellar gas, once considered to consist almost entirely of H atoms and ions, contains a significant amount and a considerable variety of molecular species. The majority of the molecules have been detected in the radio region of the spectrum usually in emission, but occasionally in absorption, although some molecules have been discovered by their absorption of visible (CH, CH^+ and CN) and ultraviolet (H_2 and CO) starlight. The molecules are generally found in comparatively dense extended regions. Also the most dense molecular clouds are regions of active star formation. Molecular processes do not only provide us with information about the evolution of these clouds, but are also a means of determining their composition and physical properties (e.g., density, temperature, etc.).

The abundance of a particular molecular species represents the competition between the chemical processes responsible for the creation and destruction of the molecule. The principal methods normally considered for the formation of interstellar molecules from individual atoms are direct radiative attachment and catalytic formation on the surface of dust grains. In the first process, two atoms, for example, can stick together

to form a molecule, with their binding energy going off as a photon. In the second process, successive atoms hit a grain, stick to the surface momentarily, and then combine to form a molecule, giving off their binding energy as heat transmitted to the grain; the molecule then either escapes by evaporation or by some other process, perhaps involving photon excitation of the molecule to a level which is not bound to the grain. The destruction of interstellar molecules is due to the absorption of photons. Direct photodissociation can occur when the energy of the photon is larger than the binding energy of the molecule. Lower energy photons can cause dissociation by exciting the molecule to an intermediate state which subsequently dissociates (e.g., in predissociation, spontaneous radiative dissociation, and photoionization). Both formation and disruption can be modified by exchange interactions between molecules and either atoms or other molecules. For detailed accounts of formation and disruption see the reviews of Dalgarno (1975) and Watson (1974).

The only available information about molecular clouds is their spectra, i.e. the radiation added to or removed from the radiation-field along the line of sight. Crucial to this task is an understanding of the processes by which molecules emit and absorb photons. If the cloud is in equilibrium with a radiation-field, the number of photons emitted will equal the number absorbed. In this situation one will not "see" a spectral

line since no net photons will then be added to or removed from the field along the line of sight. The processes which disturb this equilibrium are molecular collisions. The spectra actually observed will depend on the composition and physical conditions in the clouds. Therefore if we have sufficient knowledge about the process of spectral line formation, this may be used in conjunction with the observations to infer the conditions in the interstellar clouds.

The temperature of interstellar clouds is quite low, $\lesssim$ 100 K. At these low temperatures, vibrational excitation due to collision processes is highly improbable. For example, the energy of the first excited vibrational level of CO above the ground state corresponds to a temperature of $\simeq$ 3000 K. The levels can, however, be populated by the passage of a shock wave when the density and temperature of the cloud are high for a short period of time (Aannestad and Field (1973), Hollenbach and Shull (1977)). Other mechanisms are ultraviolet fluoresence (Black and Dalgarno (1973)), and the absorption of high energy photons (Black and Dalgarno (1976)). Another source of vibrational excitation is the molecular formation process itself (Spitzer and Cochran (1973)). The formation mechanism may be more efficient in populating very high rovibrational states, but it occurs only once during the lifetime of the molecule whereas the other excitation processes would be expected to occur more

frequently. The different excitation mechanisms result in different energy level populations, and therefore the intensity of the spectral lines gives information as to the source of the excitation (Gautier et al. (1976)). If the excitation has been caused by a shock wave, the location of the vibrational emission region can be used to determine the origin of the shock. Also the velocity of the shock may be determined by the details of the emission spectra (Simon et al. (1979)).

Interstellar clouds lose energy by the conversion of kinetic energy of excitation of the cloud constituents. The excited atoms and molecules emit photons which eventually escape from the cloud. In diffuse clouds the major energy loss arises from the excitation of the fine-structure levels of ionized carbon (e.g. see Dalgarno and McCray (1972)). The rotational excitation of molecules is an important process in determining the cooling of clouds.

The sources of the heating of interstellar clouds are manifold. In addition to the macroscopic such as hydromagnetic waves (Arons and Max (1975)) and the dissipation of turbulent motion (Dalgarno and McCray (1972)), atomic and molecular processes working in response to the absorption of interstellar ultraviolet radiation and galactic cosmic rays are potentially large sources. The various cooling and heating mechanisms give rise to thermal and pressure gradients that affect the dynamical evolution of the cloud and may indeed trigger its collapse to the point where star formation begins. Details of

these processes are given in the review of Flower (1983).

In conclusion rovibrational excitation cross sections are needed not only to derive the energy loss from a cloud, but also to interpret the radio data on molecular line emission and absorption. All these astrophysical processes are discussed by Dalgarno (1975).

2. Cross Sections and Rate Coefficients

Consider the simple case of atom-diatomic molecule scattering. The probability that the molecule will change levels by energy transfer during a collision, and that the projectile will be scattered at a given angle, is expressed in terms of a differential cross section, which has the units of area and which has the following physical interpretation. The cross section will depend on the initial (γ) and final (γ') quantum numbers for the collision, and also on the relative collision velocity $\underline{v}$. If we assume that the origin of coordinates is at the target and allow the projectile to approach along the z-axis (Figure 1) the differential cross section for a collision velocity $\underline{v}$, is given by

$$\frac{d\sigma}{d\Omega}(\gamma \to \gamma'; \theta, \phi / v)$$

= number of particles giving rise to the transition $\gamma \to \gamma'$ deflected into solid angle $d\Omega(\theta, \phi)$, per unit time, per unit incident flux.

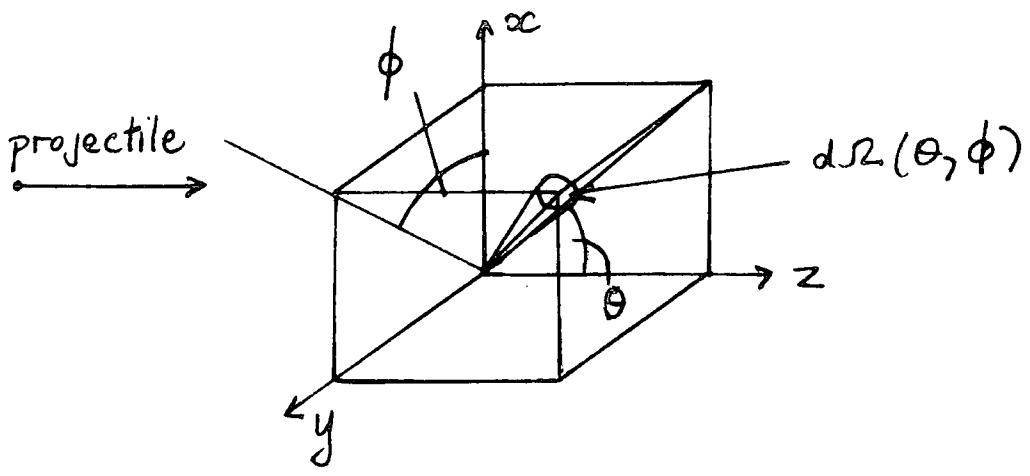

Figure 1.

Measurements are made in the laboratory frame (where the target may be at rest). To compare with theoretically determined quantities, it is necessary to convert what actually is observed in the laboratory frame to what would have been observed in the centre of mass frame. The total cross section is the integral of the differential cross section over all angles

$$\sigma(\gamma \to \gamma' | v) = \int \frac{d\sigma}{d\Omega}(\gamma \to \gamma'; \theta\, \phi | v)\, d\Omega . \qquad \text{I.2.1}$$

This cross section also has the units of area. The total (integral) cross section is the total number of particles causing the transition $\gamma \to \gamma'$, deflected into any angle per unit flux, per unit time.

Since unit flux is one particle per unit area, per unit time, the total cross section represents the

effective area presented by the target which gives rise to a transition $\gamma \to \gamma'$. The differential cross section is the effective area of the target which gives rise to the transition $\gamma \to \gamma'$ and deflection into the solid angle $d\Omega(\theta,\phi)$. If one constructs a circular region of area $\sigma(\gamma \to \gamma' | v)$ centred at the target and perpendicular to the projectile-target relative velocity, then a transition will occur if the projectile passes through the circle (Figure 2).

Figure 2.

The cross section $\sigma(\gamma \to \gamma' | v)$ thus gives an "effective interaction radius" $b_{max} = (\sigma(\gamma \to \gamma' | v)/\pi)^{\frac{1}{2}}$ such that a transition will occur if the projectile approaches closer to the target than b_{max}. The rate at which transitions $\gamma \to \gamma'$ occur is given by the flux of particles passing through the area $\sigma(\gamma \to \gamma' | v)$,

$$K_{\gamma \to \gamma'} = n v \sigma(\gamma \to \gamma' | v), \qquad \text{I.2.2}$$

where n is the number density of projectiles. In general there will be a distribution of collision velocities, so that

$$K_{\gamma \to \gamma'} = n \int_0^\infty v \sigma(\gamma \to \gamma' | v) f(v) dv. \qquad \text{I.2.3}$$

$f(v)$ is usually taken to be the Maxwellian velocity distribution at temperature T,

$$f(v) = f(v;T) = 4\pi\left(\frac{\mu}{2\pi kT}\right)^{3/2} v^2 \exp\left(\frac{-\mu v^2}{2kT}\right), \quad \text{I.2.4}$$

where k is Boltzmann's constant and μ is the reduced mass for the collision. $K_{\gamma\to\gamma'}$ may be then expressed

$$K_{\gamma\to\gamma'}(T) = \left(\frac{8kT}{\mu\pi}\right)^{\frac{1}{2}}\left(\frac{1}{kT}\right)^2 \int_0^\infty \sigma(\gamma\to\gamma'/E) E e^{-E/kT} dE, \quad \text{I.2.5}$$

where we have converted from velocity to kinetic energy using

$$E = \frac{1}{2}\mu v^2.$$

3. Experimental Determination of Cross Sections

There are essentially two experimental techniques for determining rovibrational cross sections, molecular or ion beam scattering experiments, and bulk relaxation techniques. Scattering experiments have the advantage that state to state cross sections may be determined, however such experiments are limited to certain molecular and atomic species by technical difficulties. In bulk relaxation experiments none of those difficulties are encountered, however these techniques allow only the determination of relaxation rate coefficients.

In molecular or ion beam scattering experiments two beams of particles intersect each other, usually at right angles. The pressure of the beams and in

the apparatus are of the order of 10^{-6}torr corresponding to a mean free path of 10 to 100 metres. Thus the molecules in the two beams do not undergo collisions except in the region of the intersection (known as the scattering region). A detector, which can be rotated about the scattering region, measures the intensity of the scattered particles as a function of the scattering angle.

Essentially two fundamentally different experimental techniques have been employed to detect inelastic scattering. One is the state selection method and the other the energy change method.

In the state selection experiment the molecules are prepared in a definite state before scattering and are then analysed for their final quantum state after scattering by an appropriate "state filter", which permits only molecules in the desired state to arrive at the detector. State-selection experiments use focusing properties of electric fields, or various spectroscopic techniques. The resolving power is usually very high and largely independent of the beam velocities. However, the techniques are only applicable to heavy molecules with large dipole moments (e.g. TlF, CsF, KCl).

In the energy change method the inelastic events are detected indirectly by making use of energy conservation. If both beams are monoenergetic and are well

collimated, then the conversion of translational to internal energy in an inelastic event will lead to a change in the relative velocity after scattering. This will be observed by a small change in the laboratory velocity of both scattered particles. The intensity of molecules with an altered velocity is a measure of the inelastic cross section.

Beam experiments in their present state of development suffer from several disadvantages. State selection experiments are limited to special cases and the lower resolution of energy change methods makes the measurement of state to state rovibrational cross sections extremely difficult, especially for neutral beams. The use of ions in beam experiments has the significant advantage that they are easily accelerated to high energies, where vibrational excitation occurs. Moreover, they are easily energy analysed and detected. Therefore beam experiments can resolve rovibrational cross sections in systems such as $Li^+ + H_2$ because of the ease of detection of the Li^+, and the high rotational constant of H_2. However, for most systems (e.g. $H_2 + CO$) vibrational relaxation rates are determined by collisions with probabilities of the order of 10^{-4}, and beam experiments are only sensitive to fairly large transition probabilities of the order of 1% or greater.

Bulk relaxation experiments do not suffer from any of these problems, such experiments have the common

feature of disturbing a system from its equilibrium distribution and measuring the rate of return to equilibrium. Typical experiments include laser Raman excitation, sound absorption, nuclear magnetic resonance spin - lattice relaxation, and double-resonance spectral techniques.

In laser Raman experiments, Raman active molecules are stimulated by a short laser pulse to the first vibrational state in a low temperature gas cell. As the molecules relax to the ground state there is a small temperature increase, which leads to a density change, which is detected by a laser Schlieren technique (Ducuing et al. (1970)). The method has the advantage that nonpolar molecules such as H_2 and N_2 are excited into a defined vibrational state in a low temperature heat bath.

In sound absorption experiments, one measures the attenuation of ultrasonic waves as a function of distance travelled in a gas. Part of the attenuation comes from converting translational into rovibrational molecular energy, and therefore, the rate coefficient may be measured.

In a nuclear magnetic resonance spin-lattice relaxation, a non-thermal distribution of nuclear spin states is created by magnetic fields and pulses of resonant radio frequencies. The rate of return to equilibrium can then be monitored. If this experiment

is performed in the gas phase, the relaxation occurs mainly by the coupling of nuclear spin and molecular rotation. Thus collisions which change the rotational state will also thermalize the nuclear spin states, and one measures the rotational rates weighted by the coupling constants, which are known.

In the double-resonance one disturbs the equilibrium rotational populations by pumping with strong radiation at a resonant frequency which disturbs the population in resonant levels. This disturbance propagates to other levels through collisional redistribution and is sampled by noting the change in intensity in other transitions. These changes in intensity are related to the relative rates of collisional transfer between all the levels. For a more detailed account of these and other experimental techniques see the review of Toennies (1976).

4. Theoretical Determination of Cross Sections

One of the most useful simplifying approximations for molecular collisions is the Born-Oppenheimer assumption of separable electronic and nuclear motions. Because the electrons are much lighter than the nuclei, they move much more rapidly so that we may expect them to adiabatically adjust to the instantaneous position of the nuclei. Therefore, we have simplified the problem by dividing it into two separate problems. A determination of the potential energy surface due

to the motion of the electrons and then we consider the motion of the nuclei on this potential surface.

4.1 The determination of Potential Energy Surfaces

The interaction potential between a diatomic molecule AB, approximated as a rigid rotor, and a diatomic molecule CD, approximated as a vibrating rotor is given by $V(\underline{R},\underline{r}) = E_{AB+CD}(\underline{R},\underline{r}) - E_{CD}(\underline{r}) - E_{AB}$ where $\underline{R}$ is the vector joining the centres of mass of the molecules AB and CD, and $\underline{r}$ lies along the inter-nuclear axis of CD. $E_{AB+CD}(\underline{R},\underline{r})$ is the total electronic energy of the total system for position vectors $\underline{R}$ and $\underline{r}$, and $E_{CD}(\underline{r})$ and E_{AB} are the total energies of the isolated molecules (i.e. for $R = \infty$).

Interaction potentials manifest themselves in a variety of static and dynamic phenomena. For example, the equilibrium structure of solids, virial coefficients of gases, viscosity, etc. Measurements of such phenomena are often used to obtain information about the inter-action potential, but, despite the variety of available methods, relatively little information has been obtained this way. The potential is obtained only by comparing observations with predictions based on model potentials. Because the models are rather inflexible, and because different experiments tend to sample different parts or different averages of the interaction, it is often found that a potential which models one type of data will be inadequate for another (e.g. see Shafer and Gordon (1973)).

The problem of determining the interaction potential between two systems is essentially the quantum chemical problem of determining the total energy of the electrons and nuclei of the systems. Since the electronic motion is very much faster than the nuclear motion, the problem reduces to determining the electronic energy as a function of fixed nuclear geometry (Born-Oppenheimer) approximation. The major contributions to the energy are the kinetic energy of the electrons and the Coulomb interaction among the electrons and nuclei. The interaction energy is the difference between the total energy of the combined system and that of the separated system. This can lead to large cancellation with subsequent loss of accuracy. In general, different techniques are useful at different separations, and it is convenient to distinguish between long range, short range, and intermediate distances.

At large distances AB and CD can be described as non-overlapping change distributions, and the interaction reduces to the electrostatic problem of interacting permanent and induced multipole moments. The potential consists of three terms. The electrostatic energy due to the interaction of permanent multipole moments, the induction energy, due to the interaction of permanent moments with those induced in the other collision partner, and the dispersion energy. Because the interaction is small, it is accurately represented

as a perturbation of the separated systems: the interaction energy can be calculated directly by perturbation techniques avoiding the problem of cancellation.

At small distances, the AB and CD change distributions overlap strongly and the interaction becomes repulsive. In this region the system is best described as a single molecule, and molecular orbital techniques such as the Hartree-Fock method are applicable. In the Hartree-Fock or self consistent field method, each electron is considered to move in the electrostatic field created by the other electrons. To describe the motion of one electron one must know the solutions for all the other electrons which determine the electrostatic field. In practice, one achieves this by an iterative technique. A reasonable initial guess is made to the solutions and these are used in the Hartree-Fock equations to produce new solutions which become the next guess. This cycle is repeated until the solutions are the same as the input. Hence the name self consistent field.

The wavefunctions of the electrons (or orbitals) must be expanded in some sort of basis functions. For molecular systems one often uses atomic orbitals - or at least orbitals centred on the various atoms - for the basis. This leads to the commonly seen SCF-LCAO for self consistent field-linear combination of atomic orbitals. One often sees "MO" appended

to this to indicate that the LCAO are formed into molecular orbitals.

The Hartree-Fock method has certain inherent limitations, for example it does not correctly describe the instantaneous correlation of electron motions. The resulting error in the energy is called correlation energy. However at short range this correlation energy is much smaller than the electrostatic energy, and therefore this is not a serious problem.

At intermediate distances the long range attractive forces and the short range repulsive forces compete to form a potential well, and this is the most difficult region for which to obtain an accurate interaction. The long range perturbation expansion fails as the change distributions begin to overlap. Molecular orbital methods generally become inadequate in this region because the correlation energy is comparable to the interaction energy and moves rapidly with distance as the orbitals change from atomic to molecular in character. To obtain accurate results at intermediate distances, configuration interaction techniques which explicitly include correlation effects must be used. In Hartree-Fock methods only one set, or configuration, of molecular orbitals is employed, whereas in configuration interaction calculations, the wavefunctions employed are linear combinations of all possible configurations. Hence configuration interaction calculations allow

a better description of the wavefunctions as they change from molecular to atomic. However, such calculations require roughly an order of magnitude more computer time than Hartree-Fock calculations, and this represents a major project for all but the smallest systems. These techniques outlined for the calculation of potential energy surfaces are described in more detail by Schaefer (1972).

The ab initio methods described above rely on approximate solution of the appropriate Schrödinger equation. A variety of less rigorous techniques for obtaining interaction potentials have also been developed, such as the electron gas model of Gordon and Kim (1972).

The energy of a uniform electron gas is a function only of its density. Gordon and Kim (1972) use this fact plus two other assumptions. In each volume element, the electron density is approximately constant, and the energy contribution is related to this density by the uniform electron gas formulae; the total energy of the system is obtained by integrating over all space. Secondly the electron density of the combined system is taken as the sum of the Hartree-Fock densities of the separated systems; this assumption effectively limits the method to interactions between closed shell systems where the charge distributions do not rearrange to form a chemical bond. The method fails at long range. The induction energy is not obtained since

the charge distributions are not allowed to polarise, and the dispersion energy is not obtained as the interaction vanishes for nonoverlapping charge distributions. There is evidence, however, that the model is reliable for the short range angular dependence of the potential (e.g. see Green (1974)).

4.2 Scattering Theory

Once the interaction potential has been determined, the equations describing the dynamics of the collision partners in that potential must be solved. This is known as scattering theory, and a number of techniques for solving the equations are available. The approach one uses can be fully quantum mechanical, it can make use of both quantum and classical mechanics, or can be a purely classical method.

4.2.1 Quantum Mechanics

In this approach the equation to be solved is the time independent Schrödinger equation containing the full Hamiltonian of each collision partner. This is reduced to a set of coupled second order differential equations. In the conventional close-coupling technique, the equations are solved in the space-fixed coordinate system. The total wavefunction of the system is expanded in terms of the basis states which are eigenfunctions of the total angular momentum $\underline{J}$ and the vibrational Hamiltonian. Since $\underline{J}$ is compounded from the rotational angular momenta $\underline{j}_1$ and $\underline{j}_2$, and the orbital angular

momentum $\underline{l}$, each basis set is indexed by the rotational angular momenta $\underline{j}_1$ and $\underline{j}_2$, the angular momentum $\underline{l}$, and the vibrational quantum number v_2, $(j_1 j_2 l v_2)$. The potential couples together all the basis states (i.e. $\underline{J} = \underline{j}_1 + \underline{j}_2 + \underline{l}$). $\underline{J}$ is conserved therefore the coupling matrix is diagonal in the total angular momentum. Because the orientation of the whole system in space is irrelevant the coupling matrix is independent of the z-projection of J. However for large j_1 or j_2, the number of equations to be solved can become extremely large, because of the $2j_i + 1 (i = 1,2)$ degeneracies. Depending on the algorithm used to solve the coupled equations, the computing time increases as N^2 or N^3 where N is the number of channels. Therefore except for the simplest systems, approximations must be made to the equations in order to reduce the number of channels retained.

In recent years a number of decoupling approximations have been developed which involve a simplified treatment of one or more of the terms in the full close-coupling equations, and hence their validity depends on the importance of those terms in the collision.

In Chapter II of this thesis, a full derivation of the close-coupling equations is given, and some of the decoupling approximations in current use are discussed.

4.2.2 Classical and Semi-Classical methods

There are essentially two extremes; at one extreme, quantum mechanics is suited to collisions involving light particles at low energy (i.e. few quantum states are excited). At the other extreme classical mechanics is best suited to high energy collisions (i.e. where we consider almost continuous energy levels). Generally speaking most systems studied fall between these two extremes, and for these a semi-classical approach is the most apt. In this section we outline a number of the most commonly used semi-classical and classical approaches. It is worth mentioning that only the strong-coupling correspondence principle of Percival and Richards (1970), and the semi-classical method of Billing (1974) have been extended from atom-diatom scattering to diatom-diatom scattering.

In the time-dependent close-coupling method the relative motion is treated classically and the internal motion is treated using quantum mechanics. For consistency the relative motion should be determined in a potential independent of the target orientation. This is the principal source of error in the approximation since the back coupling from the target to the trajectory is neglected. Therefore, the use of classical trajectories is only valid if the inelastic transitions which occur do not significantly affect the relative motion.

One assumes that the projectile follows a classical path determined by a spherically symmetric-potential, or a null potential (straight line paths). Once the trajectory has been determined it can be used to construct a time dependent interaction potential. The problem then consists of calculating the probability of ro-vibrational transitions due to this time dependent interaction exerted by the passing projectile.

As in quantum mechanical calculations, various simplifications of the dynamics can be made resulting in, for instance, the time-dependent sudden and time-dependent coupled states approximations. These dynamical approaches are reviewed by Balint-Kurti (1975) and Dickinson (1979).

The major fault of purely classical descriptions of the dynamics is the neglect of quantum mechanical effects. These are accounted for in the classical S-matrix method of Miller (1974) and Marcus (1972), this is a generalization of the semiclassical treatment of elastic scattering of Ford and Wheeler (1959). One determines all those classical trajectories which lead from the initial to the final state of interest. The quantum amplitude for the process is obtained by summing contributions from each trajectory with a weighting related to the density of classical paths in that neighbourhood and with relative phase between the contributions also determined classically from

the action along that path. However, for a system with several degrees of freedom, the numerical effort involved in the search for all trajectories satisfying a given set of double-ended boundary conditions becomes prohibitively large. This problem is reduced, however, if one only requires cross sections averaged over some quantum number (Miller (1971)).

The semi-classical strong-coupling correspondence principle of Percival and Richards (1970) approximates the solution of the time-dependent close-coupling equations using a classical description of the motion of the target. It incorporates the use of classical perturbation theory to determine the change in action of the target. It is expected to be most successful for large quantum numbers but comparisons with quantum calculations have shown satisfactory results for cross sections for transitions between low-lying rovibrational states (Clark (1977)). However the computing time for calculations employing this method is largely independent of the quantum numbers involved and arbitrary large quantum numbers may be handled routinely. This method is discussed in detail by Clark et al. (1977).

For vibrational excitation calculations there are two frequently used semi-classical methods. An approximation developed by Billing (1974) treats one internal degree of freedom quantum mechanically, while all the remaining degrees of freedom are treated

classically. For example, in an atom-vibrotor calculation the vibrational motion of the molecule could be treated quantum mechanically while the rotation, and the translational motion are treated classically.

The other method is based on the correspondence between the classical and quantum forced harmonic oscillator. Exact classical trajectories are employed to obtain the classical energy transfer as a function of angle. Using the Poisson distribution predicted by the forced oscillator model, vibrational excitation probabilities can be calculated (Giese and Gentry (1974)).

If quantum mechanical effects are unimportant (e.g. interference and tunnelling), a purely classical method may be used. Completely classical calculations are attractive since all the couplings are treated essentially exactly without the problems of ensuring convergence endemic in a quantum close-coupling expansion. A major problem in obtaining results from a purely classical calculation to be compared to quantum calculations or well resolved measurements is the procedure to be used to "quantise" the continuous classical variables such as angular momentum. In rotational excitation, a widely used technique is to define a final classical angular momentum j_c through the energy

$$E(j_c) = B j_c (j_c + 1) ,$$

where B is the rotational constant of the molecule and then associate a final rotational quantum number j_Q with j_c by

$$j_Q = j' \quad j' - \tfrac{1}{2}\alpha \leq j_c \leq j' + \tfrac{1}{2}\alpha ,$$

where $\alpha = 1$ for heteronuclear molecules, and $\alpha = 2$ for homonuclear molecules to allow for the $\Delta j = 2$ selection rule. Techniques for performing classical calculations have been reviewed by Bunker (1971) and Polanyi and Schreiber (1974).

CHAPTER II

QUANTUM THEORY OF MOLECULAR COLLISIONS

1. Introduction

In this chapter we present the quantum mechanical description of collisions of atoms and diatomic molecules with diatomic molecules. Once the interaction potential has been obtained, the equations describing the dynamics of the collision partners in that potential must be solved. The equation in question is the time-independent Schrödinger equation containing the full Hamiltonian of each collision partner. This may be reduced to a set of coupled second order differential equations. The solution of the latter is referred to as the Close-Coupling (CC) method. This is presented in Section 2. However, for all but the simplest systems, the numerical effort involved in solving the CC equations is prohibitively large even using fast modern computers. The large number of equations that must be solved is essentially due to the coupling between rotational and orbital angular momenta.

However, in recent years there has been a considerable amount of work in the development of approximations which lead to the total or partial decoupling of the angular momenta. In Section 3 we present some angular momentum decoupling approximations. We begin by discussing the Centrifugal sudden approximation in Section

3.1 , we discuss the Energy sudden approximation in Section 3.2 , and in Section 3.3 we discuss the Infinite order sudden approximation (a hybrid of the centrifugal and energy sudden approximations), and finally in Section 4 we touch on some other alternatives which may be used when none of the above approximations are appropriate (namely the L-Dominant, the decoupled L-Dominant, and the Effective potential approximations).

For the sake of generality the theory is presented for collisions between two diatomic molecules, except for the energy sudden approximation which has never been employed in diatom-diatom calculations, and we therefore, consider the atom-diatom theory to be adequate.

2. Close-Coupling Theory

We will consider the derivation of the problem for the collision between $^1\Sigma$ state diatomic molecules. We will approximate the projectile as a rigid rotor (denoted by 1), and the target as a vibrating rotor (denoted by 2). This derivation is in the space-fixed(SF) frame and follows the derivation presented by Takayanagi (1965). We take $\underline{r}_1 = (r_1, \theta_1, \phi_1)$, and $\underline{r}_2 = (r_2, \theta_2, \phi_2)$ lying along the molecular axes of 1 and 2 respectively, and $\underline{R} = (R, \theta, \phi)$ to be the position vector of the inter-molecular axis (Figure 1).

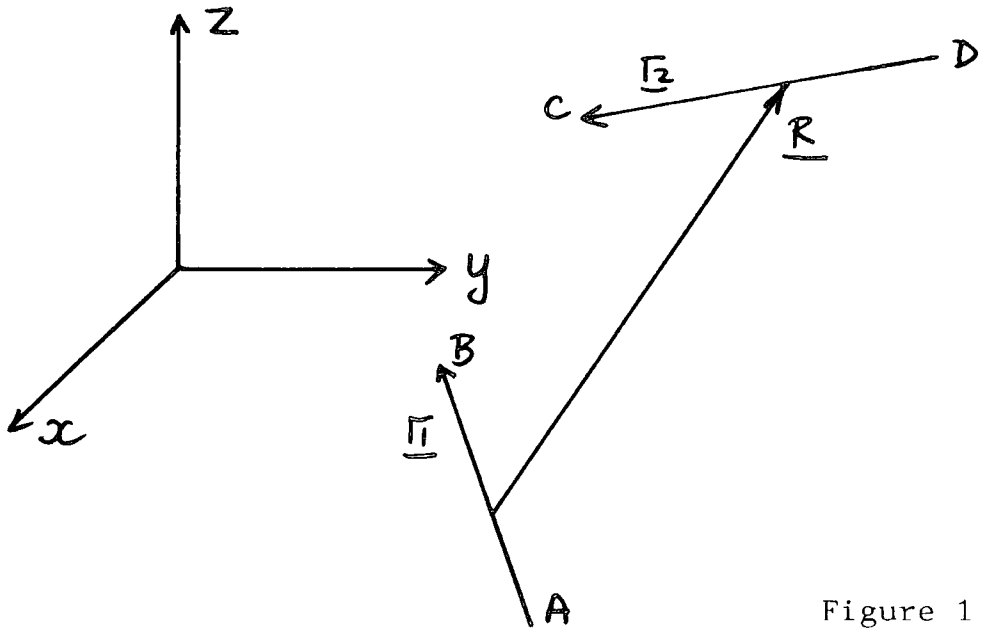

Figure 1

In this coordinate system the Schrödinger equation may be written

$$(H-E)\,\Psi(\hat{\underline{r}}_1, \hat{\underline{r}}_2, \hat{\underline{R}}) = 0\,, \qquad \text{II.2.1}$$

where Ψ denotes the total wavefunction and E is the total energy of the system. The Hamiltonian, H, may be partitioned as

$$H = -\frac{1}{2\mu}\nabla_R^2 + h_1 + h_2 + V(\hat{\underline{r}}_1, \hat{\underline{r}}_2, \hat{\underline{R}})\,, \qquad \text{II.2.2}$$

where the reduced mass of the system is given by

$$\mu = \frac{(m_A + m_B)(m_C + m_D)}{m_A + m_B + m_C + m_D}\,. \qquad \text{II.2.3}$$

V is the interaction potential as determined by the Born-Oppenheimer approximation,

$$V(\hat{\underline{r}}_1, \hat{\underline{r}}_2, \hat{\underline{R}}) \xrightarrow[R\to\infty]{} 0\,, \qquad \text{II.2.4}$$

and h_1 and h_2 are the Hamiltonians of the isolated

molecules 1 and 2 respectively

where $h_1 = B_{j_2}$, II.2.5a

and $h_2 = -\frac{1}{2\mu_2}\nabla^2_{r_2} + V(r_2)$. II.2.5b

$v(r_2)$ and μ_2 are the internuclear potential and reduced mass of molecule 2 respectively. B is the rotational constant of molecule 1 in its ground vibrational state. The kinetic energy operators may be separated into radial and angular parts,

$$-\frac{1}{2\mu}\nabla^2_R = -\frac{1}{2\mu R}\frac{\partial^2}{\partial R^2}R + \frac{\underline{l}^2}{2\mu R^2} \quad , \qquad \text{II.2.6a}$$

and $$-\frac{1}{2\mu_2}\nabla^2_{r_2} = -\frac{1}{2\mu_2 r_2}\frac{\partial^2}{\partial r_2} r_2 + \frac{\underline{j}^2}{2\mu_2 r_2^2} \quad , \qquad \text{II.2.6b}$$

where $\underline{l}$ is the orbital angular momentum operator, and $\underline{j}_1$ and $\underline{j}_2$ are the rotational angular momentum operators of molecules 1 and 2 respectively. Use is made of the conservation of angular momentum of the system in the collision,

$$\underline{J} = \underline{j}_1 + \underline{j}_2 + \underline{l} = \underline{j}_1' + \underline{j}_2' + \underline{l}' \quad , \qquad \text{II.2.7}$$

where the primes denote values after the collision.

The boundary conditions of II.2.1 are (choosing the initial relative motion to be in the z direction)

$$\Psi \xrightarrow[R\to 0]{} 0 \quad \text{since } V_{R\to\infty} \to \infty \quad , \qquad \text{II.2.8a}$$

$$\Psi \xrightarrow[R\to\infty]{} \exp(ik v_{2 j_1 j_2} z)\, \chi_{v_2 j_2}(r_2)\, Y_{j_2 m_2}(\hat{r}_2)\, Y_{j_1 m_1}(\hat{r}_1)$$

$$+ \sum_{\text{primed indices}} \exp(ik v_{2 j_1' j_2'} R)\, f(v_2 j_1 m_1 j_2 m_2 \to v_2' j_1' m_1' j_2' m_2' / \hat{R}) \qquad \text{II.2.8b}$$

$$\times\, \chi_{v_2' j_2'}(r_2)\, Y_{j_2' m_2'}(\hat{r}_2)\, Y_{j_1' m_1'}(\hat{r}_1) \, .$$

The first term is consistent with the incident direction of relative motion being the z-axis, $\chi_{v_2 j_2}(r_2) Y_{j_2 m_2}(\hat{r}_2)$ are the rovibrational eigenstates of molecule 2 and satisfy

$$(h_2 - \varepsilon_{v_2 j_2}) \chi_{v_2 j_2}(r_2) Y_{j_2 m_2}(\hat{r}_2) = 0 , \qquad \text{II.2.9a}$$

where $\varepsilon_{v_2 j_2}$ is the rovibrational eigenenergy of molecule 2 in vibrational state v_2 and rotational state j_2.

$Y_{j_1 m_1}(\hat{r}_1)$ is the rotational eigenstate of molecule 1 (in its ground vibrational state)

$$(h_1 - B_{j_1}(j_1+1)) Y_{j_1 m_1}(\hat{r}_1) = 0 . \qquad \text{II.2.9b}$$

The magnitude of the incident wavevector $k_{v_2 j_1 j_2}$ is defined by

$$k_{v_2 j_1 j_2} = \left[\frac{2\mu}{\hbar^2}(E - B_{j_1}(j_1+1) - \varepsilon_{v_2 j_2})\right]^{\frac{1}{2}} . \qquad \text{II.2.10}$$

The second term in II.2.8b describes the scattered wave, the scattering amplitude $f(v_2 j_1 m_1 j_2 m_2 \to v_2' j_1' m_1' j_2' m_2' | \hat{R})$ yields the state to state differential cross section

$$\frac{d\sigma}{d\Omega}(v_2 j_1 m_1 j_2 m_2 \to v_2' j_1' m_1' j_2' m_2' | \hat{R}) \qquad \text{II.2.11}$$

$$= \frac{k_{v_2' j_1' j_2'}}{k_{v_2 j_1 j_2}} |f(v_2 j_1 m_1 j_2 m_2 \to v_2' j_1 m_1 j_2 m_2 | \hat{R})|^2$$

Since the total angular momentum J and its projection M on the SF z-axis are conserved it is convenient to expand the total wavefunction in terms of eigenstates of J and M. The rotational angular momentum of the

two molecules $\underline{j}_1$ and $\underline{j}_2$ are coupled to form $\underline{j}_{12}$ with projection m_{12} on the SF z-axis, i.e.,

$$\underline{j}_{12} = \underline{j}_1 + \underline{j}_2 , \qquad \text{II.2.12a}$$

and

$$m_{12} = m_1 + m_2 , \qquad \text{II.2.12b}$$

which is subsequently coupled to the orbital angular momentum vector $\underline{\ell}$ to form the total angular momentum J (e.g. Alexander and Depristo (1977)).

$$\mathcal{Y}(j_1 j_2 j_{12} \ell J M / \hat{\underline{r}}_1 \hat{\underline{r}}_2 \hat{\underline{R}})$$

$$= \sum_{\substack{m_1 m_2 \\ m_{12} m_\ell}} C(j_1 m_1 j_2 m_2 / j_{12} m_{12}) C(j_{12} m_{12} \ell m_\ell / JM) \qquad \text{II.2.13}$$

$$\times Y_{j_1 m_1}(\hat{\underline{r}}_1) Y_{j_2 m_2}(\hat{\underline{r}}_2) Y_{\ell m_\ell}(\hat{\underline{R}}) ,$$

where $C(j_1 m_1 j_2 m_2 / j_{12} m_{12})$ is a Clebsh-Gordan coefficient.

$$\Phi^{JM}_{j_1 j_2 j_{12} \ell v_2}(\hat{\underline{r}}_1, \hat{\underline{r}}_2, \hat{\underline{R}}) = \sum_{\ell' j_1' j_2'} \frac{u^{J}_{j_1 j_2 j_{12} \ell v_2 \, j_1' j_2' j_{12} \ell' v_2'}(R)}{R}$$

$$\times \frac{\chi_{v_2' j_2'}(r_2)}{r_2} \mathcal{Y}(j_1' j_2' j_{12} \ell' JM / \hat{\underline{r}}_1 \hat{\underline{r}}_2 \hat{\underline{R}}) . \qquad \text{II.2.14}$$

Substitution of II.2.14 into II.2.1 and using II.2.9a,b and the orthonormal properties of

$$\mathcal{Y}(j_1 j_2 j_{12} \ell JM / \hat{\underline{r}}_1 \hat{\underline{r}}_2 \hat{\underline{R}}) \quad \text{and} \quad \chi_{v_2 j_2}(r_2) ,$$

$$\iiint \mathcal{Y}(j_1 j_2 j_{12} \ell JM) \mathcal{Y}^*(j_1' j_2' j_{12}' \ell JM) \, d\hat{\underline{R}} \, d\hat{\underline{r}}_1 \, d\hat{\underline{r}}_2$$

$$= \delta_{j_1 j_1'} \delta_{j_2 j_2'} \delta_{j_{12} j_{12}'} \delta_{\ell \ell'} \qquad \text{II.2.15a}$$

$$\int \chi_{v_2 j_2}(r_2) \chi^*_{v_2' j_2'}(r_2) \, dr_2 = \delta_{v_2 j_2, v_2' j_2'} , \qquad \text{II.2.15b}$$

we find that the radial functions in II.2.14 satisfy the following set of differential equations:

$$\left[\frac{d^2}{dR^2} - \frac{l'(l'+1)}{R^2} + k^2_{v_2' j_1' j_2'}\right] U^{J j_1 j_2 j_{12} l v_2}_{j_1' j_2' j_{12}' l' v_2'}(R)$$

$$= \frac{2\mu}{\hbar^2} \sum_{\substack{\text{double} \\ \text{primed} \\ \text{indices}}}' V^J_{v_2' j_1' j_2' j_{12}' l', v_2'' j_1'' j_2'' j_{12}'' l''} U^{J j_1 j_2 j_{12} l v_2}_{j_1'' j_2'' j_{12}'' l'' v_2''}(R). \quad \text{II.2.16}$$

The coupling matrix is given by

$$V^J_{v_2' j_1' j_2' j_{12}' l', v_2'' j_1'' j_2'' j_{12}'' l''}$$

$$= \iiint \chi_{v_2' j_2'}(r_2)\, y(j_1' j_2' j_{12}' l' J M)\, V(\hat{r}_1, \hat{r}_2, \hat{R})$$

$$\times y^*(j_1'' j_2'' j_{12}'' l'' J M)\, \chi^*_{v_2'' j_2''}(r_2)\, d\hat{r}_1 d\hat{r}_2 d\hat{R}. \quad \text{II.2.17}$$

The interaction potential is expanded in a triple series of spherical harmonics

$$V(\hat{r}_1, \hat{r}_2, \hat{R}) = \sum_{\lambda_1 \lambda_1 \lambda_{12}} A_{\lambda_1 \lambda_2 \lambda_{12}}(r_1 r_2 R)\, Y_{\lambda_1 \lambda_2 \lambda_{12}}(\hat{r}_1 \hat{r}_2 \hat{R}), \quad \text{II.2.18a}$$

where

$$Y_{\lambda_1 \lambda_2 \lambda_{12}}(\hat{r}_1 \hat{r}_2 \hat{R}) = \sum_{\mu_1 \mu_2 \mu_{12}} C(\lambda_1 \mu_1 \lambda_2 \mu_2 / \lambda_{12} \mu_{12})$$

$$\times Y_{\lambda_1 \mu_1}(\hat{r}_1)\, Y_{\lambda_2 \mu_2}(\hat{r}_2)\, Y^*_{\lambda_{12} \mu_{12}}(\hat{R}), \quad \text{II.2.18b}$$

where $\lambda_1 + \lambda_2 + \lambda_{12}$ is an even integer.

Using standard angular momentum algebraic techniques the potential matrix V^J may be written (Messiah (1962))

$$V^J = \sum_{\lambda_1\lambda_2\lambda_{12}} (4\pi)^{3/2} (-1)^{j_1'+j_2'+j_{12}'+J}$$

$$\times ([\lambda_{12}]^2[\lambda_1][\lambda_2][j_1][j_2'][\ell'][j_{12}'][j_1''][j_2''][\ell''][j_{12}''])^{\frac{1}{2}}$$

$$\times \begin{pmatrix} \lambda_{12} & \ell'' & \ell' \\ 0 & 0 & 0 \end{pmatrix} \begin{pmatrix} \lambda_1 & j_1'' & j_1' \\ 0 & 0 & 0 \end{pmatrix} \begin{pmatrix} \lambda_2 & j_2'' & j_2' \\ 0 & 0 & 0 \end{pmatrix}$$

$$\times \begin{Bmatrix} \ell'' & \ell' & \lambda_{12} \\ j_{12}'' & j_{12}' & J \end{Bmatrix} \begin{Bmatrix} j_{12}'' & j_2'' & j_1'' \\ j_{12}' & j_2' & j_1' \\ \lambda_{12} & \lambda_2 & \lambda_1 \end{Bmatrix}$$

$$\times \int_0^\infty \chi^*_{v_2'' j_2''}(r_2)\, A_{\lambda_1\lambda_2\lambda_{12}}(r_1 r_2 R)\, \chi_{v_2' j_2'}(r_2)\, dr_2 ,$$

where $[\lambda_{12}]$ denotes $2\lambda_{12}+1$. II.2.19

The term $(: : :)$ is a 3-j symbol, $\{: : :\}$ is a 6-j symbol, and $\{: : :\}$ is a 9-j symbol.

The orientation of the system in space is irrelevant and therefore, the coupling matrix, V^J, is independent of M (and therefore so are the radial functions U^J).

As $R \to \infty$, $V^J \to 0$ and the solutions of II.2.16 with $V^J = 0$ are, for $k^2_{v_2' j_1' j_2'} > 0$ (Abramowitz and Stegun (1965)),

$$k_{v_2' j_1' j_2'} R\, j_{\ell'}(k_{v_2' j_1' j_2'} R) \quad k_{v_2' j_1' j_2'} R\, n_{\ell'}(k_{v_2' j_1' j_2'} R), \qquad \text{II.2.20a}$$

where $j_{\ell'}$ and $n_{\ell'}$ are Spherical Bessel functions of the first and second kind. We may, instead, use Spherical

Hankel functions of the first and second kind (these are Spherical Bessel functions of the third kind).

$$h^{(1)}_{l'} = j_{l'} + i n_{l'} \qquad h^{(2)}_{l'} = j_{l'} - i n_{l'} \,. \qquad \text{II.2.20b}$$

The boundary condition (as $R \longrightarrow \infty$) for U^J can be expressed as a linear combination of $h^{(1)}_{l'}$ and $h^{(2)}_{l'}$,

$$U^{J}_{j_1' j_2' j_{12}' l' v_2'}{}^{j_1 j_2 j_{12} l v_2} \xrightarrow[R\to\infty]{} 0 \qquad k^2_{v_2' j_1' j_2'} \leq 0 \,,$$

$$U^{J}_{j_1' j_2' j_{12}' l' v_2'}{}^{j_1 j_2 j_{12} l v_2} \xrightarrow[R\to\infty]{} \left(-i k_{v_2' j_1' j_2'} R\, h^{(2)}_{l'}(k_{v_2' j_1' j_2'} R)\right) \delta_{v_2 j_1 j_2 j_{12} l, v_2' j_1' j_2' j_{12}' l'}$$

$$- \left(\frac{k_{v_2 j_1 j_2}}{k_{v_2' j_1' j_2'}}\right)^{\frac{1}{2}} S^J(v_2 j_1 j_2 j_{12} l, v_2' j_1' j_2' j_{12}' l')$$

$$\times \left(i k_{v_2' j_1' j_2'} R\, h^{(1)}_{l'}(k_{v_2' j_1' j_2'} R)\right)$$

$$k^2_{v_2' j_1' j_2'} > 0 \,, \qquad \text{II.2.21a}$$

also $U^{J}_{j_1' j_2' j_{12}' l' v_2'}{}^{j_1 j_2 j_{12} l v_2} \xrightarrow[R\to 0]{} 0 \,.$

Equation II.2.21a defines the S-matrix which is diagonal in J, since J is conserved. Channels with $k^2_{v_2' j_1' j_2'} \leq 0$ are known as closed channels, while $k^2_{v_2' j_1' j_2'} > 0$ defines open channels. II.2.21a may be rewritten

employing the asymptotic forms of the Spherical Hankel functions

$$U^{J}_{j_1 j_2 j_{12} l v_2 \; j_1' j_2' j_{12}' l' v_2'} \xrightarrow[R\to\infty]{} \exp\left[-i\left(k_{v_2' j_1' j_2'} R - \frac{l'\pi}{2}\right)\right]\delta_{v_2 j_1 j_2 j_{12} l, v_2' j_1' j_2' j_{12}' l'}$$

$$- \left(\frac{k_{v_2 j_1 j_2}}{k_{v_2' j_1' j_2'}}\right)^{\frac{1}{2}} S^{J}(v_2 j_1 j_2 j_{12} l, v_2' j_1' j_2' j_{12}' l') \exp\left[-i\left(k_{v_2' j_1' j_2'} R - \frac{l'\pi}{2}\right)\right]. \qquad \text{II.2.21b}$$

Thus U^J is expressed in terms of an incoming incident wave, and outgoing scattered waves. We require the correct linear combination of $\Psi^{JM}_{j_1 j_2 j_{12} l v_2}$ which satisfies the boundary condition II.2.8a, b. We employ the expansion of a plane wave into Spherical Bessel functions (Abramowitz and Stegun)

$$e^{i k_{v_2 j_1 j_2} z} = \sum_l (2l+1) i^l j_l(k_{v_2 j_1 j_2} R)\left(\frac{4\pi}{2l+1}\right)^{\frac{1}{2}} Y_{l0}(\hat{R}), \qquad \text{II.2.22}$$

and the expression for the product of two spherical harmonics (twice), and obtain

$$e^{i k_{v_2 j_1 j_2} z}\, \chi_{v_2 j_2}(\xi_2)\, Y_{j_1 m_1}(\hat{r}_1)\, Y_{j_2 m_2}(\hat{r}_2)$$

$$= \sum_{JM l j_{12} m_{12}} (4\pi(2l+1))^{\frac{1}{2}} i^l j_l(k_{v_2 j_1 j_2} R)\chi_{v_2 j_2}(\xi_2)$$

$$\times y(j_1 j_2 j_{12} l JM / \hat{r}_1 \hat{r}_2 \hat{R})\, C(j_{12} m_{12} l 0 / JM)$$

$$\times C(j_1 m_1 j_2 m_2 / j_{12} m_{12}). \qquad \text{II.2.23}$$

In order for the first term in the total wavefunction to go over to this asymptotically, the expansion used is

$$\Psi_{v_2 j_1 j_2 j_{12} m_{12}} = \frac{i(\pi)^{\frac{1}{2}}}{k v_2 j_1 j_2} \sum_{JM\ell j_{12} m_{12}} i^{\ell}(2\ell+1)^{\frac{1}{2}} \times \Psi(\hat{r}_1, \hat{r}_2, \hat{R}) C(j_{12} m_{12} \ell 0 / JM) C(j_1 m_1 j_2 m_2 / j_{12} m_{12}) \quad \text{II.2.24}$$

Substitution of II.2.21b, II.2.13 and II.2.14 into II.2.24 gives the asymptotic form

$$\Psi_{v_2 j_1 j_2 j_{12} m_{12}} \xrightarrow[R\to\infty]{} e^{ikv_2 j_1 j_2} Y_{j_1 m_1}(\hat{r}_1) Y_{j_2 m_2}(\hat{r}_2) \chi_{v_2 j_2}(r_2)$$

$$+ \frac{i(\pi)^{\frac{1}{2}}}{k v_2 j_1 j_2} \sum_{JM\ell} C(j_2 m_{12} \ell 0 / JM) C(j_1 m_1 j_2 m_2 / j_{12} m_{12}) i^{\ell}(2\ell+1)^{\frac{1}{2}}$$

$$\times \sum_{j_1' j_2' \ell' v_2'} R^{-1} i^{-\ell'} \left(\frac{k v_2' j_1' j_2'}{k v_2 j_1 j_2}\right) [\delta_{v_2 j_1 j_2 j_{12} \ell, v_2' j_1' j_2' j_{12}' \ell'} - S^J(v_2 j_1 j_2 j_{12} \ell, v_2' j_1' j_2' j_{12}' \ell')]$$

$$\times e^{ikv_2' j_1' j_2'} \sum_{m_{\ell'} m_{12} j_{12}'} C(j_{12}' m_{12}' \ell m_{\ell'} / JM) C(j_1' m_1' j_2' m_2' / j_{12}' m_{12}')$$

$$\times Y_{\ell' m_{\ell'}}(\hat{R}) Y_{j_1' m_1'}(\hat{r}_1) Y_{j_2' m_2'}(\hat{r}_2) \chi_{v_2' j_2'}(r_2). \quad \text{II.2.25}$$

Comparison of II.2.25 with II.2.8b gives the following expression for the scattering amplitude

$$f(v_2 j_1 m_1 j_2 m_2 \to v_2' j_1' m_1' j_2' m_2' / \hat{R})$$

$$= i\left(\frac{\pi}{k v_2 j_1 j_2 k v_2' j_1' j_2'}\right)^{\frac{1}{2}} \sum_{JM\ell\ell' j_{12} j_{12}'} \sum_{m_{12} m_{12}' m_{\ell'}}$$

$$\times i^{\ell-\ell'}(2\ell+1)^{\frac{1}{2}} C(j_1 m_1 j_2 m_2 / j_{12} m_{12}) C(j_{12} m_{12} \ell 0 / JM)$$

$$\times C(j_1' m_1' j_2' m_2' / j_{12}' m_{12}') C(j_{12}' m_{12}' \ell' m_{\ell'} / JM) \quad \text{II.2.26}$$

$$\times Y_{\ell' m_{\ell'}}(\hat{R}) T^J(v_2 j_1 j_2 j_{12} \ell, v_2' j_1' j_2' j_{12}' \ell'),$$

where T^J is the transition matrix, related to the S-matrix by

$$T^J(v_2 j_1 j_2 j_{12} l, v_2' j_1' j_2' j_{12}' l') = \delta_{v_2 j_1 j_2 j_{12} l, v_2' j_1' j_2' j_{12}' l'} - S^J(v_2 j_1 j_2 j_{12} l, v_2' j_1' j_2' j_{12}' l').$$

We may impose other boundary conditions for open channels, namely

$$U^{J j_1 j_2 j_{12} l v_2}_{j_1' j_2' j_{12}' l' v_2'} \xrightarrow[R\to\infty]{} -2i k_{v_2' j_1' j_2'} R_{jl'}(k_{v_2' j_1' j_2'} R)\delta_{v_2 j_1 j_2 j_{12} l, v_2' j_1' j_2' j_{12}' l'} - \left(\frac{k_{v_2 j_1 j_2}}{k_{v_2' j_1' j_2'}}\right)^{\frac{1}{2}} T^J(v_2 j_1 j_2 j_{12} l, v_2' j_1' j_2' j_{12}' l')\,(i k_{v_2' j_1' j_2'} R h^{(1)}_{l'}(k_{v_2' j_1' j_2'} R)) \qquad \text{II.2.27a}$$

$$U^{J j_1 j_2 j_{12} l v_2}_{j_1' j_2' j_{12}' l' v_2'} \xrightarrow[R\to\infty]{} -2i\{k_{v_2' j_1' j_2'} R_{jl'}(k_{v_2' j_1' j_2'} R)\delta_{v_2 j_1 j_2 j_{12} l, v_2' j_1' j_2' j_{12}' l'} - \left(\frac{k_{v_2 j_1 j_2}}{k_{v_2' j_1' j_2'}}\right)^{\frac{1}{2}} K^J(v_2 j_1 j_2 j_{12} l, v_2' j_1' j_2' j_{12}' l')(-k_{v_2' j_1' j_2'} R n_{l'}(k_{v_2' j_1' j_2'} R))\}. \qquad \text{II.2.27b}$$

Using II.2.27a we obtain the T-matrix directly, however II.2.27b has the advantage that the functions are real (except the -2i factor), and it is therefore, usual practice to obtain the K-matrix (known as the reactance matrix), and calculate S^J and T^J from it using

$$\underset{\sim}{S}^J \equiv \underset{\sim}{I} - \underset{\sim}{T}^J \equiv (\underset{\sim}{I} + i\underset{\sim}{K}^J)(\underset{\sim}{I} - i\underset{\sim}{K}^J)^{-1}, \qquad \text{II.2.28}$$

where $\underset{\sim}{I}$ is a unit matrix. The matrices K^J, S^J, and T^J are symmetric, this follows from the symmetry of the V^J matrix, and reflects the invariance of the dynamics under time reversal.

The commonly used total cross section is obtained from II.2.11 by averaging over initial m_i, summing over

final m_i', and integrating over angle $\underline{\hat{dR}}$,

$$\sigma(v_2 j_1 j_2 \to v_2' j_1' j_2') = \frac{\pi}{(2j_1+1)(2j_2+1)\, k^2_{v_2 j_1 j_2}}$$

$$\times \sum_J (2J+1) \sum_{l l'} |T^J(v_2 j_1 j_2 l \to v_2' j_1' j_2' l')|^2 . \qquad \text{II.2.29}$$

Because of the symmetry of T^J, $\sigma(v_2 j_1 j_2 \to v_2' j_1' j_2')$ satisfies the detailed balance condition

$$\sigma(v_2 j_1 j_2 \to v_2' j_1' j_2') k^2_{v_2 j_1 j_2} (2j_1+1)(2j_2+1)$$

$$= \sigma(v_2' j_1' j_2' \to v_2 j_1 j_2) k^2_{v_2' j_1' j_2'} (2j_1'+1)(2j_2'+1). \qquad \text{II.2.30}$$

As already stated this derivation applies to the scattering of a rotor (molecule 1) by a vibrotor (molecule 2), however results for atom-vibrotor collisions may be easily obtained by setting $j_1 = 0$ (hence $j_{12} = j_2$, $j_{12}' = j_2'$). The potential expansion takes a far simpler form (with $\lambda_1 = \mu_1 = 0$)

$$V(\underline{r}_2, \underline{R}, \theta_2) = \sum_{\lambda_2} B_{\lambda_2}(r_2, R) P_{\lambda_2}(\underline{\hat{r}}_2 \cdot \underline{\hat{R}})$$

$$= \sum_{\lambda_2} B_{\lambda_2}(r_2, R) P_{\lambda_2}(\cos\theta_2), \qquad \text{II.2.31}$$

and the potential matrix elements take the form

$$V^J_{v_2' j_2' l', v_2'' j_2'' l''}$$

$$= \sum_{\lambda_2} v_{\lambda_2}(v_2' j_2'; v_2'' j_2''; R) f_{\lambda_2}(j_2' l'; j_2'' l''; J), \qquad \text{II.2.32}$$

where $v_{\lambda_2}(v_2' j_2'; v_2'' j_2''; R)$

$$= \int_0^\infty \chi_{v_2' j_2'}(r_2) B_{\lambda_2}(r_2, R) \chi^*_{v_2'' j_2''}(r_2) dr_2 ,$$

and the $f_{\lambda_2}(j_2' l'; j_2'' l''; J)$ are the Percival Seaton coefficients (Percival and Seaton (1957)) known analytically in terms of 3-j and 6-j symbols.

Solution of II.2.16 to obtain T^J is known as the close-coupling (CC) method. The number of coupled equations in II.2.16 for each J value is in theory unbounded, however in practice the summation over j_1'' $j_2'' v_2'' l''$ must be finite, and one increases j_1'' j_2'' and v_2'' (and therefore l'') until the transitions of interest in a given problem have converged. The problem with CC equations is the rapid increase in the number of channels as j_1 and j_2 increase, due essentially to the $(2j_i + 1)$, $i = 1,2$, degenerate orientations in level j_i $(i = 1,2)$. A partial solution is provided by the properties of parity, $(-1)^{j_1+j_2+l}$, solutions of even and odd parity are uncoupled, and may be solved separately. Further simplication can be made when studying collisions of identical molecules, e.g. HF-HF, or identical homonuclear molecules, e.g. H_2-H_2. For collisions of two homonuclear diatomics, the potential must be invariant under the operations $r_1 \rightarrow -r_1$, $r_2 \rightarrow -r_2$. From II.2.19 this forces both λ_1 and λ_2 to be even. A consequence as indicated by the second, and third 3-j symbols in II.2.19, is that both j_1 and j_2 can only change by even increments. A detailed examination of this has been made by Alexander and De Pristo (1977).

Because of these problems few CC calculations have been carried out (in fact about 50 channels is the maximum possible on the fastest modern computers). This means

that apart from hydrogen and the hydrides, CC calculations of rovibrational cross sections are not possible. At energies high enough to study vibrational excitation a large number of rotational levels are accessible. Consider the collisions of N_2 and H_2 with an atom at energies high enough to excite the first excited vibrational level. In the case of N_2 there are around 30 rotational levels below the first excited vibrational state. Since N_2 is homonuclear this means 256 channels for one parity, and 240 channels for the other. We must, in addition, consider the rotational levels below the second vibrational state. Such a calculation is clearly not possible. Since H_2 is a lighter molecule the rotational levels are more widely spaced, there are about 8 levels below the first excited vibrational state giving 25 and 20 channels. Considering the rotational levels below the second excited vibrational state increases the number of channels to 50 and 40; this is a feasible calculation.

3. Approximate methods

Depending on the algorithm used to solve the coupled equations II.2.16 the computing time increases as N^2 or N^3, where N is the number of channels. It is obvious from the discussion in the previous section that except for the simplest systems (e.g. rovibrational calculations for atom-H_2 systems) CC calculations are not possible, and approximations must be made to the equations in order to reduce the number of channels retained.

The decoupling approximations discussed in this section involve a simplified treatment of one or more of the terms in the full CC equations, and their validity is therefore, dependent upon the importance of these terms in the collision. For example in the energy sudden approximation one assumes that the rotational levels of a molecule are degenerate, therefore it will be accurate in collisions where the rotational levels are not important. In general, however, the accuracy of a given approximation is determined by comparison with full CC calculations.

3.1 The Centrifugal Sudden approximation

This approximation is widely used in heavy particle scattering calculations, and is considered to be the most accurate of a hierarchy of possible approximations for treating a general class of collision systems. We will discuss the sufficiency conditions for the method later. The centrifugal sudden (CS) approximation (sometimes known as the coupled states or J_z conserving approximation) was simultaneously introduced by McGuire and Kouri (1974), and by Pack (1974). This approach for the atom-molecule system has been widely tested (e.g., McGuire and Kouri (1974), and Kouri et al. (1976)) and has been generalised to molecule-molecule systems (e.g. Heil and Kouri (1976), Heil et al. (1978), and Goldflam and Kouri (1979)). This derivation of the CS approximation is in a rotating reference frame in which the z-axis always lies along $\hat{\underline{R}}$ (i.e. a body-fixed coordinate (BF) system as shown in Figure 2). In such a frame the potential is axially symmetric, and $\hat{\underline{r}}_1' = (\theta_1', \phi_1')$, and $\hat{\underline{r}}_2' = (\theta_2', \phi_2')$.

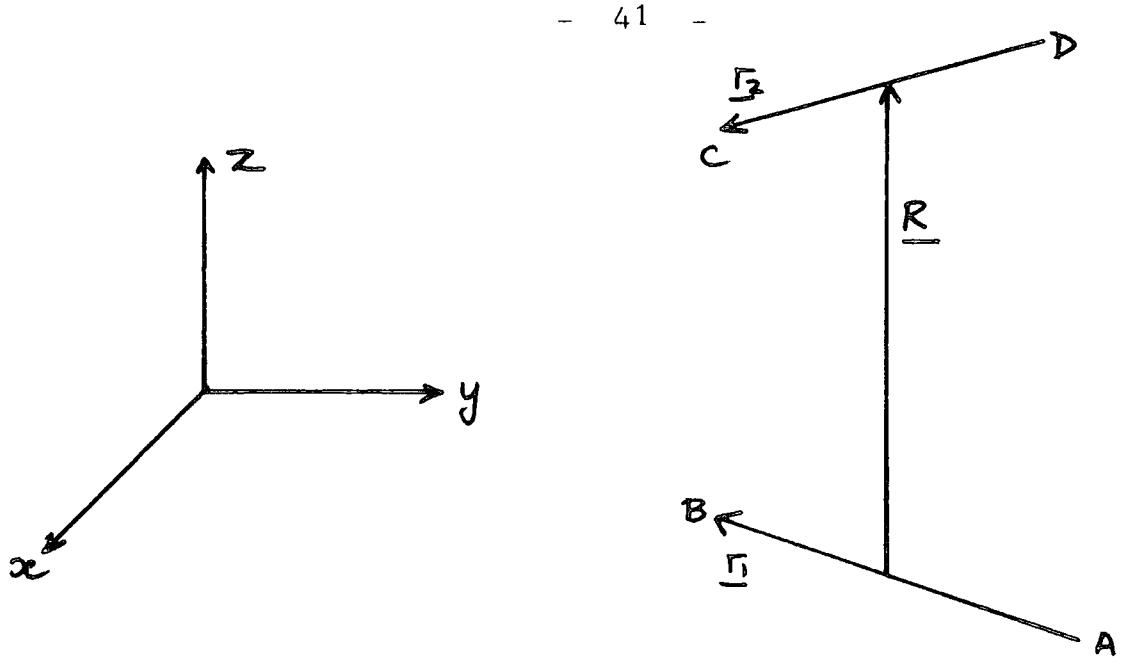

Figure 2.

The Schrödinger equation for the system may be written

$$(H-E)\,\Psi^{B} = 0, \qquad \text{II.3.1}$$

where H is defined by (cf. II.2.2)

$$H = -\frac{1}{2\mu}\nabla_R^2 + h_1 + h_2 + V(\hat{r}_1, \hat{r}_2, R), \qquad \text{II.3.2a}$$

and Ψ^{B} may be expanded in a rotational basis

$$\Psi^{B}(\hat{r}_1, \hat{r}_2, \hat{R}) = \sum_{j_1' j_2' j_{12}' \Omega'} \frac{1}{R} F^{J j_1 j_2 j_{12} \Omega v_2}_{j_1' j_2' j_{12} \Omega' v_2'}(R)\, \frac{\chi_{v_2' j_2'}(r_2)}{r_2}$$

$$\times\ \mathcal{Y}(j_1' j_2' j_{12}' \Omega, JM \mid \hat{r}_1, \hat{r}_2, \hat{R}), \qquad \text{II.3.2b}$$

where Ω is the projection of j_{12} on the body-fixed z-axis. The rotational basis function is given by

$$\mathcal{Y}(j_1 j_2 j_{12} \Omega J M / \hat{\underline{r}}_1', \hat{\underline{r}}_2', \hat{\underline{R}})$$

$$= \psi(j_1 j_2 j_{12} \Omega / \hat{\underline{r}}_1', \hat{\underline{r}}_2') N^J_{M\Omega}(\hat{\underline{R}}),$$

where $\psi(j_1 j_2 j_{12} \Omega / \hat{\underline{r}}_1', \hat{\underline{r}}_2')$

$$= \sum_{\Omega_1 \Omega_2} C(j_1 \Omega_1 j_2 \Omega_2 / j_{12} \Omega) Y_{j_1 \Omega_1}(\hat{\underline{r}}_1') Y_{j_2 \Omega_1}(\hat{\underline{r}}_2'),$$

and $$N^J_{M\Omega}(\hat{\underline{R}}) = \left(\frac{2J+1}{4\pi}\right) D^{J*}_{M\Omega}(\phi, \theta, 0).$$

$N^J_{M\Omega}$ is a normalised symmetric top eigenfunction (Rose (1957)), and $D^{J*}_{M\Omega}$ is a rotation matrix element. Substituting II.3.2b into II.3.1 we find

$$\left[\frac{d^2}{dR^2} + k^2_{v_2' j_1' j_2'}\right] F^{J j_1 j_2 j_{12} \Omega v_2}_{j_1' j_2' j_{12}' \Omega' v_2'}(R)$$

$$= \sum_{\substack{\text{double} \\ \text{primed} \\ \text{indices}}} \left(\frac{h^J_{v_2' j_1' j_2' j_{12}' \Omega' v_2'' j_1'' j_2'' j_{12}'' \Omega''}}{R} + \frac{2\mu}{\hbar^2} V^J_{v_2' j_1' j_2' j_{12}' \Omega' v_2'' j_1'' j_2'' j_{12}'' \Omega''} \right)$$

$$\times F^{J j_1 j_2 j_{12} \Omega v_2}_{j_1'' j_2'' j_{12}'' \Omega'' v_2''}(R) \qquad \text{II.3.3}$$

In the BF frame the centrifugal barrier is no longer diagonal, but given by (Launay (1976), Alexander and De Pristo (1977))

$$h^J_{v_2' j_1' j_2' j_{12}' \Omega' v_2'' j_1'' j_2'' j_{12}'' \Omega''} =$$

$$\delta_{v_2' j_1' j_2' j_{12}' \Omega' v_2'' j_1'' j_2'' j_{12}'' \Omega''} \{ \delta_{\Omega' \Omega''} [J(J+1) + j_{12}'(j_{12}'+1) - 2(\Omega')^2] \qquad \text{II.3.4}$$

$$- ([J(J+1) - \Omega'(\Omega' \pm 1)][j_{12}'(j_{12}'+1) - \Omega'(\Omega' \pm 1)])^{\frac{1}{2}} \}$$

and the intermolecular potential is expanded

$$V(\hat{r}_1', \hat{r}_2', R) = \sum_{q_1 q_2 \omega \geq 0} V_{q_1 q_2 \omega}(r_1, r_2, R)\, Y_{q_1 q_2 \omega}(\hat{r}_1', \hat{r}_2'), \qquad \text{II.3.5a}$$

where

$$Y_{q_1 q_2 \omega}(\hat{r}_1', \hat{r}_2') = 4\pi\, Y_{q_1 \omega}(\hat{r}_1')\, Y_{q_2 -\omega}(\hat{r}_2'), \qquad \text{II.3.5b}$$

where $0 \leq \omega \leq \min(q_1, q_2)$. This is invariant under rotations about the z-axis. Using this expression we are able to give an expression for the potential matrix elements (e.g. see Launay (1977), Danby (1983)),

$$V^J_{v_2' j_1' j_2' j_{12}' \Omega', v_2'' j_1'' j_2'' j_{12}'' \Omega''} = \delta_{\Omega' \Omega''} (-1)^{j_1' + j_2' + j_{12}' + \Omega'}$$

$$\times ([j_1'][j_2'][j_{12}'][j_1''][j_2''][j_{12}''][q_1][q_2])^{\frac{1}{2}}$$

$$\times \begin{pmatrix} j_1' & q_1 & j_1'' \\ 0 & 0 & 0 \end{pmatrix} \begin{pmatrix} j_2' & q_2 & j_2'' \\ 0 & 0 & 0 \end{pmatrix}$$

$$\times \sum_{q_{12}} (-1)^{q_{12}} (2q_{12} + 1)$$

$$\times \begin{pmatrix} q_1 & q_2 & q_{12} \\ -\omega & \omega & 0 \end{pmatrix} \begin{pmatrix} j_{12}' & q_{12} & j_{12}'' \\ -\Omega & 0 & \Omega \end{pmatrix} \begin{Bmatrix} j_1' & j_2' & j_{12}' \\ j_1'' & j_2'' & j_{12}'' \\ q_1 & q_2 & q_{12} \end{Bmatrix} \qquad \text{II.3.6}$$

$$\times \int_0^\infty \chi_{v_2' j_2'}(r_2)\, V_{q_1 q_2 \omega}(r_1, r_2, R)\, \chi^*_{v_2'' j_2''}(r_2)\, dr_2 .$$

The delta function $\delta_{\Omega'\Omega''}$ ensures the diagonality of the V-matrix elements in the Ω' index; this is a consequence of the invariance of the potential under rotation about R. The summation over q_{12} is such that $q_1 + q_2 + q_{12}$ is even.

The key to the CS approximation is the assumption that the nondiagonal centrifugal potential terms in II.3.4 may be ignored. Such off diagonal elements arise from the coriolis forces due to the non inertial frame. This leads to a significant reduction in the number of coupled equations since, as mentioned before, the potential matrix II.3.6 is strictly diagonal in the multiplicity Ω' In addition we set the diagonal elements of the centrifugal potential equal to $L(L + 1)\hbar^2$ where L is now a parameter. Physically one is assuming that the exact value of the orbital angular momentum is unimportant, since L can be thought of as an effective orbital angular momentum. The name j_z conserving approximation is now evident, since the projection quantum number, Ω' , is conserved during the collision. Instead of equations coupled in j_1, j_2, v_2, and ℓ we have now equations coupled in j_1, j_2 and v_2.

The equations II.3.3 may be solved subject to the boundary conditions

$$F^{J_{j_1 v_2 j_{12} \Omega v_2}}_{j_1' v_2' j_{12} \Omega' v_2'} \xrightarrow[R \to 0]{} 0 ,$$

$$F^{J_{j_1 v_2 j_{12} \Omega v_2}}_{j_1' j_2' j_{12} \Omega' v_2'} \xrightarrow[R \to \infty]{} 0 \qquad k^2_{v_2' j_1' j_2'} \leq 0 ,$$

$$F^{J}_{j_1'j_2'j_{12}'\Omega'v_2'} \xrightarrow[R\to\infty]{} (-i k_{v_2'j_1'j_2'} R h_L^{(2)}(k_{v_2'j_1'j_2'}R))\delta_{v_2j_1j_2j_{12},v_2'j_1'j_2'j_{12}'}$$
$$-\left(\frac{k_{v_2j_1j_2}}{k_{v_2'j_1'j_2'}}\right)^{\frac{1}{2}} S_L^{\Omega}(v_2j_1j_2j_{12}, v_2'j_1'j_2'j_{12}')(ik_{v_2'j_1'j_2'}R h_L^{(1)}(k_{v_2'j_1'j_2'}R))$$
$$k^2_{v_2'j_1'j_2'} > 0 . \qquad \text{II.3.7}$$

This yields an S-matrix which is block diagonal in Ω, because of the symmetry of the potential only $\Omega \geq 0$ need be considered, and the coupled equations are solved for $\Omega \leq \min(j_{12}, j_{12}')$. We may obtain an approximate space-fixed S-matrix, $\tilde{S}^J$, by employing the unitary transformation (Launay (1977)),

$$\tilde{S}^J(v_2j_1j_2j_{12}L, v_2'j_1'j_2'j_{12}'L')$$
$$= \sum_{\Omega} i^{L'-L-2L}(2L+1)^{\frac{1}{2}}(2L'+1)^{\frac{1}{2}}$$
$$\times \begin{pmatrix} j_{12}' & L' & J \\ \Omega & 0 & -\Omega \end{pmatrix}\begin{pmatrix} j_{12} & L & J \\ \Omega & 0 & -\Omega \end{pmatrix} S_L^{\Omega}(v_2j_1j_2j_{12}, v_2'j_1'j_2'j_{12}') .$$

II.3.8

The phase factor $i^{-L'-L-2L}$ guarantees that the approximate radial function, $\hat{F}^{J}_{j_1'j_2'j_{12}'\Omega'v_2'}(R)$, will fulfil the exact asymptotic boundary conditions II.2.21b. It is irrelevant for integral cross sections, but must be included to obtain correct differential cross sections (e.g. see Secrest (1975), and Schinke and McGuire (1978a)).

The centrifugal parameter L is still arbitrary and it must be identified with a physical quantity before various cross section formulae can be derived. The two natural choices for L are L and L', the initial and final orbital angular momentum respectively. Only

for the choices L ℓ, ℓ' can significant simplifications be made in the scattering amplitude. The choice of L has been fully discussed by Pack (1977), Goldflam et al. (1977), and others.

Identifying L with ℓ', when $\tilde{S}^J$ is substituted into II.2.26 one obtains (Heil et al. (1978))

$$f_{\ell'}(v_2 j_1 m_1 j_2 m_2 \to v_2' j_1' m_1' j_2' m_2' | \hat{R}) = \frac{i}{2\sqrt{k_{v_2 j_1 j_2} k_{v_2' j_1' j_2'}}} \sum_{\substack{j_{12} j_{12}' \\ \Omega}}^{\ell'} (2\ell'+1) P_{\ell'}(\cos\theta) \times C(j_1' m_1' j_2' m_2' | j_{12}' \Omega) C(j_1 m_1 j_2 m_2 | j_{12} \Omega) \times T_{\ell'}^{\Omega}(v_2 j_1 j_2 j_{12}, v_2' j_1' j_2' j_{12}'), \qquad \text{II.3.9a}$$

which is a generalisation of the atom-diatom differential scattering amplitude (McGuire and Kouri (1974)). If we identify L with ℓ, the amplitude is given by (Goldflam and Kouri (1979))

$$f_{\ell}(v_2 j_1 m_1 j_2 m_2 \to v_2' j_1' m_1' j_2' m_2' | \hat{R}) = \sum_{\substack{j_{12} j_{12}' \\ m_{12} m_{12}'}} C(j_1 m_1 j_2 m_2 | j_{12} m_{12}) C(j_1' m_1' j_2' m_2' | j_{12}' m_{12}') \times f(v_2 j_1 j_2 j_{12} m_{12} \to v_2' j_1' j_2' j_{12}' m_{12}' | \hat{R}), \qquad \text{II.3.9b}$$

where

$$f(v_2 j_1 j_2 j_{12} m_{12} \to v_2' j_1' j_2' j_{12}' m_{12}' | \hat{R})$$
$$= \sum_{\Omega} D^{j_{12}'}_{m_{12}' \Omega}(\hat{R}) \tilde{f}_l(v_2 j_1 j_2 j_{12} \Omega \to v_2' j_1' j_2' j_{12}' \Omega' | \hat{R})$$
$$\times D^{j_{12}*}_{m_{12} \Omega}(\hat{R}),$$

where

$$\tilde{f}_l(v_2 j_1 j_2 j_{12} \Omega \to v_2' j_1' j_2' j_{12}' \Omega' | \hat{R})$$
$$= \frac{i}{2\sqrt{k_{v_2 j_1 j_2} k_{v_2' j_1' j_2'}}} \sum_l (2l+1) P_l(\cos\Theta)$$
$$\times T^{\Omega}_l(v_2 j_1 j_2 j_{12} \to v_2' j_1' j_2' j_{12}').$$

The main difference between the amplitudes $f_{l'}$ and f_l is that for $L = l'$, $\Delta m_{12} = 0$, while with $L = l$, $\Delta m_{12} \neq 0$. This is significant as it is known from CC calculations (e.g. see Tarr et al. (1977), and Alexander et al. (1977)) that the exact scattering amplitude is not diagonal in m_{12}. It makes no difference whether we use $f_{l'}$ or f_l because, as noted by Khare (1977), and easily shown from the unitarity of the D matrices, both scattering amplitudes give identical results for all degeneracy averaged cross sections. It is worth noting that neither choice of L gives a fully symmetric S^J (Hunter (1975)).

Formal theoretical criteria for the applicability of the CS approximation have not yet been formulated, the accuracy of the approximation for a given system is usually assessed by comparison with CC calculations. The approximation has been successfully employed in atom-diatom, and diatom-diatom calculations. Generally speaking

the energy of the collision should be sufficiently high so that the precise value of the centrifugal term is unimportant. For purely repulsive electrostatic interaction potentials the position of the classical turning point will not vary particularly rapidly, however if the potential has an attractive well there may be three turning points all varying rapidly with ℓ, and the assumption of an effective angular momentum will not be justified. (The importance of the centrifugal term is determined by the variation of the turning points with respect to ℓ).

Kouri et al (1976) found that the impact parameter should be smaller than the classical turning point, and the energy should be well above threshold for the transition being studied, and should be at least comparable with the well depth. The latter findings limits the CS approximation to short range potentials, this is demonstrated in the results of Kouri and McGuire (1974) for the $Li^+ + H_2$ system, and in the results of Heil et al. (1978) for the $H_2 + HC\ell$ system. In both systems the long range interactions are causing the results to be in error. It is worth noting that by retaining some of the coriolis terms Kinnersley (1979) has obtained satisfactory results for $Li^+ + H_2$. The results of Heil and Kouri (1976) for $H_2 + H_2$ indicates that the CS approximation works as well for diatom-diatom collisions as for atom-diatom systems.

Since vibrational excitation occurs through hard short ranged collisions, the CS approximation would be

expected to be useful. In fact the CS calculations of Alexander and McGuire (1976) for the He + H_2 system are in excellent agreement with the CC results of Flower and Kirkpatrick (1982).

In conclusion one would expect the CS approximation to be valid in studies where the collision energy is reasonably high (to prevent the situation of three turning points), and for systems for which the potential surface contains no long range anisotropies.

3.2 The Energy Sudden Approximation

The energy sudden (ES) approximation is valid in collisions where the rotational period of the target is much longer than the collision time (i.e. the target only rotates slightly during the collision). This approximation is valid for collisions involving heavy target molecules, and high collision energies, it was introduced by Chase (1956) and has been widely used in electron-molecule scattering theory where it is known as the adiabatic-nuclei approximation. Note that the small mass of the electron makes it well suited to such collisions (e.g. see Collins and Norcross (1978)).

Few calculations have been performed employing just the ES approximation. Two atom-rotor calculations (Chu and Dalgarno (1975a), and Khare (1978)), and one rotor-rotor calculation (H_2 + N_2 studied by Bergeron et al. (1978), however the H_2 was constrained in its ground rotational state and it was therefore an atom-molecule calculation).

Nevertheless the ES approximation is worth discussing as it is a component of other decoupling approximations (notably the infinite order sudden approximation discussed in Section 2.3).

The molecule is at rest during the collision, and therefore one solves the scattering problem for all stationary rotor orientations, and uses this information to determine the state to state scattering amplitudes. The latter problem is the simpler, if $f_{v_2 \to v_2'}(\hat{r}_2, \hat{R})$ is the scattering amplitude for fixed rotor orientation,

$$f(v_2 j_2 m_2 \to v_2' j_2' m_2'; \hat{R})$$

$$= \int Y^*_{j_2' m_2'}(\hat{r}_2) f_{v_2 \to v_2'}(\hat{r}_2, \hat{R}) Y_{j_2 m_2}(\hat{r}_2) d\hat{r}_2 . \quad \text{II.3.10}$$

This formula was derived by Chase (1956), and one must calculate $f_{v_2 \to v_2'}(\hat{r}_2, \hat{R})$ at sufficient orientations to obtain a satisfactory result. Note however, that the scattering calculation is independent of the orientation of the system in space, and instead this can be considered as allowing the atom to approach the molecule from all directions. We are free to choose $\hat{r}_2$ as our polar axis which means that the interaction potential V will be axially symmetric, and therefore l_z will be conserved, although l is not (Figure 3).

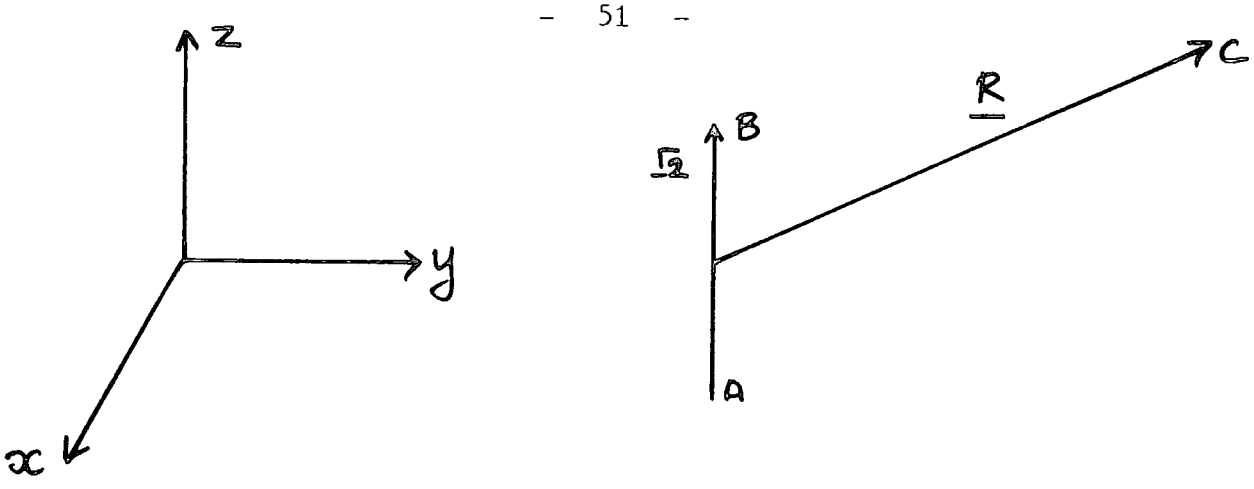

Figure 3

In this new coordinate system $\underline{R}$ is replaced by $\underline{R}' = (R, \theta', \phi')$.

Since the molecule is at rest during the collision, the rotor states may be considered degenerate, and we may denote them by $j_2 = 0$. Therefore $k_{v_2 j_2}$ and $\varepsilon_{v_2 j_2}$ are now independent of j_2 and the subscript may be omitted ($k_{v_2 j_2} = k_{v_2 0} = k_{v_2}$).

Expanding the total wavefunction as

$$\Phi(\underline{R}', \underline{r}_2) = R^{-1} \sum_{l' v_2' \eta'} u^{l v_2}_{l' v_2' \eta'}(R) \times Y_{l' \eta'}(\hat{\underline{R}}') \chi_{v_2}(r_2), \qquad \text{II.3.11}$$

the radial functions $u^{l v_2}_{l' v_2' \eta'}(R)$ satisfy

$$\left[\frac{d^2}{dR^2} + k_{v_2'} - \frac{l'(l'+1)}{R}\right] u^{l v_2}_{l' v_2' \eta'}(R) = \frac{2\mu}{\hbar^2} \sum_{l''} V^{\eta'}_{v_2' l', v_2'' l''}(R)\, u^{l v_2}_{l'' v_2'' \eta'}(R), \qquad \text{II.3.12}$$

where $V^{\eta'}_{v_2'\ell',v_2''\ell''}(R)$

$$= (2\pi)\iint \chi_{v_2'}(r_2)\, Y_{\ell'\eta'}(\theta,0)\, V(r_2,R,\theta)$$

$$\times Y^*_{\ell''\eta'}(\theta,0)\, \chi_{v_2''}(r_2)\, d(\cos\theta')\, dr_2 . \qquad \text{II.3.13a}$$

Using the single centre expansion, II.2.31, this reduces to

$$V^{\eta'}_{v_2'\ell',v_2''\ell''}(R)$$

$$= \sum_{\lambda_2} (-1)^{\eta'} (2\ell'+1)^{\frac{1}{2}} (2\ell''+1)^{\frac{1}{2}}$$

$$\times \begin{pmatrix} \ell' & \lambda_2 & \ell'' \\ 0 & 0 & 0 \end{pmatrix} \begin{pmatrix} \ell' & \lambda_2 & \ell'' \\ \eta' & 0 & -\eta'' \end{pmatrix}$$

$$\times \int \chi_{v_2'}(r_2)\; B_{\lambda_2}(r_2,R)\, \chi^*_{v_2''}(r_2)\, dr_2 . \qquad \text{II.3.13b.}$$

Since l_z is conserved, the equations are diagonal in η'. Therefore, instead of equations coupled in j_2, v_2, and ℓ, we now have sets of equations indexed by v_2 and ℓ only. If the theory had been presented for rotor-vibrotor collisions, the same conclusion would have been reached (i.e. equations indexed by j_1, j_2, v_2, and ℓ reduce to equations indexed by j_1, v_2 and ℓ). However, since the rotor (molecule 1) would not have been stationary, l_z would not have been conserved. Note that the above conclusion, namely that l_z is conserved, was drawn without any approximations to the potential surface or centrifugal potential operator.

Therefore in the rotor-vibrotor case this approximation leads to the conservation of ($l_z + j_{1z}$) (cf. CS approximation which leads to the conservation of $j_{1z} + j_{2z}$).

The equations II.3.12 may be solved subject to the boundary conditions.

$$U^{l v_2}_{l' v_2' \eta'} \xrightarrow[R \to 0]{} 0$$

$$U^{l v_2}_{l' v_2' \eta'} \xrightarrow[R \to \infty]{} 0 \quad K^2_{v_2'} \leq 0$$

$$U^{l v_2}_{l' v_2' \eta'} \longrightarrow (i K_{v_2'} R h^{(2)}_{l'}(K_{v_2'} R)) \delta_{l v_2, l' v_2'} \quad K^2_{v_2'} > 0$$

$$-\left(\frac{K_{v_2}}{K_{v_2'}}\right)^{\frac{1}{2}} S^{\eta}(l v_2, l' v_2') (i K_{v_2} R h^{(1)}_{l'}(K_{v_2'} R)) \qquad \text{II.3.14}$$

Using the sudden S-matrix , $S^{\eta}(l v_2, l' v_2')$, an approximate space-fixed S-matrix can be evaluated using

$$\tilde{S}^{J}(v_2 j_2 l, v_2' j_2' l')$$

$$= \sum_{\eta'} (2j_2+1)^{\frac{1}{2}} (2j_2'+1)^{\frac{1}{2}} \begin{pmatrix} j_2' & l' & J \\ 0 & \eta & -\eta \end{pmatrix} \begin{pmatrix} j_2 & l & J \\ 0 & \eta & -\eta \end{pmatrix} \times S^{\eta}(l v_2, l' v_2') \qquad \text{II.3.15}$$

This result comes from II.3.10, the integral may be performed analytically by rotation to a new coordinate system, and the properties of the rotation matrices employed (Khare (1978), Secrest (1975)). The space fixed S-matrix may be used in the full CC equation II.2.26 with $j_1 = 0$ to obtain the cross sections.

The coupled equations must be solved for all the values of η and for large ℓ this is highly problematic (e.g. see Chu and Dalgarno (1975a)). However using physical arguments Khare (1978) has shown that it is only necessary to consider $\eta \leq (j_2\text{max} + 1)$, since only the first few terms contribute significantly ($j_2$max is the largest j_2 accessible from the $j_2 = 0$ state). Note because of the symmetry of the potential matrix only $\eta \geq 0$ need be considered.

Using the Clebsh-Gordan series for spherical harmonics in II.3.10 an important simplification can be made,

$$f(v_2 j_2 m_2 \rightarrow v_2' j_2' m_2' / \hat{R})$$

$$= (-1)^{m_2'} (2j_2'+1)^{\frac{1}{2}} (2j_2+1)^{\frac{1}{2}} \sum_{j_2'' m_2''} (2j_2''+1)^{\frac{1}{2}}$$

$$\times \begin{pmatrix} j_2' & j_2 & j_2'' \\ -m_2' & m_2 & \Delta m_2 \end{pmatrix} \begin{pmatrix} j_2' & j_2 & j_2'' \\ 0 & 0 & 0 \end{pmatrix}$$

$$\times \left(\frac{k v_2 0 \; k v_2' j_2''}{k v_2 j_2 \; k v_2' j_2'} \right) f(v_2 00 \rightarrow v_2' j_2'' \Delta m_2 / \hat{R}), \qquad \text{II.3.16}$$

from which we may derive

$$\sigma(v_2 j_2 \rightarrow v_2' j_2')$$

$$= (2j_2'+1) \left(\frac{k v_2 0}{k v_2 j_2} \right)^{\frac{1}{2}} \sum_{j_2''} \begin{pmatrix} j_2' & j_2 & j_2'' \\ 0 & 0 & 0 \end{pmatrix} \sigma(v_2 0 \rightarrow v_2' j_2''). \qquad \text{Ii.3.17}$$

If we sum over j_2' equation II.3.17 is made to yield the result,

$$\sum_{j_2'} \sigma(v_2 j_2 \to v_2' j_2') = \left(\frac{k_{v_2 0}}{k_{v_2 j_2}}\right)^2 \sum_{j_2''} \sigma(v_2 0 \to v_2' j_2'') .$$

II.3.18

This result implies that apart from the detailed balance factor, the total integral cross section is independent of the initial rotor state. II.3.17 and II.3.18 are also valid for differential cross sections, and this property is present whenever the ES approximation is used. We only need to calculate $\sigma(v_2 0 \to v_2' j_2'')$ and all other cross sections can be trivally derived from them.

This approximation has been employed by Khare (1978) in a study of rotational excitation in Ar + N_2 and Ar + TlF. Generally speaking the results agree well with the CC results of Tsien et al. (1973), the agreement is much better for Ar + TlF, because of the heavier mass involved. At some J values it was found that $S^J(j_2 l, j_2' l')$ was very sensitive to small errors in $S^J(l, l')$. At these low J values the electrostatic potential is dominant, and an approximation can be made on the centrifugal term, and therefore, the IOS approximation would be expected to be valid, this is demonstrated by Khare (1978). The IOS was found to be satisfactory for low J, but failed at high J where the coupled states component of the approximation failed.

The problem with the ES approximation is that it

does not include the influence of closed (or almost closed) channels. If the well depth is large in comparison with the relevant kinetic energy, and the anisotropy of the interaction potential is strong, then coupling to states which are closed or almost closed can be important. However, as the collision energy increases the kinetic energy of strongly coupled states becomes greater than or equal to the well depth of the potential, and the closed channels become less important even in strongly coupled systems, and the ES approximation becomes reasonable.

3.3 The Infinite Order Sudden Approximation

This approximation is a combination of the energy sudden, and the centrifugal sudden approximations. It was introduced by Tsien and Pack (1970), and was later generalised independently by Secrest (1975) and by Hunter (1975). There are many derivations in the literature for the atom-molecule approach in both the space-fixed frame (e.g. Tsien and Pack (1970), Secrest (1975), and Parker and Pack (1978)), and the body-fixed frame (e.g. Pack (1974), and Bowman and Leasure (1977)). The approximation has been generalised to diatom-diatom systems, rotor-rotor collisions in which one rotor was treated within the infinite order sudden (IOS) approximation and where the other rotor was treated within the CS approximation (Goldflam and Kouri (1979), and Andres et al. (1982)), and in a calculation in which both rotors where treated within the IOS approximation (Goldflam

and Kouri (1979)). The present derivation is in the body-fixed frame as in Section 3.1 , only the vibrotor (molecule 2) is treated within the IOS approximation, the rotor (molecule 1) is treated within the CS approximation. The IOS approximation can be considered as an energy sudden approximation to the centrifugal sudden approximation. In the CS, the diagonal elements of the centrifugal potential are set equal to $L(L+1)\hbar^2$, and in the ES the rotor states of the molecule are assumed to be degenerate (i.e. we replace $k_{v_2 j_1 j_2}$ by $K_{v_2 j_1}$).

The potential may be expanded as in II.3.5a, however we will employ a simplified version of this in which the terms with $w \neq 0$ are neglected (this will be justified later), the potential expansion may be written,

$$\bar{V}(\theta_1', r_1, \theta_2', r_2, R) = \sum_{q_1 q_2} \bar{V}_{q_1 q_2 0}(r_1, r_2, R) \times (2q_1+1)^{\frac{1}{2}}(2q_2+1)^{\frac{1}{2}} P_{q_1}(\cos\theta_1') P_{q_2}(\cos\theta_2'). \qquad \text{II.3.19}$$

Expanding the total wavefunction Ψ^{IOS} as

$$\Psi^{IOS}(\hat{\underline{r}}_1', \underline{r}_2, R) = \sum_{v_2' j_1' \Omega_1'} \frac{\chi_{v_2'}(r_2)}{r_2} \frac{F^{J}_{j_1' \Omega_1' v_2'}(R; \theta_2')}{R} Y_{j_1' \Omega_1'}(\hat{\underline{r}}_1'), \qquad \text{II.3.20}$$

we obtain

$$\left[\frac{d^2}{dR^2} + K_{v_2' j_1'} - \frac{L(L+1)}{R^2}\right] F^{L j_1 \Omega_1 v_2}_{j_1' \Omega_1' v_2'}(R;\theta_2') = \frac{2\mu}{\hbar^2} \sum_{\substack{\text{double} \\ \text{primed} \\ \text{indices}}} V_{v_2' j_1' \Omega_1', v_2'' j_1'' \Omega_1'}(R,\theta_2') F^{L j_1 \Omega_1 v_2}_{j_1'' \Omega_1'' v_2''}(R;\theta_2').$$

II.3.21

The potential matrix elements are given by

$$V_{v_2' j_1' \Omega_1', v_2'' j_1'' \Omega_1'}(R;\theta_2') = \sum_{q_1 q_2} (2q_2+1)^{\frac{1}{2}} \times (-1)^{\Omega_1} \delta_{\Omega_1' \Omega_1''} \left[(2j_1'+1)(2q_1+1)(2j_1''+1)\right]^{\frac{1}{2}} \times \begin{pmatrix} j_1' & q_1 & j_1'' \\ 0 & 0 & 0 \end{pmatrix} \begin{pmatrix} j_1' & q_1 & j_1'' \\ -\Omega_1' & 0 & \Omega_1 \end{pmatrix} P_{q_2}(\cos\theta_2') \times \int_0^\infty \chi_{v_2'}(r_2)\, \bar{V}_{q_1 q_2 0}(r_1, r_2, R)\, \chi^*_{v_2''}(r_2)\, dr_2 .$$

II.3.22

Because the operators which depend on the angle, θ_2' between R and r_2 have been removed, we see that II.3.21 depends on θ_2' only parametrically through $V_{v_2' j_1' \Omega_1', v_2'' j_1'' \Omega_1'}(R;\theta_2')$ and can be solved for each θ_2' desired holding θ_2' fixed. Computationally II.3.21 is far simpler to solve than either II.3.3 or II.3.12 since now the coupled equations are only indexed by v_2 and j_1. The equations II.3.21 may be solved subject to the boundary conditions

$$F^{L j_1 \Omega_1 v_2}_{j_1' \Omega_1' v_2'}(R;\theta_2') \xrightarrow[R\to 0]{} 0 ,$$

$$F^{L j_1 \Omega_1 v_2}_{j_1' \Omega_1' v_2'}(R;\theta_2') \xrightarrow[R\to\infty]{} 0 \qquad K^2_{v_2' j_1'} \le 0 ,$$

$$F^{L j_1 \Omega_1 v_2}_{j_1' \Omega_1' v_2'}(R;\theta_2') \xrightarrow[R\to\infty]{} (-i K_{v_2' j_1'} R h_L^{(2)}(K_{v_2' j_1'} R))\delta_{v_2 j_1, v_2' j_1'}$$

$$-\left(\frac{K_{v_2 j_1}}{K_{v_2' j_1'}}\right)^{\frac{1}{2}} S_L(v_2 j_1 \Omega_1, v_2' j_1' \Omega_1' | \theta_2')(i K_{v_2' j_1'} R h_L^{(1)}(K_{v_2' j_1'} R)) \qquad \text{II.3.23}$$

$$K^2_{v_2' j_1'} > 0 ,$$

yielding a scattering matrix $S_L(v_2 j_1 \Omega_1, v_2' j_1' \Omega_1' | \theta_2')$ which is block diagonal in Ω_1, quadrature over θ_2' yields

$$S_L(v_2 j_1 \Omega_1 j_2 \Omega_2, v_2' j_1' \Omega_1' j_2' \Omega_2')$$

$$= \delta_{\Omega_2 \Omega_2'} \int_0^{\pi} Y_{j_2 \Omega_2}(\hat{r}_2') S_L(v_2 j_1 \Omega_1, v_2' j_1' \Omega_1' | \theta_2') Y^*_{j_2' \Omega_2'}(\hat{r}_2)\, d\hat{r}_2 . \qquad \text{II.3.24}$$

We note at this point that the conservation of Ω_2, implied by II.3.24 together with the conservation of Ω, implied by the invariance of the interaction potential II.3.19 under rotations about the intermolecular axis, result in the conservation of Ω_1. It follows that only those terms with w = 0 need to be retained in the potential expansion II.3.5a.

The S-matrix defined by II.3.24 can not be used in II.3.8 to obtain an approximate space-fixed S-matrix, since the transformation, II.3.8. assumes that the eigenfunctions $Y_{j_1 \Omega_1}(\hat{r}_1')$ and $Y_{j_2 \Omega_2}(\hat{r}_2')$ are coupled together (note however that the transformation can be used in atom-diatom calculations, since $j_1 = 0$). To

obtain the scattering amplitude we first find the body-fixed scattering amplitude for fixed vibrotor orientation Θ_2' . The asymptotic form of the wave function II.3.20 may be written

$$\Psi^{IOS} \xrightarrow[R\to\infty]{} \exp(iK_{v_2 j_1} z)\,\chi_{v_2}(r_2)\,Y_{j_1\Omega_1}(\hat{r}_1) + \sum_{\substack{\text{primed}\\ \text{indices}}} \exp(iK_{v_2' j_1'} R)\, f(v_2 j_1 \Omega_1 \to v_2' j_1' \Omega_1'\ \Theta_2'|\hat{R})\, \chi_{v_2'}(r_2)\, Y_{j_1'\Omega_1'}(\hat{r}_1'), \qquad \text{II.3.25}$$

to find $f(v_2 j_1 \Omega_1 \to v_2' j_1' \Omega_1' \Theta_2'|\hat{R})$ we find the correct linear combination of Ψ^{IOS} which goes over to II.3.25 asymptotically, and follow the procedure outlined in Section 2. If we take the orbital angular momentum parameter equal to the initial value, l , one finds that the fixed vibrotor scattering amplitude is given by

$$f(v_2 j_1 \Omega_1 \to v_2' j_1' \Omega_1\ \Theta_2'|\hat{R}) = \frac{i}{2}\,(K_{v_2 j_1} K_{v_2' j_1'})^{-1/2} \sum_l (2l+1)\, P_l(\cos\theta) \times T_l(v_2 j_1 \Omega_1 \to v_2' j_1' \Omega_1|\Theta_2'). \qquad \text{II.3.26}$$

The SF scattering amplitude is then given by

$$f(v_2 j_1 m_1 j_2 m_2 \to v_2' j_1' m_1' j_2' m_2'|\hat{R}) = \left(\frac{K_{v_2 j_1} K_{v_2' j_1'}}{k_{v_2 j_1 j_2} k_{v_2' j_2' j_2'}}\right)^{1/2} \sum_{\Omega_1} D^{j_1'}_{m_1'\Omega_1}(\hat{R})\, D^{j_1 *}_{m_1\Omega_1}(\hat{R}) \times \int_0^\pi Y_{j_2\Omega_2}(\hat{r}_2')\, f(v_2 j_1 \Omega_1 \to v_2' j_1' \Omega_1\ \Theta_2'|\hat{R})\, Y_{j_2'\Omega_2'}(\hat{r}_2')\, d\hat{r}_2 \times \sum_{\Omega_2} D^{j_2'}_{m_2'\Omega_2}(\hat{R})\, D^{j_2 *}_{m_2\Omega_2}(\hat{R}). \qquad \text{II.3.27}$$

This is a generalisation of the result given by Parker and Pack (1978) for atom-diatom scattering.

The differential cross sections are given by

$$\frac{d\sigma}{d\Omega}(v_2 j_1 j_2 \rightarrow v_2' j_1' j_2' / \underline{\hat{R}}) = \frac{1}{4(2j_1+1)(2j_2+1)k^2_{v_2 j_1 j_2}} \times \sum_{\substack{\Omega_1 \\ \Omega_2}} \left| \sum_{l} (2l+1) P_l(\cos\theta) T_l(v_2 j_1 \Omega_1 j_2 \Omega_2, v_2' j_1' \Omega_1 j_2' \Omega_2) \right|^2, \quad \text{II.3.28}$$

where $\Omega_1 = \min(j_1, j_1')$ and $\Omega_2 = \min(j_2, j_2')$.

Since the ES approximation has been employed it is only necessary to calculate results for transitions for which the initial value of $j_2 = 0$, and therefore the summation over Ω_2 collapses. The integral cross sections are found using

$$\sigma(v_2 j_1 0 \rightarrow v_2' j_1' j_2') = \frac{\pi}{k^2_{v_2 j_1 0}(2j_1+1)} \times \sum_{l\Omega_1} (2l+1) |T_l(v_2 j_1 \Omega_1 0 0, v_2' j_1' \Omega_1 j_2' 0)|^2, \quad \text{II.3.29}$$

and rotationally summed cross sections are evaluated using (e.g. see Goldflam et al. (1977) and Parker and Pack (1978))

$$\sum_{j_2} \sigma(v_2 j_1 0 \rightarrow v_2' j_1' j_2') = \frac{\pi}{k^2_{v_2 j_1 0}(2j_1+1)} \sum_{l\Omega_1} (2l+1) \times \frac{1}{2} \int_0^{\pi} |T_l(v_2 j_1 \Omega_1, v_2' j_1' \Omega_1 / \theta_2')|^2 \sin\theta_2' \, d\theta_2'. \quad \text{II.3.30}$$

To evaluate $S_L(v_2 j_1 \Omega_1, v_2' j_1' \Omega_1 | \theta_2')$ we must solve the coupled equations at a sufficient number of orientations to obtain satisfactory results. It is usual to employ Gaussian quadrature, however if we have to calculate very many cross sections, we can decrease the number of integrals by expanding the T-matrix in Legendre polynomials (for each partial wave).

$$T_L(v_2 j_1 \Omega_1, v_2' j_1' \Omega_1 | \theta_2') = \sum_\lambda A_\lambda^L (v_2 j_1 \Omega_1, v_2' j_1' \Omega_1) P_\lambda(\cos\theta_2') \qquad \text{II.3.31}$$

This allows the integral in II.3.24 to be evaluated analytically, however, it does not allow a reduction in the number of orientations, θ_2', that must be considered. The number of terms in the series is determined by the number of θ_2' values considered.

If the S-matrix is strongly dependent on θ_2', calculations at many orientations may be required. A numerical technique to reduce the number of θ_2' values required has been discussed by Secrest (1979). The approach is to interpolate the amplitude and phase of the S-matrix which vary more slowly with θ_2' than the real and imaginary parts.

In atom-molecule calculations a useful feature of the IOS approximation is that a single centre expansion of the potential has no particular advantage. In CC

and in the other approximate methods (also in the IOS approximation when $j_1 \neq 0$) the potential matrices involve integrals over triple products of spherical harmonics which can be evaluated analytically. In IOS atom-molecule calculations there are no such integrals.

Green (1978) has tested the IOS approximation against CC or CS results for HCℓ + Ar, HC + He, CO + He, and HCN + He. He found reasonable agreement for all the systems at $E_T = 100\ cm^{-1}$, except HCℓ + Ar. This is not surprising since at a given energy we would expect the sudden approximation to be less valid for the HCℓ + Ar system (Ar is heavier than He, and would therefore approach the target at a lower speed).

Generally speaking one would expect the IOS approximation to be well suited to problems of rovibrational excitation. Vibrational excitation occurs through hard short range collisions, and therefore we would expect the CS approximation to be valid, also vibrational excitation requires high collision energies, we would expect the ES approximation to be valid. In addition note that CC calculations are computationally expensive for heavy molecules with closely packed rotational levels, the ES approximation would be ideally suited to such molecules (and hence the IOS).

The large rotational energy spacing of the H_2 molecule means that collisions involving this molecule provide a stringent test of the IOS method. Schinke and McGuire

(1978a) have compared IOS and CC results for $H_2 + H^+$ at E = 3.7eV and the general level of agreement is satisfactory, however the IOS results for the $\Delta j_2 = 2$ transition are in error. Although the CS approximation is not suited to long range potentials (there are long range isotropic and anisotropic terms due to the charge on the proton), the agreement between the CS results and the CC results of McGuire (1976) is good for the $j_2 = 0 \rightarrow 2$ transition. The conclusion that may be drawn from this is that the sudden approximation is failing for $\Delta j_2 = 2$ transitions; the long range interaction means that the H^+ is spending a relatively long time in the interaction region. The increasing failure of the IOS as the angular momentum increases is consistent with this. As expected the agreement is improved at higher collision energies. The $H_2 + H^+$ system is used to test our IOS programmes (Chapter IV).

In the IOS method, we are making both the CS and ES approximations. Therefore the two preceding discussions apply (Sections 3.1 and 3.2)). However it is worth mentioning that the factorization relations presented in Section 3.2 apply provided only the ES condition is met. Also note that the method should be considered even in cases where the validity conditions are not well satisfied (providing one requires only qualitatively accurate results). The approximation is very simple, and can yield results with very little computational effort, especially since only the cross sections out of the $j_2 = 0$ level are required. The factorization relation II.3.17

given in Section 3.2 may be generalized to diatom-diatom scattering without any additional factors (e.g. see Andres et al. (1982))

$$\sigma(v_2 j_1 j_2 \rightarrow v_2' j_1' j_2') = (2j_2'+1)\left(\frac{k_{v_2 j_1 0}}{k_{v_2 j_1 j_2}}\right)^{\frac{1}{2}} \sum_{j_2''} \begin{pmatrix} j_2' & j_2 & j_2'' \\ 0 & 0 & 0 \end{pmatrix} \sigma(v_2 j_1 0 \rightarrow v_2' j_1' j_2'') . \qquad \text{II.3.32}$$

4. Other quantum mechanical decoupling approximations

In this section we discuss some less important decoupling approximations that may be employed when the approximations discussed in Section 3 are not valid.

4.1 The Effective Potential Methods

The basic difficulty in handling quantum mechanical diatom (or atom) - diatom calculations is the large number of internal molecular states that can be involved. The largest contribution to the number of molecular states generally comes from the 2j + 1 degenerate rotational projection m states for each rotational level labelled by j. Note that most experiments do not directly measure all of the potentially large amounts of data generated by conventional collision calculations. Typical experiments measure cross sections or rates that are appropriate averages over the m states. Therefore, the numerous m states are the root of the computational difficulties, but their information content is frequently averaged over to compare with experiment. The presence of vibrational states does not alter these arguments.

The effective potential (EP) approach was developed by Rabitz (1972) to handle the aforementioned difficulties. The EP approach reduces the dimensionality of the problem by projecting out or preaveraging over the m states before carrying out the dynamics. This was the first of the decoupling schemes for rotational excitation. This method is reviewed by Rabitz (1976). For a potential of the form II.2.18a, the effective potential matrix elements may be written (Zarur and Rabitz (1974))

$$V_{v_2' j_1' j_2', v_2 j_1 j_2} = \sum_{\lambda_1\lambda_2\lambda_{12}} V^{\lambda_1\lambda_2\lambda_{12}} \int \chi^{*}_{v_2' j_2'}(r_2) A_{\lambda_1\lambda_2\lambda_{12}}(\Gamma_1 r_2 R) \chi_{v_2 j_2}(r_2) dr_2 . \qquad \text{II.4.1.}$$

where

$$V^{\lambda_1\lambda_2\lambda_{12}} = N_0 \exp(i\eta) \langle j_1' j_2' \| T_{\lambda_1\lambda_2\lambda_{12}} \| j_1 j_2 \rangle .$$

where

$$N_0 = [(2j_1'+1)(2j_2'+1)(2j_1+1)(2j_2+1)]^{-1/4},$$

$$\eta = \frac{\pi}{2}\left[|j_1'+j_2'-j_1-j_2| + j_1'+j_2'+j_1+j_2\right],$$

and the reduced matrix element $\langle j_1' j_2' \| T_{\lambda_1\lambda_2\lambda_{12}} \| j_1 j_2 \rangle$

$$= \left[\frac{(2j_1'+1)(2j_2'+1)(2j_1+1)(2j_2+1)(2\lambda_{12}+1)}{(4\pi)^{3/2}}\right]^{\frac{1}{2}} \times \begin{pmatrix} j_1' & \lambda_1 & j_1 \\ 0 & 0 & 0 \end{pmatrix} \begin{pmatrix} j_2' & \lambda_2 & j_2 \\ 0 & 0 & 0 \end{pmatrix}.$$

Due to the preaveraging over m states the detailed balance condition II.2.30 is no longer valid, and the following relation holds:

$$k^2_{v_2 j_1 j_2}\, \sigma(v_2 j_1 j_2 \to v_2' j_1' j_2') = k^2_{v_2' j_1' j_2'}\, \sigma(v_2' j_1' j_2' \to v_2 j_1 j_2) . \qquad \text{II.4.2}$$

Normally there would be a factor

$$(2j_1'+1)(2j_2'+1)/(2j_1+1)(2j_2+1)$$

on the right hand side of II.4.2, however in the EP method the 2j + 1 m states are replaced by one state.

If strong coherence effects associated with particular m values were to carry through the dynamics, then this procedure would be in some doubt. One would expect that systems with few m states would be the most likely to show such coherence effects, and H_2 at low energies is perhaps the most extreme case of this type. However, the comparison of the EP results for H_2 + He (Zarur and Rabitz (1973)) with CC results is satisfactory. Comparisons with CC calculations indicates that the EP method is best for systems with weak anisotropies, and for energies well above threshold (e.g., H_2 + H_2 studied by Ramaswamy et al. (1977), and He + H_2 studied by Chu and Dalgarno (1975b)).

Another type of effective potential method is the breathing sphere (BS) approximation (e.g. Secrest (1979)). It is a model in which one eliminates the angular dependence of the molecules by averaging the interaction potential over all orientations, and then solves the resulting close-coupling equations for the spherically averaged potential. Alternatively one can look at the problem as constraining the molecules in their ground rotational states ($j_1 = 0$, $j_2 = 0$) and include

no other rotational states in the calculation (i.e. completely ignore rotational excitation). In either case the resulting coupled equations are the same. There is one channel for each vibrational state carried and the number of coupled equations for each partial wave is equal to the number of vibrational states included. The total angular momentum is just the relative angular momentum of the diatom (or atom)-diatom system. Integral cross sections may be calculated using (cf. II.3.10)

$$\sigma(v_2 \rightarrow v_2') = \frac{\pi}{k_{v_2}^2} \sum_l (2l+1) \left| T_l(v_2, v_2') \right|^2 . \qquad \text{II.4.3}$$

The BS approximation is capable of giving physically useful results, but rotational degrees of freedom are important in vibrational energy transfer (see Chapter V).

4.2 The L-Dominant and Decoupled L-Dominant approximations

The L-dominant (LD) and decoupled L-dominant approximations were developed by Depristo and Alexander (1975 and 1976 respectively) and later generalised to diatom-diatom collisions (Depristo and Alexander (1977)). They were designed to take advantage of situations where the interaction is dominated by the centrifugal terms, where long range electrostatic interactions still act at large values of the orbital angular momentum (situations where the approximations described in Section 3 are not valid).

The LD approximation is based upon the observation that in pure rotational excitation problems at large J, the largest elements of the standard CC S-matrix, $S^J(j_1 j_2 l, j_1' j_2' l')$, are those for which $l, l' \leq J$. Equivalently indexing the channels by j_{12} and $\lambda = l + j_{12} - J$ (hence $0 \leq \lambda \leq 2j_{12}$), the most important channels are those with $\lambda \leq \lambda_{12}$. Therefore in the LD approximation one only solves the CC equations retaining channels with $\lambda \leq \lambda_{12}$. The calculation is intermediate in size between CC and CS.

In the DLD approximation coupling between the channels $j_{12}\lambda$ and $j_{12}\lambda'$ is ignored, since for large J and small λ the potential matrix elements (II.2.19) are dominated by terms with $\Delta\lambda = 0$.

In collisions dominated by long range interactions (e.g. H^+ + CN, Depristo and Alexander (1976)) the DLD approximation works well, but is less satisfactory in systems where short range forces are dominant (e.g. He + HD, Green (1976)). Vibrational excitation occurs through hard short range collisions, and therefore, one would expect the LD and DLD approximations to fail in such studies.

CHAPTER III

NUMERICAL SOLUTION OF THE COUPLED EQUATIONS

1. Introduction

In this chapter we will be concerned with the method of solution of coupled second order differential equations of the form

$$\frac{d^2}{dR^2} G_n(R) = \sum_{n'=0}^{N} G_{n'}(R)\, W_{nn'}(R), \qquad \text{III.1.1}$$

which arise frequently in the theoretical study of atomic and molecular collisions. There exist many numerical methods of solution, the methods are independent of the scattering problems, however there are a number of factors that determine which method is best suited to a particular problem. All the methods will give an accurate solution to the problem given sufficient computer time. The best method is the one giving the required accuracy with the least computer time. There are many factors involved in determining the speeds of methods. Some methods are fast at low precision but become slow at high precision. Some methods require a large amount of computer time initially, but become extremely efficient when a large number of solutions are required at a range of energies. There are over twenty numerical methods in the literature, however they may be placed into four broad categories.

There are two types of numerical approaches, the more traditional of these consists of solving the coupled equations numerically, this is the approximate-solution (AS) approach. The second involves solving the coupled equations exactly, and approximating the potential matrix in some way, this is referred to as the approximate-potential (AP) approach.

For each of these two approaches there are two techniques for developing the solution. We may start the solution well into the classically forbidden region (where the potential energy is far greater than the total energy), and then we follow the solution, step by step, into the asymptotic region. This is known as solution following, and is probably the most common technique for the AS approach; it is exemplified by the method of Sams and Kouri (1969), and the de Vogelaere method developed by Lester (1968). Examples of its use in the AP approach are the methods of Gordon (1969), Light (1971), and Cheung and Wilson (1969).

The invariant imbedding technique consists of solving the scattering problem for a piece of the potential, and then a connection technique is employed to combine the R-matrices for the parts of the potential. Eventually the scattering matrix for the entire potential is found. It has been employed in the AS approach, it was first used in the amplitude density method (Johnson and Secrest (1966)). This method is now never used except in

exceptional circumstances; however, the connection formulae derived from it are still of great value. The log-derivative method of Johnson (1973), which is based on the invariant-imbedding technique of Calogero (1967), is the principal method in this category, and is still used.

There is only one member of the final category, the R-matrix propagator method of Light and Walker (1976). The method of Light and Walker (1976) was originally developed for reactive scattering, but has been modified to solve problems in elastic scattering by Stechel, Walker and Light (1978).

Finally, it is worth mentioning another method which can not be placed in any of the above categories. This is the L^2 R-matrix method and only recently has it been adapted to study molecular scattering problems (Bocchetta (1983)).

2. General Comparison of the Methods

Methods employing the AS approach tend to be simple, and extremely easy to programme, however since they follow the solution explicitly they generally require steps 10 to 20 times smaller than the wavelength. As the energy increases, the wavelength decreases and more steps must be taken over the integration range. Since AP approaches follow the potential rather than the solution, the step size is almost independent of the

collision energy. For the same reason AP methods can take larger steps than AS methods. In general, AS approaches are capable of higher accuracy at reasonable machine cost. Higher accuracy can be obtained in the AP approaches by taking smaller step sizes, however when this is done all the advantage over the AS approaches is lost, as the work required to improve accuracy grows much faster in the AP approaches than in AS approaches. The AP approach (despite allowing larger step sizes) also requires much more effort per step than the AS approach. The major advantage of AP approaches is that since they are essentially energy independent most of the information calculated at the first energy may be stored and used in subsequent energies. While this is a rather attractive feature, it may become unrealistic in large calculations involving many channels, and requiring small step sizes.

To describe the system properly it is often necessary to include closed channels in the calculation. Such channels result in instability problems in the solution-following techniques. The problem comes from the fact that computers use finite arithmetic. The closed channel solutions grow extremely fast, and it is possible that some of the weakly growing solutions may be many orders of magnitude smaller than the dominant solutions. Since we are carrying only a finite number of digits in the calculation, this leads to the loss of linear

independence. Consequently stabilizations must be performed as the solution is integrated out. Stabilization is usually achieved by multiplying the solution vectors, and their derivatives by a unitary transformation. In comparison the invariant-imbedding techniques are inherently stable and require no stabilization whatsoever.

The extreme stability of the invariant-imbedding technique is required in systems where the potential has a structure such that the solution-following techniques become unstable and no amount of stabilizing will correct. In these situations the R-matrix propagator method requires small steps, and the log-derivative method is preferable.

3. Suitability of the R-matrix Propagator Method for IOS Calculations

If we consider the collision between a vibrotor at an arbitrary orientation θ_2, treated within the IOS approximation, and a rotor treated within the CS approximation, the coupling matrix $\underset{\sim}{W}^{\Omega_1}_{nn'}(R)$ may be written, for a fixed value of Ω_1.

$$\underset{\sim}{W}^{\Omega_1}_{v_2 j_1, v_2' j_1'}(R) = V_{v_2 j_1 \Omega_1, v_2' j_1' \Omega_1}(R, \theta_2) + \delta_{v_2 j_1, v_2' j_1'} \left(\frac{L(L+1)}{R^2} - k^2_{v_2 j_1} \right) . \qquad \text{II.3.1}$$

In determining the suitability of the R-matrix propagator method to solve this problem we must consider two factors. First we notice that the coupled equations will be coupled in both v_2 and j_1. At each value of Ω_1 that

we consider we will have a coupling matrix of dimension (N x N) where N is the product ($v_2$max x $j_1$max). $v_2$max is the highest vibrational state considered, and $j_1$max is the maximum value of j_1 permissible at a given value of Ω_1 . Secondly notice that the angular momentum parameter, L, will have the same value in each channel, and only enters into the diagonal elements of the coupling matrix.

If we are only interested in atom-vibrotor collisions, we may set $j_1 = j_1' = 0$, and the equations are only coupled in v_2. Generally speaking the vibrational energy levels of molecules are relatively widely spaced, and since we are only interested in reasonably low collision energies we need retain only a few vibrational states. For such a small number of channels the numerical effort of an AP method will not be largely in excess of that required by an AS method. In addition an AP method has the advantage of requiring larger step sizes than an AS method. However, if we now reintroduce the rotational levels of the rotor (j_1) the choice of method appears less clear cut, the addition of only two rotational channels increases the dimensions of the coupling matrix by a factor of two. We must therefore consider other factors before a reasonable choice can be properly made.

Since the angular momentum parameter, L, comes into the coupled equations in a similar manner to the

total collision energy, E, the properties of AP methods which allow the generation of results at many energies, can also be used to generate results at many L values. To obtain the total cross section it is necessary to solve the coupled equations at many values of L. We may use information calculated at the initial value of L to evaluate results at subsequent values of L. However, there is one essential difference between the ways L and E come into the calculation. E is independent of the integration coordinate, R, but $L(L+1)/R^2$ is not. For the rotor-vibrotor systems studied (H_2 + CO, HD + CO) it turns out that the step size is not very strongly dependent upon L, therefore the generation of solutions for large numbers of L values with little numerical effort is possible. In the case of HD + CO, in addition to the three vibrational channels to describe the CO molecule, it was necessary to retain six rotational channels to describe the HD molecule correctly. Consequently the coupling matrix for $\Omega = 0$ was of dimension (18 x 18), at subsequent partial waves we found that the computer time required was $\sim$ 50% of that required at the initial value of L. However, we realised that for such large matrices, matrix multiplication was extremely costly, and when the appropriate routines were optimised for the Cray-1 computer system a far greater saving was obtained. The HD + CO calculations are discussed in Chapter VII.

In some systems the R dependence of the L term is more important in the choice of step size. In such cases, the approximate potential used can be modified to deal with this dependence analytically. The step size can be made virtually independent of L, and the generation of large numbers of L values is possible. This procedure is discussed in Section 4.4.

These methods of evaluating results at large numbers of partial waves could also be employed in effective potential calculations. This decoupling approximation also makes use of an effective angular momentum parameter.

Since we are dealing with the IOS, and CS approximations (which are just that-approximations) the accuracy of the results is required to no more than three to four significant figures. The AP methods are capable of achieving this level of accuracy without employing excessively small step sizes.

In view of the mathematical form of the IOS equations and the level of accuracy required we consider that an AP method rather than an AS approach is more suited to our calculations. In addition we prefer to employ an invariant imbedding technique rather than a solution following technique, due to their inherent stability. There is only one algorithm in this category, the R-matrix propagator technique of Stechel, Walker, and Light (1978), and therefore this algorithm was employed in our calculations.

4. The R-matrix Propagation Method

4.1 General Theory

The R-matrix propagator method was originally developed for reactive scattering calculations by Light and Walker (1976), and was later extended to treat inelastic scattering problems by Stechel, Walker and Light (1978) (hereafter referred to as SWL). This method is based upon the propagation of the R-matrix. This is the matrix relating functions to their derivatives at a given value of the integration coordinate. Since it is an invariant-imbedding technique it is not sensitive to the numerical problems associated with the propagation of closed channel solutions, and in addition SWL report that it is fast and accurate.

It is fairly easy to understand, and relatively simple to programme. It involves various matrix operations (e.g., multiplication, diagonalization, inversion, etc.) which can be achieved by means of standard routines. Essentially one starts by solving the problem for a part of the potential, taking the potential to be zero beyond certain limits. Then one solves the problem for an adjacent part of the potential. One then combines the two solutions to obtain the solution for the potential consisting of both parts. Proceeding in this way, concatenating parts of the potential, eventually the entire problem is solved.

We may write the general form of the coupled equations III.1.1 in matrix form,

$$\frac{d^2}{dR^2}\underset{\sim}{G}(R) = \underset{\sim}{W}(R)\,\underset{\sim}{G}(R) \,. \qquad \text{III.4.1}$$

The basis of the R-matrix propagation method is the Magnus exponential method. In this method the equations given in III.4.1 are written as twice as many coupled first order equations,

$$\frac{d}{dR}\begin{bmatrix} \underset{\sim}{G}(R) \\ \underset{\sim}{G}'(R) \end{bmatrix} = \underset{\sim}{A}\begin{bmatrix} \underset{\sim}{G}(R) \\ \underset{\sim}{G}'(R) \end{bmatrix} , \qquad \text{III.4.2}$$

where $\underset{\sim}{A}$ is a (2N x 2N) matrix defined by

$$\begin{bmatrix} \underset{\sim}{0} & \underset{\sim}{I} \\ \underset{\sim}{\omega} & \underset{\sim}{0} \end{bmatrix} ,$$

where $\underset{\sim}{0}$ and $\underset{\sim}{I}$ are the zero and unit matrix respectively. A propagator $\underset{\sim}{U}$ is defined to relate solutions across an interval ΔR,

$$\begin{bmatrix} \underset{\sim}{G}(R+\Delta R) \\ \underset{\sim}{G}'(R+\Delta R) \end{bmatrix} = \begin{bmatrix} U_1 & U_2 \\ U_3 & U_4 \end{bmatrix}\begin{bmatrix} G(R) \\ G'(R) \end{bmatrix} = \underset{\sim}{U}\begin{bmatrix} \underset{\sim}{G}(R) \\ \underset{\sim}{G}'(R) \end{bmatrix} , \qquad \text{III.4.3}$$

where the (2N x 2N) matrix $\underset{\sim}{U}$ is related to the first order coupling matrix $\underset{\sim}{A}$ by the Magnus exponentiation

$$\underset{\sim}{U} = \exp\left\{ (\Delta R)\underset{\sim}{A} - \frac{(\Delta R)^3}{12}\begin{bmatrix} \underset{\sim}{\omega}' & 0 \\ 0 & -\underset{\sim}{\omega}' \end{bmatrix} + \cdots \right\} , \qquad \text{III.4.4}$$

where $\underset{\sim}{\omega}'$ is the derivative of $\underset{\sim}{\omega}$. The method of SWL is to diagonalize $\underset{\sim}{\omega}$ and to retain only the first term of the exponential series, this corresponds to taking a constant reference potential across each sector. However SWL do not recommend the exponential method

(In this method of solution the step propagators are multiplied together to form the propagator over the entire integration range). If there are locally closed channels in the calculation, the exponential growth of the solutions associated with them may lead to a loss of linear independence in the full set of solutions. In fact any propagator may be used, and instead of equation III.4.3, SWL employ

$$\begin{pmatrix} \underset{\sim}{G}_A \\ \underset{\sim}{G}_B \\ \underset{\sim}{G}_C \\ \vdots \end{pmatrix} = \begin{pmatrix} \underset{\sim}{R}_{AA} & \underset{\sim}{R}_{AB} & \underset{\sim}{R}_{AC} & \cdots \\ \underset{\sim}{R}_{BA} & \underset{\sim}{R}_{BB} & \underset{\sim}{R}_{BC} & \cdots \\ \underset{\sim}{R}_{CA} & \underset{\sim}{R}_{CB} & \underset{\sim}{R}_{CC} & \cdots \\ \vdots & \vdots & \vdots & \end{pmatrix} \begin{pmatrix} \underset{\sim}{G}'_A \\ \underset{\sim}{G}'_B \\ \underset{\sim}{G}'_C \\ \vdots \end{pmatrix} \qquad \text{III.4.5}$$

to propagate the scattering information. The R-matrix relates the translational functions to their derivatives at the boundaries of the region over which the Schrödinger equation has been solved. A,B,C... denote a set of surfaces in configuration space on which information relating wavefunctions and their (outwardly normal) derivatives is required. For example for the three dimensional reactive scattering of an atom and diatomic molecule, there are three asymptotic rearrangement channels and therefore the R-matrix is blocked 3 x 3, however in elastic scattering sufficient information is available on a single surface. We are now in a position to describe

how the R-matrix solution to the coupled equations may be constructed.

The approach is to divide the integration range into smaller regions in which the local R-matrix may be determined. This is shown schematically in Figure 1. The global R-matrix, which is of dimension (N x N) is constructed by assembling the local R-matrices determined in each sector. The global R-matrix is an (N x N) matrix because it only retains information about a single surface, but the sector R-matrices are (2N x 2N) matrices since they carry information from one surface to another. In accordance with neglecting the higher order terms in III.4.4 we assume that the coupling matrix $\underset{\sim}{W}$ is constant over the width of a sector (i.e. $\underset{\sim}{W}' = 0$). The coupling matrix is diagonalised at the centre of each sector,

$$\underset{\sim}{\bar{T}}^{(i)} \underset{\sim}{W}(R_i) \underset{\sim}{T}^{(i)} = \lambda^2(i) ,$$

III.4.6

where $\underset{\sim}{\bar{T}}^{(i)}$ is the transpose and inverse of $\underset{\sim}{T}^{(i)}$ since $\underset{\sim}{W}$ is assumed to be symmetric (i.e. $\underset{\sim}{T}^{(i)}$ is orthogonal).

We thus transform from the original basis ϕ to a new basis ψ which are linear combinations of the original,

$$\psi_n^{(i)} = \sum_{n'} T_{n'n}^{(i)} \phi_{n'} .$$

III.4.7.

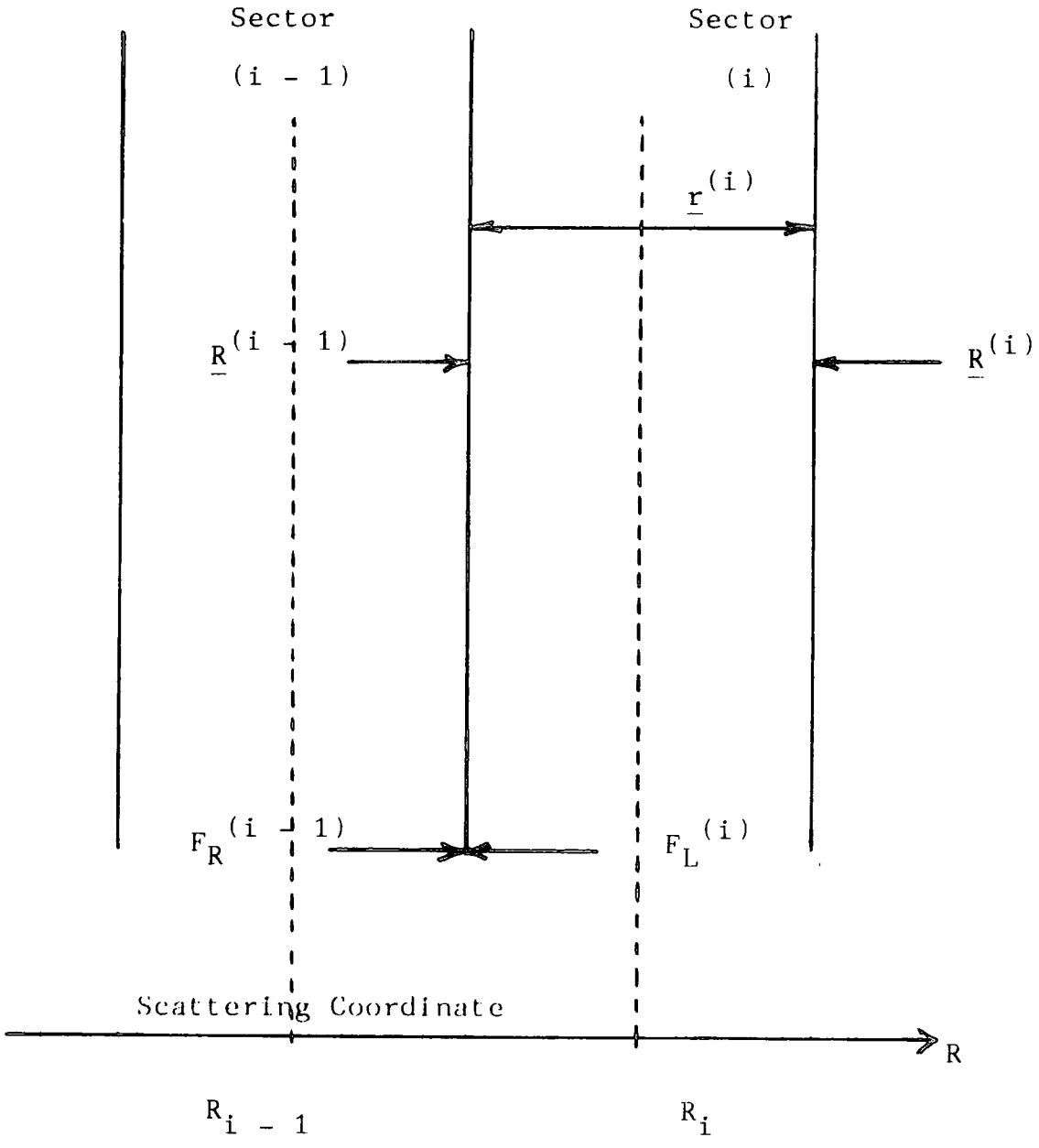

Figure 1 The sectorization of configuration space, and the assembly of sector R-matrices to form the global R-matrix

This transformation results in the elimination of all the coupling in the differential equations for the new translational functions $F_n^{(i)}(R)$,

$$\frac{d^2}{dR^2} F_n^{(i)}(R) = (\lambda_n^{(i)}(R))^2 F_n^{(i)}(R) ,$$

III.4.8

where $$F_n^{(i)}(R) = \sum_{n'} T_{n'n}^{(i)} G_{n'}(R) .$$

Within a given sector (i) the values of the translational functions at the right and left hand boundaries of the sector are given by (assembling the functions $R_n^{(i)}(R)$ in a column vector)

$$\underset{\sim}{F}_L(i) = \underset{\sim}{F}^{(i)}(R_i - \tfrac{1}{2} h_i)$$
$$\underset{\sim}{F}_R(i) = \underset{\sim}{F}^{(i)}(R_i + \tfrac{1}{2} h_i) .$$

III.4.9

Since the coupling has been removed from III.4.1 the sector R-matrix $r^{(i)}$ in the sector (i) may be written (in the locally diagonal representation)

$$\begin{bmatrix} \underset{\sim}{F}_L(i) \\ \underset{\sim}{F}_R(i) \end{bmatrix} = \begin{bmatrix} \underset{\sim}{\Gamma}_1^{(i)} & \underset{\sim}{\Gamma}_2^{(i)} \\ \underset{\sim}{\Gamma}_3^{(i)} & \underset{\sim}{\Gamma}_4^{(i)} \end{bmatrix} \begin{bmatrix} -\underset{\sim}{F}_L'(i) \\ \underset{\sim}{F}_R'(i) \end{bmatrix} .$$

III.4.10

The similarity with the Magus exponential method III.4.3 is now clear. The values of the elements $\underset{\sim}{\Gamma}_1^{(i)}$, $\underset{\sim}{\Gamma}_2^{(i)}$ ... depend upon the value of $\lambda_n^{(i)}(R)$. This is discussed in Section 4.4 .

One must ensure the continuity of the total wave-function and its normal derivative at each sector boundary, we therefore transform from the $\underset{\sim}{F}(i-1)$ representation to the $\underset{\sim}{G}$ representation and back to the $\underset{\sim}{F}(i)$ representation,

$$\underset{\sim}{F}_R(i-1) = \underset{\sim}{\bar{T}}^{(i-1)}\underset{\sim}{G} = \underset{\sim}{\bar{T}}^{(i-1)}\underset{\sim}{T}^{(i)}\underset{\sim}{F}_L(i), \qquad \text{III.4.11}$$

$$\underset{\sim}{F}'_R(i-1) = \underset{\sim}{Q}(i-1,i)\underset{\sim}{F}'_L(i), \qquad \text{III.4.12}$$

where $\underset{\sim}{Q}(i-1,i) = \underset{\sim}{\bar{T}}^{(i-1)}\underset{\sim}{T}^{(i)}$.

Note that since the transformation matrices $\underset{\sim}{\bar{T}}^{(i-1)}$ and $\underset{\sim}{T}^{(i)}$ are orthogonal, the matrix $\underset{\sim}{Q}$ is also orthogonal.

The method functions by assembling the sector R-matrices given by III.4.10 recursively beginning near the origin, and progressing towards the asymptotic region. At each step a new global R-matrix is evaluated by assembling a new sector R-matrix with the old global R-matrix. The global R-matrix is always defined so that it relates the radial functions to its derivatives at the outer boundary of the last sector, i.e.,

$$\underset{\sim}{F}_R(i) = \underset{\sim}{\mathcal{R}}^{(i)}\underset{\sim}{F}'_R(i). \qquad \text{III.4.13}$$

The R-matrix $\underset{\sim}{\mathcal{R}}^{(i)}$ is the inverse of the log-derivative matrix defined by Johnson (1973).

To find the new global R-matrix we employ the relation

$$\underset{\sim}{R}^{(i)} = \underset{\sim}{\Gamma}_4^{(i)} - \underset{\sim}{\Gamma}_3^{(i)} \underset{\sim}{Z}^{(i)} \underset{\sim}{\Gamma}_2^{(i)},$$

II.4.14a

where $$\underset{\sim}{Z}^{(i)} = (\underset{\sim}{\Gamma}_1^{(i)} + \underset{\sim}{\bar{Q}}(i-1,i)\, \underset{\sim}{R}^{(i-1)}\, \underset{\sim}{Q}(i-1,i))^{-1}.$$

III.4.14b

Note that the recursion relations III.4.14a, b produce a symmetric R-matrix (provided $\underset{\sim}{R}^{(i-1)}$ and $\underset{\sim}{\Gamma}^{(i)}$ are symmetric).

4.2 Boundary Conditions

The R-matrix recursion is initialized near the origin (in the classically forbidden region), with the initial $\underset{\sim}{R}^{(1)}$ matrix defined by

$$(\underset{\sim}{R}^{(1)})_{jk} = \delta_{jk} / \lambda_j /^{-1}. \qquad \text{III.4.15}$$

The relation III.4.15 assumes the potential is large and repulsive near the origin (which is usually the case), for other types of potentials, $\underset{\sim}{R}^{(1)}$ must be chosen to reflect the behaviour of the regular solution near the origin. When one reaches the asymptotic region, one transforms back to the original basis set ϕ, using the transformation

$$\underset{\sim}{G}_R(M) = \underset{\sim}{I}^{(M)} \underset{\sim}{E}_R(M) \qquad \text{III.4.16a}$$

$$\underset{\sim}{G}'_R(M) = \underset{\sim}{I}^{(M)} \underset{\sim}{E}'_R(M), \qquad \text{III.4.16b}$$

where M is the number of sectors. Combining III.4.16a,b with the equation for the last R-matrix determined by the recursion to the right hand side of the last sector M as in III.4.13 gives the equation for the final global R-matrix,

$$\underset{\sim}{\mathcal{R}}^{Final} = \underset{\sim}{T}^{(M)} \underset{\sim}{\mathcal{R}}^{(M)} \underset{\sim}{\bar{T}}^{(M)} \qquad \text{III.4.17a}$$

$$\underset{\sim}{G}_R(M) = \underset{\sim}{\mathcal{R}}^{Final} \underset{\sim}{G}'_R(M). \qquad \text{III.4.17b}$$

The asymptotic translational functions will have the form

$$\underset{\sim}{G} = \underset{\sim}{A} - \underset{\sim}{B}\underset{\sim}{S}^0 \qquad \text{III.4.18a}$$

$$\underset{\sim}{G}' = \underset{\sim}{A}' - \underset{\sim}{B}'\underset{\sim}{S}^0, \qquad \text{III.4.18b}$$

where A and B are diagonal matrices of incoming and outgoing asymptotic functions respectively, and $\underset{\sim}{S}^0$ is essentially the scattering matrix. Using equations III.4.18a, b we obtain

$$\underset{\sim}{A} - \underset{\sim}{B}\underset{\sim}{S}^0 = \underset{\sim}{\mathcal{R}}^{Final}(\underset{\sim}{A}' - \underset{\sim}{B}'\underset{\sim}{S}^0) \qquad \text{III.4.19}$$

from which we can obtain the "S-matrix"

$$\underset{\sim}{S}^0 = (\underset{\sim}{\mathcal{R}}^{Final}\underset{\sim}{B}' - \underset{\sim}{B})^{-1}(\underset{\sim}{\mathcal{R}}^{Final}\underset{\sim}{A}' - \underset{\sim}{A}). \qquad \text{III.4.20}$$

One will recall that in Chapter II, the boundary conditions were written explicitly in terms of Spherical Bessel functions, and Spherical Hankel functions. To determine the S-matrix in the IOS approximation we have (cf. II.3.23)

$$\underset{\sim}{G} \xrightarrow[R\to\infty]{} \left(-ik_{v_2'j_1'} R h_L^{(2)}(k_{v_2'j_1'}R)\right)\delta_{v_2j_1,v_2'j_1'} - \left(\frac{k_{v_2j_1}}{k_{v_2'j_1'}}\right)^{\frac{1}{2}} S_L(v_2j_1\Omega_1, v_2'j_1'\Omega_1/\Theta_2)\left(ik_{v_2'j_1'} R h_L^{(1)}(k_{v_2'j_1'}R)\right).$$

$$k^2_{v_2'j_1'} > 0 \qquad \text{III.4.21}$$

Comparing III.4.21 and III.4.18a we find

$$\underset{\sim}{A} = -ik r_{v_2' j_1'} R h_L^{(2)}(k r_{v_2' j_1'} R),$$

$$\underset{\sim}{B} = ik r_{v_2' j_1'} R h_L^{(1)}(k r_{v_2' j_1'} R),$$

and $$S^0_{v_2 j_1, v_2' j_1'} = \left(\frac{k r_{v_2 j_1}}{k r_{v_2' j_1'}}\right)^{\frac{1}{2}} S_L(v_2 j_1 \Omega_1, v_2' j_1' \Omega_1 / \Theta_2).$$

Alternatively we could work in terms of the reactance matrix (K-matrix). This is computationally easier as all the functions are real (cf. II.2.27b). We find

$$\underset{\sim}{A} = k r_{v_2' j_1'} R j_L(k r_{v_2' j_1'} R), \qquad k^2_{v_2' j_1'} > 0$$

$$\underset{\sim}{B} = k r_{v_2' j_1'} R n_L(k r_{v_2' j_1'} R),$$

and $$S^0_{v_2 j_1, v_2' j_1'} = \left(\frac{k r_{v_2 j_1}}{k r_{v_2' j_1'}}\right)^{\frac{1}{2}} K_L(v_2 j_1 \Omega_1, v_2' j_1' \Omega_1 / \Theta_2).$$

If the channel is closed (i.e. $k^2_{v_2' j_1'} \leq 0$) the asymptotic boundary condition may be expressed as a linear combination of exponentially growing solutions, e^{kR}, where $k = |k r_{v_2' j_1'}|$, and exponentially decaying solutions e^{-kR}. However physically the exponentially growing solution is not acceptable since all the flux enters via open channels, and therefore we are justified in expressing the boundary conditions just in terms of e^{-kR}, i.e.,

$$\underset{\sim}{Q} \xrightarrow[R\to\infty]{} A_{v_2 j_1, v_2' j_1'} e^{-|k r_{v_2' j_1'}| R}.$$

$$k^2_{v_2' j_1'} \leq 0 \qquad \text{III.4.22}$$

In practice we fit the boundary condition in terms of modified Bessel functions of the third kind (Abramowitz and Stegun (1965)) which are exponentially decaying functions, and so III.4.22 may be rewritten

$$\underset{\sim}{Q} \xrightarrow[R\to\infty]{} A_{v_2 j_1, v_2' j_1'} z \sqrt{\frac{\pi}{2z}}\, K_{L+\frac{1}{2}}(z), \qquad \text{III.4.23}$$

where $z = |k v_2' j_1'| R$.

4.3 Long Range Interaction Potentials - Asymptotic Series Expansions

For very long range potentials such as those going as $1/R^3$, it is necessary to integrate quite far before the potential has decayed sufficiently so that the wave function can be fitted to the Spherical Bessel functions or Spherical Hankel functions. If all the long range terms of the potential are of the form $1/R^n$, where n is an integer (as is usually the case), it is possible to find a complete set of asymptotic solutions for the long range potential and match these to the solution to determine the scattering information. In this section we first take a closer look at the conventional method of fitting the asymptotic boundary condition and subsequently extend our discussion to the use of asymptotic series expansions in dealing with long range potentials. For simplicity we will only consider atom-vibrotor scattering (i.e. $j_1 = 0$).

In the IOS approximation the coupled differential equations take the form (cf. II.3.21)

$$\left(-\frac{d^2}{dR^2} + \frac{L(L+1)}{R^2} - k^2_{v_2'}\right) G^{Lv_2}_{v_2'}(R,\theta_2)$$

$$+ \sum_{v_2''} V_{v_2',v_2''}(R,\theta_2)\, G^{Lv_2}_{v_2''}(R,\theta_2) = 0 . \qquad \text{III.4.24}$$

If R is sufficiently large so that all the short range (exponential) terms of the interaction potential have become negligible, we may write

$$V_{v_2',v_2''}(R,\theta_2) \sim \frac{2\mu}{\hbar^2}\,\delta_{v_2'v_2''}\,\frac{v_n}{R^n} \quad (n \geq 2), \qquad \text{III.4.25}$$

and III.4.24 has the asymptotic form

$$\left(-\frac{d^2}{dR^2} + \frac{\lambda(\lambda+1)}{R^2} - k^2_{v_2'}\right) G^{Lv_2}_{v_2'}(R,\theta_2)$$

$$+ O\left(\frac{1}{R^3}\right) = 0, \qquad \text{III.4.26}$$

where $\lambda(\lambda+1) = L(L+1) + \frac{2\mu}{\hbar^2} v_2$.

If we integrate the coupled equations sufficiently far into the asymptotic region so that the term $\lambda(\lambda+1)/R^2$ is negligible, the boundary condition may be written

$$G^{Lv_2}_{v_2'}(R,\theta_2) \underset{R\to\infty}{\sim} \delta_{v_2 v_2'} \sin\left(k_{v_2'}R - \tfrac{1}{2}\lambda\pi\right)$$

$$+ K_L \cos\left(k_{v_2'}R - \tfrac{1}{2}\lambda\pi\right).$$

where $K_L = K_L(v_2 j_1 \Omega_1, v_2' j_1' \Omega_1 / \theta_2)$

III.4.27

In practice, however, the convergence of the solutions obtained by III.4.27 is extremely slow, and it is more efficient to employ Bessel functions of the first and second kind (denoted by J_λ and Y_λ respectively), Abramowitz and Stegun (1965),

$$G_{v_2'}^{Lv_2}(R,\theta_2) \underset{R\to\infty}{\sim} \left(\frac{1}{2}\pi R\right)^{\frac{1}{2}} \left(J_{\lambda+\frac{1}{2}}(k_{v_2'}R)\,\delta_{v_2v_2'} + \left(\frac{k_{v_2}}{k_{v_2'}}\right)^{\frac{1}{2}} K_L\, Y_{\lambda+\frac{1}{2}}(k_{v_2'}R)\right).$$

III.4.28

If we take $v_2 = 0$, and $\lambda = L$, then we obtain a boundary condition that may be used when the interaction potential is negligible, and not the centrifugal term (cf. II.2.27b),

$$G_{v_2'}^{Lv_2}(R,\theta_2) \underset{R\to\infty}{\sim} \delta_{v_2v_2'} R k_{v_2'} j_L(k_{v_2'}R) - \left(\frac{k_{v_2}}{k_{v_2'}}\right)^{\frac{1}{2}} K_L R k_{v_2'} n_L(k_{v_2'}R).$$

III.4.29

If, however, the long range potential III.4.25 contains terms with $n \geq 3$, it is necessary, as mentioned previously, to integrate the coupled equations out to extremely large R values before the boundary condition can be fitted using III.4.29. This problem may be overcome by the use of asymptotic series expansions. When all the long range terms are of the form R^{-n}, it is possible to integrate sufficiently out into the

asymptotic region to where all the short range terms in the potential have become negligible. One then finds a complete set of asymptotic solutions for the long range potential and matches these to the solution to obtain the K-matrix. In this case the asymptotic form III.4.25 may be written

$$\left(-\frac{d^2}{dR^2} + \frac{L(L+1)}{R^2} - k^2_{v_2'} + \frac{2\mu}{\hbar^2}\frac{v_n}{R^n}\right) G^{Lk_2}_{v_2'}(R,\theta_2) = 0 . \qquad n \geq 3 \qquad \text{III.4.30}$$

The asymptotic solution for the long range potential in scattering calculations was first employed in electron scattering by Burke and Schey (1962), and was later adapted to molecular collisions by Brandt and Truhlar (1973).

Secrest (1979) has suggested asymptotic series expansions of the form

$$\left.\begin{matrix} f(R) \\ g(R) \end{matrix}\right\} = a(R) \left\{\begin{matrix} \sin x \\ \cos x \end{matrix}\right. + b(R) \left\{\begin{matrix} \cos x \\ \sin(-x) \end{matrix}\right. , \qquad \text{III.4.31}$$

where $x = kR - \lambda\pi/2$.

(the subscript v_2' has been dropped)

Asymptotic series expansions of this type are based on the assumption that convergence will be improved by fitting not to sin x and cos x, as in III.4.27, but to these functions modified by their derivatives.

While such expansions have proved to be of great value in heavy particle scattering calculations (e.g. Pfeffer and Secrest (1983), and Gerratt and Roberts (1983) - both will be discussed in Chapter IV) the trigonometric functions do not include the effects of the centrifugal term, and we consider that asymptotic series expansions incorporating Spherical Bessel functions would be more satisfactory. Such expansions are suggested by Gailitis (1976),

$$\left.\begin{matrix} F(R) \\ G(R) \end{matrix}\right\} = A(R) \left\{\begin{matrix} \bar{j}_L(kR) \\ \bar{n}_L(kR) \end{matrix}\right. + B(R) \left\{\begin{matrix} \bar{j}_L'(kR) \\ \bar{n}_L'(kR) \end{matrix}\right. , \qquad \text{III.4.32}$$

where $\bar{j}_L(kR) = kR\, j_L(kR)$ and $\bar{n}_L(kR) = kR\, n_L(kR)$.

To obtain the series expansions for A(R) and B(R) we first obtain the differential equations for A(R) and B(R) by substituting III.4.32 into III.4.30.

$$A''(R) - 2B(R)\frac{L(L+1)}{R^3} - 2B'(R)\left(k^2 - \frac{L(L+1)}{R^2}\right) = \frac{2\mu}{\hbar^2}\frac{v_n}{R^n}A(R) \qquad \text{III.4.33a}$$

$$B''(R) + 2A'(R) = \frac{2\mu}{\hbar^2}\frac{v_n}{R^n}B(R) \qquad \text{III.4.33b}$$

As $R \to \infty$ we require that $A(R) \to 1$ and $B(R) \to 0$, and therefore write the series expansions for A(R) and B(R)

$$A(R) = 1 + \sum_{m=0}^{\infty} \alpha_m R^{-m-p} \quad p \geq 1 \qquad \text{III.4.34a}$$

$$B(R) = \sum_{m=0}^{\infty} \beta_m R^{-m-q} \quad q \geq 1, \qquad \text{III.4.34b}$$

where p, and q are constants.

Identifying coefficient of the same power of R in III.4.33a,b, we obtain:-

$$p = n, \quad q = n - 1$$

$$\alpha_0 = \frac{\mu v_n}{2k^2\hbar^2}, \quad \beta_0 = \frac{\mu v_n}{(n-1)k^2\hbar^2}, \quad \beta_1 = 0,$$

$$\beta_2 = \frac{-n\mu v_n}{4k^4\hbar^2} + \frac{nL(L+1)\mu v_n}{(n^2-1)k^4\hbar^2},$$

and the recursion relations for the higher order coefficients in III.4.34a,b

$$\alpha_{M-2}(M+n-2)(M+n-1) - 2L(L+1)\beta_{M-2} \times (M+n-2) + 2k^2\beta_M(M+n-1) = 2\mu v_n \alpha_{M-n} \qquad \text{III.4.35a}$$

$$\beta_{M-1}(M+n-2)(M+n-1) - 2\alpha_{M-1}(M+n-1) = 2\mu v_n \beta_{M-n+1}. \qquad \text{III.4.35b}$$

If additional terms are retained in the long range potential,

$$V_{v_2 v_2'}(R,\theta_2) \underset{R\to\infty}{\sim} \frac{2\mu}{\hbar^2}\delta_{v_2 v_2'}\left(\frac{v_n}{R^n} + \frac{v_{n+1}}{R^{n+1}} + \cdots\right), \quad n \geq 3 \qquad \text{II.4.36}$$

in general $\beta_i \neq 0$ and the recursion relations are appropriately modified. The derivation of III.4.33a,b, and their solution is shown in Appendix 1 at the back of this thesis.

It is clear that the use of asymptotic series expansions in systems with long range potentials varying as R^{-n} (where $n \geq 3$) has one very important advantage. Since one need only integrate the coupled equations to where the short range terms of the interaction potential have become negligible we have a means of reducing the computer time required to solve the fixed angle coupled equations.

In Chapter IV we shall illustrate the advantage of the functions III.4.32 over the more conventional Spherical Bessel functions with reference to $H_2 + H^+$ collisions. The $H_2 + H^+$ potential surface contains long range isotropic and anisotropic terms due to the charge on the proton.

4.4 Derivation of the Sector R-matrix

In this section we present the derivation of the sector R-matrix. Within a sector the equations are completely uncoupled, the equations in question are written

$$\frac{d^2}{dR^2} F_n^{(i)}(R) = (\lambda_n^{(i)}(R))^2 F_n^{(i)}(R) . \qquad \text{III.4.37}$$

We begin by assuming that the eigenvalues $\lambda_n(R)$ of the coupling matrix are constant across a given sector, and later generalize to more complex situations. The eigenvalues can have any known form, however, the transformation matrix $\underset{\sim}{T}$ must remain constant across the sector to maintain the decoupling of the equations.

The elements of $\underset{\sim}{r}_1$, $\underset{\sim}{r}_2$, $\underset{\sim}{r}_3$ and $\underset{\sim}{r}_4$ form a 2 x 2 block matrix,

$$\begin{bmatrix} F_n(a) \\ F_n(b) \end{bmatrix} = \begin{bmatrix} (r_1)_{nn} & (r_2)_{nn} \\ (r_3)_{nn} & (r_4)_{nn} \end{bmatrix} \begin{bmatrix} -F_n'(a) \\ F_n'(b) \end{bmatrix}, \qquad \text{III.4.38}$$

where a and b are the sector boundaries ($a = R_i - \frac{1}{2}h$, $b = R_i + \frac{1}{2}h$). The elements of the sector R-matrix ($\underset{\sim}{r}_1$, $\underset{\sim}{r}_2$, $\underset{\sim}{r}_3$, and $\underset{\sim}{r}_4$) must be diagonal to prevent mixing of the solutions. Equation III.4.38 is a simple second order differential equation, and has two linearly independent solutions $A^{(i)}(R)$ and $B^{(i)}(R)$, and thus the general solution may be written

$$F_n^{(i)}(R) = \alpha A_n^{(i)}(R) + \beta B_n^{(i)}(R) \qquad \text{III.4.39a}$$

$$\frac{d}{dR} F_n^{(i)}(R) = \alpha \frac{d}{dR} A_n^{(i)}(R) + \beta \frac{d}{dR} B_n^{(i)}(R), \qquad \text{III.4.39b}$$

where α and β are arbitrary constants. The Wronskian of two linearly independent solutions $A_n^{(i)}(R)$ and $B_n^{(i)}(R)$ is denoted by $\underset{\sim}{W}$ and is a constant.

$$W = A_n^{(i)}(R)B_n^{(i)\prime}(R) - B_n^{(i)}(R)A_n^{(i)\prime}(R) \qquad \text{III.4.40}$$

The R-matrix relation III.4.38 holds for any solution of III.4.37, and therefore is independent of α and β. We choose two solutions satisfying the following simple boundary conditions

$$F_1(a)=1 \qquad F_1'(a)=0 \qquad \text{III.4.41a}$$

$$F_2(b)=1 \qquad F_2'(b)=0\,, \qquad \text{III.4.41b}$$

where 1, and 2 refer to two separate boundary conditions of the F's, and the subscript n has been dropped. The R-matrix is now easily obtained in terms of F_1 and F_2 from

$$r_1 = -F_2(a)/F_2'(a) \qquad r_2 = 1/F_1(b) \qquad \text{III.4.42a}$$

$$r_3 = -1/F_2(a) \qquad r_4 = F_1(b)/F_1'(b). \qquad \text{III.4.42b}$$

The solutions satisfying the boundary conditions III.4.39a,b are

$$F_1(R) = W^{-1}[B'(a)A(R) - A'(a)B(R)] \qquad \text{III.4.43a}$$

$$F_2(R) = W^{-1}[B'(b)A(R) - A'(b)B(R)], \qquad \text{III.4.43b}$$

this can be easily verified. Substituting III.4.43a,b into III.4.38 we obtain the general form for the sector R-matrices

$$r_1 = \frac{B'(b)A(a) - A'(b)B(a)}{A'(b)B'(a) - B'(b)A'(a)} \qquad \text{III.4.44a}$$

$$r_2 = W/[B'(a)A'(b) - A'(a)B'(b)] \qquad \text{III.4.44b}$$

$$r_3 = W/[A'(b)B'(a) - B'(b)A'(a)] \qquad \text{III.4.44c}$$

$$r_4 = \frac{B'(a)A(b) - A'(a)B(b)}{B'(a)A'(b) - A'(a)B'(b)} \quad . \qquad \text{III.4.44d}$$

Notice that $r_2 = r_3$ and therefore the sector R-matrix is symmetric, and this will lead to a unitary S-matrix. For the constant potential we have

$$A(R) = e^{-|\lambda_n|R}, \; B(R) = e^{|\lambda_n|R} \quad \lambda_n^2 > 0 \qquad \text{III.4.45a}$$

$$A(R) = \cos(|\lambda_n|R), \; B(R) = \sin(|\lambda_n|R) \quad \lambda_n^2 \leq 0. \qquad \text{III.4.45b}$$

Using III.4.42a,b with $b = a + h_i$, we then obtain

$$(r_1)_{nn'} = (r_4)_{nn'} = \delta_{nn'} \begin{cases} |\lambda_n|^{-1} \coth |h_i \lambda_n| & \lambda_n^2 > 0 \\ -|\lambda_n|^{-1} \cot |h_i \lambda_n| & \lambda_n^2 \leq 0 \end{cases} \qquad \text{III.4.46a}$$

$$(r_2)_{nn'} = (r_3)_{nn'} = \delta_{nn'} \begin{cases} |\lambda_n|^{-1} \operatorname{csech} |h_i \lambda_n| & \lambda_n^2 > 0 \\ -|\lambda_n|^{-1} \operatorname{csec} |h_i \lambda_n| & \lambda_n^2 \leq 0 \; . \end{cases} \qquad \text{III.4.46b}$$

It was stated earlier that the eigenvalues $\lambda_n(R)$ can have any known form, it is possible to adopt any

form which gives known solutions, A(R) and B(R), to III.4.39a,b. In situations where the potential and hence $\lambda_n(R)$ are rapidly varying with respect to R, employing a sector R-matrix appropriate to the varying $\lambda_n(R)$ would allow larger step sizes. We could take advantage of such a situation in the IOS approximation in which the coupling matrix takes the form

$$W^{\Omega_1}_{v_2 j_1, v_2' j_1'}(R) = V_{v_2 j_1 \Omega_1, v_2' j_1' \Omega_1}(R, \theta_2) + \delta_{v_2 j_1, v_2' j_1'}\left(\frac{L(L+1)}{R^2} - k^2_{v_2 j_1}\right). \qquad \text{III.4.47}$$

Dropping the superscript Ω_1, and employing matrix notation we may write

$$\underset{\sim}{W}(R) = \underset{\sim}{W}^A(R) + \underset{\sim}{I}\left(\frac{L(L+1)}{R^2}\right), \qquad \text{III.4.48}$$

where

$$W^A_{v_2 j_1, v_2' j_1'} = V_{v_2 j_1 \Omega_1, v_2' j_1' \Omega_1}(R, \theta_2) - \delta_{v_2 j_1, v_2' j_1'} k^2_{v_2 j_1}.$$

The transformation $\underset{\sim}{T}$ which diagonalizes $\underset{\sim}{W}(R)$ will also diagonalize $\underset{\sim}{W}^A(R)$, since it is independent of L

$$\underset{\sim}{\bar{T}}\,\underset{\sim}{W}^A\,\underset{\sim}{T} = \underset{\sim}{q}^2 \qquad \text{III.4.49a}$$

$$\underset{\sim}{\bar{T}}\,\underset{\sim}{W}\,\underset{\sim}{T} = \underset{\sim}{q}^2 + \underset{\sim}{I}\left(\frac{L(L+1)}{R^2}\right). \qquad \text{III.4.49b}$$

All the off-diagonal elements of $\underset{\sim}{W}$ are contained in $\underset{\sim}{q}^2$, and therefore it is reasonable to consider $\underset{\sim}{q}^2$ as constant over the sector width. The appropriate

form of the eigenvalues of $\underset{\sim}{W}$ are

$$(\lambda_n(R))^2 = q_n^2 + \frac{L(L+1)}{R^2} \quad . \qquad \text{III.4.50}$$

This may be substituted into equation III.4.37, and we may find values for A(R) and B(R). For $q_n^2 < 0$ the solutions are in terms of Spherical Bessel functions, and for $q_n^2 \geq 0$ we must consider modified Spherical Bessel functions of the first and second kind (Abramowitz and Stegun (1965)).

$$A(R) = \begin{cases} |q_n| R j_L(|q_n|R) & q_n^2 < 0 \\ |q_n| R \sqrt{\frac{\pi}{2|q_n|R}}\, I_{L+\frac{1}{2}}(|q_n|R) & q_n^2 \geq 0 \end{cases} \qquad \text{III.4.51a}$$

$$B(R) = \begin{cases} |q_n| R n_L(|q_n|R) & q_n^2 < 0 \\ |q_n| R \sqrt{\frac{\pi}{2|q_n|R}}\, I_{-L+\frac{1}{2}}(|q_n|R) & q_n^2 \geq 0 \end{cases} \qquad \text{III.4.51b}$$

Substituting III.4.51a,b into III.4.44 a,b,c, and d we obtain the sector R-matrices.

This technique is of value when studying systems with interaction potentials that are long ranged and have a deep well. It is of greatest use when the collision energies of interest require that calculations be made at a large number of partial waves. The technique has two advantages, the step size may be increased and in addition the step size is virtually independent of L. We therefore may generate results at a large number of partial waves with little numerical effort.

The step size will not, however, be independent of L, as the diagonal elements of the coupling matrix increase the off diagonal elements will become less significant. Nevertheless we would expect this effect to be weak.

The propagators III.4.51a,b are more complex than those derived using a constant potential III.4.45a,b but their evaluation can be made more efficient if we take advantage of the recursion relations that exist between Bessel functions (see Abramowitz and Stegun (1964)). Employing the relations for Spherical Bessel functions, and writing

$$S_L(|q_n|R) = |q_n|R\, j_L(|q_n|R) \quad \text{or } |q_n|R\, n_L(|q_n|R), \qquad \text{III.4.52}$$

we obtain the following relations (for $q_n^2 < 0$)

$$S_{L+1}(|q_n|R) = \frac{(L+1)}{|q_n|R} S_L(|q_n|R) - \frac{1}{|q_n|} S'_L(|q_n|R) \qquad \text{III.4.53a}$$

$$S'_{L+1}(|q_n|R) = \frac{1}{|q_n|}\left[S_L(|q_n|R) - \frac{(L+1)}{|q_n|R} S_{L+1}(|q_n|R)\right], \qquad \text{III.4.53b}$$

similar relations may be derived for $q_n^2 \geq 0$. Therefore the information required to evaluate the propagators $A(a)$, $A'(a)$, $B(a)$, $B'(a)$ can be generated using the corresponding values used in the previous partial wave. The major draw-back of this technique

is the amount of storage required, we would need to know the values of $A(a)$, $A'(a)$, $B(a)$ and $B'(a)$ at each sector boundary for each q_n, and in addition we require the value of R at each sector boundary and the values of q_n at the centre of each sector. Therefore for an N-channel problem we would need to store (5N + 1) numbers. In rotor-vibrotor calculations this amount of storage might be prohibitively large however, in atom-vibrotor calculations when we only retain a few vibrational channels, this storage should present no problems.

4.5 The Step size Algorithm

In the R-matrix propagator method one assumes that the coupling matrix $\underset{\sim}{W}$ is constant over the width of the sector, this in turn leads to the assumption that the derivative $\underset{\sim}{W}'$ is zero over the width of the sector. Therefore a scheme is required in which one reduces the matrix of derivatives $\underset{\sim}{W}'$ into a single parameter suitable for determining the sector width. We will assume that the function $V'(R)$ is a satisfactory measure of the rate of change of the coupling potential, and the new sector width is given by

$$h_{i+1} (\equiv \text{VSTEP}) = \text{BETA} \left[\left(\frac{2\mu}{\hbar^2} V'(R) \right)^2 \right]^{-1/6}, \qquad \text{III.4.54}$$

where BETA is a constant. The rate of change of the average eigenvalue is a satisfactory measure of the rate of change of the potential $V'(R)$.

$$\frac{2\mu}{\hbar^2} V'(R) = \frac{1}{N} \sum_{n=1}^{N} \left(\frac{\lambda_n^2(i) - \lambda_n^2(i-1)}{R_i - R_{i-1}} \right) \qquad \text{III.4.55}$$

Unfortunately, at local minima, and maxima in the potential (where $V'(R) \rightarrow 0$), III.4.55 overestimates the next sector width. This can be overcome by limiting the new sector width relative to the last, employing

$$h_{i+1} (\equiv GSTEP) = h_i \times FACT. \qquad \text{III.4.56}$$

Another measure of the change of the coupling matrix is the overlap matrix $\underset{\sim}{Q}$. For small sectors $\underset{\sim}{Q}$ is almosta unit matrix, if $\underset{\sim}{T}^{(i-1)} = \underset{\sim}{T}^{(i)}$ then

$$\underset{\sim}{Q}(i-1, i) = \underset{\sim}{T}^{(i-1)} \underset{\sim}{T}^{(i)} = \underset{\sim}{I}.$$

The rate of change of the transformation matrix $\underset{\sim}{T}^{(i)}$ from sector to sector is limited via the relation

$$h_{i+1} (\equiv CSTEP) = CUPMAX \times \left(\frac{N-1}{2 \times CUPLR} \right)^{\frac{1}{2}}. \qquad \text{III.4.57}$$

where $$CUPLR = \frac{\underset{\sim}{T}(1 - \underset{\sim}{Q})}{N (R_i - R_{i-1})^2}.$$

In III.4.57 CUPMAX is an input tolerance specifying the maximum magnitude of a typical off diagonal element of $\underset{\sim}{Q}$.

A final fine control upon the step size is imposed by specifying the parameters STPMIN and STPMAX. The new sector is required to fall within the permissible

range of sector widths (STPMIN, STPMAX).

Thus the algorithm is dependent upon five parameters, namely:-

STPMIN, STPMAX, BETA, FACT, CUPMAX

where BETA controls the sector widths, and is based on the rate of change of the eigenvalues of $\underset{\sim}{W}$.

FACT limits the maximum rate of change in the sector width and CUPMAX controls the new sector width, and is based on the rate of change of the matrix $\underset{\sim}{Q}$.

All these parameters must be specified to obtain the best results for the problem being studied.

Of these parameters, only VSTEP will be affected by the choice of the eigenvalue $\lambda_n(R)$. In Section 4.4 we discussed two possible forms for $\lambda_n(R)$. We first assumed that $\lambda_n^2(R)$ was constant over the sector width, where,

$$\text{A} \quad \lambda_n^2(R) = q_n^2 + \frac{L(L+1)}{R^2} .$$

Secondly, we considered a scheme in which the centrifugal term was treated analytically, and q_n^2 was taken as constant across the width of the sector,

$$\text{B} \quad \lambda_n^2 = q_n^2 .$$

A places the greatest constraint upon VSTEP in that it assumes that both the diagonalization and the centrifugal term are constant within the sector, whereas B only assumes the former to be constant across the width of the sector.

As discussed in Section 4.4 scheme B has the advantage that the step size is virtually independent of L, and consequently large numbers of partial waves may be generated with little numerical effort. This can be achieved by employing scheme A, however we have the additional constraint that the step size must be sufficiently small to ensure numerical accuracy at the highest partial wave, and this can then be used at all the partial waves considered. In situations where the step size is highly dependent upon L, it may be necessary to divide the range of partial waves considered in the calculation into smaller subgroups, and determine an appropriate step size for each group.

The step size algorithm makes no mention of L or the total collision energy, E. However it is worth mentioning that the step size will be weakly dependent upon L (and E) even when scheme B is employed. As stated in Section 4.4, as the diagonal elements of the coupling matrix $\underset{\sim}{W}$ increase the off diagonal elements will become less important.

4.6 Propagating Variable Numbers of Closed Channels

In solving a scattering problem, one is usually only interested in transitions among a certain set of states. The transitions to states far in energy from the initial states of interest are only negligibly excited. Nevertheless, it is frequently found that they must be included in the calculation to obtain

accurate values for the transitions to states which are of interest. In addition it is often necessary to carry closed channels to obtain fully converged transitions. The closed channels, and the channels belonging to states which are weakly excited are necessary to describe the system properly in the perturbed region where the interaction is strong. In particular the closed channels are required to accurately describe the deformation of the collision partners. The translational functions of such states carry no useful scattering information as they are so deeply buried under the potential barrier that they never gain any appreciable amplitude.

In the R-matrix propagator algorithm it is possible to carry the optimum number of channels in a given sector. Dropping channels from the propagation is extremely simple, and is achieved by truncating the R-matrix (the relevant row and column are removed). The truncated R-matrix will still be symmetric, and consequently the final S-matrix will be unitary. "Picking up" new channels is easily achieved by propagating the original global R-matrix on the outer surface $\underset{\sim}{R}^{(i)}$ and bringing it up to the larger dimension by adding elements using the appropriate initial conditions.

SWL specify two methods for determining the number of closed channels needed to be propagated across a sector. The first is a rather simple energy-based

criterion. It is possible to specify a tolerance based upon the extent to which a channel is closed, any channel more deeply buried than specified by the parameter may be dropped. In addition we may determine the extent to which a deeply buried channel is coupled to less deeply buried channels, this may be achieved by considering the off diagonal elements of the matrix $\underline{Q}$. The quantity γ_j is an estimate of the extent to which channel (j) is coupled to channels (1, 2 ... j-1)

$$\gamma_j = \frac{1}{(2j-2)(R_i - R_{i-1})} \left[\sum_{k=1}^{j-1} (Q_{jk}^2 + Q_{kj}^2) \right]^{\frac{1}{2}}.$$

CHAPTER IV

ROVIBRATIONAL EXCITATION OF H_2 BY H^+

1. Introduction

Due to its large rotational energy level spacing the H_2 molecule provides a rigorous test of approximate treatments of the rotational motion of molecules, particularly the energy sudden and the infinite order sudden approximations. (see Chapter II, Sections 3.2 and 3.3).

The interaction potential for $H_2 + H^+$ contains long range isotropic, and anisotropic components due to the charge on the proton. The presence of such terms means that the accuracy of the coupled states component of the IOS approximation will be reduced. The accuracy of the sudden component is also reduced, since this approximation requires that the rotational period of the molecule be large compared to the collision time, which is proportional to the range of the interaction potential. The long range interactions have the result of increasing the collision time, and the proton spends a long time in the interaction region. The presence of long range interaction terms also makes the calculation of cross sections for the $H_2 + H^+$ system difficult since large integration ranges are necessary. This means a large number of steps in the algorithm, which may be small steps to minimize error in each sector, and hence reduce the accumulated round-off error in the final result.

Three ab initio potential surfaces for the $H_2 + H^+$ system (Csizmadia et al. (1970), Bauschlicher et al. (1973),

and Carney and Porter (1974)), have been compared and discussed by Giese and Gentry (1974). Giese and Gentry concluded that an analytic fit to a restricted set of points from the SCF-MO-configuration interaction calculation of Csizmadia et al., suitably adjusted, would provide the best representation of the $H_2 + H^+$ potential surface. The calculations of Csizmadia et al. are by far the most extensive and cover a comprehensive range of nuclear geometries.

Giese and Gentry (1974) have performed semi-classical calculations of vibrational excitation of H_2 by H^+ using their DECENT model (Distribution among quantum states) of Exact Classical Energy Transfer). The classical energy transfer (as a function of angle) is obtained by means of exact classical 3-d trajectories. By employing the correspondence principle between a classical, and quantum forced harmonic oscillator they obtained differential and integral cross sections. Although the results of Giese and Gentry agree well with the experimental data of Udseth et al. (1973) it was postulated by Schinke (1977) that there are some aspects (e.g. rainbow structures) that might be improved by the application of more quantum like scattering theories. Consequently Schinke (1977) performed time dependent close-coupling calculations which employed an energy sudden treatment of the rotation. The overall agreement with the results of Giese and Gentry is satisfactory and, in addition, the results of Schinke contain additional rainbow structures. Schinke concluded that the use of the straight line impact parameters restricted

the time dependent close coupling method to collision energies $\gtrsim$ 15 eV.

McGuire (1976) has performed CC and CS calculations treating the H_2 molecule as a rigid rotor. The potential surface of Giese and Gentry was employed with the H_2 internuclear separation set at its equilibrium value. The object of the calculations was to ascertain the feasibility of a close-coupling study in the approximated coupled states form. Calculations carried out by Schinke and McGuire (1978a) employing the IOS approximation were compared with the CS results and it was concluded that the IOS approximation was valid for $H_2 + H^+$ for collision energies $\gtrsim$ 3.7 eV. These IOS calculations were extended by Schinke and McGuire (1978b), by the inclusion of the vibrational degree of freedom which was treated by the close-coupling technique.

Programmes which perform IOS calculations of rovibrational excitation cross sections were written in FORTRAN IV, and developed on the IBM 370/168 computer at Newcastle University. The aim of this study was to test these programmes by repeating the calculation of Schinke and McGuire (1978b) at E = 4.67 eV. It is worth mentioning that the results of this calculation are of little value, apart from ascertaining that the computer programmes, which are used to obtain the results presented in the following chapters, are functioning correctly; the potential surface of Giese and Gentry (1974) (GG) employed by Schinke and McGuire has been shown to be in error by

Schinke et al. (1980). In an appendix at the end of this chapter we will present results illustrating the advantage of asymptotic series expansions of the type introduced by Gailitis (1976), over the conventional method of fitting the asymptotic boundary condition.

2. The Interaction Potential

The calculation of Schinke and McGuire (1978b) employs the analytic potential surface of Giese and Gentry (1974) (GG). GG report the total potential of the $H_2 + H^+$ system (they include the potential of the isolated H_2 molecule in their calculation). Therefore, one advantage of the GG potential is that it may be used to determine the exact vibrational wavefunctions of the H_2 molecule. Such a calculation has been undertaken by Schinke (1977), and these wavefunctions are employed by Schinke and McGuire (1978b). Unfortunately, the method used by Schinke to determine these wavefunctions destroys their orthonormality, and leads to unphysical behaviour for the higher vibrational states. Consequently we prefer to calculate our own exact wavefunctions, the calculation of which is described in Section 3, together with a discussion of the problems associated with Schinke's wavefunctions.

The potential of GG is a fit to 138 ab initio configuration interaction energies of Csizmadia et al. (1970) to the following ten parameter analytic function. All ten parameters (underlined) were optimized by an iterative least-squares fit of this function to the 138 calculated points. The co-ordinate system used is shown in Figure 1.

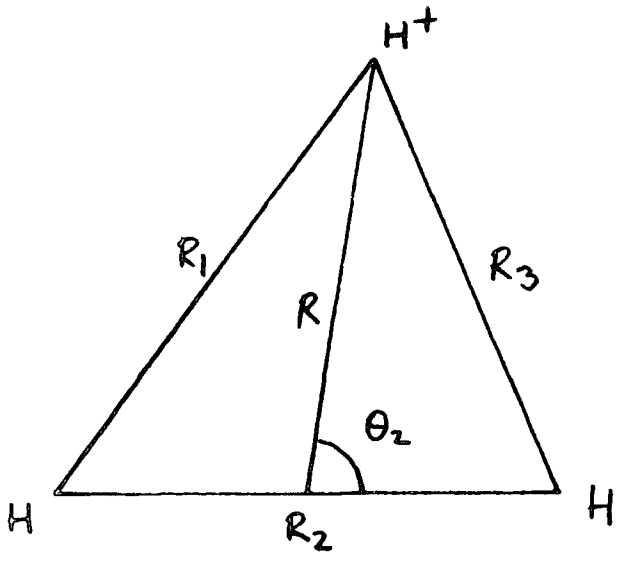

Figure 1.

The potential is expressed in terms of the three interatomic distances R_k (k = 1,2,3), where R_2 is the H_2 internuclear separation (thus $R_2 = r$), and is given in atomic units by

$$V = \sum_{k=1}^{3} H(R_k) + PF_1 + QF_2 + \underline{0.073225}F_3 + 0.17449. \qquad \text{IV.2.1}$$

$H(R_k)$ is a minor variant of a Hulburt-Hirschfelder potential function (Hulburt and Hirschfelder (1941)) and may be written as

$$H(R_k) = A\left[-2E + E^2 - 0.1145Z^3E^2(1-Z)\right], \qquad \text{IV.2.2}$$

where $E = e^{-Z}$

$Z = B(R_k/R_e - 1)$

$B = 1.4426 - \underline{0.126871}F_4$

$R_e = 1.40083 + \underline{0.27923}F_4$

$A = 0.17449 - (\underline{0.014665} + \underline{0.022721}\,R_k)F_4$

and P is the charge-induced dipole contribution

$$P = -(A_0 + A_2 P_2(\cos\theta_2))R^{-4}. \qquad \text{IV.2.3}$$

A_0 and A_2 are determined from cubic fits to the spherical and angle-dependent polarizabilities versus R_2 (Kolos and Wolniewicz (1965), Truhlar (1972)).

The numerical values are

$$A_o = 2.6091 + \int [2.246 + (0.3181 - 0.1194\rho)\rho]\,d\rho ,$$

$$A_2 = 0.60735 + \int [1.3588 + (0.5573 - 0.3170\rho)\rho]\,d\rho ,$$

where $\rho = R_2 - 1.40083$. IV.2.4

The charge-quadrupole contribution Q is given by $Q = Q_2 P_2 R^{-3}$, where Q_2 is determined from a cubic fit to the quadrupole moment versus R_2,

$$Q_2 = 0.45883 + \int [0.53223 + (0.03234 - 0.091474\rho)\rho]\,d\rho .$$

Finally, F_1, F_2, F_3 and F_4 are roll-off and roll-on functions given by

$$F_1 = R^5/(133.6729 + R^5) \qquad \text{IV.2.5a}$$

$$F_2 = R^4/(29.6088 + R^4) \qquad \text{IV.2.5b}$$

$$F_3 = 1/\{1 + \exp[2.1135(R - 2.4421)]\} \qquad \text{IV.2.5c}$$

$$F_4 = 1/(1 + 0.000164289\,R^6). \qquad \text{IV.2.5d}$$

The use of the summation over the diatomic potential functions $H(R_k)$ allows the width, depth and position of the potential minimum to vary slowly as the proton approaches. The above fit is a good representation of the $H_2 + H^+$ potential, however, only the quantities A_o, A_2, and Q_2 are independent of R and can be calculated at all the required quadrature points once and used for all values of R. The computationally expensive tasks such as exponentiation are contained in $H(R_k)$. At each step in the integration range these matrix elements must be evaluated numerically. However, these calculations are only necessary at the initial partial wave, subsequent partial waves require no explicit reference to the potential.

In CC and CS calculations the form of the potential

is a more severe problem. To undertake such calculations the potential surface is more conveniently expressed in terms of a single centre expansion,

$$V(R,r,\theta_2) = \sum_{\lambda} v_\lambda(R,r) P_\lambda(\cos\theta_2). \quad \text{IV.2.6}$$

In the CC and CS calculations of McGuire (1976) the interaction potential was expressed as in IV.2.6 by means of a coordinate transformation.

The GG potential given by IV.2.1 is the total potential of the system. The interaction potential is given by

$$V_{int}(\underline{R},\underline{r}) = V(\underline{R},\underline{r}) - V_{H_2}(\underline{r}), \quad \text{IV.2.7}$$

where $V_{H_2}(\underline{r})$ is the potential of the isolated H_2 molecule, and is given by IV.2.1 with R = ∞

$$V_{H_2}(\underline{r}) = A'[-2E' + (E')^2 - 0.1145(Z')^3(E')^2(1-Z')] + 0.17449, \quad \text{IV.2.8}$$

where

$A' = 0.17449$, $E' = e^{-Z'}$,

$Z' = 1.4426(r/1.40083-1)$.

3. The H_2 vibrational wavefunctions

The potential of GG includes the potential of the isolated H_2 molecule (IV.2.8), therefore the calculation of exact vibrational wavefunctions is possible. To determine exact H_2 bound states $\phi^{ex}_{v_2}$ and energies $\mathcal{E}^{ex}_{v_2}$ we must solve

$$\left[-(2\mu_{H_2})^{-1}\frac{d^2}{dr^2} + V_{H_2}(r) - \mathcal{E}^{ex}_{v_2}\right]\phi^{ex}_{v_2} = 0. \quad \text{IV.3.1}$$

This method has been employed by Schinke (1977); the desired wavefunctions were expanded into the normalised harmonic functions ϕ^{HO}_i according to

$$\phi_{v_2}^{ex} = \sum_i C_i \phi_i^{HO}. \qquad \text{IV.3.2}$$

The harmonic basis functions ϕ_i^{HO} are solutions of

$$\left[-(2\mu_{H_2})^{-1}\frac{d^2}{dr^2} + V^{HO}(r) - \mathcal{E}_i^{HO}\right]\phi_i^{HO} = 0, \qquad \text{IV.3.3.}$$

where $V^{HO}(r) = \frac{k}{2}(r-r_e)$,

and are given by

$$\phi_i^{HO}(r) = \exp\left(-\frac{Q^2}{2}\right) N_i H_i(Q), \qquad \text{IV.3.4.}$$

where $Q = (\mu k)^{\frac{1}{2}}(r-r_e)$,

N_i is a normalisation coefficient,

and H_i is a Hermite polynomial.

Substituting IV.3.2 into IV.3.1 and making use of IV.3.3 and the orthonormal properties of ϕ_i^{HO} we obtain the homogeneous set of linear equations for the coefficients c_i

$$(\underset{\sim}{V} + \underset{\sim}{\Delta})\underset{\sim}{c} = 0, \qquad \text{IV.3.5.}$$

where the matrices V and $\underset{\sim}{\Delta}$ are defined by

$$V_{ij} = \int_0^\infty dr\, \phi_i^{HO}(V_{H_2} - V^{HO})\phi_j^{HO}$$

$$\Delta_{ij} = (\mathcal{E}_i^{HO} - \mathcal{E}^{ex})\delta_{ij}.$$

The desired energies $\mathcal{E}_{v_2}^{ex}$ are then the solutions of the secular equation

$$|\underset{\sim}{V} + \underset{\sim}{\Delta}| = 0. \qquad \text{IV.3.6.}$$

As Schinke (1977) points out the harmonic wavefunctions are of a simple form, and this increases the use of his exact wavefunctions in further applications. However, harmonic wavefunctions have two serious disadvantages for this type of calculation. The exact H_2 wavefunctions

are substantially different from the HO functions for reasonably high vibrational states, and a large number of basis functions are required in the expansion. The major problem is that for higher vibrational states ($i \geq 10$) the HO functions are non-zero for $r < 0$. This is clearly unphysical as it corresponds to the two nuclei of the H_2 molecule passing through each other. This could be easily overcome by extending the integration range in the V_{ij} elements, and indeed this is essential if the orthonormal properties of the wave functions are to be preserved. Whilst the V_{H_2} potential is not infinite for $r < 0$ it is larger than the harmonic potential V^{HO}. Therefore extending the integration range would result in a shift of emphasis from the potential well in which we are primarily interested, to the region for which $r < 0$.

Schinke does not extend the integration range (Kirkpatrick (1983)), and hence destroys the orthonormality of the HO wavefunctions which are employed to derive the secular equation (IV.3.6). Schinke uses 20 HO wavefunctions in his expansion. The expansion coefficients used in his calculation are shown in Table 1. For the higher order wavefunctions, $V_2 \geq 4$, the basis used is insufficient, this is most evident for $V_2 = 6$; compare $C_{6,19}$ with $C_{6,6}$.

In the present IOS calculation the exact wavefunctions were recalculated using Morse oscillator wavefunctions. The Morse potential and corresponding eigenfunctions and

TABLE 1

Expansion coefficients, Cv_2i, of the vibrational basis states employed by Schinke (1977).

i	$v_2 = 0$	$v_2 = 1$	$v_2 = 2$	$v_2 = 3$	$v_2 = 4$	$v_2 = 5$	$v_2 = 6$
0	0.98924	-0.13199	0.02928	-0.03512	0.03022	-0.02126	0.01426
1	0.14160	0.91099	-0.34437	0.11093	-0.07474	0.06783	-0.05556
2	-0.00421	0.37450	0.67933	-0.51369	0.24862	-0.14282	0.11137
3	0.03460	0.06605	0.57768	0.26929	-0.50248	0.37348	-0.23332
4	0.01112	0.07537	0.21227	0.60622	-0.20469	-0.23465	0.34202
5	-0.00047	0.04585	0.14929	0.36869	0.36577	-0.49440	0.17604
6	0.00266	0.01193	0.11484	0.25262	0.39956	-0.05132	-0.38364
7	0.00130	0.00918	0.05492	0.21649	0.32015	0.21168	-0.34572
8	-0.0006	0.00666	0.03190	0.14259	0.30800	0.24808	-0.09666
9	0.00027	0.00217	0.02320	0.08986	0.25168	0.29905	0.03075
10	0.00019	0.00137	0.01262	0.06508	0.18779	0.31351	0.11111
11	-0.00001	0.00111	0.00713	0.04374	0.14519	0.28292	0.24079
12	0.00003	0.00042	0.00500	0.02754	0.10864	0.23235	0.22695
13	0.00003	0.00024	0.00297	0.01920	0.08017	0.21120	0.31950
14	0.0	0.00020	0.00165	0.01253	0.05454	0.14742	0.18046
15	0.0	0.00009	0.00118	0.00858	0.04404	0.14298	0.32688
16	0.00001	0.00004	0.00068	0.00504	0.02542	0.07681	0.09873
17	0.0	0.00004	0.00043	0.00403	0.02301	0.09175	0.28077
18	0.0	0.00002	0.00022	0.00173	0.00935	0.02699	0.00861
19	0.0	0.00001	0.00018	0.00168	0.01132	0.05487	0.23006

eigenvalues are given by (Mies 1964)

$$V^{MO}(r) = D\left[e^{-\phi(r-r_e)} - 1\right]^2 \qquad \text{IV.3.7a}$$

$$\phi_i^{MO}(r) = A_i\, y^{-1/2} W_{\varepsilon/2,\varepsilon/2-1/2-i}(y) \qquad \text{IV.3.7b}$$

$$\varepsilon_i^{MO} = \frac{4D}{\varepsilon}\left\{(i+\tfrac{1}{2}) - \frac{1}{\varepsilon}(i+\tfrac{1}{2})^2\right\}, \qquad \text{IV.3.7c}$$

where

$$y = \varepsilon e^{-\phi(r-r_e)}, \quad A_i^2 = \frac{(\varepsilon-1-2i)\phi}{i!\,\Gamma(\varepsilon-i)},$$
$$\varepsilon^2 = 8\mu_{H_2} D_2/\phi^2,$$

and $W_{\varepsilon/2,\varepsilon/2-\frac{1}{2}-i}(y)$ is a Whittaker function (Abramowitz and Stegun (1965)).

The parameters D, ϕ, and r_e are chosen to approximate V^{MO} as V^{H_2}. Values (in a.u.) are

D = 0.17449 well depth,

r_e = 1.40083 equilibrium separation,

ϕ = 0.9900134.

The parameter ϕ was chosen by Kirkpatrick (1983) by fitting the Morse eigenvalues to Schinke's energy levels. A linear least squares fit of $\varepsilon^{ex}_{v_2}/(v_2 + \frac{1}{2})$ versus $(v_2 + \frac{1}{2})$ was employed to obtain a gradient of $-4D/\varepsilon^2$ and intercept $4D/\varepsilon$, this gave a value of ε of 36.16 (dimensionless), combining this with the value of the reduced mass used by Schinke, μ_{H_2} = 918.07576 a.u. (Kirkpatrick (1983)) gave the above value of ϕ. ϕ is quoted to so many figures to ensure that the parameters used in ϕ^{MO} are self-consistent, and to maintain the orthonormality of the wavefunctions. This is very important since the calculation of Morse wavefunctions involves very large and very small numbers. For example

$$M(\mathcal{E}) \sim 10^{38}$$

and there is a double exponentiation $\exp(-\frac{1}{2}\mathcal{E}e^{-(r-r_e)})$. The Morse potential tends to a finite value as $r \to \infty$, and consequently only a discrete number of bound states can be supported. The number of bound states is determined by $W_{\mathcal{E}/2, \mathcal{E}/2-\frac{1}{2}-i}(y)$; the existence of which requires that $2i < \mathcal{E} - 1$. The calculated value of $\mathcal{E}$ gives an upper value of $i = 17$. This in itself puts an upper bound on the size of the basis set employed in the calculation. It was decided, after considerable experimentation, that we should employ seventeen wavefunctions, i = 0,16, in the expansion. The V_{ij} elements were evaluated using a 96-point Gauss Legendre quadrature in the range $0 \leq r \leq 12$ a.u. The expansion coefficients, $C_{v_2 i}$ for v_2 = 0,6 and i = 0,16, are tabulated in Appendix 2. The coefficients illustrate that the size of the basis used is adequate for the exact wavefunctions employed in this calculation. A comparison between the Morse oscillator expansion (MOEX) wavefunctions, and Schinke's harmonic oscillator expansion (HOEX) wavefunctions is given in Figure 2. None of the problems discussed with respect to harmonic wavefunctions apply to Morse wavefunctions.

There are only significant discrepancies between the exact wavefunctions in the region $0 \lesssim r \lesssim 0.5$a.u., and it is worth mentioning that SM maintained a lower limit of r = 0.5a.u. when evaluating their potential matrix elements in order to minimize the effects of the

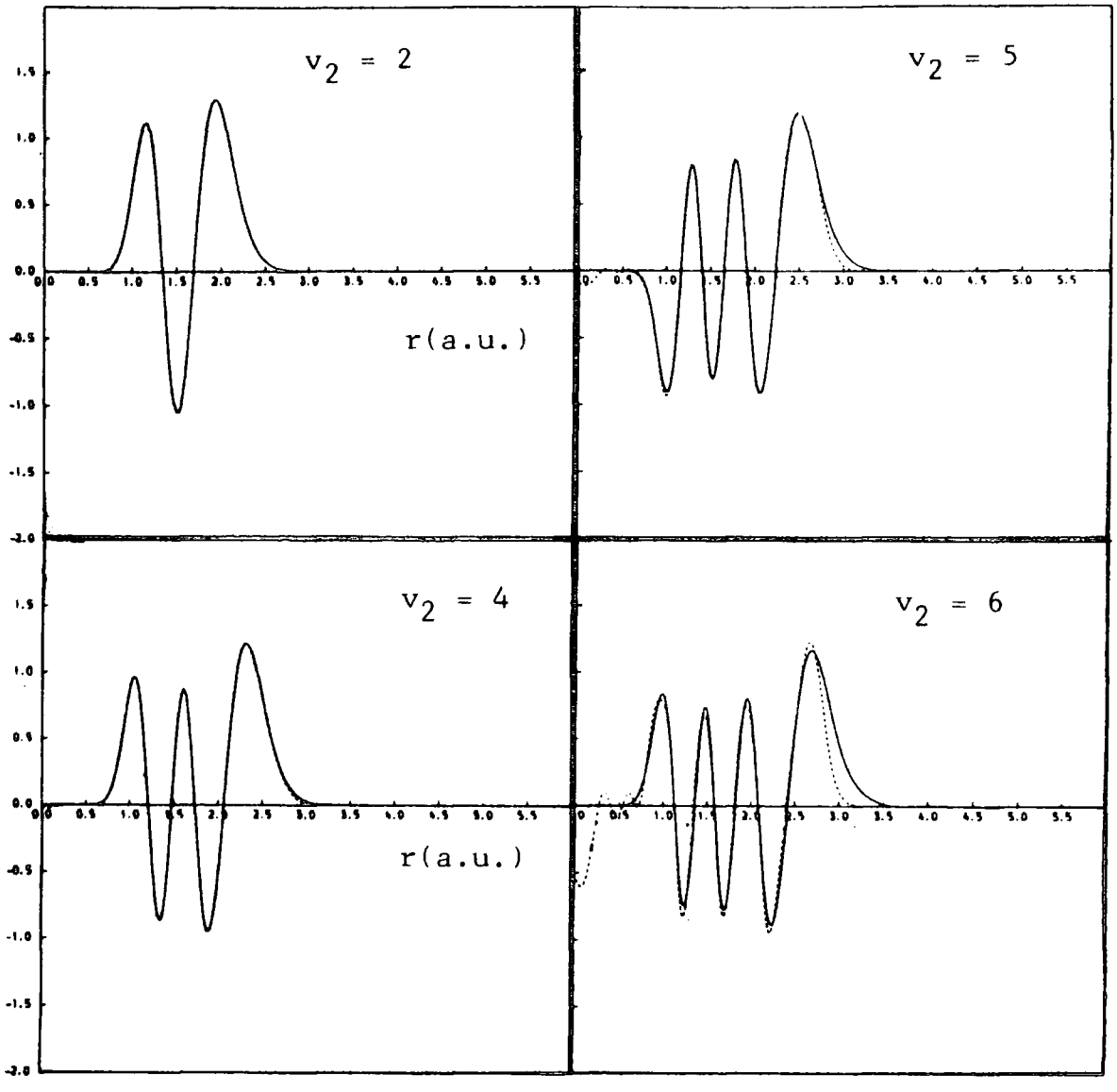

Figure 2 Comparison of the Morse oscillator expansion (MOEX) wavefunctions with Schinke's HOEX wavefunctions.

Full curves : MOEX wavefunctions; broken curves : HOEX wavefunctions.

Wavefunctions in units of a.u.

spurious oscillations. It is interesting to compare the eigenenergies of the HOEX wavefunctions with those of the MOEX wavefunctions. They are shown in Table 2. Despite the problems associated with Harmonic wavefunctions it is evident that $\mathcal{E}_{v_2}^{HOEX}$ and $\mathcal{E}_{v_2}^{MOEX}$ agree to within 1% for $0 \leq v_2 \leq 6$. Also shown in Table 2 are the values of $\mathcal{E}_{v_2}^{MOEX}$ obtained using 64- and 48-point Gauss Legendre quadratures to evaluate the V_{ij} elements. The 96-point quadrature employed is more than adequate. In conclusion it is unlikely that the use of the MOEX wavefunctions rather than the HOEX wavefunctions will significantly affect the results of the scattering calculations, but as mentioned earlier, we did not want to employ the unphysical HOEX wavefunctions of Schinke.

4. Numerical details

As already stated, the aim of this calculation is to reproduce the results of Schinke and McGuire (1978b) (hereafter referred to as SM). SM report rovibrational cross sections at two collision energies, E = 4.67eV and E = 10eV, because of the limitations on computer time it was only possible to repeat the calculations at E = 4.67eV, however this is sufficient to verify that the computer programmes are working correctly.

Following SM we retain seven vibrational states in the fixed angle coupled equations for partial waves in the range $0 \leq L \leq 100$. For partial waves with $L > 100$ SM report the vibrational coupling is negligible, and they

TABLE 2

Values of $\varepsilon^{MOEX}_{v_2}$ obtained using an N-point Gauss Legendre quadrature to evaluate the Vij elements. (a) N = 96, (b) N = 64, (c) N = 48, compared with the eigenenergies, $\varepsilon^{HOEX}_{v_2}$, of Schinke's vibrational wavefunctions.

	v_2=	0	1	2	3	4	5	6
$\varepsilon^{MOEX}_{v_2}$	(a)	0.994392-2	0.289413-1	0.468745-1	0.637421-1	0.795329-1	0.942310-1	0.107817-0
	(b)	0.994916-2	0.289411-1	0.468753-1	0.637468-1	0.795274-1	0.941899-1	0.107782-0
	(c)	0.994245-2	0.289612-1	0.468715-1	0.635457-1	0.796155-1	0.939794-1	0.108243-0
$\varepsilon^{HOEX}_{v_2}$		0.994410-2	0.289412-1	0.468753-1	0.637424-1	0.795405-1	0.943606-1	0.108437-0

Eigenenergies in a.u.

determine the vibrationally elastic S-matrix elements using WKB phase shifts calculated on the $V_{00}(R,\theta_2)$ potential matrix element. The vibrationally averaged surface, $V_{00}(R,\theta_2)$, is given by

$$V_{00}(R,\theta_2) = \langle v_2=0 | V(R,r,\theta_2) | v_2'=0 \rangle \quad \text{IV.4.1}$$

We, however, retain two vibrational channels in the fixed angle coupled equations to determine such S-matrix elements. This difference in approach is unlikely to obscure the comparison as the WKB method has been shown to be extremely accurate for large L values (e.g. see Pfeffer and Secrest (1977)), and is applicable under conditions for which the IOS method is normally expected to be valid. The other numerical details employed in this calculation are discussed in detail in the rest of this section, and where possible have been compared with the methods used by SM. The reduced mass of the $H_2 + H^+$ system was taken to be μ = 1224.101013a.u. as employed by SM (Kirkpatrick (1983)).

4.1 The vibrational quadrature

The evaluation of the potential matrix elements in an IOS calculation require the solution of the integral of the type (cf. II.3.22)

$$V_{v_2 v_2'}(R,\theta_2) = \int_0^\infty \chi_{v_2} V(R,r,\theta_2) \chi_{v_2'} dr . \quad \text{IV.4.2}$$

SM report that in their calculation which employs the HOEX wavefunctions, the potential matrix elements were calculated using a 28-point Gauss-Legendre quadrature in the range $0.2 \leq r \leq 3.0$a.u.

In the present calculation we employ the MOEX wavefunctions, and using these the integral may be rewritten (cf. IV.3.7b)

$$V_{v_2 v_2'}(R,\theta_2) = \int_0^\infty \left(\sum_i C_{v_2 i}\,\phi_i^{MO}\right) V(R,r,\theta_2) \left(\sum_{i'} C_{v_2' i'}\,\phi_{i'}^{MO}\right) dr$$

$$= \int_0^\infty N_{v_2 i} N_{v_2' i'}\, y^{\varepsilon - i - 1 - i'} e^{-y} L_i^{\varepsilon-2i-1}(y) L_{i'}^{\varepsilon-2i'-1}(y) \quad \text{IV.4.3.}$$

$$V(R,r,\theta_2)\,dr + \cdots\cdots$$

where $N_{v_2 i} = C_{v_2 i} A_i (-1)^i i!$

$W_{\varepsilon/2,\,\varepsilon/2-v_2-i}(y)$ has been written in terms of a generalised Laguerre polynomial $L_i^{\varepsilon-2i-1}(y)$ i.e.

$$W_{\varepsilon/2,\,\varepsilon/2-v_2-i}(y) = e^{-v_2 y}\, y^{\varepsilon/2-i} (-1)^i\, i!\, L_i^{\varepsilon-2i-1}(y)$$

(Abramowitz and Stegun (1965)). Since the magnitude of the wavefunctions is zero for $r < 0$, the range of integration can be extended to $-\infty$ to ∞, and using the fact that $y = \varepsilon e^{-\phi(r-r_e)}$ the integral may be rewritten as

$$V_{v_2 v_2'}(R,\theta_2)$$

$$= \int_0^\infty \phi^{-1} N_{v_2 i} N_{v_2' i'}\, e^{-y} y^{\varepsilon - i - i' - 2} L_i^{\varepsilon-2i-1}(y)\, L_{i'}^{\varepsilon-2i'-1}(y)$$

$$V(R,r,\theta_2)\,dy + \cdots\cdots \quad \text{IV.4.4}$$

This makes the integral for $V_{v_2 v_2'}(R,\theta_2)$ ideally suited to evaluation by Gauss-Leguerre quadrature which employs the weight function e^{-y}. This scheme has the advantage of eliminating the use of input limits since the weight function e^{-y} forces the quadrature points over the correct range. The weight function e^{-y} need not be calculated. The quantities $y^{\varepsilon-i-i'-2}$, $L_i^{\varepsilon-2i-1}(y)$, and $L_{i'}^{\varepsilon-2i'-1}(y)$ are independent of R and can be calculated at the required quadrature points on initialization of the potential routine and used repeatedly for all values of R.

Table 3 contains a comparison of potential matrix elements $V_{0 v_2'}(R,\theta_2)$ for $\theta_2 = \pi/2$, $v_2' = 0,6$ and R=3,10,20a.u.

TABLE 3

Values of $V_{0v_2'}(R,\theta_2 = \pi/2)$ using MOEX wavefunctions, calculated by N-point Gauss Laguerre quadrature. (a) N = 28, (b), N = 48, (c) N = 64, and using HOEX wavefunctions, calculated by N-point Gauss Legendre quadrature (d) N = 28.

R(a.u.)	v_2'= 0	1	2	3	4	5	6
3	(a)-0.66357178-1	-0.81549090-2	0.10320330-2	0.89284587-5	-0.14310809-3	0.13260069-3	-0.10252166-3
	(b) "	"	"	0.89284844-5	-0.14310816-3	0.13260083-3	-0.10252191-3
	(c) "	"	"	0.89284851-5	"	"	"
	(d)-0.66356271-1	-0.81544933-2	0.10297962-2	0.90110097-5	-0.14544774-3	0.12458966-3	-0.14296324-3
10	-0.30979120-3	-0.14570058-3	0.23929393-4	-0.48324368-5	0.10043571-5	-0.50702382-7	-0.19646103-6
	"	"	"	-0.48324358-5	0.10043547-5	-0.50697437-7	-0.19647000-6
	"	"	"	"	0.10043546-5	-0.50697271-7	-0.19647031-6
	-0.30978661-3	-0.14569820-3	0.23927137-4	-0.48322186-5	0.99421227-6	-0.80229672-7	-0.29720226-6
20	-0.41039920-4	-0.83254944-5	0.11568101-5	-0.20701703-6	0.45982526-7	-0.95449620-8	-0.10471550-9
	"	"	"	-0.20701691-6	0.45982526-7	-0.95443115-8	-0.10592254-9
	"	"	"	"	0.45982516-7	-0.95442899-8	-0.10596181-9
	-0.41039430-4	-0.83252533-5	0.11565882-5	-0.20697745-6	0.44927752-7	-0.13876025-7	-0.17348870-7

Matrix Elements, $V_{0v_2'}(R, \theta_2)$, in a.u.

calculated by 28-, 48-, and 64- point Gauss Leguerre quadrature. The discrepancies between values obtained using 28 and 64 points are extremely small even at large values of R, where the potential is extremely small. Also shown are the values of $V_{0v_2'}(R,\theta_2)$, $v_2' = 0,6$ calculated using a 28- point Gauss Legendre quadrature in the range $0.2 \leq r \leq 3.0$a.u. (employing the HOEX wavefunctions calculated by Kirkpatrick (1983)). For the matrix elements of major interest ($v_2' \leq 3$), there are no significant differences between the results obtained using the Gauss Leguerre quadratures, and the Gauss Legendre quadrature . SM report that seven vibrational states must be included to obtain reliable results for $\Delta v_2 \leq 3$ transitions, and therefore the higher matrix elements must also be considered. As can be seen in Table 3 the 28-point Gauss Legendre quadrature can fail badly for small matrix elements with a highly oscillatory integrand, such as $V_{06}(R = 20, \pi/2)$.

It was decided to employ a 64-point Gauss Leguerre quadrature in this work. The evaluation of the potential matrix elements accounts for a large percentage of the total computer time for this calculation ($\sim$50% for a 28-point quadrature). However, the use of an approximate potential algorithm allows the efficient generation of many partial waves, the evaluation of the matrix elements is only required at the initial partial wave. Subsequent values of L require no explicit reference to the potential matrix elements. The matrix elements can be calculated using

a large number of quadrature points without significantly increasing the total time required. SM employ de Vogelaere's algorithm to solve the coupled equations, and therefore have to evaluate the matrix elements at each partial wave.

The differences between the results obtained using a 28-point Gauss Legendre, and a 64-point Gauss Laguerre quadrature will affect the cross sections to a degree, however, the most severe differences occur at large R values ($R \gtrsim 20$a.u.) and it is only necessary to integrate the fixed angle coupled equations out to $R \approx 20$a.u. to obtain satisfactory results for the vibrationally inelastic transitions, maintaining accuracy in $|S_L(v_2, v_2' | \theta_2)|^2$ to three significant figures (i.e. vibrational excitation is not particularly important at large R values). Cross sections for the vibrationally elastic transition in the vibrational ground state require a much larger integration range to achieve the same level of convergence (the solution of the coupled equations for fixed orientations is discussed in Section 4.2). However, such cross sections are essentially determined by the higher partial waves. As L increases vibrational coupling becomes less important and it is possible to propagate fewer channels to obtain satisfactory results. SM report that at higher partial waves (they do not state what they mean by higher) it was only necessary to retain five vibrational states and for $L > 100$ it is worth repeating that the vibrationally elastic S matrix elements were determined using the WKB approximation.

4.2 Solution of the coupled equations for fixed orientation

The calculation of cross sections employing the IOS approximation involves two operations. The coupled second order differential equations are solved at given rotor orientations to produce the S-matrices, which are then used to calculate the cross sections. The calculation of the S-matrices is by far the most problematic operation and takes about 95% of the total computer time, and therefore, is discussed in detail in this section.

A computed version of the R-matrix propagator method to solve coupled differential equations was written in FORTRAN IV and developed on the IBM 370/168 computer at NUMAC by Kirkpatrick (1983). This integration routine incorporates the step length algorithm as discussed in Chapter III. The form of the sector R-matrix was chosen to be that appropriate to a constant potential across the sector (i.e. III.4.46). The programme is able to efficiently generate many energies and partial waves.

This routine has been checked by Kirkpatrick (1983) by reproducing the results of SWL obtained for the model atom-forced harmonic oscillator system described by Secrest and Johnson (1966), and also MOLSCAT was used to verify the algorithm for rovibrational IOS calculations (the system studied was H_2 + He).

It was decided in this calculation to use the algorithm with a fixed step length. It is difficult to assess the possible advantage of employing the variable

step size algorithm in this calculation. Kirkpatrick (1983) notes that it is excessively dependent on the rate of change of the potential. In calculations employing the H_2 + He potential of Gordon and Secrest (1979), Kirkpatrick (1983) found that a variable step size gave only a 20% reduction in computer time over a fixed step size (maintaining accuracy to 4 figures). The GG potential is far more complex than that of Gordon and Secrest (1979) (which is a smoothly decaying exponential), and therefore the use of the algorithm might have resulted in a substantial reduction of computer time. However, Kirkpatrick (1983) also reports that the algorithm is highly prone to failure. At one extreme the algorithm allows large steps in the asymptotic region, but also forces the step size in the classically forbidden region to be far smaller than required, while at the other extreme if the tolerances are relaxed allowing larger steps near R = 0, the larger step sizes further out become too large to maintain accuracy. It was decided, therefore, to employ a constant step size in this and in all subsequent work (H_2 + CO, HD + CO).

In all our calculations, the sector R-matrices used were appropriate to approximating the elements of the locally diagonal matrix as constant (III.4.46). As discussed in Chapter III.4.4 there are advantages in employing more complex sector R-matrices which are appropriate to approximating the elements of the locally diagonal matrix as $[\text{constant} + L(L+1)/R^2]$. Indeed the H_2 + H^+ system is ideally suited as a test case with which

to investigate the efficiency of Bessel function propagators, its potential surface has a deep well and is long ranged. In addition at the energies of interest large numbers of partial waves are required ($\gtrsim$200 at E = 10eV, and $\gtrsim$ 100 at E = 4.67eV). However, the aim of the present calculation is to check the computer programmes for use with other systems, e.g. H_2 + CO, and HD + CO, whose potential surfaces do not warrent the use of such propagators so therefore any modification of the existing routines was not considered worthwhile. Both these schemes require that the step size be sufficiently small so that the diagonalization, performed at the centre of the sector, be accurate over the entire width of the sector. In the former scheme it must be sufficiently small so that the coupling matrix (including the $L(L+1)/R^2$ term) can be accurately approximated as constant within the sector. The rate of change of the term $L(L+1)/R^2$ increases with L and therefore a step size which is sufficiently small to accurately calculate results for the highest L value required will also be sufficient for the lower values. It is therefore, worthwhile using a smaller step size than required at the first partial waves.

Preliminary calculations were carried out by Kirkpatrick (1983) for the H_2 + H^+ system. He studied the system at E = 10eV, and determined that in order to maintain $|S_L(0,v_2'|\theta_2)|^2$ accurate to three significant figures for v_2 = 0,1,2 and 3 it was necessary to employ about 3000

steps of fixed length in the range $0.15 \lesssim R \lesssim 30$a.u. Since we employ an approximate potential algorithm the step size should be essentially independent of the collision energy (Chapter III.2), therefore that determined at E = 10eV should be satisfactory at E = 4.67eV. After considerable experimentation it was found that to maintain the same level of accuracy that the above integration range and step size were satisfactory. However, an exception was the vibrationally elastic transition in the vibrational ground state (for the linear orientation, $\cos \theta_2 = 1$); here the leading long range anisotropic term in the potential surface has maximum effect (IV.2.4). Table 4 shows the convergence of the partial cross sections, $\sigma^L(v_2=0 j_2=0 \rightarrow v_2'=0 j_2''=0/\theta_2)$, for the linear orientation, $\theta_2 = 0$, with respect to the integration coordinate, R. To obtain these one orientation partial cross-sections the programme evaluates the product $Y^*_{j_2''0}(\theta_2 0) T_L(v_2, v_2'/\theta_2)\Big|_{j_2''=0}$ this is equivalent to evaluating the integral (cf. II.3.24)

$$\int_0^{\pi} Y^*_{j_2''0}(\theta_2,0)\, T_L(v_2, v_2'/\theta_2) \sin\theta_2 \, d\theta_2 , \qquad \text{IV.4.5}$$

employing a one orientation quadrature with the weight function set equal to one. The resulting one orientation cross sections are proportional to $|T_L(v_2, v_2'/\theta_2)|^2$.

It is clear from Table 4 that the convergence of $\sigma^L(00 \rightarrow 00/\theta_2=0)$ is extremely slow, however, it was not considered worthwhile extending the integration range in the present calculations as physically near- collinear collisions have a small probability of actually occurring,

TABLE 4

The convergence of vibrationally elastic partial cross sections, $\sigma^{L}(00 \rightarrow 00 | \theta_2)$, at the linear orientation, $\theta_2 = 0$.
Integration range $0.15 \lesssim R \lesssim X$ a.u.
Cross sections in Å^2.

X(a.u.)	L = 0	50	75	125
20	0.21849600-3	0.13904351+0	0.64909899+0	———
30	0.21809306-3	0.13286757+0	0.63955445+0	0.92426370+0
40	0.21855717-3	0.13054751+0	0.63581842+0	0.93338700+0
50	———	0.12943995+0	0.63397099+0	0.93743308+0

TABLE 5

The approximate computer times required for the solution of the coupled equations at one orientation using the Cray-1 computer.
(a) Initial partial wave, (b) Subsequent partial waves.

	7 vibrational channels	2 vibrational channels
Time(s)	(a) 17.5	4.8
	(b) 7.5	0.6

(3000 steps of fixed length in the range $0.15 \lesssim R \lesssim 30$ a.u.)

and indeed exactly collinear collisions have a zero probability of occurring due to the $\sin\theta_2$ weighting in the integral for the S-matrix (IV.4.5).

In Table 5 are the approximate computer times required for the solution of the coupled equations at one orientation, using the Cray-1 computer, retaining 7 and 2 vibrational channels. The times for the initial and subsequent partial waves are given. The coupled equations are to be solved at 14 orientations in these calculations, and seven channels are to be retained for $0 \leq L \leq 100$, so that the increase in computer time due to an extended integration range would have been unacceptable.

Once the equations have been integrated out to the upper limit of the integration range, the code continues outwards until the largest relative change in the S-matrix elements is less than a given tolerance. This ensures that the integration range employed is sufficient.

SM report plots of $|S_L(0,v_2'|\theta_2)|^2$ versus L at E = 4.67eV for θ_2 = 0°, 51.43°, and 90°, and v_2' = 1 and 2. Our preliminary calculations involved reproducing these results to check that our description of the system was adequate and to find programming errors before undertaking the full scattering calculations. The results of SM are shown in Figure 3, together with the result obtained using the MOEX wavefunctions. For all three orientations and for v_2' = 1, and 2, the overall agreement is satisfactory. The discrepancies are seen to increase with v_2' and with decreasing L. Here the differences in the potential matrix

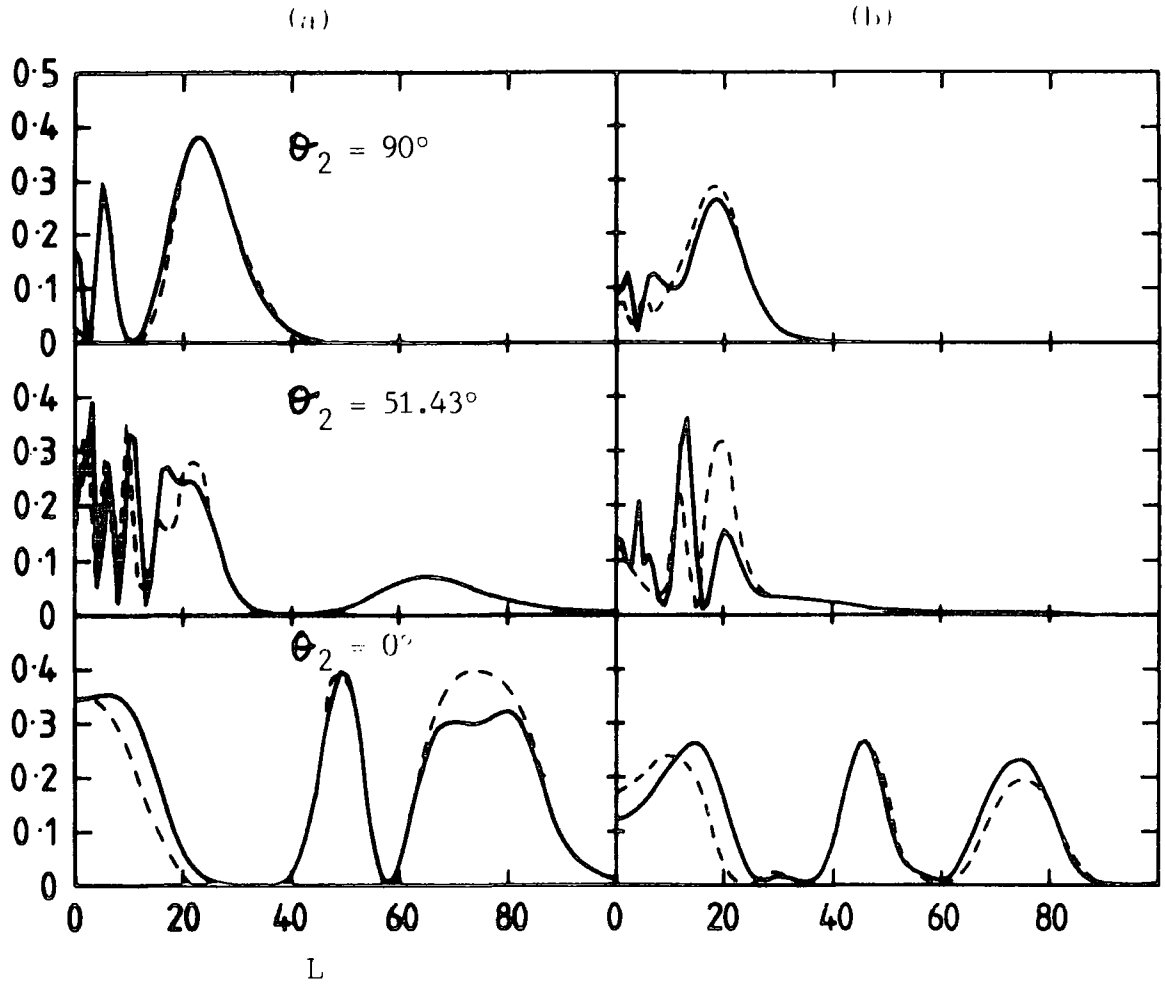

Figure 3

Transition probabilities for vibrational excitation $|S_L(0,v_2'|\theta_2)|^2$ versus partial wave L at E 4.67 eV for three orientations θ_2.

Full curves : Present calculation.

Broken curves : SM.

Column (a) $v_2' = 1$, column (b) $v_2' = 2$.

$|S_L(0,v_2'|\theta_2)|^2$ in a.u.

elements due to the use of a 64-point Gauss Leguerre quadrature rather than a 28-point Gauss Legendre quadrature are having greatest effect, since the potential is more important at these low L values. The exception to this rule is the plot of $|S_L(0,1|\theta_2)|^2$ for $\theta_2 = 0°$, where large discrepancies are seen at large L values. This poor agreement would seem to indicate either the presence of a programming error, which is becoming more apparent as L increases, or the deterioration of our numerical accuracy with L. The satisfactory agreement at large L for the other two orientations would appear to rule out both the above possibilities (also notice the satisfactory agreement at $\theta_2 = 0°$ for $L \gtrsim 80$).

Schinke (1980) has shown that partial cross sections with $L \approx 75$ are extremely sensitive to the form of the interaction potential. Schinke presents a plot of vibrationally elastic partial cross sections, $\sigma^L(01 \rightarrow 07)$ against L at E = 4.67eV. There is a large maximum at L = 75 when the GG potential is employed, however when the more accurate potential of Schinke et al. (1980) is employed this maximum is reduced by a factor ~ 10 Schinke attributes this to the fact that partial waves with $L \approx 75$ sample a broad shallow well in the P_2 anisotropy of the interaction potential. It is possible that the discrepancy seen in the plot of $|S_L(0,1|\theta_2)|^2$ at $\theta_2 = 0°$ at $L \approx 75$ is due to the slight differences in the potential matrix elements for $v_2 \leq 4$ ($v_2 = 5$, and 6 will probably not be particularly

important in this region, as mentioned previously SM retain only five vibrational states at higher partial waves). Notice that at $\theta_2 = 0°$, the $P_2(\cos\theta_2)$ polynomial has its maximum value, and hence at this orientation the P_2 anisotropy will have maximum effect.

In view of the reasonable agreemnt obtained at the values of θ_2 studied we consider that our description of the system and our numerical methods are accurate.

4.3 The Angular Quadrature

Once the orientation S-matrices have been obtained it is necessary to integrate them over orientation to obtain the body fixed S-matrix (II.3.26). The orientation S-matrices are calculated at the points relevant to the quadrature scheme used. In this calculation we only need consider integrals appropriate to the evaluation of $\sigma(v_2 0 \rightarrow v_2' j_2'')$. All other cross sections can be derived employing (II.3.17).

$$\sigma^L(v_2 j_2 \rightarrow v_2' j_2') = (2j_2'+1)\left(\frac{k_{v_2 0}}{k_{v_2 j_2}}\right)^2 \sum_{j_2''} \begin{pmatrix} j_2' & j_2 & j_2'' \\ 0 & 0 & 0 \end{pmatrix}^2 \sigma^L(v_2 0 \rightarrow v_2' j_2'')$$

IV.4.6

To calculate all cross sections involving states up to $j_{2\,max}'$ we require all $\sigma^L(v_2 0 \rightarrow v_2' j_{2\,max}'')$ because of the properties of the three j symbols, for a complete summation. The evaluation of $\sigma^L(v_2 0 \rightarrow v_2' j_2'')$ involves solution of the integral

$$\int_0^{\pi} Y^*_{j_2'' 0}(\theta_2, 0)\, S_L(v_2, v_2' / \theta_2) \sin\theta_2 \, d\theta_2 .$$

IV.4.7.

The integral IV.4.7 must be evaluated using a quadrature of sufficient order to obtain converged cross sections for $j_2'' = 0$ to $2j_{2\,max}''$.

Convergence becomes worse with increasing j_2'' due to the increasing oscillatory behaviour of $Y^{*}_{j_2''0}(\theta_2, 0)$. $\sigma^{L}(v_2 0 \rightarrow v_2' j_2'')$ must be calculated to sufficiently high j_2'' values to complete the summation in IV.4.6; however note that as j_2'' increases the magnitude of such cross sections decrease, and in addition the 3-j symbols decrease as $(j_2 - j_2'')$ and $(j_2' - j_2'')$ increase. Therefore it is evident that to maintain accuracy in the results of interest it is not necessary to calculate cross sections with large j_2'' values to the same degree of precision. Hence it may be possible to reduce the number of quadrature points and allow the accuracy of the high j_2'' cross sections to waver.

The obvious quadrature scheme to use is Gauss Legendre. The limits of a Gauss Legendre quadrature integral are $\cos\theta_2 = -1$ and 1 ($\theta_2 = 0$ to π). When the target is a heteronuclear molecule there is only one method of application we must employ an N-point quadrature in the above range, however, if we are dealing with a homonuclear target molecule the S-matrix is symmetric about $\pi/2$ and the integral IV.4.7 may be written

$$\int_0^{\pi} Y^{*}_{j_2''0}(\theta_2, 0)\, S_L(v_2, v_2' / \theta_2) \sin\theta_2 \, d\theta_2$$

$$= \int_0^{\pi/2} Y^{*}_{j_2''0}(\theta_2, 0) S_L(v_2, v_2' / \theta_2) \sin\theta_2 d\theta_2 \quad j_2'' \text{ even}$$

$$= 0 \qquad j_2'' \text{ odd} \,. \quad \text{IV.4.8}$$

Therefore, since an N point quadrature is required in the range 0 to $\pi/2$, one can choose points from a 2N point quadrature and only use half of them or one can adjust the points and weights of a standard N point quadrature as outlined by Abramowitz and Stegun (1965),

now if $$\int_{-1}^{1} f(x)\,dx = \sum_i w_i f(x_i) \qquad \text{IV.4.9a}$$

then $$\int_{0}^{1} f(x)\,dx = \sum_i \left(\frac{w_i}{2}\right) f\left(\frac{x_i}{2} + \frac{1}{2}\right) \qquad \text{IV.4.9b}$$

SM choose not to implement a Gaussian quadrature, rather they interpolate the T-matrix elements by expansion in Legendre polynomials. For each partial wave the T-matrix is written (cf. II.3.28).

$$T_L(v_2, v_2' / \theta_2) = \sum_\lambda A^L_\lambda (v_2, v_2') P_\lambda (\cos\theta_2) . \qquad \text{IV.4.10}$$

The expansion coefficients $A^L_\lambda(v_2, v_2')$ are determined by the set of linear equations

$$\sum_{\lambda=0}^{N^*} A^L_\lambda (v_2, v_2') \sum_{i=1}^{N} P_\lambda (\cos(\theta_2)_i) P_{\lambda'} (\cos(\theta_2)_i)$$

$$= \sum_{i=1}^{N} T_L (v_2, v_2' / (\theta_2)_i) P_{\lambda'} (\cos(\theta_2)_i), \qquad \text{IV.4.11}$$

where $\lambda , \lambda' = 0, 2 \ldots . N^*$, $N^* \leq 2(N-1)$.

$(\theta_2)_1 = 0°$ and $(\theta_2)_N = 90°$ because only Legendre polynomials of even order are included due to the symmetry about 90°. Two advantages of this quadrature scheme are that the expansion order may be enlarged by adding more orientations $(\theta_2)_i$ without neglecting the previously calculated values, also the values of θ_2 chosen can be concentrated in the region where the integrand is varying most rapidly. However SM report that this scheme does not allow a reduction in the number of orientation angles

θ_2 that must be considered in the integrand IV.4.6.

The computer programmes written to perform these calculations employ the more usual scattering formalism, and consequently we prefer to use Gauss Legendre quadrature. In their paper SM compare their 12-point quadrature with a 14-point Gauss Legendre quadrature (they do not state which type this is). The comparison is made by examining rigid rotor differential cross sections for the rotational transitions $j = 1 \rightarrow 5$ and $j = 1 \rightarrow 7$ (SM are not interested in transitions for which $\Delta j > 6$, as there is no experimental data for such transitions). The level of agreement between the two quadratures for the $j = 1 \rightarrow 7$ transition indicates that the use of a 14-point Gauss Legendre quadrature rather than the 12-point quadrature will not obscure the comparison between the vibrationally elastic cross sections, however SM do not compare these quadratures for the vibrationally inelastic cross sections.

In Figure 4 we show the variation of the real and imaginary parts of $S_L(0,v_2'|\theta_2)$ for L = 25 and v_2' = 0,1, 2, and 3. Values of $S_L(0,v_2'|\theta_2)$ have been calculated at 20 equidistant values of θ_2. It is clear that at this low value of L, where vibrational excitation is important, that for the $H_2 + H^+$ system the vibrationally inelastic S-matrix elements become stronger functions of θ_2 as v_2' increases. Therefore it is difficult to know, a priori, just how the use of the Gaussian scheme rather than that used by SM will affect the level of agreement between

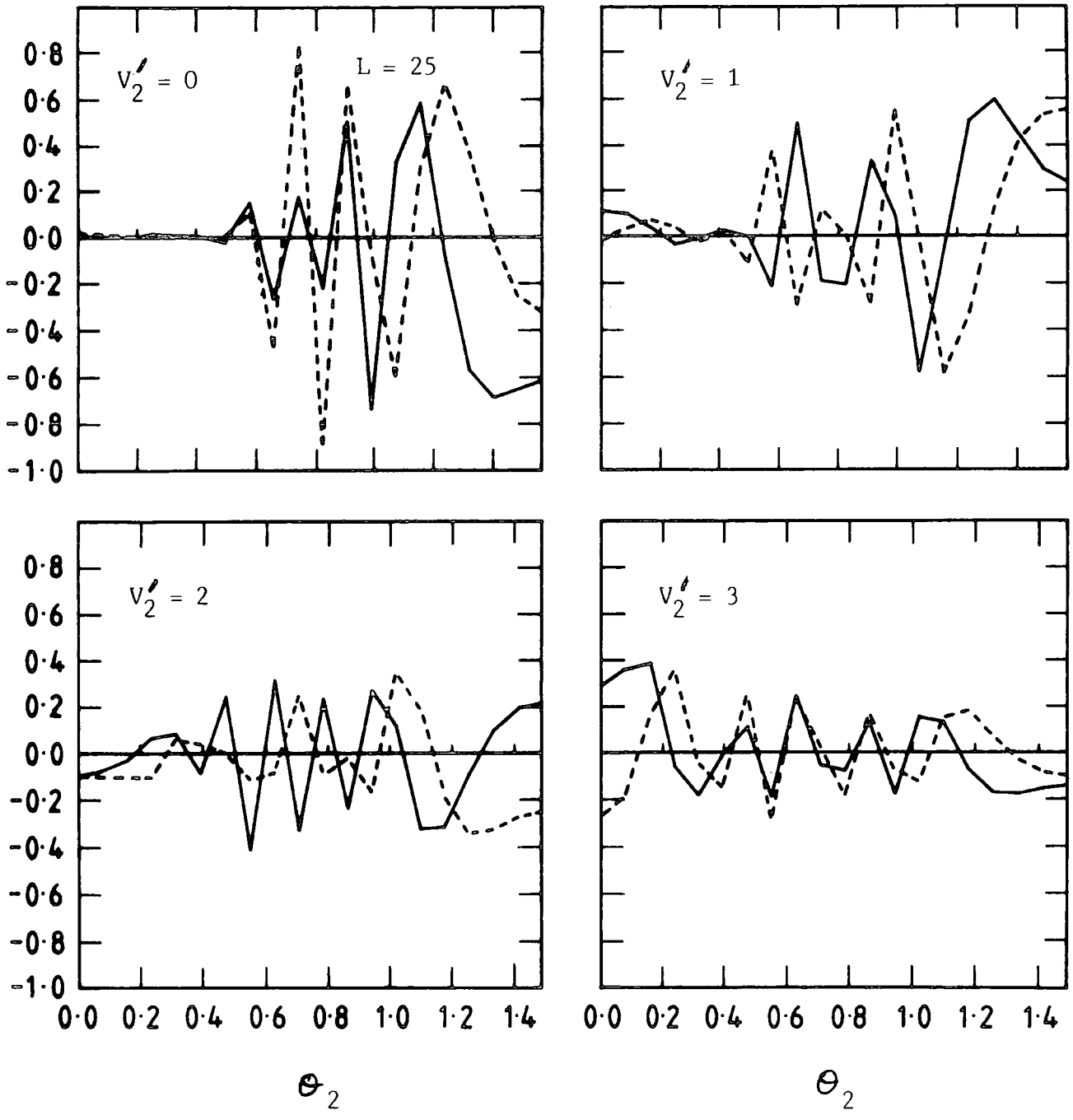

Figure 4

The variation of $S_L(V_2=0, V_2'/\theta_2)$ as a function of θ_2 for L = 25 and V_2' = 0,1,2,3 at E = 4.67 eV.

Full curves : Real part of S-matrix; broken curves : imaginary part of S-matrix.

S-matrices in a.u., θ_2 in radians.

the vibrationally inelastic cross sections. It is hoped that a difference of two quadrature points will not have a significant effect, even for $S_L(0,3/\theta_2)$.

Kirkpatrick (1983) has compared the efficiency of the two types of Gaussian quadratures described earlier, with regard to the H_2 + He system, and reports that it is more efficient to employ half the points of a 2N quadrature. For H_2 + He the S-matrix elements are smoothly varying functions of θ_2 (even at L = 0), however in sharp contrast, for H_2 + H^+ the S-matrix elements are highly oscillatory functions of the orientation angle θ_2, for $L \lesssim 25$ (as illustrated in Figure 4). So at first sight the work of Kirkpatrick may not appear relevant. However one may show that using half the points of a 2N quadrature is more efficient by considering the error functions of the two types of Gauss Legendre quadratures. It can be shown that if $f(x)$ is continuous for $-1 \leq x \leq 1$, the error of the 2N point Gaussian rule (IV.3.9a) is of the form $d_n f^{(2n)}(\xi)$ (Abramowitz and Stegun (1965)) where $-1 \leq \xi \leq 1$ and

$$d_n = \frac{2^{(2n+1)}\,(n!)^4}{(2n+1)\,[(2n)!]^3}\Bigg|_{n=2N}, \qquad \text{IV.4.12a}$$

which decreases rapidly as 2N increases. For the Gaussian rule (IV.3.9b), it may be shown that for an N point quadrature the error is given by (Abramowitz and Stegun)

$$(b-a)^{2n+1} d_n f^{(2n)}(\xi)\Big|_{n=N}, \qquad \text{IV.4.12b}$$

where b = 1, and a = 0.

For a given value of N the error in using half the points of a 2N quadrature is far less than the error involved in using the adjusted points and weights of an N-point quadrature. Therefore we choose to employ the former scheme, and employ 14-point from a 28-point quadrature.

5. Results and discussion

In Table 6 we present the integral cross sections for the vibrationally elastic process, for both para-H_2 ($j_2 = 0$) and ortho-H_2 ($j_2 = 1$). The agreement between the results of the present calculation and the results of SM is satisfactory for all rotational transitions except $j_2 = 0 \rightarrow 2$ and $j_2 = 1 \rightarrow 3$. The range of partial waves ($L \leq 175$) employed in the calculation was insufficient to converge the integral cross section for the $j_2 = 0 \rightarrow 2$ transition (and consequently the integral cross section for the $j_2 = 1 \rightarrow 3$ transition which is essentially determined by $\sigma(00 \rightarrow 02)$). As pointed out by Schinke and McGuire (1978a) the sudden approximation overestimates the long range part of the $\Delta j_2 = 2$ transitions caused by the charge-quadrupole interaction. As discussed previously (Chapter II.3.2) the sudden approximation requires that the rotational period of the target be large compared to the collision time (which is proportional to the range of the interaction potential). The charge-quadrupole interaction has the effect of increasing the effective collision time and making the IOS approximation inapplicable

TABLE 6

Vibrationally elastic integral cross sections

$\sigma(0j_2 \rightarrow 0j_2')$ in $Å^2$ at E = 4.67eV.

(a) Schinke and McGuire (1978b).

(b) Present calculation.

(c) Rigid rotor coupled states results, McGuire (1976)

j_2'			
para-H_2(j_2 = 0):			
0	(a) 67.7	(b) 65.25	(c) 61.9
2	14.0	8.72 + 2.34*	8.10
4	3.04	2.88	1.50
6	1.27	1.20	0.614
8	0.567	0.481	0.443
10	0.293	0.263	0.370
ortho-H_2(j_2 = 1):			
1	73.3	67.69	64.2
3	9.77	7.35	4.97
5	2.28	2.16	1.25
7	0.938	0.874	0.610

* Estimated contribution for $L > 175$

for Δj_2 2 transitions. For $L \gtrsim 55$ SM show that only the P_2 anisotropy of the GG potential surface survives, therefore higher rotational transitions (e.g. $j_2 = 0 \rightarrow 4$, $0 \rightarrow 6$ ...) must be the result of multiple $\Delta j_2 = 2$ transitions in this region. The overestimation of the rotational transitions involving $\Delta j_2 = 2$ is clearly seen when one compares the results of SM (or the present calculation) with the coupled-states rigid rotor cross sections of McGuire (1976) which are also shown in Table 6. As Schinke and McGuire (1978a) point out the above effect is more severe for $j_2 = 0 \rightarrow 2$, and consequently this is the only unconverged transition for para-H_2.

The contribution to the integral cross section for the $j_2 = 0 \rightarrow 2$ transition, from partial cross sections with $L > 175$ was estimated in the following manner. The partial cross sections $\sigma^L(00 \rightarrow 02)$ for $150 \leq L \leq 175$, were plotted versus L. In this region the variation of $\sigma^L(00 \rightarrow 02)$ with respect to L is essentially linear and may be represented by

$$\sigma^L(00 \rightarrow 02) = aL + b, \qquad \text{IV.5.1}$$

where a and b are constants.

Using the plot it was possible to calculate a and b (a = -6.2530(-4), and b = 1.6413(-1)) which gave a maximum possible value of L = 261. Integration of equation IV.5.1 gave the contribution to $\sigma(00 \rightarrow 02)$ for $176 \leq L \leq 261$ to be 2.34 Å^2.

In Figure 5 we present differential cross sections for the first four rotational excitations of ortho-H_2 in its ground vibrational state. It may be seen that the overall agreement between the results of the present calculations, and the results of SM is good. The only significant discrepancies are seen in the $j_2 = 1 \rightarrow 3$ cross sections in the low angle region ($\theta \lesssim 15^\circ$) the cross sections calculated by SM increase beyond 10^2Å^2 for $\theta < 5^\circ$ (although it is quite difficult to see this in the Figure). Such cross sections are essentially determined by the higher partial waves ($L \gtrsim 100$). Since the differential cross sections were evaluated using S-matrix elements computed in the range $0 \leq L \leq 175$, the discrepancies are due to the "missing contribution" to $j_2 = 1 \rightarrow 3$ for $L > 175$.

It is worth mentioning that Schinke (1980) has shown that the rainbow maxima in the $j_2 = 1 \rightarrow 5$ and $j_2 = 1 \rightarrow 7$ differential cross sections are caused by the P_2 term of the interaction potential (i.e. he has shown that the rainbow maxima result from partial waves $L \gtrsim 55$). These rainbow maxima are spurious, and are reduced when the more accurate potential surface of Schinke et al. (1980) is employed. The present calculations confirm that the maxima are due to inaccuracies in the GG potential and the form the wavefunctions have no effect whatsoever on the maxima. This is in contrast to Kirkpatrick (1983) who postulated that the maxima might be due to the "inaccurate" HOEX wavefunctions.

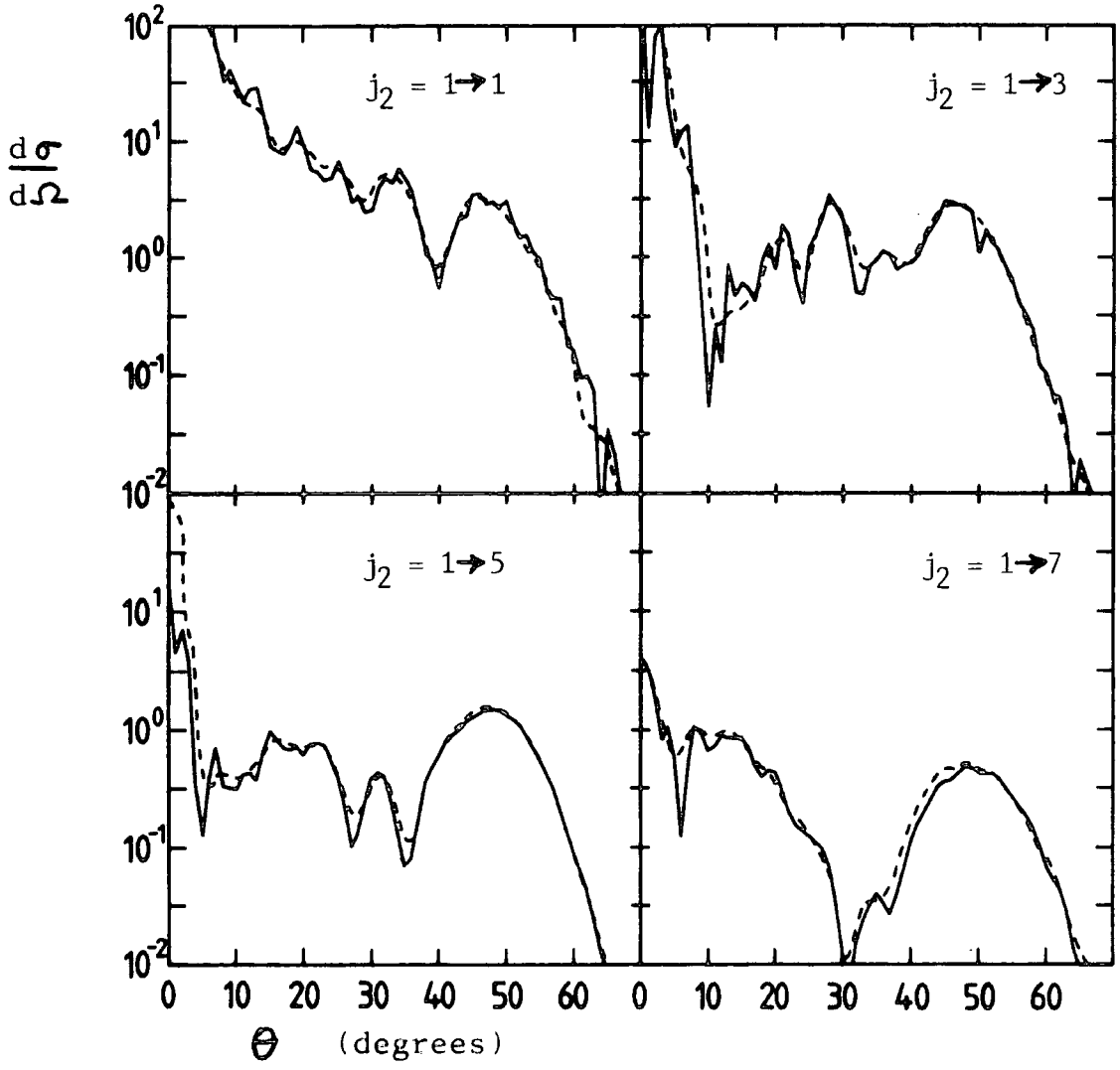

Figure 5

Vibrationally elastic differential cross sections $\frac{d\sigma}{d\Omega}(o_{j_2} \rightarrow o_{j_2'}/\theta)$. A comparison of the present calculations (———) with the results of SM (------).

Cross sections in $\mathring{A}^2$.

Rovibrational cross sections for the vibrationally inelastic process $v_2 = 0 \rightarrow v_2' = 1,2,3$ are presented in Table 7. The agreement between the results of the present calculations and those of SM is satisfactory. The only exception is the cross section for the process $v_2 = 0$ $j_2 = 0 \rightarrow v_2' = 3\ j_2'' = 2$. This is most likely due to a typographical error in the paper of SM, since for all other given rotational transitions the cross sections decrease monotonically with increasing v_2'.

It appears that neither the use of MOEX wavefunctions rather than HOEX wavefunctions, or the use of a Gaussian quadrature rather than the 12-point equidistant quadrature of SM have a significant effect on the numerical values of the vibrationally inelastic cross section. However, generally speaking integral cross sections are not a particularly sensitive measure of the phase of the S-matrix elements, and hence the quadrature employed in a calculation, a far more rigorous test of different quadrature schemes are differential cross sections (e.g. see Pfeffer and Secrest (1977)). It is probable that if the differential cross sections for the transitions given in table 7 were compared that the agreement would not be as satisfactory (especially in the higher angle region $\theta \gtrsim 40°$, where the cross sections are determined essentially by the lower partial waves).

Despite the different numerical methods employed in the present calculations and by SM the overall agreement between all the results presented is satisfactory. It

TABLE 7

Vibrationally inelastic integral cross sections

$\sigma(0j_2 \rightarrow v_2' j_2')$ in $Å^2$ at E = 4.67eV.

(a) Schinke and McGuire (1978b).

(b) Present calculation.

	v_2' = 1	2	3
para-H_2 (j_2 = 0):			
0	(a) 0.107	0.027	0.025
	(b) 0.110	0.031	0.019
2	0.188	0.048	0.057
	0.183	0.048	0.020
4	0.232	0.058	0.025
	0.224	0.056	0.028
6	0.215	0.054	0.026
	0.204	0.062	0.027
8	0.136	0.043	0.026
	0.133	0.060	0.026
10	0.072	0.034	0.017
	0.081	0.042	0.020
ortho-H_2 (j_2 = 1):			
1	0.183	0.046	0.036
	0.184	0.051	0.028
3	0.216	0.054	0.027
	0.186	0.054	0.025
5	0.228	0.057	0.026
	0.219	0.060	0.028
7	0.180	0.049	0.027
	0.173	0.062	0.027

is evident that the use of the MOEX wavefunctions rather than the HOEX wavefunctions does not significantly affect the results of the scattering calculation (as postulated in Section 3). This is not particularly surprising as the wavefunctions are qualitatively very similar, this however, is in sharp contrast with the conclusions of Kirkpatrick (1983), who postulates that all the cross sections (both vibrationally elastic and inelastic) would be significantly affected by the use of "improved" wavefunctions. He studies fixed angle orientation S-matrices at L = 25, 50, 75 and 100 at E = 10eV, calculated using both the Morse and HOEX oscillator wavefunctions. He admits that his calculations are by no means conclusive, for example, it is not obvious what effect differences in fixed angle S-matrices will have on cross sections, and it is worth noting that his study is at E = 10eV not 4.67eV. The conclusions he draws are not directly applicable to this calculation, for example vibrational excitation is more important at E = 10eV.

Fortunately the different quadrature schemes used in the two calculations have not obscured the comparison. If, as mentioned above, differential cross sections had been compared, the differences in the two quadratures would probably have been more apparent. There is no guarantee that the 12 point quadrature employed by SM is sufficient to converge any of the cross sections. SM indicate that this quadrature was not considered

completely satisfactory but was the maximum practicable due to the large amount of computer time required for the calculations. It is probable that twelve orientations will be insufficient to give an accurate integration of the S-matrix elements over θ_2, for $L \lesssim 25$, where the fixed angle S-matrices are highly oscillatory functions of the orientation angle, θ_2.

In conclusion, in view of the level of agreement between our own calculations and those of SM we believe that we can be reasonably sure that our IOS programmes are working correctly.

APPENDIX

The Use of Asymptotic Series Expansions in Heavy particle Scattering

The theory of asymptotic series expansions was discussed in Chapter III.4.3 . In this appendix we shall present the result of calculations illustrating the advantages of asymptotic series expansions of the type introduced by Gailitis (1976) over the conventional method of fitting the boundary condition (cf. II.2.27b).

$$G^{LV_2}_{V_2'}(R,\theta_2)$$

$$\underset{R\to\infty}{\sim} \delta_{V_2V_2'} R k_{V_2'} j_L(k_{V_2'}R) - \left(\frac{k_{V_2}}{k_{V_2'}}\right)^{\frac{1}{2}} K_L R k_{V_2'} n_L(k_{V_2'}R). \qquad \text{IV.A.1}$$

Equation IV.A.1 may be employed once the interaction potential has become negligible, however in the case of $H_2^+ + H^+$ it is necessary to integrate the coupled equations out to extremely large R values before the boundary conditions can be fitted. The interaction potential contains long range isotropic, and anisotropic components due to the charge on the proton. The charge-induced dipole contribution (IV.2.3)

$$P = -(A_0 + A_2 P_2(\cos\theta_2))R^{-4}, \qquad \text{IV.A.2}$$

and the charge-quadrupole contribution (IV.2.4)

$$Q = Q_2 P_2(\cos\theta_2) R^{-3}. \qquad \text{IV.A.3}$$

As discussed in Chapter III.4.3 if all the long range terms in the interaction potential are of the form $1/R^n$, where n is an integer, it is possible to integrate sufficiently out into the asymptotic region to where all the short range terms in the potential have become negligible. One then finds a complete set of asymptotic solutions for the long range potential and matches these to the solution to obtain the K-matrix. In this case the coupled differential equations have the asymptotic form (cf.III.4.30).

$$\left(-\frac{d^2}{dR^2} + L(L+1) - k^2_{v_2} + \frac{2\mu}{\hbar^2}\frac{v_n}{R^n}\right) g^{Lv_2}_{v_2'}(R,\theta_2) = 0$$

$$n \geq 3 . \qquad \text{IV.A.4}$$

The asymptotic solution for the long range potential has already been successfully used in heavy particle scattering (Pfeffer and Secrest (1983), Gerratt and Roberts (1983)). Both these calculations employed asymptotic series expansions (ASE) of the type introduced by Secrest (1979) (cf. III.4.31).

$$\left.\begin{matrix} f(R) \\ g(R) \end{matrix}\right\} = a(R)\left\{\begin{matrix} \sin x \\ \cos x \end{matrix}\right. + b(R)\left\{\begin{matrix} \cos x \\ \sin(-x) \end{matrix}\right. .$$

IV.A.5.

The series expansions for a(R) and b(R) are found by substituting f(R) or g(R) into IV.A.4.

Pfeffer and Secrest (1983) have studied the $N_2 + Li^+$ system whose potential surface contains long range terms which decay as $1/R^3$, $1/R^4$, and $1/R^5$. Using the above

technique Pfeffer and Secrest (1983) found that it was possible to stop the integration after integrating only one tenth of the range required to arrive at the region in which they could terminate using Riccati Bessel functions.

Gerratt (private communication) reports that these functions have been successfully employed in a study of vibrational excitation in atom-diatom collisions (Gerratt and Roberts (1983)). The R-matrix method (Bocchetta (1983)) was employed in a region $0 \leq R \leq R_A$ (R_A was determined by the requirement that only the van der Waals ($^1/R^6$) contribution to the potential should be significant for $R > R_A$). The use of these functions eliminated the need to integrate the coupled differential equations from $R = R_A$ to a point where the van der Waals potential had become negligibly small.

We prefer to employ ASE of the type introduced by Gailitis (1976) (III.4.32).

$$\begin{Bmatrix} F(R) \\ G(R) \end{Bmatrix} = A(R) \begin{Bmatrix} \bar{J}_L(kR) \\ \bar{n}_L(kR) \end{Bmatrix} + B(R) \begin{Bmatrix} \bar{J}_L'(kR) \\ \bar{n}_L'(kR) \end{Bmatrix} . \quad \text{IV.A.6}$$

As mentioned in Chapter III.4 these functions are preferable to IV.A.5 in that the effect of the long range term $L(L+1)/R^2$ is already incorporated in the Spherical Bessel functions. In this study we retain the leading long range term of the $H_2 + H^+$ potential (IV.A.3), and therefore the Schrodinger equation takes the asymptotic form

$$\left(\frac{-d^2}{dR^2} + \frac{L(L+1)}{R^2} - k_{v_2}^2 + \frac{2\mu}{\hbar^2} \frac{\sqrt{3}}{R^3} \right) G_{v_2'}^{L v_2}(R, \theta_2) = 0 , \quad \text{IV.A.7}$$

where $v_3 = Q_2 P_2(\cos\theta_2)$.

The calculations are essentially a continuation of the study presented in the main body of this chapter, and therefore the numerical details developed for that calculation are employed in the present work. In this study we are concerned with the evaluation of fixed orientation partial cross sections, $\sigma^L(v_2 j_2 \rightarrow v_2' j_2' / \theta_2)$, it will be recalled that the convergence of the vibrationally elastic cross sections in the vibrational ground state was extremely slow, especially at the collinear orientation (Table 4, Section 4.2). Therefore we examine the convergence of such cross sections, $\sigma^L(00 \rightarrow 00/\theta_2=0)$ in greater detail, and use the results in order to illustrate the advantages of the ASE over the conventional Bessel functions.

To calculate the series A(R) and B(R) and their derivatives, a routine was written in FORTRAN IV and developed on the IBM 370/168 computer at NUMAC. This routine incorporates a capability to monitor the behaviour of the terms of both series. The series we are dealing with are asymptotic, that is to say, the series given by A(R) and B(R) do not converge. As more and more terms are added to the series, the added terms become smaller and the series approach the correct solution up to a point. Beyond that point the added terms begin to get larger, and the series diverge. Thus it is important to stop computing terms in the series at the proper place.

The programme stops adding terms to each series if the terms of either A(R) andB(R) start to diverge. This is sufficient to ensure that the functions IV.A.6 and their derivatives are convergent (e.g. see Kreyszig (1972)). It is difficult to know just how accurate the solution is at this point, when equation IV.A.7 is solved one obtains an R-matrix of questionable accuracy.

If however, this point is not reached it is not necessary to continue adding terms which do not form a significant contribution to the series, and therefore the series must be truncated at suitable points. The relative importance of each term is determined by (e.g. for B(R))

$$TEST > \left| \frac{b_n}{SUM} \right|, \qquad \text{IV.A.8}$$

where b_n is the current (nth) term of the series, and $SUM = \sum_{m=0}^{n} \beta_m R^{-m-2}$. "TEST" is an input tolerance which must be specified. If the quotient on the righthand side of IV.A.8 is less than TEST, then the series is terminated.

In the present calculations the former condition was never reached, and the latter test was used to truncate the series. Table 8 shows values of $|S_L(0,0|\theta_2)|^2$ evaluated at E = 4.67 eV, and at L = 0 and 5 with $\theta_2 = 0$, using different values of TEST. As can be seen the agreement between results evaluated using TEST = 10^{-9}, 10^{-10}, and 10^{-11} is excellent. In calculations employing the IOS

TABLE 8

A comparison of $|S_L(0,0|\theta_2)|^2$ at $\theta_2 = 0°$ evaluated using different values of the parameter TEST at L = 0 and 5.

(a) 10^{-9}, (b) 10^{-10}, (c) 10^{-11}

	$\|S_L(0,0\|\theta_2=0°)\|^2$ (a.u.)^2	
L =	0	5
(a)	0.37304935	0.31158844
(b)	"	"
(c)	"	"

~3000 steps in the range
$0.15 \lesssim R \lesssim 30$ a.u.

approximation it is sufficient to evaluate results correct to no more than three or four significant figures. Evidently TEST could have been relaxed to maintain this level of accuracy, however, it was found that varying the value of TEST had an insignificant effect on the total computer time, the vast majority of which is used in the R-matrix routine. A value of TEST = 10^{-9} was employed in all these calculations.

In Table 9 we compare the convergence, with respect to the integration coordinate R, of $\sigma^L(00\rightarrow00|\theta_2=0)$ for L = 0, 5 and 10 at E = 4.67eV, evaluated using fits to the functions IV.A.6 or to Spherical Bessel functions in the asymptotic region. It is apparent from Table 9 that the ASE results are 'more or less' converged at $R \simeq 40$a.u., whereas the Spherical Bessel function results are not - even at R = 140a.u. Gerratt (private communication) reports that he obtained similar results in his study of vibrational excitation in atom-diatom collisions. One will recall however, that such collinear collisions have a zero probability of occurring (the results presented in Table 9 are purely for the purpose of illustration). Nevertheless the results obtained for near collinear collisions (which are not particularly important, but do contribute to the final results) will be very similar in both their magnitude and convergence properties.

In the $H_2 + H^+$ calculations presented in this chapter

TABLE 9

Single orientation partial cross sections, $\sigma(00 \to 00 | \theta_2 = 0)$, calculated at E = 4.67 eV. Boundary conditions are imposed in terms of either Spherical Bessel functions or of asymptotic series expansions (ASE).

Cross sections are given in $\mathring{A}^2$.

L =	0		5		10	
R(a.u.)	Bessel functions	ASE	Bessel functions	ASE	Bessel functions	ASE
10	0.2570-3	0.2397-3	0.5106-1	0.4458-1	0.9395-1	0.8865-1
20	0.2185-3	0.2207-3	0.4814-1	0.4642-1	0.9193-1	0.9044-1
30	0.2181-3	0.2199-3	0.4743-1	0.4665-1	0.9131-1	0.9063-1
40	0.2186-3	0.2198-3	0.4715-1	0.4671-1	0.9106-1	0.9067-1
60	0.2190-3		0.4694-1		0.9088-1	
80	0.2192-3		0.4686-1		0.9081-1	
100	0.2193-3		0.4683-1		0.9078-1	
120	0.2194-3		0.4681-1		0.9076-1	
140	0.2195-3		0.4679-1		0.9075-1	

it will be recalled that the coupled differential equations were integrated out to R $\tilde{\sim}$ 30a.u., and the boundary conditions were fitted employing Spherical Bessel functions. This upper limit on the integration range was imposed by the computer time available for those calculations. It is difficult to know how the final cross sections would have been changed by extending the integration range, however it is evident that results obtained for the transition $v_2 = 0\, j_2 = 0$ to $v_2' = 0\, j_2' = 0$ were not fully converged. Employing the ASE, the same integration range would have ensured 'more or less' converged results. In Figure 6 we plot the increment in the partial cross sections, $\Delta\sigma^L = |\sigma^L(r_1) - \sigma^L(r_2)|$, as a function of the local scattering coordinate.

$$\sigma^L(r_1) = \sigma^L(00 \rightarrow 00 / \theta_2 = 0) \text{ at } R = r_1$$

and $r_2 > r_1$.

The better convergence properties of the ASE are evident from this figure.

Pfeffer and Secrest (1983) report that in their study of the rovibrational excitation of N_2 by Li^+ at E = 4.23eV, the use of the functions IV.A.5 reduced the integration range by a factor ten. It is worth noting that as in our calculations the vibrational motion of the target molecule was treated within the close coupling approximation , and the rotational motion was treated within the IOS approximation. Also the leading long range term of the interaction potential is the charge-quadrupole interaction varying as R^{-3}. However, one

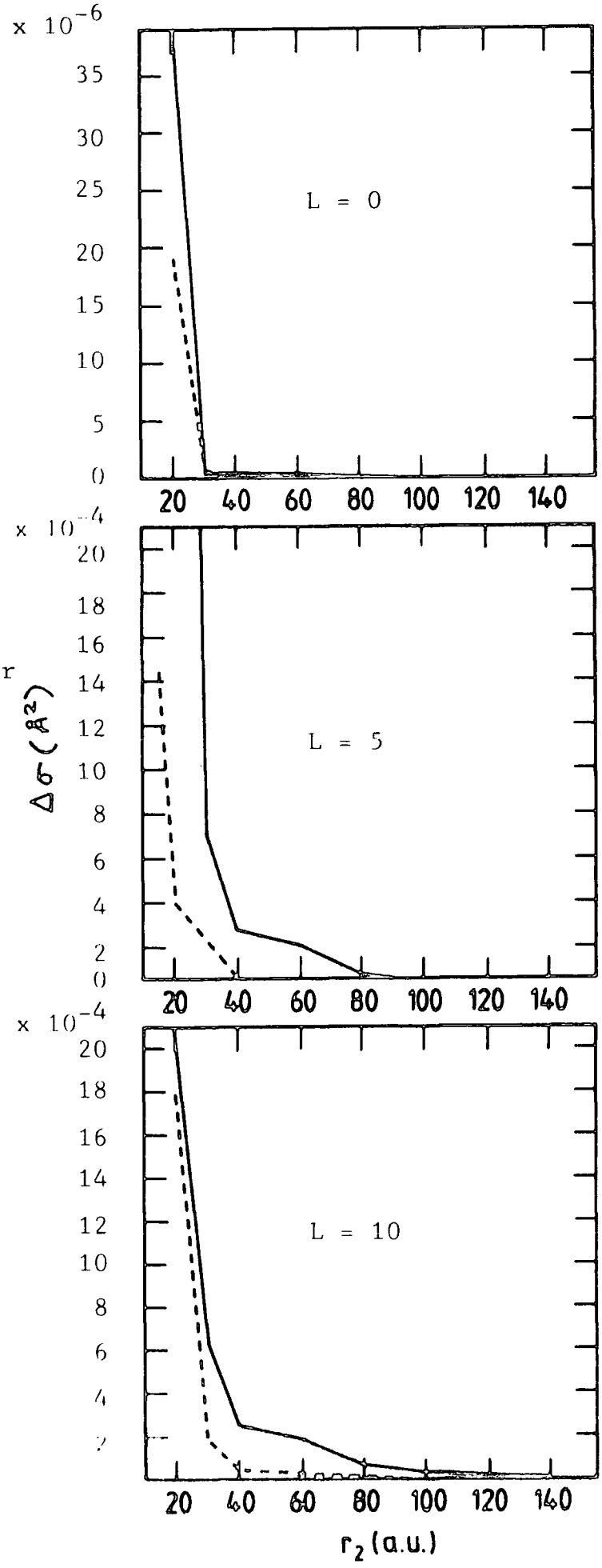

Figure 6

Plots of $\Delta\sigma$ (Å^2) against r_2 (a.u.), for three values of L. Full curves : using Spherical Bessel functions; broken curves : using asymptotic series expansions.

would expect the ASE to be advantageous when applied to $N_2 + Li^+$ for the following reason.

The potential term in IV.A.7 is more important due to the higher reduced mass of the $Li^+ + N_2$ system, and the higher quadrupole moment of the N_2 molecule. In Table 10 we give the relevant numerical values. It is interesting that Pfeffer and Secrest (1983) also report that the ASE method worked best at small L (they do not specify what they mean by small). As mentioned previously, we would expect the ASE of the type introduced by Gailitis (1976) to be advantageous over a larger range of L than the ASE suggested by Secrest (1979), since in the former functions IV.A.6 the effect of the centrifugal term, L, is included in the Spherical Bessel functions.

TABLE 10

$H_2 + H^+$

Reduced mass of system = 1224.101013 a.u.

Quadrupole moment of H_2 = 0.459 a.u.

$N_2 + Li^+$ (Pfeffer and Secrest (1983))

Reduced mass of system = 12347.587078 a.u.

Quadrupole moment of N_2 = 0.943 a.u.

The quadrupole moments are given for the H_2 and N_2 molecules set at their equilibrium geometries.

CHAPTER V

ROVIBRATIONAL EXCITATION OF $^{12}C^{16}O$ by PARA-H_2

1. Introduction

The study of the rovibrational excitation of CO is important for two reasons. The CO molecule is the most abundant heavy molecule in the interstellar medium, and it can be collisionally excited by the other most abundant species in the interstellar clouds, like H_2, H, H^+, and He. Secondly, a knowledge of relaxation rates and deactivation cross sections is an essential prerequisite for the dynamical study of CO lasers.

One of the systems that has been most thoroughly studied experimentally in recent years is H_2 + CO. The first study of the vibrational activation of CO (v_2 = 0) in collisions with H_2 was carried out by Hooker and Millikan (1963). The H_2 + CO system was used in the first measurement of vibrational relaxation times in the low temperature range 100 - 300K by Miller and Millikan (1970). Subsequent to these studies, considerable effort has been devoted to determining the rate of vibrational deactivation of CO by H_2 (e.g. Starr et al. (1974), Stephenson and Mosburg (1974), Andrews and Simpson (1975), (1976), and Allen et al. (1979)). Andrews and Simpson (1976) have obtained results for normal -H_2, para-H_2 and ortho -H_2 in the temperature range 77-340K using laser fluorescence experiments. The CO gas is vibrationally

excited using a pulsed chemical CO laser, and the rate of fluorescence decay is measured. Starr et al. (1974) have obtained results for normal -H_2 in the temperature range 100 - 650 K using a frequency doubled CO_2 laser.

In comparison very little theoretical work has been devoted to the rovibrational excitation of CO by H_2. The major reason for this has been the absence of a suitable potential energy surface. In order to study the rovibrational excitation of CO one requires a potential energy surface incorporating the angular, intermolecular, and internuclear variation of the interaction. Such potential energy surfaces have been recently published (Poulsen (1982), van Hemert (1983), and Bačić, Schinke and Diercksen (1984a)). Poulsen (1982) has obtained an analytical representation of the ab initio SCF points of Prissette et al. (1978) and Flower et al. (1979). The dependence of the interaction on the CO and H_2 internuclear distances was obtained by representing the interaction as a superposition of atom-atom interactions.

Poulsen (1982) only employs the short range part of the SCF calculations. The multipole part of the potential was given as the usual interaction between permanent multipoles. For all the multipoles, functional forms that modelled their dependence on the internuclear coordinates were suggested. The long range dispersion was chosen from the coefficients for CO and H_2 as given in the literature (Parker and Pack (1976), Meyer (1976)).

Van Hemert (1983) has employed the electron gas model of Gordon and Kim (1972) to calculate the H_2 + CO interaction at 4158 points. Van Hemert (1983) also reports an analytical expression of the H_2 + CO interaction derived from his electron gas calculations and the second order long range (dispersion and induction) interactions of the system calculated by perturbation theory. The electron gas model calculations explicitly give the variation of the interaction with the internuclear separations.

Very recently, after these calculations had been completed, a H_2 + CO potential surface was constructed by Bačić, Schinke, and Diercksen (1984a). Extensive SCF calculations (including the electrostatic, induction, and charge transfer effects) performed for a number of H_2 and CO bonds lengths by Diercksen and Kraemer (1984) were combined with damped long range dispersion energies to determine an analytical potential surface including the variation of the CO internuclear distance.

Poulsen and Billing (1982) have employed the potential of Poulsen (1982) in semi-classical calculations in which the vibration of the CO and the rotation of H_2 are treated quantum mechanically, and the rotation of CO and the relative translational motion are treated classically. The rate of vibrational deactivation of CO (v_2 = 1) in collisions with para- and ortho -H_2 which simultaneously undergoes the rotational transitions Δj_i = 0, 2 or 4 is studied. Good agreement is found

with the experimental relaxation rates in the temperature range $100 \leq T \leq 2000K$.

Drolshagen and Gianturco (1983, 1984) have performed quantum mechanical calculations of cross sections for the vibrational excitation of CO by H_2 and of H_2 by CO. Both the CO and H_2 molecules are treated within the breathing sphere (BS) approximation. Cross sections for the vibrational excitation of H_2 by CO are found to be much smaller than the corresponding cross sections for the excitation of CO by H_2. Calculations are carried out in the energy range $E \lesssim 4$ eV. The agreement with the experimental relaxation rate of CO (v_2 1) is unsatisfactory.

Bačić, Schinke and Diercksen (1984a) have carried out quantum mechanical calculations employing the potential surface constructed from the SCF calculations of Diercksen and Kraemer (1984). The rotation of the CO is treated within the IOS, BS and CS approximations. The H_2 molecule is constrained to its ground rotational state, and the de-excitation of CO ($v_2 = 1$) is studied in the energy range $\lesssim 0.5$ eV. The IOS and CS relaxation rates agree well with the experimental measurements in the temperature range $100 \leq T \leq 300K$, however the results computed using the BS approximation are found to be unsatisfactory.

Computationally the CO molecule is not suited to rigorous CC calculations. Since CO has a small rotational constant, there are many closely packed rotational

levels; the $2j_2 + 1$ rotational degeneracy means that the number of coupled equations becomes excessively large. However, because the rotational levels are closely packed CO is ideally suited to approximate treatments of the rotational motion, particularly the energy sudden and the infinite order sudden approximations (Chapter II, Sections 3.2 and 3.3 respectively). In the present calculations we will treat the rotational degree of freedom of the CO within the IOS, and BS approximations. Since the potential energy surfaces (van Hemert (1983), and Poulsen (1982)), the dynamical approximations and the description of the vibrational motion of the CO are the major objects of this study we will confine ourselves to H_2 constrained in its ground rotational state ($j_1 = 0$).

2. The Interaction Potentials

As stated in Section 1 there are three interaction potential surfaces available in the literature suitable to study the rovibrational excitation of CO by H_2 (Poulsen (1982), van Hemert (1983), and Bačić, Schinke and Diercksen (1984a)). However, when these calculations were begun the latter potential was not available, and consequently only the potentials of Poulsen (1982) and van Hemert (1983) are employed in our study.

2.1 The Potential of Poulsen

The potential of Poulsen (1982) (hereafter referred to as the P potential) is an analytical fit to the ab initio SCF calculations of Prissette et al. (1978) and

Flower et al. (1979). This calculation considers 19 configurations at 10 intermolecular distances from 4 to 10 a.u. keeping the two molecules at their equilibrium geometries. The total interaction potential has three parts, a short range part V^{SR}, the long range multipole interaction V^{MP}, and the dispersion energy V^{disp}, i.e.,

$$V = V^{SR} + V^{MP} + V^{disp} \qquad \text{V.2.1}$$

the SCF calculations give the first two parts

$$V^{SCF} = V^{SR} + V^{MP} \qquad \text{V.2.2}$$

The short range potential was therefore, obtained by fitting an analytical expression to $V^{SCF} - V^{MP}$. The short range part is extracted from the SCF points using

$$V^{SR} = V^{SCF} - V^{MP} = V^{SCF} - V^{SCF}_{Q_{H_2}\mu_{CO}} - V^{SCF}_{Q_{H_2}Q_{CO}} \qquad \text{V.2.3}$$

where the superscript SCF indicates that the dipole (μ) and quadrupole (Q) moments obtained with the SCF basis set were used. An analytical function is fitted to the short range potential defined by V.2.3. When fitting, the equilibrium bond lengths of H_2 and CO used in the SCF calculation were employed. As mentioned above the ab initio calculations consider the equilibrium bond lengths. A model was therefore used from which the dependence of the interaction on the intranuclear distances was derived. The coordinate system used is

shown in Figure 1.

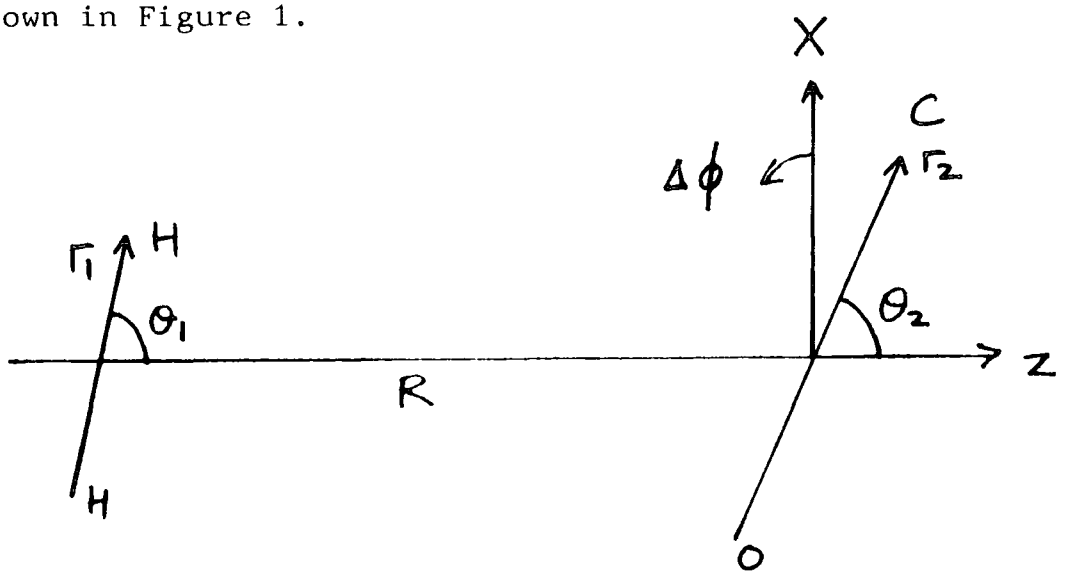

Figure 1.

The analytical representation was expanded in R and in the spherical harmonics $Y_{LM}(\theta_1,\phi_1)$ for H_2 with L = 0 and 2. One of the uses of this potential surface will be to examine the near-resonance process

$$CO(v_2=1) + H_2(j_1=2) \rightarrow CO(v_2=0) + H_2(j_1=6) + 87.03\ cm^{-1}. \qquad V.2.4$$

This transition may be induced to first order by a $P_4(\cos\theta_1)$ term and to second order by $P_2(\cos\theta_1)$. The P_4 coefficient could not be obtained by fitting an expanded form to the SCF points, because the number of configurations is too limited to determine both the P_2 and P_4 coefficients. An estimate was obtained by a further expansion of the analytical form including now Y_{LM} with L = 4 and using the same parameters as obtained in the fit with only L = 0 and 2.

The short range potential, ignoring terms with $\Delta\phi$, is given by (in Å).

$$V^{SR} = \sum_{i=1}^{4} [V_{0i} Y_{00}(\cos\theta_1) + V_{2i} Y_{20}(\cos\theta_1) + V_{4i} Y_{40}(\cos\theta_1)], \qquad \text{V.2.5}$$

where

$$V_{0i} = (4\pi)^{\frac{1}{2}} V_{Ai} (2 + S_i) \; ; \; i = 1,4$$
$$V_{2i} = (4\pi/5)^{\frac{1}{2}} V_{Ai} \, 2t_i/3 \; ; \; i = 1,4$$
$$V_{4i} = (4\pi/9)^{\frac{1}{2}} V_{Ai} A_{i+i}^2 r_1^4 R^{-2}/280 \; ; \; i = 1, \text{and } 3$$
$$V_{4i} = (4\pi/9)^{\frac{1}{2}} A_{i+i}^3 V_{Ai} r_1^4 [A_{i+i}/840 + (140R)^{-1}] ; \; i = 2 \text{ and } 4,$$

where

$$V_{A1} = f_5 A_1 \exp(-A_2 R - A_2 f_{14})$$
$$V_{A2} = -A_3 \exp(-A_4 R - A_4 f_2)$$
$$V_{A3} = A_5 \exp(-A_6 R + A_6 f_{34})$$
$$V_{A4} = -A_7 \exp(-A_8 R + A_8 f_4),$$

where the 's-type' functions are given by

$$S_1 = A_2 r_1^2 [A_{10} A_2/12 - (6R)^{-1} + (1-\epsilon) r_2 \cos\theta_2 R^{-2}/6 + A_2 r_1^2 R^{-2}/120]$$
$$S_2 = A_4 r_1^2 [A_4/12 - (6R)^{-1} + A_4^3 r_1^2/960 - A_4^2 r_1^2 R^{-1}/240]$$
$$S_3 = A_6 r_1^2 [A_{11} A_6/12 - (6R)^{-1} - \epsilon r_2 \cos\theta_2 R^{-2}/6 + A_6 r_1^2 R^{-2}/120]$$
$$S_4 = A_8 r_1^2 [A_8/12 - (6R)^{-1} + A_8^3 r_1^2/960 - A_8^2 r_1^2 R^{-1}/240],$$

where the 't-type' functions are given by

$$t_1 = A_2 r_1^2 [A_{10} A_2/4 + (4R)^{-1} - (1-\epsilon) r_2 \cos\theta_2 R^{-2}/4 - A_2 r_1^2 R^{-2}/56]$$
$$t_2 = A_4 r_1^2 [A_4/4 + (4R)^{-1} + A_4^3 r_1^2/224 - A_4^2 r_1^2 R^{-1}/224]$$
$$t_3 = A_6 r_1^2 [A_{11} A_6/4 + (4R)^{-1} + \epsilon r_2 \cos\theta_1 R^{-2}/4 - A_6 r_1^2 R^{-2}/56]$$
$$t_4 = A_8 r_1^2 [A_8/4 + (4R)^{-1} + A_8^3 r_1^4/224 - A_8^2 r_1^2 R^{-1}/224]$$

and where the functions f_{14}, f_2, f_{34}, f_4, and f_5 are given by

$$f_2 = (1-\epsilon) r_2 \cos\theta_2 + 0.5 (1-\epsilon)^2 r_2^2 \sin^2\theta_2 R^{-1}$$

$$f_4 = \epsilon r_2 \cos\theta_2 - 0.5 \epsilon^2 r_2^2 \sin^2\theta_2 R^{-1}$$

$$f_{14} = f_2 - 0.5 (1-\epsilon)^3 r_2^3 \sin^2\theta_2 \cos\theta_2 R^{-2}$$

$$f_{34} = f_4 - 0.5 \epsilon^3 r_2^3 \sin^2\theta_2 \cos\theta_2 R^{-2}$$

$$f_5 = \{A_9 + \cos^2[1.5(\pi-\theta_2)]\}(A_9+1)^{-1} \text{ if } \theta_2 \geq \pi/3$$

$$f_5 = 1 \qquad \text{otherwise.}$$

The function f_5 was included to improve the anisotropy around the C end of the CO molecule,

$$\epsilon = m_C / (m_O + m_C) \qquad \text{V.2.6}$$

where m_c and m_o are the masses of the C and O atoms respectively, the following values were assumed (Prissette et al. (1978)).

$$m_C = 12.001, \quad m_O = 15.9994.$$

The parameters A_1 to A_{11} are given in Table 1.

TABLE 1

Parameters of the short range H_2 + CO potential

A_1 = 248.55 eV	A_2 = 3.0168 Å^{-1}	A_3 = 1.0493 eV
A_4 = 1.549 Å^{-1}	A_5 = 338.81 eV	A_4 = 3.5776Å^{-1}
A_7 = 0.35584 eV	A_8 = 1.9601Å^{-1}	A_9 = 2.0749
A_{10} = 0.00	A_{11} = 0.24	

The multipole part of the potential is taken as the usual interaction between the permanent multipoles of the two molecules (e.g. see Flower et al. (1979), Leavitt (1980)), where

$$V^{MP} = V_{Q\mu} + V_{QQ} + V_{Q_4\mu} + V_{Q_4Q} \qquad \text{V.2.7}$$

$$V_{Q\mu} = -4\pi(15)^{-1/2} Q^{HH} \mu^{CO} R^{-4} \qquad \text{V.2.7a}$$
$$\times (3 Y^{HH}_{20} Y^{CO}_{10} + 3^{1/2} Y^{HH}_{2\pm1} Y^{CO}_{1\mp1})$$

$$V_{QQ} = 4\pi 5^{-1} Q^{HH} Q^{CO} R^{-5} \qquad \text{V.2.7b}$$
$$(6 Y^{HH}_{20} Y^{CO}_{20} + 4 Y^{HH}_{2\mp1} Y^{CO}_{2\mp1} + Y^{HH}_{2\pm2} Y^{CO}_{2\mp2})$$

$$V_{Q_4\mu} = -4\pi(27)^{-1/2} Q^{HH}_4 \mu^{CO} R^{-6} \qquad \text{V.2.7c}$$
$$\times (5 Y^{HH}_{40} Y^{CO}_{10} + 10^{1/2} Y^{HH}_{4\pm1} Y^{CO}_{1\mp1})$$

$$V_{Q_4Q} = 4\pi(45)^{-1/2} Q^{HH}_4 Q^{CO} R^{-7} \qquad \text{V.2.7d}$$
$$\times (15 Y^{HH}_{40} Y^{CO}_{20} + 120^{1/2} Y^{HH}_{4\pm1} Y^{CO}_{2\mp1} + 15^{1/2} Y^{HH}_{4\pm2} Y^{CO}_{2\mp2})$$

where

$$Y^{HH}_{l_1\pm m} Y^{CO}_{l_2\mp m} = (1+\delta_{m,0})^{-1} [Y_{l_1 m}(\theta_1,\phi_1) Y_{l_2 -m}(\theta_2,\phi_2) + Y_{l_1 -m}(\theta_1,\phi_1) Y_{l_2 m}(\theta_2,\phi_2)],$$

where Q^{HH} and Q^{HH}_4 are the quadrupole and hexadecapole moments of the H_2 molecule respectively, and where μ^{CO} and Q^{CO} are the dipole and quadrupole moments of the CO molecule respectively.

In the paper by Poulsen (1982) the factor $(1+\delta_{m,0})^{-1}$ is missing (Bačić, Schinke, and Diercksen (1984b)). This is unimportant for the present calculations, since the multipole moment interactions are not used, however, we did not realise that this factor was missing, and

consequently some of the results presented in Chapters VI and VII are in error. We will discuss the major implications of this error in the potential routine in the relevant chapters. The following multipole moments are considered to be the most accurate in the literature.

The quadrupole moment function of H_2 used is the fit of Truhlar (1972) to the results of Kolos and Wolniewicz (1965)

$$Q^{HH} = 0.4876 + 1.069\,\text{Å}^{-1}(r_1 - r_{1,eq}) + 0.12273\,\text{Å}^{-2}(r_1 - r_{1,eq})^2 - 0.6559\,\text{Å}^{-3}(r_1 - r_{1,eq})^3\,(eV\text{Å}^5)^{\frac{1}{2}}, \qquad \text{V.2.8a}$$

where $r_{1,eq}$ is the H_2 equilibrium bond length. Karl et al. (1975) have calculated the hexadecapole moment and its derivatives for a series of bond lengths, using the results of Kolos and Wolniewicz (1965). Poulsen (1982) has fitted a six term moment function (for $0.6 \leq r_1 \leq 2.2$ a.u.) to their results, and obtained

$$Q_4^{HH} = 0.08408 + 0.3992\,\text{Å}^{-1}(r_1 - r_{1,eq}) + 0.6742\,\text{Å}^{-2}(r_1 - r_{1,eq})^2 + 0.2906\,\text{Å}^{-3}(r_1 - r_{1,eq})^3 - 0.3274\,\text{Å}^{-4}(r_1 - r_{1,eq})^4 - 0.2462\,\text{Å}^{-5}(r_1 - r_{1,eq})^5\,(eV\text{Å}^9)^{\frac{1}{2}}. \qquad \text{V.2.8b}$$

For the dipole moment of CO, the empirical expression derived by Chackerian (1976) is employed,

$$\mu^{CO} = -0.096566 + 2.4790\,\text{Å}^{-1}(r_2 - r_{2,eq}) - 0.2182\,\text{Å}^{-2}(r_2 - r_{2,eq})^2 - 2.006\,\text{Å}^{-3}(r_2 - r_{2,eq})^3 + 1.126\,\text{Å}^{-4}(r_2 - r_{2,eq})^4\,(eV\text{Å}^3)^{\frac{1}{2}}. \qquad \text{V.2.9a}$$

where $r_{2,eq}$ is the CO equilibrium bond length.

The quadrupole of CO was taken to be

$$Q^{CO} = -1.543 + 1.879 \text{Å}^{-1}(r_2 - r_{2,eq}) + 2.118 \text{Å}^{-2}(r_2 - r_{2,eq})^2 (eV\text{Å}^5)^{\frac{1}{2}}$$

V.2.9b

where the equilibrium value is the experimental value reported by Meerts et al. (1977) and the derivatives in V.2.9b were obtained by fitting a three term moment function to the results of Amos (1979).

The dispersion energy is given by

$$V^{disp} = -19.18 eV \text{Å}^6 R^{-6} [1 + 0.105 P_2(\cos\theta_1) + 0.083 P_2(\cos\theta_2)] \qquad \text{V.2.10}$$

where the isotropic and $P_2(\cos\theta_2)$ coefficients are reported by Parker and Pack (1976). The $P_2(\cos\theta_1)$ anisotropy coefficient is given by Meyer (1976).

As with the GG interaction potential (Chapter IV.2) very little initialization can be performed since it is impossible to separate the variables R and r_2 to any large extent. One can only calculate the functions f_{14}, f_2, f_{34}, f_4 and f_5 (apart from the R^{-1} and R^{-2} factors), and the multipole moment functions during the potential initialization. The computationally expensive tasks such as exponentiation must be evaluated at each value of R, however this is only necessary at the initial partial wave, and in addition some exponentiation can be done analytically (e.g., A_4^3, A_4^2, $(4\pi)^{\frac{1}{2}}$, etc.).

2.2 The Potential of van Hemert

Van Hemert (1983) has employed the electron gas model of Gordon and Kim (1972) to calculate the H_2 + CO interaction at 4158 points. Van Hemert (1983) also reports an analytical expression of the H_2 + CO interaction potential derived from his electron gas calculations and the correct second order long range (induction and dispersion) contributions as given by perturbation theory.

The potential (hereafter referred to as the VH potential) is expressed explicitly in terms of radial and angular variables, by the use of the spherical expansion method (van der Avoird et al. (1980), Berns and van der Avoird (1980)). For two linear (diatomic) molecules in Σ states, the distance and orientation dependence of the interaction is written (in a.u.).

$$V(\hat{r}_1, \hat{r}_2, \hat{R}) = (4\pi)^{3/2} \sum_{L_1=0}^{L_1^{MAX}} \sum_{L_2=0}^{L_2^{MAX}} \sum_{L=0}^{L^{MAX}} V_{L_1 L_2 L}(R, r_1, r_2)\, A_{L_1 L_2 L}(\hat{r}_1, \hat{r}_2, \hat{R}) \qquad \text{V.2.11}$$

where $\underline{R} = (R, \theta, \phi)$, $\hat{r}_1 = (\theta_1, \phi_1)$, and $\hat{r}_2 = (\theta_2, \phi_2)$ and where the expansion coefficients, $V_{L_1 L_2 L}$, are functions of distance only and completely determine the orientational dependence of the potential. Since the interaction potential is invariant under rotation of the arbitrary coordinate system we may set $\theta = \phi = 0$, and employ a coordinate system of the type given in Figure 1. The paper of van Hemert (1983) does not, however, clearly define the coordinate system to be used. For the H_2 + CO system there are two alternatives. $\theta_1 = \theta_2 = 0$

can define the linear configuration in which the O is closest to the H_2 molecule (as in Figure 1), alternatively $\theta_1 = \theta_2 = 0$ may define a linear configuration with C closest to the H_2 molecule. In an earlier publication, van Hemert (1981), the latter configuration is taken, however some preliminary calculations studying the R dependence of the interaction potential with respect to θ_2 have indicated that van Hemert (1983) has adopted a coordinate system as given in Figure 1.

If we set $\phi_1 = 0$ the angular functions $A_{L_1L_2L}$ can be expressed as

$$A_{L_1L_2L} = \sum_{M=0}^{\min(L_1,L_2)} X_{L_1L_2LM} P_{L_1}^M(\cos\theta_1) P_{L_2}^M(\cos\theta_2) \cos M\phi_2 , \qquad \text{V.2.12}$$

where

$$X_{L_1L_2LM} = \left[\frac{(2L_1+1)(2L_2+1)(2L+1)}{64\pi^3}\right]^{\frac{1}{2}} \times \left[\frac{(L_1-M)(L_2-M)}{(L_1+M)(L_2+M)}\right]^{\frac{1}{2}} \begin{pmatrix} L_2 & L_1 & L \\ M & -M & 0 \end{pmatrix} (2-\delta_{M0})(-1)^M ,$$

and P_L^M are associated Legendre functions according to the definition in Brink and Satchler (1975).

Since the interaction potential can be decomposed into short range, first order (multipole moment interactions), and second order (induction and dispersion interactions) long range contributions, the $V_{L_1L_2L}$ can be analyzed in the same terms

$$V_{L_1L_2L}(R,r_1,r_2) = V^{SR}_{L_1L_2L}(R,r_1,r_2) + V^{(1)LR}_{L_1L_2L}(R,r_1,r_2) + V^{(2)LR}_{L_1L_2L}(R,r_1,r_2) . \qquad \text{V.2.13}$$

By examination of a plot of the logarithms of the short range expansion coefficients as a function of R, for different r_1 and r_2 values, the following analytical form for $V_{L_1L_2L}(R,r_1,r_2)$ was suggested.

$$V^{SR}_{L_1L_2L}(R,r_1,r_2) = sgn_{L_1L_2L} \exp(a_{L_1L_2L} + b_{L_1L_2L}R + c_{L_1L_2L}R^2 + d_{L_1L_2L}R^3)$$

V.2.14a

where $L_1^{MAX} = 2$, $L_2^{MAX} = 4$, and $L^{MAX} = 7$,

where $sgn_{L_1L_2L}$ indicates that the expansion coefficients should be negative for $L_1L_2L = (2,1,1)$ and $(2,2,2)$,

and where

$$a_{L_1L_2L}(r_1,r_2) = a^{(0)}_{L_1L_2L} + a^{(1)}_{L_1L_2L}\bar{r}_1 + a^{(2)}_{L_1L_2L}\bar{r}_2 + a^{(12)}_{L_1L_2L}\bar{r}_1\bar{r}_2$$

V.2.14b

where $\bar{r}_1 = r_1 - r_{1,eq}$ and $\bar{r}_2 = r_2 - r_{2,eq}$
and where $a^{(0)}$, $a^{(1)}$, $a^{(2)}$, $a^{(12)}$ are numerical parameters. Similar expressions hold for $b_{L_1L_2L}(r_1,r_2)$, $c_{L_1L_2L}(r_1,r_2)$, and $d_{L_1L_2L}(r_1,r_2)$. This form does not account for the probably small, non-linear terms in r_1 and r_2. The small cross term is included, however, since it may contribute significantly in rovibrational calculations. The coefficients $a_{L_1L_2L}$, $b_{L_1L_2L}$, $c_{L_1L_2L}$, and $d_{L_1L_2L}$ in V.2.14a and their dependence upon r_1 and r_2 (V.2.14b) were determined simultaneously in a polynomial least squares fit of the logarithms of the spherical expansion coefficients.

Only the isotropic dispersion energy is given by van Hemert (1983), and this is given by

$$V^{(2)LR}_{000}(R,r_1,r_2) = -[C_6^e R^{-6} + C_8^e R^{-8} + C_{10}^e R^{-10}] f_2^{(2)}(r_2) f_1^{(2)}(r_1)$$

V.2.15

where C_6^e, C_8^e, and C_{10}^e are the dispersion coefficients for CO and H_2 at their equilibrium bond length, and have the following values (in a.u.)

$$C_6^e = 3.16,\ C_8^e = 790,\ \text{and}\ C_{10}^e = 22\,200,$$

and where

$$f_1^{(2)}(r_1) = 1 + 0.636\,\bar{r}_1$$

$$f_2^{(2)}(r_2) = 1 + 0.391\,\bar{r}_2 .$$

C_6 was obtained from known polarizabilities and from the known C_6 values of the pure components, and the higher dispersion coefficients, C_8, C_{10}, were obtained with the help of sum rule ratios where one assumes equal mean excitation energies for all multipole transitions (Mulder et al. (1980)). It is assumed that C_8 and C_{10} depend on the intermolecular distance to the same measure as C_6.

Equation V.2.15 can be extended for use at intermediate distances by multiplying the right-hand side with a damping function $f_R^{(2)}(R)$ (e.g. see Meath and Allmatt (1979))

$$f_R^{(2)}(R) = \exp\left[-\gamma\,(1.28\,R_m/R - 1)^2\right], \quad R < 1.28\,R_m$$
$$= 1, \quad R \geq 1.28\,R_m$$

V.2.16

where R_m = 7.55 a.u., and γ = 0.7.

The long range multipole interactions are given by

$$V^{(1)LR}_{L_1L_2L}(R, r_1, r_2) = C^{L_1L_2L}_{L_1+L_2+1}(r_1, r_2)\, R^{-(L_1+L_2+1)},$$

V.2.17

where $L_1^{MAX} = 2$, $L_2^{MAX} = 4$, and $L^{MAX} = 7$,

and where

$$C^{L_1 L_2 L}_{L_1+L_2+1}(r_1, r_2) = C^{L_1 L_2 L}_{L_1+L_2+1}(r_{1,eq}, r_{2,eq}) f_1^{(1)}(r_1) f_2^{(1)}(r_2)$$

with $f_x^{(1)} = 1 + (dQ_{Lx}/dr_x)\bar{r}_x$,

where $Q_{Lx}(r)$ is the permanent 2^L-pole moment of molecule X with bond length r. The paper of van Hemert (1983) gives formal expressions for $C^{L_1 L_2 L}_{L_1+L_2+1}(r_{1,eq}, r_{2,eq})$, for other intramolecular distances the coefficients, $C^{L_1 L_2 L}_{L_1+L_2+L}(r_1, r_2)$ must be found by evaluating dQ_{Lx}/dr_x assuming that

$$\frac{dQ_{Lx}}{dr_x} = [Q_{Lx}(r_+) - Q_{Lx}(r_-)]/(r_+ - r_-),$$

where r_+ and r_- are the largest and smallest intramolecular distances considered.

In contrast to the P potential, this is an extremely simple interaction potential to compute. In these calculations only the short range and dispersion terms are employed, and we note that a great deal of the work involved in computing these terms can be done once at each orientation at the initial value of R, and used repeatedly throughout the integration. The functions $A_{L_1 L_2 L}$, $a_{L_1 L_2 L}$, $b_{L_1 L_2 L}$, $c_{L_1 L_2 L}$, $d_{L_1 L_2 L}$, $f_1^{(2)}$, and $f_2^{(2)}$ are all, as one can see, independent of R.

It is worth adding that the potential surface employed by Bačić, Schinke and Diercksen (1984a) (and also 1984b, see Chapter VI.1) should in theory, be the most accurate description of the H_2+CO interaction. It (the 'DK' potential) was constructed from the elaborate SCF calculations of Diercksen and

Kraemer (1984) obtained at three CO bond distances (r_2 = 1.898 a.u., 2.132 a.u., and 2.234 a.u.), and has been shown to provide the most satisfactory description of the rotational excitation of CO by D_2 (see Schinke et al. (1984) - this paper contains a summary of the results obtained using all the three potentials). However as we shall show, principally in Section 5, but also in Chapter VI.4 we doubt that rotational excitation is a sufficiently stringent test of an interaction potential, and using our calculations of the rovibrational excitation of CO by H_2 together with the results obtained by Bačić, Schinke and Diercksen (1984a,b) we are able to make a more 'complete' comparison of the interaction potentials.

3. Description of the System

3.1 IOS Calculations

As already mentioned these IOS calculations are performed with the H_2 molecule constrained in its ground rotational (j_1 = 0) state. For para-H_2 in its ground rotational state the interaction potential takes the form:

$$V^{IOS}(\underline{r}_2, R) = \frac{1}{4\pi} \int V(\underline{r}_1, \underline{r}_2, R)\, d\hat{r}_1 \Big|_{r_1 = r_{1,eq}} . \qquad \text{V.3.1}$$

The internuclear separation of the H_2 molecule is fixed at its equilibrium value reflecting the fact that the probability for the vibrational excitation of H_2 is negligibly small. This has been demonstrated in the breathing sphere (BS) calculations of Drolshagen

and Gianturco (1983). The anisotropy of the interaction potential due to the asymmetry of the H_2 molecule is implicitly averaged out (i.e. only the leading, $P_0(\cos\theta_1)$, term of the interaction potential is retained). The potential of Poulsen (1982), employed in these calculations, may be written

$$V^{IOS}(\underline{r}_2, R) = V_1^{SR} + V_1^{disp} \qquad \text{V.3.2}$$

where $V_1^{SR} = \left(\frac{1}{4\pi}\right)^{\frac{1}{2}} \sum_{i=1}^{4} V_{0i}$

and $V_1^{disp} = -19.18\,eV\,\text{Å}^6\, R^{-6}\left[1 + 0.083\, P_2(\cos\theta_2)\right]$.

The potential of van Hemert (1983) takes the form

$$V^{IOS}(\underline{r}_2, R) = (4\pi)^{3/2} \sum_{L_2} V_{0L_2L_2}(r_2, R)\, A_{0L_2L_2}(\theta_2) \qquad \text{V.3.3}$$

where $A_{0L_2L_2}(\theta_2) = X_{0L_2L_20} P^0_{L_2}(\cos\theta_2)$,

where $X_{0L_2L_20} = \begin{pmatrix} L_2 & 0 & L_2 \\ 0 & 0 & 0 \end{pmatrix} \left[\frac{(2L_2+1)^2}{64\pi^3}\right]^{\frac{1}{2}}$.

The short range contribution is given by

$$V^{SR}_{0L_2L_2}(r_2, R) = \exp\left(a_{0L_2L_2} + b_{0L_2L_2} R + c_{0L_2L_2} R^2 + d_{0L_2L_2} R^3\right) \qquad \text{V.3.4}$$

where $a_{0L_2L_2} = a^{(0)}_{0L_2L_2} + a^{(2)}_{0L_2L_2} \bar{r}_2$ and similar expressions hold for $b_{0L_2L_2}$, $c_{0L_2L_2}$, and $d_{0L_2L_2}$. The parameters $a^{(0)}_{0L_2L_2}$, $a^{(2)}_{0L_2L_2}$, $b^{(0)}_{0L_2L_2}$ ---- are tabulated in Table 2 for $0 \leq L_2 \leq 4$, and $L_1 = 0$. With these parameters V.3.4 is valid in the region $3.5 \leq R \leq 8.5$ a.u. The dispersion contribution is given

TABLE 2

Parameters used in V.3.3 for the description of the inter- and intramolecular distance dependence of the spherical expansion coefficients for the first order potential.

L_1	L_2	L	$a^{(o)}$	$a^{(2)}$	$b^{(o)}$	$b^{(2)}$
0	0	0	0.3389+1	-0.1294+1	-0.1843+1	0.7871+0
0	1	1	-0.3737+1	0.3828+1	0.3622+0	-0.2514+1
0	2	2	0.1235+1	-0.1285+1	-0.1143+1	0.6835+0
0	3	3	-0.2508+1	0.8553+0	-0.3741+0	-0.6706+0
0	4	4	-0.2687+0	0.7675+0	-0.1436+1	-0.6719+0

L_1	L_2	L	$c^{(o)}$	$c^{(2)}$	$d^{(o)}$	$d^{(2)}$
0	0	0	0.9654-1	-0.1253+0	-0.9360-2	0.8422-2
0	1	1	-0.1598+0	0.5038+1	0.1600-2	-0.3011-1
0	2	2	-0.2105-1	-0.1128+0	-0.1504-2	0.8145-2
0	3	3	-0.9517-1	0.1304+0	0.1417-2	-0.5859-2
0	4	4	0.3009-1	0.1405+0	-0.3514-2	-0.7125-2

by

$$V_{000}^{(2)LR}(R,r_2) = -\left[C_6^e R^{-6} + C_8^e R^{-8} + C_{10}^e R^{-10}\right] f_2^{(2)}(r_2). \qquad \text{V.3.5}$$

Both Poulsen (1982) and van Hemert (1983) take the equilibrium intranuclear distances of CO and H_2 to be the experimental values given by Prissette et al. (1978), i.e.

$r_{1,eq}$ 1.4 a.u., and $r_{2,eq}$ 2.132 a.u.

The vibrational basis functions of CO were taken to be Morse oscillator wavefunctions. The normalised Morse eigenfunctions and eigenvalues are given by Mies (1964). See Chapter IV.3 for details.

$$\psi_{v_2}^{MO}(r_2) = A_{v_2} y^{-1/2} W_{\varepsilon/2,\varepsilon/2-1/2-v_2}(y), \qquad \text{V.3.6}$$

$$\varepsilon_{v_2}^{MO} = \frac{4D}{\varepsilon}\left\{\left(v_2+\tfrac{1}{2}\right) - \frac{1}{\varepsilon}\left(v_2+\tfrac{1}{2}\right)^2\right\}, \qquad \text{V.3.7}$$

where $y = \varepsilon e^{-\phi(r_2 - r_{2,eq})}$, $A_{v_2}^2 = \dfrac{(\varepsilon - 1 - 2v_2)\,\phi}{v_2!\,\Gamma(\varepsilon - v_2)}$,

$\varepsilon^2 = 8\mu_{CO} D/\phi^2$, and $D = \hbar\omega\varepsilon/4$,

where ε = 261.22 and $\hbar\omega$ = 0.26898eV (Mies (1964)).

μ_{CO} is the reduced mass of the CO molecule, and takes the numerical value, 12499.6 a.u.

Using these parameters the remaining parameters D, and ϕ are found to be:

D = 0.64556 a.u. $\qquad\qquad$ ϕ = 0.9726472 a.u.

As for the H_2 Morse oscillator wavefunctions, ϕ is quoted to so many figures so that the parameters

used in $\psi^{MO}_{v_2}$ are self-consistent and maintain the orthonormality of the wavefunctions. For CO this is extremely important since we deal with very large and very small numbers

$$\Gamma(\Sigma) \sim 10^{500}, \quad \exp\left(-\tfrac{1}{2}\Sigma_i e^{-(r_2 - r_{2,eq})}\right).$$

The calculation of the wavefunctions is discussed in Appendix 3 at the back of this thesis.

Both the reduced masses of CO, μ_{CO}, and of the H_2 + CO system, μ, were calculated using nuclide masses (Weast (1975)),

H = 1.0079 amu

C = 12 amu

O = 15.9994 amu

where 1 amu is defined as 1/12 of the mass of ^{12}C, and employing the fact that

1 a.u. = electron rest mass energy

= 5.4858026-4 amu

we find that μ_{CO} and μ take the numerical values:

μ_{CO} = 12499.6 a.u.

μ = 3427.79 a.u.

3.2 Breathing Sphere Calculations

Within the BS approximation (Chapter II.4) in addition to neglecting the rotational degree of freedom of H_2, we also neglect the rotational degree of freedom of CO. Therefore we average the interaction potential over both the H_2 and CO orientations, and the potential (isotropic) may be written

$$V^{BS}(\underline{r}_2, R) = \frac{1}{(4\pi)^2} \iint V(\underline{r}_1, \underline{r}_2, R)\, d\hat{r}_1 \Big/ r_1 = r_{1,eq}\, d\hat{r}_2$$

$$= \frac{1}{4\pi} \int V^{IOS}(r_2, R)\, d\hat{r}_2 . \qquad \text{V.3.8}$$

Only the potential of van Hemert (1983) is employed in these calculations, and within the BS approximation takes the extremely simple form

$$V^{BS}(\underline{r}_2, R) = (4\pi)^{3/2} V_{000}(r_2, R)\, A_{000} \qquad \text{V.3.9}$$

where $A_{000} = \left(\frac{1}{4\pi}\right)^{\frac{1}{2}} \left(\frac{1}{64\pi^3}\right)^{\frac{1}{2}}$.

Calculations are performed employing both harmonic and Morse oscillator wavefunctions to describe the vibrational motion of the CO molecule. The details of the Morse oscillator wavefunctions have already been presented in Section 3.1. The harmonic basis functions are the solutions of (see Chapter IV.4).

$$\left[-\frac{\hbar^2}{2\mu_{CO}} \frac{d^2}{dr_2^2} + V^{HO}(r_2) - \mathcal{E}^{HO}_{v_2} \right] \psi^{HO}_{v_2} = 0 \qquad \text{V.3.10}$$

where the harmonic potential is given by

$$V^{HO}(r_2) = \mu_{CO} \omega^2 (r_2 - r_{2,eq})/2 \ ,$$

and the harmonic basis functions may be written

$$\psi^{HO}_{v_2} = \exp\left(-\frac{Q^2}{2}\right) N_{v_2} H_{v_2}(Q) \ ,$$

where $H_{v_2}(Q)$ is a Hermite polynomial, N_{v_2} is a normalization coefficient, and

$$Q = \left(\frac{\mu_{CO}\omega}{\hbar}\right)^{\frac{1}{2}} (r_2 - r_{2,eq}) .$$

The eigenenergies are given by

$$\varepsilon_{v_2}^{HO} = \left(v_2 + \tfrac{1}{2}\right)\hbar\omega .$$

These calculations were performed primarily to make a comparison with the BS results of Drolshagen and Gianturco (1983, 1984), and therefore we take the numerical value of $\hbar\omega$ employed by those authors.

$$\hbar\omega = 0.269 eV$$

The values of the reduced masses μ_{CO} and μ, and the equilibrium intranuclear distances $r_{1,eq}$ and $r_{2,eq}$ are taken to be those employed in the IOS calculations.

4. Numerical Methods

4.1 IOS calculations

IOS calculations have been performed employing the P and VH interaction potentials. The energy range studied in these calculations is $1.1\,\hbar\omega \leqslant E \leqslant 2.9\,\hbar\omega$, were the unit of energy, $\hbar\omega$ = 0.26898eV. The P potential is employed at ten collision energies, $E_n = (0.9 + 0.2n)\hbar\omega$, where n = 1,2,3...10, while the VH potential is employed at just two energies, $1.1\hbar\omega$ and $2.9\hbar\omega$, so that these potential surfaces can be compared. The results of interest are the cross sections for the vibrational deactivation processes, $v_2 = 1$ to $v_2' = 0$, and $v_2 = 2$ to $v_2' = 1$ and 0.

4.1.1 Evaluation of the potential matrix elements

As stated in Chapter IV.4 the evaluation of the potential matrix elements in an IOS calculation require the solution of an integral of the type (cf. II.3.22).

$$V_{v_2,v_2'}(R,\theta_2) = \int_0^\infty \psi_{v_2}^{MO} V(\underline{R},\underline{r}_2,\theta_2)\psi_{v_2'}^{MO} d\underline{r}_2 \quad \text{V.4.1}$$

The evaluation of the Morse oscillator wavefunctions, $\psi_{v_2}^{MO}$, is dealt with in some detail in Appendix 3 at the back of this thesis. We mention that these wavefunctions are employed to describe the vibrational motion of the CO molecule in the majority of the calculations presented in this thesis (i.e. the calculations presented in this chapter, and Chapters VI & VII). As stated in Appendix 3, in addition to the open vibrational channels retained in these calculations, it is necessary, so that the CO molecule is properly described, to include closed channels. When the calculations were started it was not known how many closed channels would be required to achieve satisfactory results. The energy spacing of the vibrational levels of CO is large ($\sim 2000\ cm^{-1}$), and thus one would expect the levels to be weakly coupled by the potential. Thus at the reasonably low collision energies studied in these calculations ($E \lesssim 1eV$) it will probably be necessary to include one (or possibly two) closed channels to obtain satisfactory cross sections for the transitions $v_1 = 1$ to $v_2' = 0$, and $v_2 = 2$ to $v_2' = 1$ and 0 (see for example Gianturco et al. (1980),

this is a study of vibrational excitation in the He + CO system, however, the conclusions regarding the convergence of the results as a function of the number of vibrational channels retained in the coupled equations should be qualitatively similar). However, so that the convergence of the results could be properly tested we employed the first six ($v_2 \leq 5$) Morse wavefunctions in these preliminary calculations, although, as indicated above, it is unlikely that all six wavefunctions will be used in any of the production calculations.

The integral V.4.1 is evaluated by means of a Gauss Legendre quadrature, we must therefore specify the upper and lower limits of integration, r_{max} and r_{min} respectively. Table 3 contains a comparison of potential matrix elements $V_{0v_2'}(R,\theta_2)$ for $\theta_2 = 0°$, $v_2' = 0,5$, and R = 3,10,20 a.u., calculated using the following values of r_{max}, and r_{min}; r_{max} = 2.8 a.u. and r_{min} = 1.4 a.u. or 1.6 a.u., r_{max} = 3.0 a.u. and r_{min} = 1.4 a.u. or 1.6 a.u. The results were evaluated using the P potential, and employing a 96-point Gauss Legendre quadrature which should be extremely accurate for this purpose, and is, we mention, the highest number of points that can be generated using our computer programme. The use of a more efficient quadrature would mean that the points and weights would have to be typed into our computer programme by hand (assuming such high order quadratures exist). As can be seen the results are only weakly

TABLE 3

Comparison of potential matrix elements, $V_{ov_2'}(R,\theta_2)$(a.u.), at $\theta_2 = 0°$ evaluated using different integration ranges over the vibrational co-ordinate, r_2.

(a) r_{min} = 1.4 a.u., r_{max} = 2.8 a.u., (b) r_{min} = 1.4a.u., r_{max} = 3.0a.u., (c) r_{min} = 1.6 a.u., r_{max} = 2.8 a.u., (d) r_{min}= 1.6 a.u., r_{max} = 3.0 a.u.

v_2' =	0	1	2	3	4	5
R(a.u.)						
3.0 (a)	0.420001+0	0.218133-1	-0.904691-4	-0.201919-5	0.669781.6	-0.117672-6
(b)	"	"	"	"	"	"
(c)	"	"	"	"	"	-0.117665-6
(d)	"	"	"	"	"	-0.117672-6
10.0	-0.440384-4	0.206937-6	-0.131319-7	0.118117-8	-0.127741-9	0.158726-10
	"	"	"	"	"	0.158728-10
	"	"	"	"	"	0.158725-10
	"	"	"	"	"	0.158726-10
20.0	-0.545506-6	0.654289-10	-0.433318-11	0.387240-12	-0.420282-13	0.525761-14
	"	"	"	"	"	0.525765-14
	"	"	"	"	"	0.525758-14
	"	"	"	"	"	0.525761-14

dependent upon the limits r_{max} and r_{min}, for the values of the limits used in these calculations. Varying r_{max} or r_{min} by 0.2 a.u. has an insignificant effect on the results at all the values of R shown. The values of R_{max} and R_{min} will be taken to be 1.4 a.u., and 2.8 a.u. respectively in all the calculations employing our Morse wavefunctions.

Employing an integration range, $1.4 \leq r_2 \leq 2.8$ a.u., over the vibrational coordinate, r_2, we evaluated the potential matrix elements using different Gauss Legendre quadratures. In Table 4 we give a comparison of the numerical values of $V_{0v_2'}(R,\theta_2)$ for $v_2' \leq 5$ evaluated using 96-, 64-, and 48- point quadratures in calculations employing the P potential. Results are shown at $\theta_2 = 0°$ and at R = 3,10 20 a.u. The agreement between the results obtained using 96- and 64- point quadratures is very good for $v_2' \leq 5$. A 96- point quadrature will be employed in all our preliminary calculations employing the P potential, and only the directly relevant (open) channels will be retained in the coupled equations. We mention that closed channels should have no effect upon the step size and the integration range. Once these parameters have been determined, the convergence of the results as a function of the number of vibrational channels retained in the calculations will be examined, and Table 4 will be used to 'select' a suitable quadrature for our production calculations employing the P potential.

TABLE 4

Comparison of potential matrix elements, $Vov'_2(R, \theta_2)$(a.u.), at $\theta_2 = 0^\circ$ evaluated using the P potential, and different N-point Gauss Legendre quadratures. (a) N = 96, (b) N = 64, (c) N = 48.

v'_2 =	0	1	2	3	4	5
R(a.u.)						
3.0 (a)	0.420001+0	0.218133-1	-0.904691-4	-0.201919-5	0.669781-6	-0.117672-6
(b)	"	"	"	"	0.669779-6	-0.117740-6
(c)	"	"	"	"	"	-0.117661-6
10.0	-0.440284-4	0.206937-6	-0.131319-7	0.118117-8	-0.127741-9	0.158726-10
	"	"	"	"	"	0.158732-10
	"	"	"	"	"	0.158722-10
20.0	-0.545506-6	0.654289-6	-0.433318-11	0.387240-12	-0.420282-13	0.525761-14
	"	"	"	"	"	0.525776-14
	"	"	"	"	"	0.525755-14

In Table 5 we show a comparison of the potential matrix elements, $V_{0 v_2'}(R,\theta_2)$, for $v_2' \leq 5$, evaluated using the VH potential, using 96-, 64- and 48- point Gauss Legendre quadratures in the range $1.4 \leq r_2 \leq 2.8$ a.u. Results are shown for R = 3,10, and 20 a.u., and at $\theta_2 = 0°$. As for the P potential, very good agreement is found between the results obtained using 96- and 64- point quadratures for $v_2' \leq 5$. We mention that although the r_2 dependence of the H_2 + CO interactions as described by the P and VH potentials (at a given value of R) are probably quite different, both potentials will vary smoothly with r_2, compared to the oscillatory behaviour of the wavefunctions. Thus one would expect the convergence of the potential matrix elements, as a function of the number of quadrature points used to evaluate them, to be similar for the two potentials, as is the case. In all the preliminary calculations employing the VH potential we will employ a 96- point quadrature. It is worth mentioning that it was found that the potential matrix elements, evaluated using the VH potential, diverged for intermolecular separations, $R > 20$ a.u. The reasons for this will be discussed in Section 4.1.2(ii) together with the method employed to alleviate this problem.

4.1.2 Solution of the coupled equations for fixed orientations

In this section we will determine the parameters necessary for the accurate integration of the fixed

TABLE 5

Comparison of potential matrix elements, $V_{0v_2'}(R,\theta_2)$ (a.u.), at $\theta_2 = 0°$ evaluated using the VH potential, and different N-point Gauss Legendre quadratures. (a) N = 96, (b) N = 64, (c) N = 48.

v_2' =	0	1	2	3	4	5
R(a.u.)						
3.0 (a)	0.380968+0	-0.123627-3	0.828817-4	-0.109856-4	0.139727-5	-0.220989-6
(b)	"	"	"	"	"	-0.221008-6
(c)	"	"	"	"	"	-0.220981-6
10.0	-0.374990-4	-0.516173-6	0.581298-7	-0.198180-8	0.222682-9	-0.260251-10
	"	"	"	"	"	-0.260232-10
	"	"	"	"	"	-0.260258-10
20.0	-0.496826-6	-0.104874-7	0.439488-9	-0.310781-10	0.292315-11	-0.333863-12
	"	"	"	"	"	-0.333839-12
	"	"	"	"	"	-0.333873-12

orientation coupled equations in the IOS calculations employing both the P and VH potentials. The parameters of interest are the integration range, $R_{min} \longrightarrow R_{max}$ (where R_{min} and R_{max} are the lower and upper limits of the integration range respectively), and the number of integration steps in the range $R_{min} \longrightarrow R_{max}$ which we will denote by N. Therefore it follows that the step size is given by

$$X = (R_{MAX} - R_{min})/N.$$

The determination of all these parameters will be discussed in some detail, one will recall that the integration of the coupled equations is by far the most important aspect of a scattering calculation (Chapter IV.4) since it accounts for about 95% of the total computer time. In the present calculations the fixed angle coupled equations are solved employing the R-matrix propagator algorithm using propagators corresponding to a constant reference potential (Chapter III.4.4). A fixed step size was used in all the calculations, some of the problems encountered in the use of the step size algorithm were discussed in Chapter IV.4. We first determine the above parameters for the P potential, and then repeat the tests for the VH potential.

4.1.2(i) The P potential

It will be recalled that X is energy dependent (although weakly), this is discussed in Chapter III.4.5 There is, therefore, the possibility that the step size determined at the highest collision energy may not be

sufficiently small to maintain accuracy at some of the lower energies. As discussed in Chapter III as the energy increases, since the energy is only present in the diagonal elements of the coupling matrix, the off diagonal elements of the coupling matrix become less important. Consequently the step size required to maintain accuracy can be increased. We begin by examining the energy dependence of the step size required to maintain accuracy. Since we do not know the values of the parameters R_{min} and R_{max} we employ what we consider to be a generous integration range in which R_{min} = 1 a.u., and R_{max} = 40 a.u. At 40 a.u. vibrational excitation should not be important, in addition a starting value of r_{min} = 1 a.u. should be satisfactory for the H_2 + CO system as this is well in the classically forbidden region.

In Table 6 we present a comparison of results obtained employing several step sizes at the lowest and highest collision energies considered in these calculations (E = 1.1 $\hbar\omega$ and E = 2.9 $\hbar\omega$ respectively) and at L = 0. It is clear that at both energies the results converge monotonically to the correct answer as the number of sectors is increased. This monotonic convergence is an extremely useful feature, Kirkpatrick (1983) reports that if one employs the step size algorithm, the results tend to oscillate. As mentioned previously (Chapter III) approximate potential algorithms require a lot of numerical effort to obtain highly accurate results,

TABLE 6

Comparison of $|S_L(v_2, v_2' | \theta_2)|^2$ obtained using the P potential, and different numbers of steps over the integration range at L = 0.

(a) 195 steps, (b) 390 steps, (c) 780 steps, (d) 3900 steps.

θ_2 =	0^o	90^o	180^o
E = 1.1 ħw			
$v_2 = 1 \rightarrow v_2' = 0$	(a) 0.543172-6	0.792105-7	0.506654-7
	(b) 0.549581-6	0.800173-7	0.512574-7
	(c) 0.550265-6	0.801073-7	0.513210-7
	(d) 0.550392-6	0.801254-7	0.513327-7
E = 2.9 ħw			
$v_2 = 1 \rightarrow v_2' = 0$	(a) 0.547403-2	0.110918-2	0.280446-2
	(b) 0.553915-2	0.111796-2	0.283291-2
	(c) 0.554369-2	0.111832-2	0.283506-2
	(d) 0.554371-2	0.111828-2	0.283534-2
$v_2 = 2 \rightarrow v_2' = 0$	0.100165-5	0.405892-7	0.137423-6
	0.102429-5	0.412326-7	0.140279-6
	0.102593-5	0.412679-7	0.140513-6
	0.102612-5	0.412682-7	0.140541-6
$v_2 = 2 \rightarrow v_2' = 1$	0.726507-3	0.146264-3	0.186629-3
	0.734216-3	0.147415-3	0.188675-3
	0.734834-3	0.147494-3	0.188849-3
	0.734923-3	0.147500-3	0.188861-3

$|S_L(v_2, v_2' | \theta_2)|^2$ in units of $(a.u.)^2$

R_{min} = 1 a.u., R_{max} = 40 a.u.

N.B. The following information may be useful for Chapter VI. If E_T denotes the initial kinetic energy relative to the $v_2 = 1$ $j_1 = 0$ threshold then at 1.1 hw, E_T = 233.5549 cm^{-1}, and at 2.9 hw, E_T = 4138.5631 cm^{-1}.

although they can obtain reasonable accuracy with much less effort. This is reflected in the results of Table 6 where the use of 195 steps gives reasonable results. It is clear from Table 6 that the convergence of the results is similar at both energies (i.e. the step size required to maintain accuracy is not noticeably energy dependent in the energy range we study).

The step size is dependent on the partial wave parameter. As already mentioned, in these calculations the sector R-matrices used were appropriate to approximating the elements of the locally diagonal matrix as constant (III.4.46). Therefore the step size should be sufficiently small so that the coupling matrix (including the $L(L + 1)/R^2$ term) can be accurately approximated as constant within the sector. As discussed in Chapter III the rate of change of the term $L(L + 1)/R^2$ increases with L and therefore, a step size which is sufficiently small to accurately calculate results for the highest L value will also be sufficient for the lower values.

In Table 7 we show a comparison of results obtained employing different step sizes at E = 2.9$\hbar\omega$ and at L = 30, 50, 70, 90. Results are shown for $\theta_2 = 90°$. At the two highest values of L shown we have omitted the values of $|S_L(v_2, v_2'/\theta_2)|^2$ for $v_2 = 2$ to $v_2' = 0$ and 1 since they are extremely small, and it is impossible to maintain accuracy (i.e. we are dealing with numerical zeros). Notice that the values of $|S_L(v_2, v_2'/\theta_2)|^2$ for

TABLE 7

Comparison of $|S_L(v_2, v_2' | \theta_2)|^2$ (a.u.)^2 obtained using the P potential, and different numbers of steps over the integration range at E = 2.9 eV (a) 195 steps, (b) 390 steps, (c) 780 steps, (d) 3900 steps. $\theta_2 = 90°$

L =		30	50	70	90
$v_2 = 1 \rightarrow v_2' = 0$	(a)	0.210190-3	0.361491-5	0.362019-9	0.237123-14
	(b)	0.211469-3	0.362395-5	0.360206-9	0.235448-14
	(c)	0.211498-3	0.362187-5	0.359454-9	0.234923-14
	(d)	0.211480-3	0.362078-5	0.359182-9	0.234742-14
$v_2 = 2 \rightarrow v_2' = 0$		0.273617-9	0.879154-16		
		0.276877-9	0.877852-16	———	———
		0.276902-9	0.875555-16		
		0.276852-9	0.874628-16		
$v_2 = 2 \rightarrow v_2' = 1$		0.520620-5	0.972781-10		
		0.523568-5	0.968915-10	———	———
		0.523614-5	0.966936-10		
		0.523563-5	0.966202-10		

R_{min} = 1 a.u., R_{max} = 40 a.u.

these transitions are already extremely small at L = 50. In view of the results presented in Table 7 we claim that the step size required to maintain accuracy is weakly dependent upon L, for the range of L values considered in these calculations. At E = 2.9 $\hbar\omega$, if one considers all partial waves with $L \leq 80$, this is sufficient to evaluate integral rotationally summed cross sections converged to much less than 1% for all the vibrational transitions studied.

As mentioned in ChapterIII we begin the integration in the classically forbidden region (i.e. we start the integration at a point where the interaction potential is much greater than the collision energy). Thus a value of R_{min} determined at E = 2.9 $\hbar\omega$ and L = 0 should be satisfactory at all other partial waves, and at all energies less than 2.9 $\hbar\omega$. The convergence of the results as a function of R_{min} was examined keeping R_{max} constant at 40 a.u., and employing a step size of 0.01 a.u. (corresponding to N = 3900 in Table 6). The results of our calculations are shown in Table 8. As expected R_{min} = 1 a.u. is more than sufficient to maintain accuracy, the results obtained with R_{min} = 1,2 and 3 a.u. are in excellent agreement for the transitions shown.

Determining satisfactory values for R_{max} is rather more difficult. Essentially at a given collision energy R_{max} is determined by two factors. If the asymptotic boundary condition is fitted in terms of Spherical Bessel functions (Chapter III) the effect of the centrifugal

TABLE 8

Comparison of $|S_L(v_2, v_2' | \theta_2)|^2$ (a.u.)^2 obtained using the P potential, and different values of R_{min} at E = 2.9 eV and L = 0.

(a) R_{min} = 1 a.u., (b) R_{min} = 2 a.u., (c) R_{min} = 3 a.u.

θ_2 =		0^o	90^o	180^o
$v_2=1 \rightarrow v_2'=0$	(a)	0.554371-2	0.111828-2	0.283534-2
	(b)	"	"	"
	(c)	"	"	"
$v_2=2 \rightarrow v_2'=0$		0.203623-5	0.412682-7	0.140541-6
		"	"	"
		"	"	"
$v_2=2 \rightarrow v_2'=1$		0.734923-3	0.147500-3	0.188871-3
		"	"	"
		"	"	"

R_{max} = 40 a.u., X = 0.01 a.u.

potential is implicitly included in the Bessel functions. Thus we need to integrate the coupled equations to a value of R_{max} at which the interaction potential has become negligible. Therefore one could determine R_{max} at E = 1.1 $\hbar\omega$ and L = 0, however there is another factor, as L increases one finds that R_{max} increases (e.g. see Table 4, Chapter IV.4). When L increases the classical turning point moves to a larger R value. One must fit the boundary condition in the classically allowed region where the solution to the Schrödinger equation is a linear combination of oscillatory functions (e.g. III.4.24) and not an exponentially decaying function.

In Table 9 we show the convergence of $|S_L(v_2, v_2'|\theta_2)|^2$ as a function of R_{max} at E = 1.1 $\hbar\omega$ and L = 0, 10, and 20. The results were obtained maintaining R_{min} = 1 a.u., and X = 0.01 a.u. It is clear that if one maintains a value of R_{max} = 25 a.u. at all the values of L shown then one may obtain results converged to within a few per cent. We note that although we maintain this value of R_{max} for partial waves with L $\geq$ 20, it becomes progressively more difficult to maintain accuracy since the values of $|S_L(v_2, v_2'|\theta_2)|^2$ become extremely small. (Indeed, at this energy we found that to evaluate an integral rotationally summed cross section converged to within 1% we only needed to consider all L $\lesssim$ 30).

In Table 10 we show the results of calculations at E =2.9 $\hbar\omega$ and L = 0, 50, 70, and 90 at one CO orientation,

TABLE 9

Comparison of $|S_L(v_2, v_2'|\theta_2)|^2$ (a.u.)^2 obtained using the P potential, and different values of R_{max} at E = 1.1 ħw.

(a) R_{max} = 20 a.u., (b) R_{max} = 25 a.u., (c) R_{max} = 30 a.u.

θ_2 =		0°	90°	180°
L				
0	(a)	0.550275-6	0.801278-7	0.513012-7
	(b)	0.550410-6	0.801220-7	0.513555-7
	(c)	0.550405-6	0.801263-7	0.513326-7
10		0.188512-6	0.224245-7	0.206638-7
		0.188535-6	0.224223-7	0.206622-7
		0.188527-6	0.224235-7	0.206617-7
20		0.119863-8	0.531074-10	0.563807-9
		0.119793-8	0.530723-10	0.566084-9
		0.119787-8	0.530704-10	0.566042-9

R_{min} = 1 a.u., X = 0.01 a.u.

TABLE 10

Comparison of $|S_L(v_2 v_2' | \theta_2)|^2$ (a.u.)^2 obtained using the P potential, and different values of R_{max} at E = 1.9 and 2.9 ħw at $\theta_2 = 0°$.

(a) R_{max} = 20 a.u., (b) R_{max} = 25 a.u., (c) R_{max} = 30 a.u.

L =		0	50	70	90
E = 2.9 ħw					
$v_2=1 \rightarrow v_2'=0$	(a)	0.554382-2	0.109423-3	0.656646-7	0.279149-12
	(b)	0.554372-2	0.109421-3	0.656648-7	0.276843-12
	(c)	0.554371-2	0.109421-3	0.656651-7	0.276696-12
$v_2=2 \rightarrow v_2'=0$		0.102618-5	0.558360-12	———	———
		0.102612-5	0.558315-12		
		0.102612-5	0.558320-12		
$v_2=2 \rightarrow v_2'=0$		0.734951-3	0.204087-7	———	———
		0.734922-3	0.204074-7		
		0.734924-3	0.204076-7		
E = 1.9 ħw					
$v_2=1 \rightarrow v_2'=0$	(a)	0.367333-3	0.675062-8	———	———
	(b)	0.367322-3	0.674968-8		
	(c)	0.367326-3	0.674968-8		

R_{min} = 1 a.u., X = 0.01 a.u.

$\theta_2 = 0°$. The results illustrate that as the partial wave parameter increases the integration range must be extended, however notice that for the range of L values considered the increase in R_{max} is not significant. A value of R_{max} = 25 a.u. is able to converge the results to within a few per cent at all the L values shown (and for all the transitions shown). In addition one may see that the value of R_{max} does not increase significantly with decreasing energy (e.g. compare E = 2.9 $\hbar\omega$ and L = 0 with the results for E = 1.1 $\hbar\omega$ and L = 0 in Table 9). In Table 10 we also show results for E = 1.9 $\hbar\omega$ and L = 0, and 50 (the value of $|S_L(v_2)v_2'|\theta_2)|^2$ decreases rapidly for L > 50). Again a value of R_{max} = 25 a.u. is satisfactory at this energy. We note that the convergence of the results is similar in all orientations, as is illustrated in Table 9. In practice we studied the dependence of the results on R_{max} at all the ten energies considered in the calculations, the results in Tables 9 and 10 are intended to illustrate that, as already mentioned, we found that R_{max} does not vary significantly within the range of L values or the range of energies studied in these calculations. In conclusion, in view of the convergence tests presented for R_{min}, R_{max}, and X we consider that satisfactory results may be obtained by setting R_{min} = 2 a.u., R_{max} = 25 a.u., and X = 0.05 a.u. (corresponding to N = 780 steps in Table 6).

4.1.2(ii) The VH Potential

As already mentioned in this section, it was found that for intermolecular separations $R \gtrsim 20$ a.u. the potential matrix elements calculated using the VH potential are divergent. A detailed examination of this potential indicated that the short range (0,1,1) term, $V^{SR}_{0,1,1}$ is responsible for this unphysical behaviour. The VH potential employed in these calculations takes a relatively simple form (V.3.3), nevertheless it is easy to make a typing error in one of the expansion parameters given in Table 2. However we found no errors in the parameters (or the potential routines), and it is worth mentioning that using our routines we have successfully reproduced the plots of $V^{SR}_{L_1L_2L}$ versus R given for the equilibrium separations $r_{1,eq}$ and $r_{2,eq}$ in the paper of van Hemert (1983).

In Table 11 we show the numerical values of the short range terms, $V^{SR}_{L_1L_2L}$, for $L_1 = 0$ and $L_2 = 0,1,2,3,4$ at R = 10,15,20, and 25 a.u., and at $\bar{r}_2 = 0.0, \pm 0.54$ a.u. The (0,1,1) term starts to diverge at relatively small values of $R(\gtrsim 15$ a.u.), at small values of $\bar{r}_2$ (e.g. -0.54 a.u.). Note however, that these small values of $\bar{r}_2$ are not particularly important, since the vibrational basis functions (for $v_2 \leq 5$) are extremely small at such values of $\bar{r}_2$. As mentioned above, only for intermolecular separations $R \gtrsim 20$ a.u. did the potential matrix elements start to diverge (and hence have a significant effect

R(a.u.) =		10.0	15.0	20.0	25.0
$\bar{r}_2$(a.u.)	(a)	0.10328895135E-06	0.44651798320E-17	0.17731623177E-37	0.18819681775E-72
-0.54	(b)	0.89181315887E-06	0.48107510704E-07	0.33816632006E+00	0.21377411237E+21
	(c)	0.27309239130E-06	0.16617378719E-13	0.12322041009E-25	0.13130591477E-44
	(d)	0.28513241106E-06	0.14647481829E-10	0.58007891098E-14	0.55530652125E-15
	(e)	0.15786132167E-06	0.53612345713E-11	0.39876005497E-16	0.84409404026E-22
		0.39396648292E-06	0.15132753307E-14	0.51817243284E-30	0.14137775107E-55
0		0.50687571575E-06	0.29288393226E-12	0.20986346212E-20	0.61912554353E-30
		0.10115770593E-05	0.67447951323E-11	0.53234243276E-18	0.16098364723E-27
		0.58655464608E-06	0.17825786984E-10	0.11267771610E-15	0.42876853671E-21
		0.26761940403E-06	0.20809429159E-11	0.26831778578E-19	0.41124665232E-31
		0.15026736900E-05	0.51285778236E-12	0.15142588328E-22	0.10620619805E-38
0.54		0.28809060357E-06	0.17831102986E-17	0.13023967828E-40	0.0
		0.37470401212E-05	0.27376316173E-08	0.22998500451E-10	0.19736913391E-10
		0.12066195897E-05	0.21693741309E-10	0.21887138913E-17	0.33106482823E-27
		0.45369026848E-06	0.80771012003E-12	0.18054575243E-22	0.20036133532E-40

Table 11 The variation of the short range terms, $V^{SR}_{0,L_2,L}$ (a.u.) with respect to the intermolecular separation, R.
(a) $L_2 = 0$, (b) $L_2 = 1$, (c) $L_2 = 2$, (d) $L_2 = 3$, (e) $L_2 = 4$.
The $V^{SR}_{0,1,1}$ and $V^{SR}_{0,3,3}$ terms are underlined.

on the values of the S-matrices). It is worth mentioning that in their study of the rotational excitation of CO by D_2 using the VH potential, Billing and Poulsen (1983) found that several of the short range terms are divergent, namely (0,1,1), (0,3,3), (2,2,0), and (2,2,2), however the (0,1,1) and (0,3,3) terms only diverged for $R > 60$ a.u. Since they study rotational excitation they must maintain $\bar{r}_2 = 0$, and indeed it is clear from Table 11, that for the (0,1,1) term the problem becomes less severe as $\bar{r}_2$ increases. In addition notice that the rate of decrease of the (0,3,3) term is significantly slower than the other terms (except the (0,1,1) term) at $\bar{r}_2 = -0.54$ a.u.

In Table 12 we compare the values of $|S_L(v_2, v_2'|\theta_2)|^2$ evaluated using the full IOS potential given by V.3.3 at all values of R in the integration range with results obtained with the (0,1,1) term set to zero for $R > 15$ a.u. The calculations were performed employing a small step size (0.01 a.u.), and maintaining $R_{min} = 1$ a.u. and $R_{max} = 20$ a.u. Results are shown for $E = 1.1$ and 2.9 $\hbar\omega$ at $L = 0$ and at $\theta_2 = 0^o$. As may be seen the restriction placed on $V^{SR}_{0,1,1}$ for $R > 15$ a.u. has no significant effect on the results. In addition it is apparent that no more than one closed channel need be included at the energies studied in these calculations, the convergence of the results as a function of the vibrational basis will be discussed in more detail in Section 4.1.3, however we mention at

TABLE 12

A comparison of $|S_L(v_2, v_2'|\theta_2)|^2$ (a.u.)^2 evaluated using the VH potential at L = 0 and $\theta_2 = 0^\circ$.

(a) Full IOS potential given by V.3.3.

(b) $V^{SR}_{0,1,1}(r_2, R) = 0$ for $15 < R \leq 20$ a.u.

E ($\hbar\omega$) =	1.1	2.9		
Number of rotational channels	$v_2 = 1 \rightarrow v_2' = 0$	$v_2 = 1 \rightarrow v_2' = 0$	$v_2 = 2 \rightarrow v_2 = 1$	$v_2 = 2 \rightarrow v_2 = 0$
2	(a) 0.97323129-8 (b) 0.97322960-8	———	———	———
3	0.11098171-7 0.11098153-7	(a) 0.24431415-3 (b) 0.24431415-3	0.24601365-4 0.24601360-4	0.15799795-8 0.15799805-8
4	0.11697055-7 0.11697038-7	0.24485070-3 0.24485060-3	0.30720869-4 0.30720863-4	0.18986246-8 0.18986249-8
5	———	0.24445117-3 0.24451165-3	0.30868157-4 0.30868151-4	0.19078414-8 0.19078418-8

this stage that convergence is found to be worst at the 'collinear' orientations, $\theta_2 = 0^o$ and 180^o (see Table 20, Section 4.1.3). In conclusion we consider that setting $V^{SR}_{0,1,1} = 0$ for $R > 15$ a.u. would appear to a reasonable solution to the above problem.

It is possible that there are a number of typographical errors in the paper of van Hemert (1983), however we doubt this. One will recall that using the parameters of Table 2, the short range potential of van Hemert (1983) is valid in the range $3.5 \geq R \geq 8.5$ a.u., and therefore it is more likely that the potential fit is 'breaking down' for $R > 8.5$ a.u.

In Table 13 we examine the energy dependence of the sector width, a comparison of results obtained employing several step sizes at E = 1.1 and 2.9 $\hbar\omega$ and at L = 0 is shown. Generally speaking the convergence of the results as a function of the number of steps in the integration range is less satisfactory than for those evaluated employing the P potential (cf. Table 6), however notice that the matrix elements are much smaller in the present calculations. Indeed, it is extremely difficult to maintain accuracy at $\theta_2 = 180^o$, where the matrix elements are very small. It is not clear why the magnitude of $|\mathcal{L}(v_2, v_2'|\theta_2)|^2$ should be so strongly diminished at this orientation, as mentioned above we believe that this potential is programmed correctly. Nevertheless, such small elements should not be particularly important, the contributions

TABLE 13

Comparison of $|S_L(v_2, v_2'|\theta_2)|^2$ (a.u.)^2 evaluated using the VH potential, and different numbers of steps over the integration range at L = 0.

(a) 390 steps, (b) 780 steps, (c) 3900 steps.

θ_2 =	0^o	90^o	180^o
E = 1.1 $\hbar\omega$			
$v_2=1 \rightarrow v_2'=0$	(a) 0.966552-8	0.491236-7	0.446622-11
	(b) 0.968689-8	0.492512-7	0.482391-11
	(c) 0.969240-8	0.492872-7	0.492373-11
E = 2.9 $\hbar\omega$			
$v_2=1 \rightarrow v_2'=0$	(a) 0.243481-3	0.424361-3	0.129801-5
	(b) 0.244149-3	0.425246-3	0.130127-5
	(c) 0.244307-3	0.425435-3	0.130174-5
$v_2=2 \rightarrow v_2'=0$	0.156833-8	0.586880-8	0.411421-13
	0.157716-8	0.589237-8	0.415443-13
	0.157926-8	0.589720-8	0.415823-13
$v_2=2 \rightarrow v_2'=1$	0.244994-4	0.548479-4	0.408167-7
	0.245715-4	0.549541-4	0.409302-7
	0.245887-4	0.549747-4	0.409416-7

R_{min} = 1 a.u., R_{max} = 40 a.u.

at $\theta_2 \approx 0^\circ$ and $\theta_2 \approx 90^\circ$ are a factor of $\sim 10^3$ larger and are therefore the major contributors (even despite the small sin θ_2 weight factor at $\theta_2 \approx 0^\circ$). As for the P potential, we conclude that the step size is not highly dependent on the energy.

In Table 14 we study the L dependence of the step size, results are shown at E = 2.9 $\hbar\omega$ and L = 30, 50, and 70 at $\theta_2 = 90^\circ$. At $L > 70$ the results become extremely small, and it is impossible to maintain accuracy. The results indicate that the VH potential does not only produce results which are very different in magnitude to these evaluated using the P potential, but also the L distribution of results is probably quite different for the two potentials, indeed we mention that the range of L values needed to be considered at a given energy is slightly smaller for the VH potential. For example, at E = 2.9 $\hbar\omega$ we require all $L \leq 70$, compared with $L \leq 80$ needed in the same calculation employing the P potential (to ensure that the integral cross sections are converged to within 1%). From the results presented in Tables 13 and 14 we conclude that a step size of 0.05 a.u. (corresponding to 780 steps in Table 14) will be satisfactory to evaluate the results converged to within a few percent at the energies studied (E = 1.1 and 2.9 $\hbar\omega$) and at the values of L studied ($L \leq 70$).

As for the P potential we determine a suitable value for R_{min} at the highest collision energy, and lowest partial wave. The results of our calculations

TABLE 14

Comparison of $|S_L(v_2, v_2' | \theta_2)|^2$ (a.u.)^2 obtained using the VH potential, and different numbers of steps over the integration range at E = 2.9 ħw.

(a) 390 steps, (b) 780 steps, (c) 3900 steps. $\theta_2 = 90^\circ$

L =		30	50	70
$v_2 = 1 \rightarrow v_2' = 0$	(a)	0.939152-4	0.160521-5	0.134979-9
	(b)	0.940646-4	0.160591-5	0.134829-9
	(c)	0.940927-4	0.160586-5	0.134526-9
$v_2 = 2 \rightarrow v_2' = 0$		0.478953-10	0.216384-16	
		0.480228-10	0.216324-16	———
		0.480441-10	0.359366-16	
$v_2 = 2 \rightarrow v_2' = 1$		0.202576-5	0.194849-10	
		0.202800-5	0.194594-10	———
		0.202830-5	0.193257-10	

at E = 2.9 $\hbar\omega$ and L = 0 are shown in Table 15. The results evaluated maintaining R_{min} = 1,2 and 3 a.u. are in excellent accord. A value of R_{min} = 2 a.u. will be employed in all our calculations.

In Table 16 we examine the convergence of the results as a function of R_{max} at E = 1.1 $\hbar\omega$ and L = 0, and 10. We mention that at this energy we only require partial waves with $L \lesssim 20$, the results shown in Table 16 indicate that a value of R_{max} = 25 a.u. is satisfactory at all the values of L considered at this energy. Notice that we have omitted the results at $\theta_2 = 180^o$, because of the small values of $|S_L(v_2, v_2' | \theta_2)|^2$ at this orientation it is difficult to maintain accuracy. In Table 17 we show the results of calculations at E = 2.9 $\hbar\omega$ and at L = 0, 50, and 70 at $\theta_2 = 0^o$. We notice that, as for the results evaluated using the P potential, the value of R_{max} required to maintain accuracy does not vary significantly with L. Although E = 1.1 and 2.9 $\hbar\omega$ are the only collision energies studied in these calculations, the numerical methods developed in this section are used for our breathing sphere calculations (Section 4.2). Thus we also show results evaluated at E = 1.9 $\hbar\omega$ and L = 0, 50 in Table 17, to give a better idea of the energy dependence of R_{max}. As can be seen from Tables 16 and 17, the value of R_{max} required to evaluate satisfactory results does not vary significantly with either the collision energy or the partial wave parameter.

TABLE 15

Comparison of $|S_L(v_2, v_2' | \theta_2)|^2$ (a.u.)^2 obtained using the VH potential, and different values of R_{min} at $E = 2.9\ \hbar\omega$ and $L = 0$.

(a) $R_{min} = 1$ a.u., (b) $R_{min} = 2$ a.u., (c) $R_{min} = 3$ a.u.

θ_2 =		0^o	90^o	180^o
$v_2=1 \rightarrow v_2'=0$	(a)	0.244307-3	0.425435-3	0.130173-5
	(b)	"	"	"
	(c)	"	"	"
$v_2=2 \rightarrow v_2'=0$		0.157926-8	0.589720-8	0.415623-13
		"	"	"
		"	"	"
$v_2=2 \rightarrow v_2'=1$		0.245887-4	0.549747-4	0.409416-7
		"	"	"
		"	"	"

$R_{max} = 40$ a.u., $X = 0.01$ a.u.

TABLE 16

Comparison of $|S_L(v_2, v_2' | \theta_2)|^2$ (a.u.)^2 obtained using the VH potential, and different values of R_{max} at $E = 1.1\ \hbar\omega$.

(a) $R_{max} = 20$ a.u., (b) $R_{max} = 25$ a.u., (c) $R_{max} = 30$ a.u

θ_2 =		0^o	90^o
L			
0	(a)	0.973249-8	0.498876-7
	(b)	0.976812-8	0.491184-7
	(c)	0.969240-8	0.492872-7
10		0.319256-8	0.136018-7
		0.337400-8	0.136823-7
		0.334605-8	0.135893-7

$R_{min} = 1$ a.u., $X = 0.01$ a.u.

TABLE 17

Comparison of $|S_L(v_2, v_2'|\theta_2)|^2$ (a.u.)^2 obtained using the VH potential, and different values of R_{max} at E = 1.9 and 2.9 $\hbar\omega$ at $\theta_2 = 0^o$.

(a) R_{max} = 20 a.u., (b) R_{max} = 25 a.u., (c) R_{max} = 30 a.u.

L =		0	50	70
E = 2.9 $\hbar\omega$				
$v_2=1 \rightarrow v_2'=0$	(a)	0.244316-3	0.702591-5	0.109478-7
	(b)	0.244305-3	0.703090-5	0.106089-7
	(c)	0.244307-3	0.703027-5	0.106144-7
$v_2=2 \rightarrow v_2'=0$		0.157998-8	0.332031-14	———
		0.157962-8	0.326795-14	
		0.157926-8	0.317196-14	
$v_2=2 \rightarrow v_2'=1$		0.245012-4	0.168242-8	———
		0.245971-4	0.172874-8	
		0.245887-4	0.169934-8	
E = 1.9 $\hbar\omega$				
$v_2=1 \rightarrow v_2'=0$	(a)	0.125501-4	0.522292-9	———
	(b)	0.125585-4	0.583155-9	
	(c)	0.125570-4	0.598745-9	

In this respect the conclusions are qualitatively similar to those drawn for the P potential, although as may be seen the VH potential will probably produce rather different numerical values for the cross sections. It is, however, difficult to be conclusive at this stage since not all the L values have been examined, and the L distributions of the partial cross sections appear to be very different for the two potentials (cf. Tables 16 and 17 with Tables 9 and 10). Also it is not clear (despite the strong θ_2 dependence of the S-matrices as computed using the VH potential) that when the angular integration (over θ_2) has been carried out, that the potentials will produce significantly different results at a given value of L (at a given collision energy). For example, the two potentials produce rather different results at $\theta_2 \approx 180^\circ$, however the sin θ_2 weighting at such orientations is extremely small (and is zero at 180°), and therefore it is unlikely that this significant difference in the single orientation results will have such a profound effect upon the final results. The values of the parameters R_{min}, R_{max}, and X used in these calculations are identical to those used for the P potential (i.e. R_{min} = 2 a.u., R_{max} = 25 a.u., and X = 0.05 a.u.).

4.1.3 Description of the CO molecule

In this section we examine the convergence of the results with respect to the number of vibrational channels retained in the fixed angle coupled equations.

4.1.3(i) The P potential

In Table 18 we present the results of calculations performed at two collision energies, E = 1.9 $\hbar\omega$ and 2.9 $\hbar\omega$. One would expect convergence to be worst at these collision energies, since 1.9 $\hbar\omega$ and 2.9 $\hbar\omega$ are just below the v_2 2 and v_2 3 thresholds respectively. Results are shown at three CO orientations, θ_2 = 0°, 90°, 180°. One will recall that closed channels are required to accurately describe the deformation of the target (Chapter II.4.6). Since in the present study the H_2 molecule is a spherically symmetric particle, one may think of the collision as one involving an atom and a diatomic molecule, rather than two diatomic molecules. Thus the collinear approaches are given by θ_2 = 0° and 180°, physically one would expect the deformation of the target to be greatest at these collinear ('head on') collisions, certainly this would appear to be reflected in the results shown in Table 18.

It is clear from the results presented in Table 18 that to obtain satisfactory results, converged to within 1%, for all the transition shown, and at all the energies studied in these calculations, it is necessary to include all the open, and one closed vibrational channel. This is confirmed for the $v_2 = 1$ to $v_2' = 0$ process by BSD in their study of the CO + $H_2(j_1 = 0)$ system using the DK potential.

TABLE 18

Comparison of $|S_L(v_2, v_2'|\theta_2)|^2$ obtained using the P potential, and retaining different numbers of vibrational channels in the coupled equations at L = 0.

(a) 2 channels, (b) 3 channels, (c) 4 channels, (d) 5 channels.

θ_2 =		0°	90°	180°
E = 1.9 $\hbar\omega$				
$v_2=1 \rightarrow v_2'=0$	(a)	0.367282-3	0.659697-4	0.102243-3
	(b)	0.424871-3	0.672928-4	0.141248-3
	(c)	0.425085-3	0.672930-4	0.141544-3
E = 2.9 $\hbar\omega$				
$v_2=1 \rightarrow v_2'=0$	(b)	0.554327-2	0.111831-2	0.283510-2
	(c)	0.555726-2	0.111832-2	0.285922-2
	(d)	0.555693-2	0.111825-2	0.285917-2
$v_2=2 \rightarrow v_2'=0$		0.102593-5	0.412676-7	0.140512-6
		0.126618-5	0.420444-7	0.218819-6
		0.127161-5	0.420880-7	0.221177-6
$v_2=2 \rightarrow v_2'=1$		0.734842-3	0.147493-3	0.188848-3
		0.908000-3	0.150288-3	0.305620-3
		0.911883-3	0.150453-3	0.308867-3

$|S_L(v_2, v_2'|\theta_2)|^2$ in units of $(a.u.)^2$

It will be recalled that in Section 4.1.1 we compared the values of the potential matrix elements evaluated using different Gauss Legendre quadratures. In Table 4 results are shown calculated using 96-, 64-, and 48-point quadratures. It may be seen that for the vibrational states required in these calculations, $v_2 \leq 3$, the agreement between the results evaluated using these quadratures is excellent (even at R = 20 a.u. where the interaction potential is extremely small and it is difficult to maintain accuracy). Since we employ an approximate potential algorithm, no explicit reference to the potential matrix elements is required after the calculation at the initial partial wave, therefore we are able to generate a large number of results with very little numerical effort. Notice that we have already shown that the step size required to maintain accuracy does not vary significantly with L. In the present calculations we chose to employ a 96- point Gauss Legendre quadrature, this means that the calculation at the initial partial wave is quite expensive, in Table 19 we give the approximate computer times required for the evaluation of $V_{v_2,v_2'}(R,\theta_2)$ at 460 values of R for $v_2(v_2') \leq 3$ using the IBM 370/168 computer at NUMAC, however such a quadrature ensures extremely high numerical accuracy with no increase in computer time at subsequent partial waves.

TABLE 19

Comparison of approximate computer times required to evaluate $V_{v_2,v_2'}(R,\theta_2)$ for $v_2(v_2') \leq 3$ at 460 values of R using the IBM 370/168 at NUMAC employing different N-point Gauss Legendre quadratures.

(a) P Potential, (b) VH potential.

N		48	64	96
Time(s)	(a)	15.27	19.24	27.24
	(b)	9.41	11.35	15.22

4.1.3(ii) The VH Potential

In Table 20 we examine the convergence of $|S_L(v_2, v_2'/\theta_2)|^2$ with respect to the number of vibrational channels retained in the coupled equations. Results are shown at E = 1.1, 1.9, and 2.9 $\hbar\omega$. The convergence of the results as a function of increasing v_2 is in qualitative agreement with the results obtained with the P potential, notice it is extremely difficult to maintain accuracy at E = 1.1 $\hbar\omega$, and $\theta_2 = 180^\circ$ because of the small matrix elements at this orientation, as mentioned previously, the elements at $\theta_2 \approx 0^\circ$, and 90° are however a factor of $\sim 10^3$ larger, and would be expected to be the major contributions to the final results. Thus we only need consider vibrational channels with $v_2(v_2') \leq 3$ in these calculations, and as for the P potential, excellent agreement is found between the values of $V_{v_2, v_2'}(R, \theta_2)$ evaluated employing the three Gauss Legendre quadratures (96-, 64-, and 48- points). Again we take advantage of the approximate potential algorithm and employ a 96-point quadrature. Also given in Table 19 are the approximate computer times required for the evaluation of $V_{v_2, v_2'}(R, \theta_2)$ at 460 values of R for $v_2(v_2') \leq 3$ using the IBM 370/168 computer at NUMAC in calculations employing the VH potential. Notice that the simple form of the VH potential is reflected in the relative magnitude of the computer times required by the two potentials.

In Table 21 we give the approximate computer times required at the initial and subsequent partial waves, to integrate the fixed angle coupled differential equations

TABLE 20

Comparison of $|S_L(v_2, v_2'|\theta_2)|^2$ obtained using the VH potential, and retaining different numbers of vibrational channels in the coupled equations at L = 0.

(a) 2 channels, (b) 3 channels, (c) 4 channels, (d) 5 channels.

θ_2 =		0^o	90^o	180^o
E = 1.1 $\hbar\omega$				
$v_2=1 \rightarrow v_2'=0$	(a)	0.966436-8	0.490959-7	0.329766-11
	(b)	0.111314-7	0.552493-7	0.422946-11
	(c)	0.111222-7	0.553562-7	0.512090-11
E = 1.9 $\hbar\omega$				
$v_2=1 \rightarrow v_2'=0$	(a)	0.125488-4	0.283992-4	0.299236-7
	(b)	0.146779-4	0.323814-4	0.376952-7
	(c)	0.146832-4	0.323900-4	0.376894-7
E 2.9 $\hbar\omega$				
$v_2=1 \rightarrow v_2'=0$	(b)	0.244146-3	0.425232-3	0.130173-5
	(c)	0.244344-3	0.425471-3	0.130173-5
	(d)	0.244317-3	0.425437-3	0.130121-5
$v_2=2 \rightarrow v_2'=0$		0.157751-8	0.589139-8	0.408489-13
		0.189566-8	0.704364-8	0.499670-13
		0.190486-8	0.706919-8	0.593993-13
$v_2=2 \rightarrow v_2'=1$		0.245799-4	0.549464-4	0.410020-7
		0.306938-4	0.661795-4	0.553685-7
		0.308410-4	0.664163-4	0.560729-7

TABLE 21

A comparison of approximate computer times required to solve the fixed angle coupled equations at one orientation using the Cray-1 computer. Times are shown for both the P and VH potentials at the initial and subsequent partial waves.

(a) 3 vibrational channels, (b) 4 channels

	Time(s)	
	Initial partial wave	Subsequent partial waves
P potential	(a) 3.29	0.19
	(b) 3.40	0.25
VH potential	(a) 1.74	0.19
	(b) 1.90	0.25

460 steps in the range $2.0 \lesssim R \lesssim 25.0$ a.u.

at one orientation using the Cray-1 computer. Three and four vibrational channels are retained, and approximately 460 steps of fixed length are taken. As can be seen it is possible to generate results at subsequent partial waves with very little numerical effort. Notice, in addition, that the computer time required at subsequent partial waves is independent of the form of the interaction potential.

4.2 Breathing Sphere Calculations

In these calculations the CO molecule is approximated as a breathing sphere, it is considered to be a spherically symmetric scattering partner which interacts with the H_2 molecule via an effective, averaged potential (V.3.8) which is independent of their relative orientations. Essentially the BS approximation is a very simple (one orientation) version of the IOS approximation. Since all CO orientations are equivalent, one only needs to solve the fixed angle coupled equations at one orientation. One will recall that in the IOS approximation rotationally summed cross sections are evaluated using (cf. II.3.30).

$$\sum_{j_2'} \sigma(v_2 j_2 = 0 \rightarrow v_2' j_2') = \sigma(v_2 \rightarrow v_2')$$

$$= \frac{\pi}{k^2_{v_2 j_2 = 0}} \sum_{l} (2l+1) \frac{1}{2} \int_0^{\pi} |T_l(v_2 \rightarrow v_2' | \theta_2)|^2 \sin\theta_2 \, d\theta_2 . \qquad \text{V.4.2}$$

Since in the BS approximation the T matrix is independent of the CO orientation, θ_2, we may evaluate the integral in V.4.2 analytically to give (cf. II.4.3).

$$\sigma(v_2 \rightarrow v_2') = \frac{\pi}{k^2_{v_2}|_{z=0}} \sum_{\ell} (2\ell+1) |T_{\ell}^{BS}(v_2 \rightarrow v_2')|^2 .$$

V.4.3

These BS calculations are performed employing the VH potential, and both harmonic and Morse oscillator wavefunctions are used to describe the vibrational motion of the CO molecule. BS calculations employing harmonic oscillator wavefunctions were performed primarily in order to make a comparison with the results of Drolshagen and Gianturco (1983, 1984), we note that it is not worth going into the same degree of detail regarding the calculation of the harmonic wavefunctions as is done for the Morse wavefunctions. They are extremely simple functions (see Section 3.2) and relatively easy to calculate, qualitatively they are similar to Morse wavefunctions for reasonably low vibrational states ($v_2 \leq 5$). They are significant over the same range of r_2, the vibrational coordinate, $1.4 \leq r_2 \leq 2.8$ a.u., and the eigenenergies are roughly 2% higher than the corresponding Morse eigenenergies. We add that harmonic oscillator wavefunction are employed only in these calculations, whereas the Morse wavefunctions are employed in the calculations presented in this chapter, and in Chapters VI and VII.

As already stated in Section 3.2 we assume a value of $\hbar\omega$ = 0.269 eV for the harmonic oscillator basis functions, since this value is quoted by Drolshagen and Gianturco (1983, 1984). Calculations are performed

at ten barycentric collision energies, E_n, in the range $1.1 \leq E \leq 2.9$ $\hbar\omega$, where $E_n = (0.9 + 0.2n)$ $\hbar\omega$ $(n = 1,2,3...10)$.

The value of $\hbar\omega$ employed in our IOS calculations is slightly different ($\hbar\omega$ = 0.26898 eV). The small differences between the numerical values of $\hbar\omega$, and the Morse and harmonic eigenenergies should not seriously affect any comparisons between the calculations. In addition we perform calculations at two collision energies (E = 1.1, and 2.9 $\hbar\omega$, where $\hbar\omega$ = 0.26898 eV) employing our Morse oscillator wavefunctions.

Since these BS calculations are essentially simple IOS calculations, the numerical details developed for our IOS calculations should be satisfactory for these calculations. As stated in Section 3.2 the interaction potential is just the isotropic (CO and H_2 orientation independent) term. Ignoring the CO anisotropy terms should not significantly affect the variation of the interaction potential with respect to the intermolecular separation, R, hence we will employ the values of R_{min}, R_{max}, and X determined in the previous section. In addition the neglect of the CO anisotropy terms should not seriously affect the description of the CO molecule (i.e. we include one closed vibrational channel, and all open channels in our IOS calculations). This latter assumption is easy to check, in Table 22 we present the convergence of the results with respect to the number of vibrational states included in the coupled equations. The results are shown at E = 1.9 $\hbar\omega$ and E = 2.9 $\hbar\omega$,

TABLE 22

The convergence of $|S_L(v_2, v_2')|^2$ with respect to the number of vibrational channels at L = 0. The results are evaluated treating the rotational degree of freedom of the CO within the BS approximation, and using harmonic oscillator wavefunctions to approximate the vibrational motion.

(a) 2 channels, (b) 3 channels, (c) 4 channels, (d) 5 channels.

	$v_2=1 \rightarrow v_2'=0$	$v_2=2 \rightarrow v_2'=0$	$v_2=2 \rightarrow v_2'=1$
E(ħw)			
1.9	(a) 0.941781-5 (b) 0.947348-5 (c) 0.947238-5	———	———
2.9	(b) 0.208947-3 (c) 0.208941-3 (d) 0.208910-3	0.764802-9 0.905397-9 0.909486-9	0.144718-4 0.173181-4 0.173994-4

$|S_L(v_2, v_2')|^2$ in units of $(\text{a.u.})^2$

and at L = 0, and were evaluated using the harmonic wavefunctions. As can be seen (and as expected) the inclusion of one closed vibrational channel in the coupled equations is sufficient to ensure that the values of $|S_2(v_2, v_2')|^2$ are converged to within a few per cent for all the transitions studied in these calculations. It is clear that to converge the results for the transition $v_2 = 1$ to $v_2' = 0$ one need only retain the open vibrational channels in the range of collision energies studied ($E \lesssim 1$eV).

It is worth repeating that these BS calculations are computationally very simple, the interaction potential takes an extremely simple form, and the coupled equations need only be solved at one orientation at each partial wave. The calculations were performed on the IBM 370/168 computer at NUMAC. Even without taking advantage of the efficient generation of results at subsequent partial waves, using stored information generated at the initial value of L, the approximate computer time required for one partial wave was only 6 seconds (retaining four vibrational channels in the coupled equations).

4.3 Angular Quadrature

In these IOS calculations we evaluate two types of cross sections. Those for the individual rotational transitions in CO for $j_2 = 0$ to j_2'', evaluated using (cf. II.3.29),

$$\sigma(v_2\, 0 \rightarrow v_2' j_2'') = \frac{\pi}{k_{v_2}^2} \sum_{\ell} (2\ell+1) |T_\ell(v_2, j_2 = 0, v_2' j_2'')|^2, \qquad \text{V.4.4}$$

and cross sections summed over the final rotational states, j_2'', calculated using (cf. II.3.30)

$$\sum_{j_2'} \sigma(v_2 0 \to v_2' j_2'') = \sigma(v_2 \to v_2')$$

$$= \frac{\pi}{k_{v_2}^2} \sum_L \frac{1}{2} \int_0^\pi |T_L(v_2, v_2'|\theta_2)|^2 \sin\theta_2 \, d\theta_2 \quad \text{V.4.5}$$

In this study the rotationally summed cross sections are of primary interest since such cross sections are used to evaluate relaxation rate coefficients (Section 5) which may then be compared with the corresponding experimentally determined rates (and also rates evaluated in other theoretical studies). We note that these are the only cross sections presented in this thesis from the calculations employing the VH potential. However, generally speaking it is far easier to accurately evaluate rotationally summed cross sections than the corresponding cross sections for the individual rotational transitions. There are two reasons for this. V.4.5 does not involve the function $Y_{j_2''}^*(\theta_2, 0)$ which becomes highly oscillatory as j_2'' is increased, and secondly V.4.5 involves $|S_L(v_2, v_2'|\theta_2)|^2$ which for both the P and VH potentials is a less oscillatory function of θ_2 than either the real or the imaginary parts of $S_L(v_2, v_2'|\theta_2)$. This is illustrated in Figure 2 for the P interaction potential. We show the variation of the real and imaginary parts of $S_L(1,0|\theta_2)$ and $|S_L(1,0|\theta_2)|^2$ with respect to θ_2 at E = 2.9 $\hbar\omega$ and L = 0. It is clear that many more quadrature points

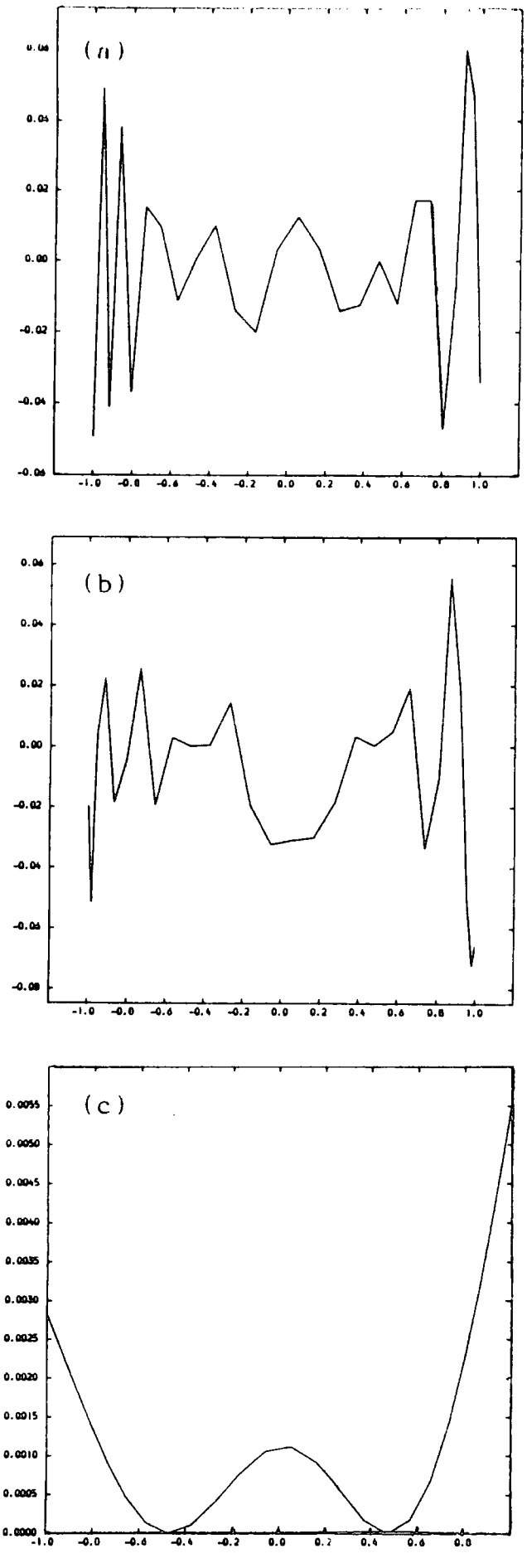

Figure 2

The variation with θ_2 of the real part (a) and imaginary part (b) of $S_L(v_2=1, v_2'=0|\theta_2)$ in units of (a.u.) at E = 2.9 $\hbar\omega$ and L = 0. Also shown (c) is the θ_2 variation of $|S_L(v_2=1, v_2'=0|\theta_2)|^2$.

are required to integrate either the real or imaginary parts of $S_L(1,0/\theta_2)$ than $|S_L(1,0/\theta_2)|^2$. Consequently we will devote the majority of this section to the evaluation of the individual rotational cross sections, $\sigma(v_2 j_2 \rightarrow v_2' j_2'')$ using the P potential, for the vibrational transition $v_2 = 1$ to $v_2' = 0$ (note that such cross sections are not presented for $v_2 = 2$ to $v_2' = 1$ and 0).

The major differences between these calculations, and those described in Chapter IV for the $H_2 + H^+$ system are the number of rotational states (j_2'') that must be included in the calculations, and the number of orientations at which the coupled equations must be solved. For a diatomic molecule such as H_2, there is a rigorous selection rule which allows only transitions for $\Delta j_2 =$ even to occur, however in the case of a heteronuclear diatomic molecule there is no corresponding selection rule and consequently odd Δj_2 transitions are also possible.

Secondly the relatively large energy spacing of the H_2 rotational states means that even at a collision energy of E = 4.67 eV relatively few rotational states are energetically accessible after the collision has taken place, and consequently it was only necessary to consider the evaluation of cross sections, $\sigma(v_2 0 \rightarrow v_2' j_2'')$, involving rotational states up to $j_2'' = 10$. In Chapter IV.5, Table 6 clearly illustrates that states with $j_2'' > 10$ need not be considered for a 'complete summation' in IV.4.6 .

$$\sigma(v_2 j_2 \rightarrow v_2' j_2') = (2j_2'+1)\left(\frac{k_{v_2 0}}{k_{v_2 j_2}}\right)^2 \sum_{j_2''} \begin{pmatrix} j_2' & j_2 & j_2'' \\ 0 & 0 & 0 \end{pmatrix}^2 \times \sigma(v_2 0 \rightarrow v_2' j_2'') \qquad \text{V.4.6}$$

CO, however, has a far smaller rotational constant than H_2 ($B_{CO} = 1.9313\ cm^{-1}$ cf $B_{H_2} = 59.3125\ cm^{-1}$) (Herzberg (1950)), and consequently there are many closely packed rotational levels. Even at the relatively low collision energies studied in these calculations ($E \lesssim 1eV$) a considerably larger number of rotational states are accessible after vibrational relaxation has taken place. For example at $E = 1.1\hbar\omega$ there are $\sim$ 34 states accessible (at $E = 1.9\hbar\omega$, $j_{2max}'' \simeq 46$, and at $E = 2.9\hbar\omega$, $j_{2max}'' \simeq 56$). We mention these are only estimates, the energy of the levels was calculated using the simple expression $\mathcal{E}_{j_2''} = B_{CO} j_2''(j_2'' + 1)$ which becomes progressively inaccurate as j_2'' increases.

As noted in Chapter IV.4 when one deals with a heteronuclear target molecule we have no choice but to employ an N-point quadrature in the range $0 \leq \theta_2 \leq \pi$ as the S-matrix is not symmetric about $\theta_2 = \pi/2$, as in the case of a homonuclear diatomic target molecule. This in itself forces a large increase in the number of orientations at which the coupled equations must be solved.

The quadrature that we employ will automatically force an upper bound on the number of rotational (j_2'') states than can be included in the calculations. By

definition if one is dealing with an N-point quadrature, then those points are the zeros of $Y_{N,0}(\theta_2,0)$ therefore $\sigma(v_2 0 \rightarrow v_2' j_2'' = N) = 0$. For $j_2'' > N$ the number of oscillations of $Y_{j_2'',0}(\theta_2 0)$ is greater than N, and the quadrature gives unsatisfactory results. Evidently if we employ an N-point quadrature, the evaluation of cross sections, $\sigma(v_2 0 \rightarrow v_2' j_2'')$ is only possible for rotational states up to $j_2'' = N - 1$.

It is not worth employing more than ~30 quadrature points since this ensures excellent convergence for rotationally summed cross sections (see Table 25). Thus at the majority of the collision energies studied in these calculations the rotational basis, employed for CO, will be inadequate (and consequently the summation over j_2'' in V.4.6 will be incomplete). Evidently we must rule out the use of V.4.6 to calculate cross sections with initial $j_2 > 0$ using cross sections evaluated for initial $j_2 = 0$ (at all but possibly the lowest energy, E = 1.1 $\hbar\omega$).

In Table 23 we show the values of $\sigma^L(v_2=1 j_2=0 \rightarrow v_2'=0 j_2'')$ for $j_2'' \leq 26$ at E = 2.9 $\hbar\omega$ and L = 0,50 calculated using 28-, 32, and 40- point Gauss Legendre quadratures (notice that only even transitions are shown, this is purely for brevity, in practice all the transitions are evaluated). As expected at each value of L, the convergence of the results obtained with the three quadrature schemes deteriorates with increasing j_2'', however it is

TABLE 23

Comparison of IOS cross sections calculated using different Gauss Legendre quadratures at E = 2.9 $\hbar\omega$ and L = 0, 50.

(a) 28 points, (b) 32 points, (c) 40 points.

L = 0	$\sigma^L(10 \to 0j_2'')$ (Å^2)	L = 0	$\sigma^L(10 \to 0j_2'')$	L = 50	$\sigma^L(10 \to 0j_2'')$ (Å^2)	L = 50	$\sigma^L(10 \to 0j_2'')$
$j_2'' = 0$ (a)	0.22522357-6	$j_2'' = 14$	0.19902748-6	$j_2'' = 0$ (a)	0.12939376-6	$j_2'' = 14$	0.23209120-6
(b)	0.22586404-6		0.27796484-6	(b)	0.12839373-6		0.23396610-6
(c)	0.22589407-6		0.28811360-6	(c)	0.12674984-6		0.24046788-6
$j_2'' = 2$	0.12485866-6	$j_2'' = 16$	0.27767298-6	$j_2'' = 2$	0.10598087-5	$j_2'' = 16$	0.33346406-6
	0.12380769-6		0.16425483-6		0.10566535-5		0.33326852-6
	0.12374680-6		0.14951836-6		0.10514208-5		0.33817034-6
$j_2'' = 4$	0.52360862-6	$j_2'' = 18$	0.36964668-6	$j_2'' = 4$	0.41622160-6	$j_2'' = 18$	0.36054723-6
	0.52291562-6		0.20379642-7		0.41475976-6		0.36197764-6
	0.52297365-6		0.30922252-7		0.41233686-6		0.36074963-6
$j_2'' = 6$	0.10532696-8	$j_2'' = 20$	0.16140612-6	$j_2'' = 6$	0.77106396-6	$j_2'' = 20$	0.26842016-6
	0.89522968-9		0.51999592-7		0.77330103-6		0.27141044-6
	0.89076211-9		0.35432335-7		0.77738518-6		0.26983052-6
$j_2'' = 8$	0.48733938-6	$j_2'' = 22$	0.88635525-8	$j_2'' = 8$	0.21159488-6	$j_2'' = 22$	0.13158979-6
	0.49423491-6		0.11953573-7		0.21579353-6		0.13186751-6
	0.49445205-6		0.34681142-7		0.22397302-6		0.13221995-6
$j_2'' = 10$	0.36865692-6	$j_2'' = 24$	0.19206948-6	$j_2'' = 10$	0.67649973-8	$j_2'' = 24$	0.37731602-7
	0.36489260-6		0.13576427-6		0.63540943-8		0.39386405-7
	0.36508273-6		0.50415399-7		0.55933101-8		0.38383227-7
$j_2'' = 12$	0.17057319-6	$j_2'' = 26$	0.13776925-6	$j_2'' = 12$	0.12489493-6	$j_2'' = 26$	0.91762018-5
	0.12832918-6		0.36628193-7		0.12557271-6		0.61767866-5
	0.12470706-6		0.58977065-7		0.12739928-6		0.56454736-5

evident that at a given energy convergence improves with L. Physically as L decreases the H_2 is able to approach closer to the CO where the anisotropy of the interaction potential is greater and therefore $S_L(v_2=1, j_2'' 0/\theta_2)$ becomes a stronger function of θ_2. Consequently as L increases fewer quadrature points are required to integrate $S_L(1,0/\theta_2)$ over θ_2.

As the collision energy, E, increases the kinetic energy available for the collision increases, consequently the H_2 is able to approach closer to the CO, we would expect therefore that decreasing E has a similar effect on the convergence of the cross sections as increasing L.

This is illustrated in Table 24 where we present the values of $\sigma^L(10 \rightarrow 0 j_2'')$ for E = 1.9 $\hbar\omega$ and L = 0, calculated using 28- and 32- point Gauss Legendre quadratures. Clearly at this energy the convergence of the results for a given value of j_2'' is far superior than for the corresponding results evaluated at E = 2.9 $\hbar\omega$.

Finally in Table 25 we compare the values of rotationally summed cross sections, $\sigma^L(v_2 \rightarrow v_2')$, for the transitions v_2 = 1 to v_2' = 0, and v_2 = 2 to v_2' = 1 and 0, obtained using 28- and 32- point Gauss Legendre quadratures. The results shown are evaluated at E = 2.9 $\hbar\omega$ and L = 0, employing both the P and VH interaction potentials. Notice that for the P potential the convergence of these rotationally summed cross sections is far better than

TABLE 24

Comparison of IOS cross sections calculated using different Gauss Legendre quadratures at E = 1.9 $\hbar\omega$ and L = 0 : (a) 28 points; (b) 32 points.

Cross sections in units of $Å^2$.

L = 0	$\sigma^L(10 \to 0j_2'')$	L = 0	$\sigma^L(10 \to 0j_2'')$
$j_2'' = 0$	(a) 0.27724758-7	$j_2'' = 14$	0.24216229-7
	(b) 0.27722092-7		0.24336987-7
$j_2'' = 2$	0.18740944-7	$j_2'' = 16$	0.62067915-8
	0.18743008-7		0.58336099-8
$j_2'' = 4$	0.23523323-7	$j_2'' = 18$	0.19206660-8
	0.23530474-7		0.25222250-8
$j_2'' = 6$	0.40410774-7	$j_2'' = 20$	0.26893630-8
	0.40388637-7		0.21472692-8
$j_2'' = 8$	0.61689808-8	$j_2'' = 22$	0.46625192-8
	0.61883541-8		0.28491694-8
$j_2'' = 10$	0.25724297-7	$j_2'' = 24$	0.15124308-8
	0.25784212-7		0.44086015-8
$j_2'' = 12$	0.44926814-7	$j_2'' = 26$	0.16927551-7
	0.44883217-7		0.70263780-8

TABLE 25

Comparison of IOS rotationally summed cross sections, $\sigma(v_2 \rightarrow v_2')$, evaluated using different Gauss Legendre quadratures: (a) 28; (b) 32.

Cross sections in $Å^2$ calculated at E = 2.9 $\hbar\omega$ and L = 0.

		P potential	VH potential
$v_2=1 \rightarrow v_2'=0$	(a)	0.46418014-5	0.10024156-5
	(b)	0.46487479-5	0.10100988-5
$v_2=2 \rightarrow v_2'=0$		0.34516585-9	0.89766816-11
		0.34637290-9	0.90089657-11
$v_2=2 \rightarrow v_2'=1$		0.18626094-5	0.16397943-6
		0.18857920-5	0.16556750-6

for the corresponding individual rotational cross sections. It is worth mentioning that since the summation over j_2'' is performed analytically in V.4.5, these rotationally summed cross sections are not restricted by the quadrature used to evaluate them (assuming of course, that the number of quadrature points is sufficient to provide converged results). Clearly for both the P and VH potentials the agreement of the results evaluated using 28- and 32- point quadratures is excellent. In conclusion we will employ the following Gauss Legendre quadratures in all our IOS calculations:

$1.1 \leq E \leq 1.9$ eV 28- points.

$2.1 \leq E \leq 2.9$ eV 32- points, $L \leq 50$.

28- points, $L > 50$.

5. Results and discussion

In this section we will present cross sections and rate coefficients for the process of collisional de-excitation evaluated in calculations employing the P and VH potential surfaces. Table 26 contains the numerical values of the rotationally summed cross sections, $\sigma(v_2 \rightarrow v_2') = \sum_{j_2} \sigma(v_2 0 \rightarrow v_2' j_2')$, for the vibrational de-excitation processes $v_2 = 1$ to $v_2' = 0$, $v_2 = 2$ to $v_2' = 0$, and $v_2 = 2$ to $v_2' = 1$, evaluated in the IOS calculations employing the P potential. Cross sections for the corresponding excitation processes may be determined using the following detailed balance relationship

$$k_{v_2 0}^2 \sigma(v_2 0 \rightarrow v_2' j_2') = k_{v_2' 0}^2 \sigma(v_2' 0 \rightarrow v_2 j_2'). \qquad \text{V.5.1}$$

TABLE 26

Rotationally summed cross sections, $\sigma(v_2 \rightarrow v_2')(\text{Å}^2)$, for the vibrational de-excitation of $^{12}C^{16}O$ by para-H_2 in its ground state. The barycentric energy, E, is expressed in units of $\hbar\omega$ = 0.26898 eV and is relative to the rovibrational ground state. Numbers in brackets are powers of 10.

E($\hbar\omega$)	σ (1→0)	σ(2→0)	σ(2→1)
1.1	0.952(-6)		
1.3	0.103(-4)		
1.5	0.488(-4)		
1.7	0.151(-3)		
1.9	0.365(-3)		
2.1	0.746(-3)	0.220(-9)	0.260(-5)
2.3	0.135(-2)	0.362(-8)	0.257(-4)
2.5	0.225(-2)	0.252(-7)	0.116(-3)
2.7	0.349(-2)	0.112(-6)	0.351(-3)
2.9	0.515(-2)	0.371(-6)	0.830(-3)

These are not reciprocal processes and this detailed balance type condition is imposed by the IOS approximation. Such a relationship is not unreasonable in the IOS approximation, where the rotor states are considered degenerate.

The cross sections for the vibrational de-excitation of CO are extremely small. An explanation can be provided within the distorted wave approximation (e.g. see Gianturco (1979)). In this approximation the cross sections are proportional to a radial integral over the corresponding coupling potential weighted by the radial functions of the initial, v_2, and final v_2', states. Because of the low collision energies the initial wavefunction is moderately oscillating while the final wavefunction is much more rapidly oscillating because of the released energy (e.g. for $v_2 = 1 \rightarrow 0$, the energy released is $\sim$ 2152 cm^{-1}) and thus the magnitude of the overlap integral is small. In addition, it is worth noting that its magnitude depends on a delicate interplay between the two wavefunctions around the classical turning point.

Figure 3 shows the distribution of the $v_2 = 1$ to $v_2' = 0$ vibrational de-excitation cross sections, $\sigma(10 \rightarrow 0j')$, amongst the final rotational states for E = 1.1, 1.9, and 2.9 ~~eV~~, evaluated in the IOS calculations employing the P potential. It is clear that as the total collision energy increases there is a tendency to populate higher rotational states of the ground

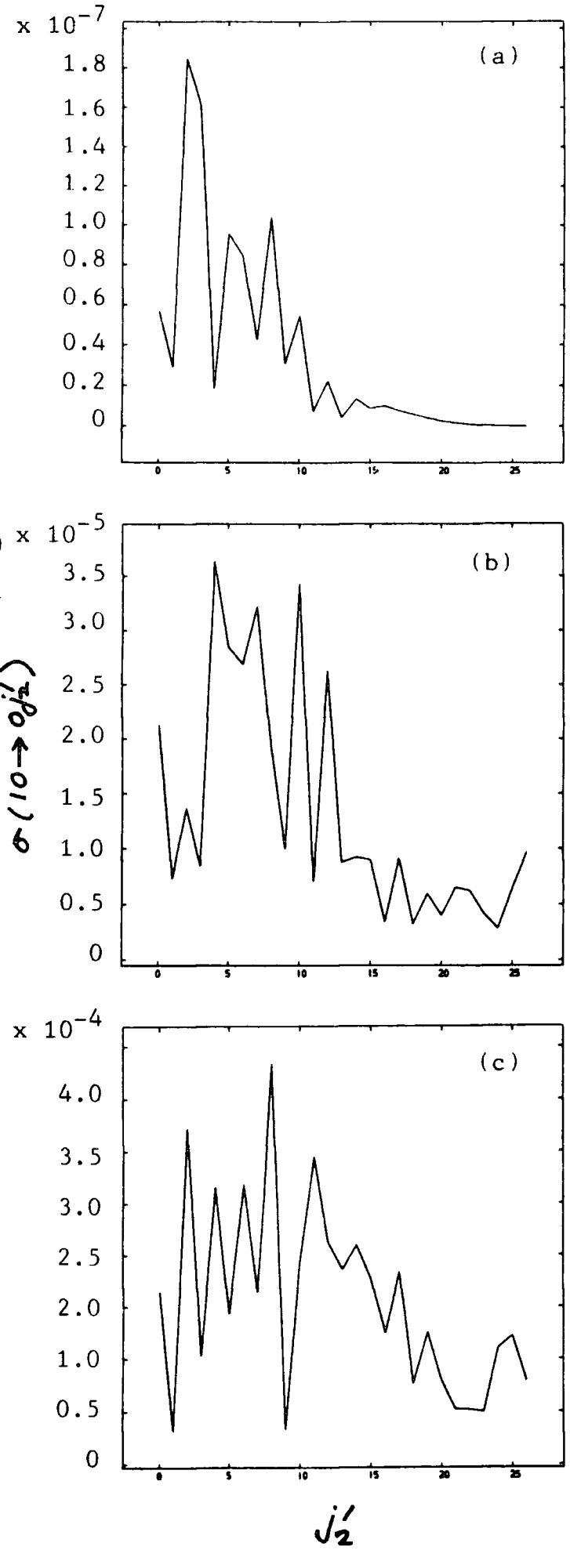

Figure 3

The distribution of the vibrational de-excitation cross section $\sigma(10 \rightarrow 0j_2')(\text{Å}^2)$ amongst the final rotational states, j_2' :

(a) E = 1.1 $\hbar\omega$;

(b) E = 1.9 $\hbar\omega$;

(c) E = 2.9 $\hbar\omega$.

vibrational state of the CO molecule. At the two higher collision energies (E = 1.9 $\hbar\omega$ and 2.9 $\hbar\omega$) the cross sections are obviously not converged with respect to the final rotational state j_2', evidently states with $j_2' > 26$ should be considered.

The oscillatory behaviour of $\sigma(10 \rightarrow 0j_2')$ with respect to j_2' is due to the anisotropy of the interaction potential. Consequently it changes with both the range of j_2' and the collision energy. It will be recalled that for the rovibrational excitation of a homonuclear diatomic molecule, such as H_2 (e.g. see the results for the rovibrational excitation of H_2 by H^+ in Chapter IV) there is a rigorous selection rule which only allows transitions for which Δj_2 = even to occur. In the case of an "almost homonuclear" diatomic molecule (i.e. a heteronuclear diatomic for which the odd anisotropy in the interaction potential is much smaller than the even anisotropy, as in the case of CO) the odd Δj_2 transitions are diminished by destructive interference, but yet have finite cross sections. This effect has been demonstrated by McCurdy and Miller (1977) using semiclassical methods, and it is worth noting that similar effects have been observed by Andres et al. (1982), and Schinke et al. (1984) in studies of the rotational excitation of CO by D_2.

In Figure 4 we show a comparison between the IOS rotationally summed cross sections for the vibrational

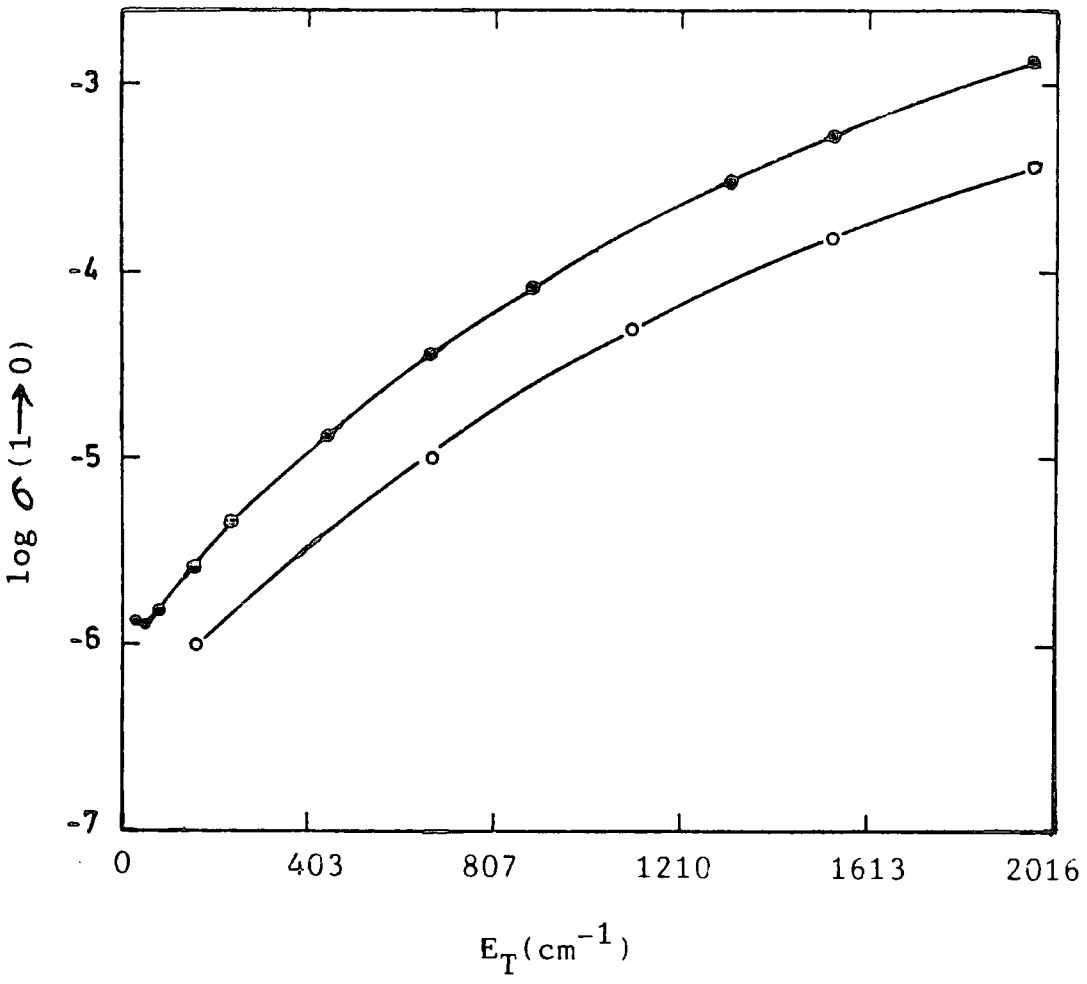

Figure 4 A comparison of the IOS calculations of rotationally summed cross sections for the vibrational de-excitation process $v_2 = 1$ to $v_2' = 0$, $\sigma(1 \rightarrow 0)$, in units of $Å^2$.

—●—●—●— : BSD; —o—o— : Present calculations. E_T is measured relative to the $v_2 = 1$ $j_1 = 0$ threshold.

relaxation process $v_2 = 1$ to $v_2' = 0$ calculated by Bačić, Schinke and Diercksen (1984a) (hereafter referred to as BSD) with the corresponding results evaluated in the present IOS calculations employing the P potential. It may be seen from Figure 4 that the cross sections evaluated by BSD are roughly a factor of 2.5 - 3.5 larger than the results of the present calculations, in the energy range shown. BSD employ the DK potential, use Morse oscillator wavefunctions to describe the vibrational motion of the CO molecule, and H_2 is constrained in its ground rotational state.

Vibrational transitions are induced by the r_2-dependence of the interaction potential. If we express the interaction potential in the form

$$V(\underline{r}_2, R) = \sum_{\lambda_2} V_{\lambda_2}(r_2, R) P_{\lambda_2}(\cos\theta_2), \qquad \text{V.5.2.}$$

we may expand in a Taylor series about the equilibrium CO internuclear separation, $r_{2,eq}$, and obtain

$$V(r_2, R) = \sum_{\lambda_2} P_{\lambda_2}(\cos\theta_2) \left[V_{\lambda_2}(r_{2,eq}, R) + (r_2 - r_{2,eq}) \frac{\partial}{\partial r_2} V_{\lambda_2}\Big|_{r_2 = r_{2,eq}} + \frac{1}{2} (r_2 - r_{2,eq})^2 \frac{\partial}{\partial r_2} V_{\lambda_2}\Big|_{r_2 = r_{2,eq}} + \cdots \right]. \qquad \text{V.5.3}$$

The successive terms of the expansion V.5.3 are responsible for the transitions with $\Delta v_2 = 0, 1, 2 \ldots$ It will be recalled that the r_2-dependence of the P and DK potentials

were obtained in rather different ways. The P potential was constructed by using the ab initio SCF potential energy points of Prissette et al. (1978) and Flower et al. (1979). The original SCF data were available only for the CO equilibrium bond distance, $r_{2,eq}$, and the dependence on r_2 was obtained by representing the interaction potential as a superposition of atom-atom interactions. On the other hand the DK potential was constructed from the elaborate SCF calculations of Diercksen and Kraemer (1984). These SCF potential energies where calculated at three CO bond distances (r_2 = 1.898a.u., 2.132a.u., 2.234a.u.). In view of the different procedures of obtaining the r_2-dependence of the interaction, the discrepancies seen in Figure 4 are perhaps not so surprising.

What is rather surprising is that BSD find that the magnitude of the vibrational de-excitation cross sections are extremely dependent upon the vibrationally elastic potential, $V_{\lambda_2}(r_{2,eq}, R)$, this term cannot directly influence the vibrational inelastic cross sections (the overlap integral involving this term will be zero).

The DK potential employed by BSD involves a damping function of the form

$$f(R) = \exp[-\gamma(D/R-1)^2] \quad \text{for } R \leq D$$

$$f(R) = 1 \quad \text{for } R > D \qquad \text{V.5.4}$$

where the parameters γ and D were determined by simultaneously fitting rotationally inelastic and total differential

cross sections for D_2 + CO (Schinke et al. (1984)).

The function V.5.4 multiplies the dispersion term of the potential and any change of these parameters must be consistent with the beam data. BSD find that changing D from 4.46Å to 4.70Å results in a shift in the zero point of the vibrational elastic potential, $V_0(r_{2,eq}, R)$, of only 0.08Å, however this is sufficient to decrease the cross section for $E \approx 80$ cm^{-1} by a factor of 1.5. The sensitivity decreases with the collision energy, the explanation of this behaviour is easy if one recalls that the cross section is mainly determined by the turning point region (at $E \approx 2000$ cm^{-1} the cross section only decreases by a factor of ~ 1.1).

The zero point of the isotropic part of the P potential is roughly 0.16Å smaller than the DK potential (with D = 4.46Å). In order to fit the diffraction oscillations of the D_2 + CO total differential cross section (Schinke et al. (1984)) it should be shifted to larger distances which would probably decrease the cross sections which are already a factor $\sim 2.5 - 3.5$ smaller than those calculated by BSD. As BSD point out the sensitivity on the absolute location of the elastic potential puts a strong restriction on the accuracy of ab initio or empirical potential surfaces. In view of the present results it is questionable whether the extrapolation from the equilibrium separation to arbitrary CO internuclear distances, as performed by Poulsen (1982), is

sufficiently accurate. However, despite the differences in the de-excitation cross sections we will show later in this section that both the P and DK potentials provide a reasonable description of the experimental results for the de-excitation of CO ($v_2 = 1$) by ortho-H_2.

The experimental data available (e.g. Andrews and Simpson (1976), and Starr et al. (1974)) is in the form of vibrational relaxation rate coefficients. For a gas in translational equilibrium, the rate coefficients for individual processes $v_2 j_2 \rightarrow v_2' j_2'$ are related to the corresponding cross sections by averaging over a Maxwellian velocity distribution (see Chapter I).

$$\alpha_{v_2 j_2 \rightarrow v_2' j_2'}(T) = \int_0^\infty v\, \sigma(v_2 j_2 \rightarrow v_2' j_2'; v) f(v;T)\, dv \qquad \text{V.5.5}$$

where $$f(v;T) = 4\pi \left(\frac{\mu}{2\pi kT}\right)^{3/2} \exp(-\mu v^2/2kT)$$

μ is the reduced mass of the system, v is the initial relative velocity of the two molecules, k is Boltzmann's constant, and T is the temperature. We can obtain the expression in terms of an average over E', the initial collision energy of the system in molecular state $(v_2 j_2)$ by using $E' = \frac{1}{2}\mu v^2$

$$\alpha_{v_2 j_2 \rightarrow v_2' j_2'}(T) = \left(\frac{8kT}{\mu k}\right)\left(\frac{1}{kT}\right)^2 \int_0^\infty E' \sigma(v_2 j_2 \rightarrow v_2' j_2'; E') \exp\left(\frac{-E'}{kT}\right) dE' \qquad \text{V.5.6}$$

Pure rotational relaxation ($\Delta v_2 = 0$) is extremely rapid (Alexander (1975)) and consequently the relaxation process observed experimentally is the overall relaxation of the rotational states of the $v_2 = 1$ state to the $v_2 = 0$ state. Within the IOS approximation V.5.6 is independent of the initial rotational state j_2 and thus it is equal to the relaxation rate averaged over j_2 independent of the particular form of the distribution function. (In the BS approximation all rotational states are omitted, with the exception of $j_2 = 0$). We therefore chose $j_2 = 0$ and write the vibrational rate (summed over final rotational state j_2')

$$\alpha_{1\to 0}(T) = \sum_{j_2'} \alpha_{10\to 0j_2'}(T) .$$

V.5.7

The interpolation of the available results (rotationally summed cross sections, $\sigma(v_2 \to v_2')$, for the process $v_2 = 1 \to 0$) required to evaluate the integral in V.5.6 was performed over log ($\sigma(v_2 = 1 \to v_2' = 0)$) as a function of log E'. A spline interpolation procedure was employed to obtain the values of the cross sections to evaluate the integral by a Gauss Legendre quadrature.

In Figure 5, we present the values of the vibrational relaxation rate evaluated using the results of the IOS calculations employing the P potential. We compare our results with the 'V-T' semiclassical results of Poulsen and Billing (1982), in which it is supposed

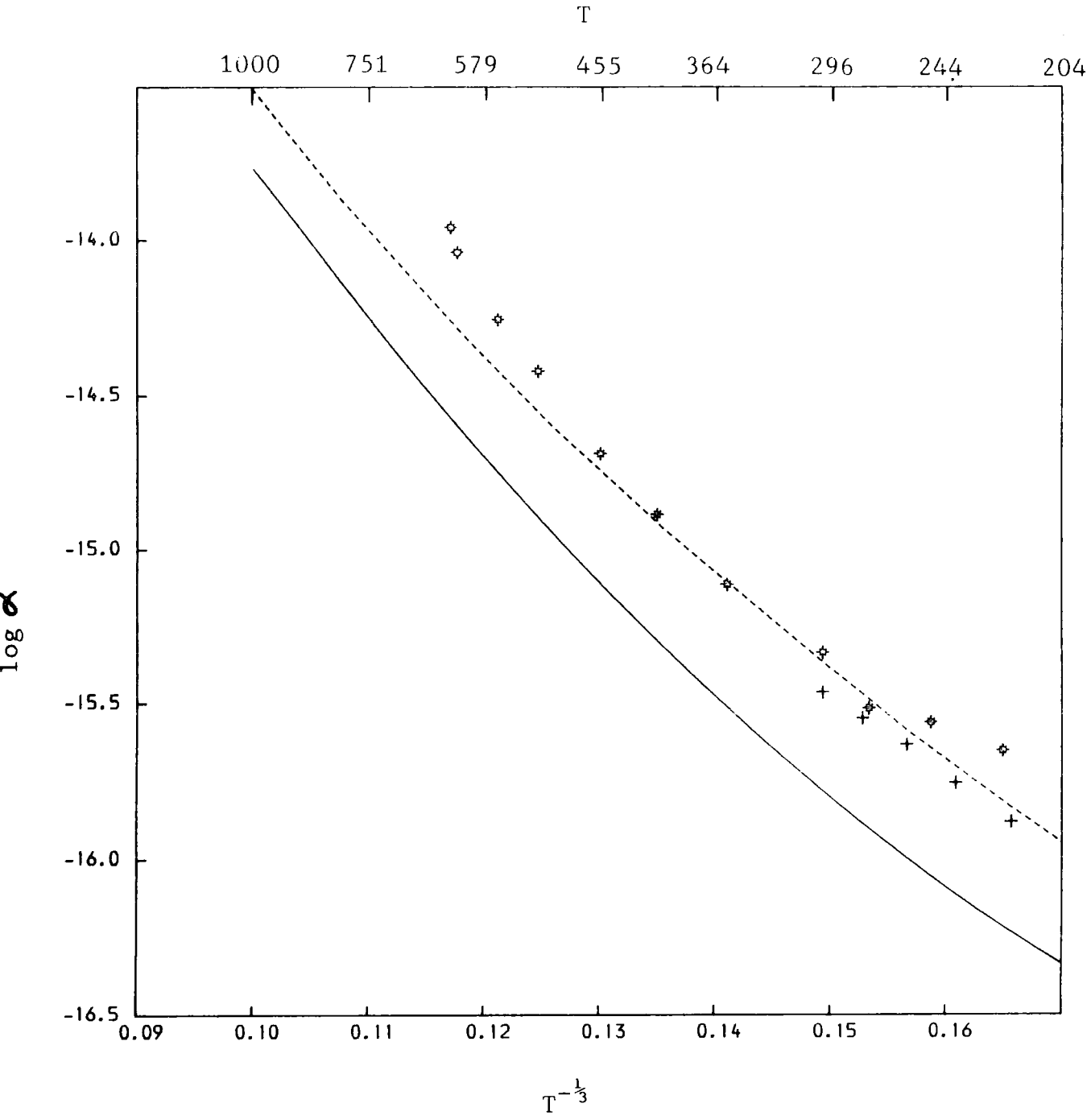

Figure 5. The variation with temperature, T(K), of the vibrational relaxation coefficient, α ($cm^3 s^{-1}$). Full curve : present calculations; broken curve : Poulsen and Billing (1982); + :Andrews and Simpson (1976); * : Starr et al. (1974).

that all the vibrational excitation energy of the CO molecule is converted into relative translational energy (i.e. the H_2 molecule does not become rotationally excited in the collision). It is worth noting that Poulsen and Billing (1982) also employ the P potential and Morse oscillator vibrational eigenfunctions.

Also shown are the experimental points of Andrews and Simpson (1976) for ortho-H_2 and of Starr et al. (1974) for normal H_2. It is more appropriate to compare the theoretical results in Figure 5 with the experimental results for ortho-H_2 than with the measurements in normal H_2. Experimentally it is found that the relaxation of CO in para-H_2 is much faster than in ortho-H_2. The difference is due to the near-resonance process (V.2.4)

$$CO(v_2=1) + H_2(j_1=2) \rightarrow CO(v_2=0) + H_2(j_1=6) + 87.03\ cm^{-1}$$

V.5.8a

which is not present for ortho-H_2, but which enhances the results obtained in normal H_2. According to Poulsen and Billing (1982) such a comparison between experiment and theory is not unreasonable, these authors find that pure vibrational-translational processes

$$CO(v_2=1) + H_2(j_1) \rightarrow CO(v_2=0) + H_2(j_1)$$

V.5.8b

are much more efficient than processes in which $\Delta j_1 \neq 0$ except for the near-resonance process above. In addition, they find that the 'V-T' cross sections are essentially

independent of the initial H_2 rotational state. While in the next chapter we show the latter statement to be true, the former conclusion is shown to be erroneous (Chapter VI).

In the calculation of Poulsen and Billing (1982), classical mechanics were used to describe the rotation of the CO molecule and the relative motion of the CO and H_2 molecules. The vibrational motion of the CO was treated quantum mechanically, this semiclassical approximation will be hereafter referred to as the SCA.

Similar results to those shown in Figure 5 have been obtained by Price et al. (1983) for the He + CO system. These authors compare the results of quantal calculations, in which the close-coupling approximation is applied to the vibrational motion and the IOS approximation to the rotational motion, with calculations employing the SCA. When the sudden approximation is also applied in the semiclassical calculations, these authors find excellent agreement between the two sets of calculations of the rate coefficient for vibrational relaxation, however when this approximation is removed, discrepancies are found which are in the same sense and similar in magnitude to those shown in Figure 5. It would appear from these results that the energy-sudden component of the IOS approximation is responsible for the discrepancies between the theoretical curves.

Recently many such speculations about the applicability

of the IOS approximation to describe vibrational relaxation have arisen in the literature (e.g. Maricq et al. (1983), Price et al. (1983), Billing and Clary (1982), and Jolicard and Billing (1984)). However BSD cast doubt on this interpretation, they point out that the test of the IOS approximation against the SCA is not unambiguous since both methods involve different approximations. These authors have calculated rotationally summed cross sections treating the CO rotational motion within the CS and IOS approximations. The CS cross sections are roughly a factor 1.5 larger than the IOS cross sections, and independent of the initial rotational state of the CO molecule for low j_2 ($j_2 \lesssim 6$). As BSD point out, if the IOS approximation is accurate for j_2 0 it is difficult to imagine that it is inaccurate by a factor 2 to 4 for initial CO rotational states lower than eight or so.

It appears, therefore that the discrepancy between the calculations is more likely due to the use of classical mechanics. Within the SCA the translational energy due to the quantum transition is not rigorously defined. It is normal to take a symmetrized energy according to the arithmetic velocity average for the initial and final channels (e.g. see Price et al. (1983)). This is satisfactory if the energy due to the quantum transition is small compared to the total energy, however, the energy transfer for the $v_2 = 1$ to $v_2' = 0$ transition (~ 2152 cm^{-1}) is significant compared with the initial

translational energies which contribute most at the lower temperatures in Figure 5 ($T \lesssim 500$ K). It is clear that the discrepancy between the two calculations decreases with increasing temperature. Both the IOS approximation and the SCA would be expected to improve with temperature.

Secondly, as BSD have shown, the turning point region is important in the calculation of vibrationally inelastic cross sections. Classical mechanics is usually not appropriate to properly describe the turning point region, especially if the transition probabilities are of the order of 10^{-5} - 10^{-4}; the classically forbidden region is not probed at all by the classical trajectories.

In Figure 6 we compare the vibrational relaxation rate evaluated using the results of the IOS calculations employing the P potential with the corresponding results obtained by BSD. The results of BSD are shown for two values of the parameter D (4.46 Å and 4.70 Å). For reference the experimental results for ortho-H_2 (Andrews and Simpson (1976)) are shown. As can be seen the results evaluated by BSD agree extremely well with the experimental data, especially if a value of D = 4.70 Å is taken. However it will be recalled that the CS cross sections evaluated by BSD are a factor of $\sim$ 1.5 larger than the corresponding IOS cross sections. Therefore if the results shown in Figure 6 are increased by a factor of 1.5 the results of BSD move above the experimental data (nevertheless the agreement will still be reasonable),

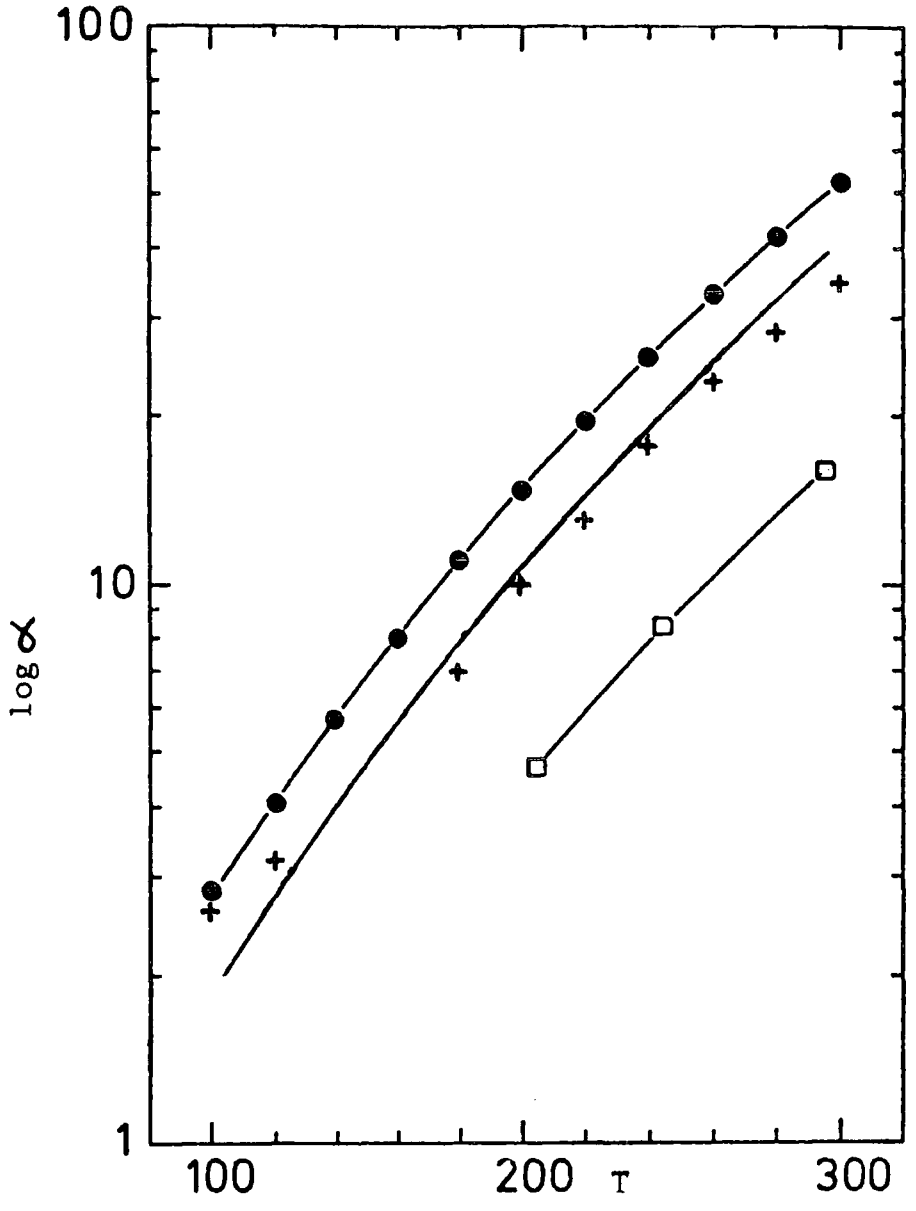

Figure 6. A comparison of IOS calculations of the variation with temperature T(K) of the vibrational relaxation coefficient, α ($10^{-17}cm^3s^{-1}$). —□—□—□— : present calculations; —•—•—•— : BSD (D = 4.46Å); ——— : BSD (D = 4.70Å).

Also shown are the experimental points of Andrews and Simpson (+ + +).

however the present results move closer to the experimental points. There is another factor, the strength of $\Delta j_1 = 2$ transitions, this will be discussed in detail in Chapter VI. For the present discussion we will assume that Poulsen and Billing (1982) are correct in their observation that transitions with $\Delta j_1 \neq 0$ are not important (except for the near-resonance process above). Thus despite the discrepancies in the cross sections evaluated using the P and DK potential, and the resulting criticism of the P potential, both potentials provide a reasonable description of the experimental results for ortho-H_2.

In Table 27 (columns 3 and 4) we compare the results of IOS calculations employing the P potential and the VH potential. The electron gas model potential of van Hemert (1983) explicitly gives the variation of the interaction potential with r_2. However, it was found by Billing and Poulsen (1983) that this potential surface gives relatively poor agreement with the experimental measurements for rotationally inelastic scattering in the D_2 +CO system. Since rotation and vibration are strongly coupled in the H_2 + CO system one would not expect the VH potential to reproduce rovibrational cross sections particularly well. As can be seen the agreement of the results, evaluated using the VH potential, with the experimental points shown in Figure 5 would be unsatisfactory.

TABLE 27

Rotationally summed vibrational de-excitation cross sections, $\sigma(v_2 \rightarrow v_2')(\text{Å}^2)$. The CO-$H_2$ interaction potential of Poulsen (1982) or van Hemert (1983) has been employed. The vibrational motion of the CO molecule is represented by Morse or harmonic oscillator wavefunctions, and the IOS or BS approximation to the CO rotational motion is used. Energies E are expressed relative to the rovibrational ground state of CO. Numbers in brackets are powers of ten.

E($\hbar\omega$)	$v_2 \rightarrow v_2$	Poulsen/ Morse/IOS	van Hemert/ Morse/IOS	van Hemert/ Morse/BS	van Hemert/ Harmonic/BS
1.1	$1 \rightarrow 0$	0.952(-6)	0.401(-6)	0.382(-7)	0.481(-7)
2.9	$1 \rightarrow 0$	0.515(-2)	0.182(-2)	0.865(-3)	0.104(-2)
2.9	$2 \rightarrow 0$	0.371(-6)	0.278(-7)	0.322(-8)	0.486(-8)
2.9	$2 \rightarrow 1$	0.820(-3)	0.289(-3)	0.980(-4)	0.122(-3)

It is clear from Table 27 that the agreement with the results obtained using the P potential deteriorates with increasing Δv_2. For $\Delta v_2 = 1$ the results differ by a factor $\sim$ 2-2·5, however for $\Delta v_2 = 2$ the agreement is extremely poor. As already mentioned vibrational transitions are induced by the r_2-dependence of the interaction potential. The successive terms of the expansion V.5.3 are responsible for the transitions $\Delta v_2 = 0,1,2...$ While it is possible that reasonable agreement in the first order term, $\frac{\partial v_{\lambda 2}}{\partial r_2}\Big/_{r_2 = r_{2,eq}}$, might be predicted by two independent determinations of the interaction potential, agreement in second order and higher order derivatives becomes progressively less likely. Consequently we are not surprised by the deterioration of the agreement with Δv_2.

It is worth noting that the vibrationally elastic potential calculated by van Hemert (1983) has a zero point which is $\sim$ 0.13Å greater than that of the P potential. Consequently the isotropic parts of the VH and DK potentials are quite similar, and we mention that the isotropic parts of the two interaction potentials were essentially derived from similar principals (as far as the dispersion energy is concerned). Nevertheless the $v_2 = 1 \rightarrow 0$ de-excitation cross sections calculated using the two potentials are very different. Evidently when comparing different potential surfaces the terms of major interest should be the terms that are directly

responsible for the transition being studied.

In order to compare with the calculations of Drolshagen and Gianturco (1983, 1984), we performed calculations in which the rotational motion of the CO was treated within the breathing sphere (BS) approximation. The interaction potential of van Hemert (1983) was employed, and harmonic oscillator wavefunctions were used to describe the vibrational motion of the CO molecule. In Table 27 (column 6) we present some of the results of these calculations. Comparison of columns 4 and 5 in Table 27 shows that cross sections computed using the BS approximation are roughly an order of magnitude smaller than the corresponding IOS results; the largest discrepancies being found at lower energy. In this respect, our conclusions are in qualitative agreement with these of Gianturco et al. (1982) for the CO + He system. In addition note that BSD find similar agreement between results obtained using the BS and IOS approximations. As already mentioned the rotational-vibrational coupling is large for H_2 + CO, and since the BS approximation neglects this coupling it must be dismissed as a realistic dynamical approach to study the H_2 + CO system.

In column 5 of Table 27 we present the results of calculations employing the BS approximation, and using Morse oscillator wavefunctions to describe the vibrational motion of the CO molecule. A comparison of the results computed using the BS approximation, but using different descriptions of the vibrational

motion of the CO molecule indicates that the calculation of rovibrational cross sections is less sensitive to the form of the vibrational eigenfunctions than to the dynamical approximation employed or to the form of the interaction potential.

In Figure 7, we compare values of the vibrational relaxation coefficient, $\alpha_{1\to 0}$, as computed by Drolshagen and Gianturco (1984), with our own results, employing the VH potential, harmonic oscillator wavefunctions, and the BS approximation. The paper of Drolshagen and Gianturco (1983) contains graphs which display the variation with energy of rotationally summed cross sections for the vibrational de-excitation processes ($v_2 = 1$ to $v_2' = 0$, and $v_2 = 2$ to $v_2' = 0$). A comparison of the results of Drolshagen and Gianturco (1983) with our own results for the transition ($v_2 = 1$ to $v_2' = 0$), by visual inspection of the relevant graph , shows that the values computed by these authors are systematically smaller than our own. We have no satisfactory explanation for the discrepancies in either the de-excitation cross sections or in the values of the vibrational rate coefficients shown in Figure 7.

Since the cross sections evaluated by Drolshagen and Gianturco (1984) are systematically lower than our own, we would expect a corresponding lowering of the relaxation rate coefficient in the entire temperature range shown in Figure 7. The lowest energy

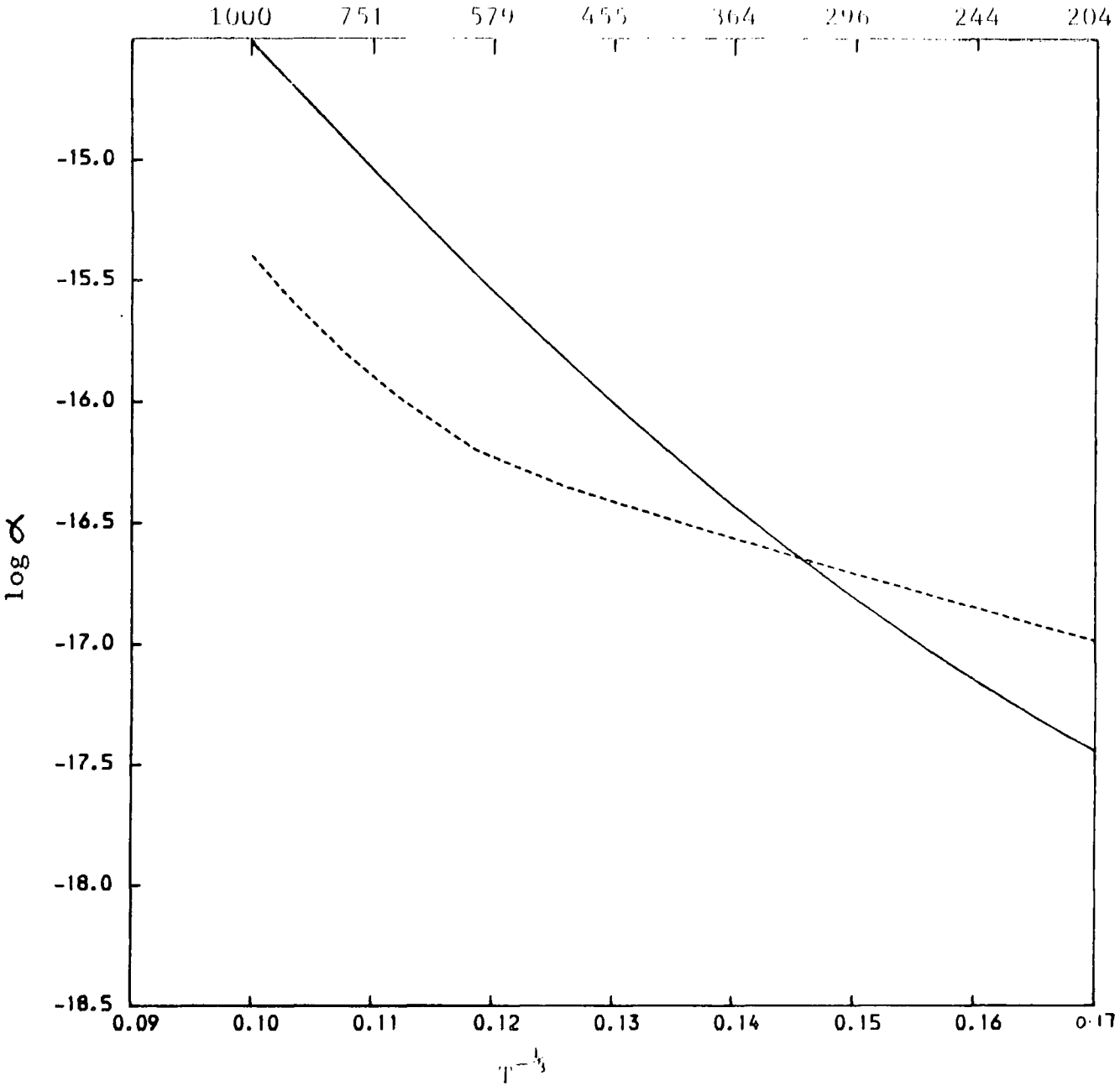

Figure 7 A comparison of BS calculations of the variation with temperature, T(K), of the vibrational relaxation coefficient, α ($cm^3 s^{-1}$). Full curve : present calculations; broken curve : Drolshagen and Gianturco (1984).

studied in this calculation is 1.1 $\hbar\omega$ (corresponding to T $\sim$ 300K), we initially thought that the relaxation rate coefficient, evaluated in our calculations, might be erroneous for T $\lesssim$ 300 K. We therefore calculated an additional cross section at E = 1.05 $\hbar\omega$, and recalculated the rate coefficient. At T $\lesssim$ 300K the values of the rate coefficient changed by less than 1%.

Drolshagen and Gianturco (1984), Gianturco (private communication) claim that the vibrational basis employed in our calculations is insufficient, and state that in their calculations three to four closed channels were required at all the collision energies studied (E $\lesssim$ 4 eV). However for the range of collision energies studied in the present calculations (E $\lesssim$ 1eV) we have demonstrated that it is sufficient to include all the open channels, and one closed channel to ensure convergence to within $\sim$ 5% (see Table 22, Section 4.2). This is confirmed by BSD who have carried out H_2 + CO calculations of the type considered here, using the BS approximation, and employing the DK potential.

It appears that there is a difference between the calculations of Drolshagen and Gianturco (1983) and the present study. In the work of Drolshagen and Gianturco (1983) the vibrational coupling is taken to be independent of R and is taken to be its value at the classical turning point (see Gianturco et al. (1980) for more details). However, employing this technique Gianturco et al. (1980)

find that at low collision energies ($E \lesssim 1eV$) only the open channels are required to achieve satisfactory results for vibrationally inelastic cross sections for the He + CO system. Consequently it is not clear to us why Drolshagen and Gianturco (1983) required three to four closed channels at all energies. In addition we note that the rate coefficient reported in the paper of Drolshagen and Gianturco (1983) are erroneous (Drolshagen and Gianturco (1984), Gianturco (private communication)), this does not make one confident of the validity of the revised rate coefficient. It is worth repeating that in view of the behaviour of the cross sections calculated in this and in the calculation of Drolshagen and Gianturco (1983), one would expect the rate coefficient of Drolshagen and Gianturco (1984) to be systematically lower than that evaluated in our calculation at the temperatures shown in Figure 7.

In conclusion, in view of the qualitative agreement between our BS calculations and those of both Gianturco et al. (1980) and BSD, and in view of behaviour of the rate coefficients calculated in this and in the calculation of Drolshagen and Gianturco (1983, 1984), we believe that both the cross sections and the rate coefficients computed by these authors are seriously in error .

6. Summary

We have performed quantum mechanical calculations of the rovibrational de-excitation of CO by H_2. In the present study the H_2 molecule is constrained in its ground rotational state ($j_1 = 0$). Calculations are performed using both the P potential, and the VH potential in which the rotational degree of freedom of the CO molecule is treated within the IOS approximation, and in which the vibrational motion is approximated by Morse oscillator wavefunctions. We find that our IOS cross sections for the vibrational de-excitation process $v_2 = 1$ to $v_2' = 0$ are roughly a factor of 3 smaller than the corresponding results evaluated by BSD employing the DK potential. We are not able to give a simple explanation of this observation, however we find the computed values of the rate coefficient for the vibrational de-excitation of CO($v_2 = 1$) by ortho-H_2 are in reasonable agreement with the experimental points of Andrews and Simpsons (1976). The results obtained by BSD are in better agreement with experiment, however we note that in view of the CS and IOS results obtained by BSD the use of the CS approximation should increase our IOS rates by a factor of 1.5, and thus the agreement with experiment would improve. The semi-classical results of Poulsen and Billing (1982) using the P potential are in excellent agreement with the experimental results,

however, in view of the results of BSD we suspect that the semi-classical approximation employed by these authors is not suitable to study the vibrational excitation of CO by H_2, and thus we consider this agreement purely accidental.

The agreement between the IOS results obtained using the P and VH potential deteriorates with increasing Δv_2. We attribute this to the difficulty of obtaining consistent higher order terms in two independent derivations of an interaction potential.

We have performed BS calculations employing the VH potential, and using both harmonic and Morse oscillator wavefunctions to describe the vibrational motion of CO. The BS approximation gives cross sections which are roughly an order of magnitude smaller than the corresponding IOS cross sections evaluated using the same potential surface. We conclude, in view of this, and the results obtained by BSD, that the BS approximation should be ruled out as a possible means of studying the vibrational de-excitation of CO by H_2. In addition, we conclude, by comparing the BS results obtained using different vibrational wavefunctions, that the calculation of rovibrational cross sections is less sensitive to the form of the vibrational eigenfunctions than to the dynamical approximations employed or to the form of the interaction potential.

The agreement with the BS results of Drolshagen

and Gianturco (1983, 1984), is unsatisfactory. The reasons for the discrepancies between both the computed values of the cross sections and the rate coefficients for the vibrational de-excitation of CO(v_2 = 1) by ortho-H_2 are unresolved. We conclude, in view of the results of Gianturco et al. (1980) and BSD, that the results presented by Drolshagen and Gianturco (1983, 1984) are seriously in error.

CHAPTER VI

NEAR-RESONANCE VIBRATIONAL RELAXATION OF $^{12}C^{16}O$ IN COLLISIONS WITH PARA-H_2

1. Introduction

As stated in Chapter V.1, since the early experiment of Hooker and Millikan (1963) there has been considerable interest in the H_2 + CO system. Measurements have been made in ortho-H_2 (j_1 = 1,3,5---), and para-H_2 (j_1 = 0,2,4---) as well as normal-H_2, over a wide range of kinetic temperatures.

It has been observed experimentally that para-H_2 is more efficient than ortho-H_2 in the vibrational deactivation of CO(v_2 = 1) (Millikan and Osburg (1964)). These authors anticipated that the difference must be due to the populations of different rotational levels, and they suggested that the following near-resonance transition makes the deactivation faster in para-H_2 (V.2.4).

$$CO(v_2=1) + H_2(j_1=2) \rightarrow CO(v_2=0) + H_2(j_1=6) + 87.03\ cm^{-1}$$

VI.1.1

More recently Andrews and Simpson (1976) have published experimental measurements for normal -H_2, para-H_2 and ortho-H_2 in the temperature range $77 \leq T \leq 340$K.

A satisfactory theoretical interpretation of this effect has been needed for several years. The earliest

attempts to explain the experimental observation are those of Sharma and Kern (1971)), and Nelson and Roberts (1973). Both studies close with a reasonable agreement between theory and experiment after making numerous assumptions and simplifications concerning the dynamics. Some of the approximations have been shown to be inappropriate for the H_2 + CO system, for example, the breathing sphere approximation for the CO rotational degree of freedom used by Nelson and Roberts (1973) and the use of straight-path classical trajectories employed by Sharma and Kern (1971) (see Chapter V.5). The lack of detailed information about the interaction potential at that time prohibited any more realistic dynamical study. While Sharma and Kern (1971) consider only the long range multipole moments with a hard sphere radius of 3.3Å, Nelson and Roberts (1973) treat the vibration-rotation coupling as a fit parameter from the beginning.

As discussed in Chapter V.1 it is only recently that potential surfaces suitable to study the vibrational de-excitation of CO by H_2 have become available in the literature (Poulsen (1982), van Hemert (1983), and Bačić, Schinke, and Diercksen (1984a)). The first realistic dynamical study of the near-resonance process (VI.1.1) was carried out by Poulsen and Billing (1982). These authors calculated relaxation rates within a semi-classical (classical path) approximation employing the P potential. The agreement with the experimental data for both para-

and ortho-H_2 is excellent. It is shown that the difference between the ortho- and para- rate is due to the near-resonance process which the authors conclude is primarily induced by the long range multipole interaction between the hexadecapole moment of H_2 and the dipole moment of CO.

It will be recalled that in the previous chapter we studied the de-excitation of CO($v_2 = 1$) by H_2 constrained in its ground rotational state ($j_1 = 0$). In the present chapter we extend the calculations presented in Chapter V by taking explicit account of the H_2 rotational degree of freedom. The sudden approximation is inapplicable to H_2, owing to the large value of its rotational constant, and therefore we employ the more accurate coupled states (CS) approximation (Chapter II). However, in relatively high energy collisions involving lighter collision partners, for example H^+, satisfactory results can be obtained employing the IOS approximation (e.g. see Schinke and McGuire (1978a)). The rotational degree of freedom of the CO is treated within the IOS approximation.

In Chapter V.5 it was shown that the P potential provides a better description of rovibrational excitation of CO by H_2 than the VH potential, consequently only the P potential will be employed in these calculations. Since we now take explicit account of the rotational motion of the H_2, the H_2 anisotropy terms of the interaction must be included. In this chapter we are primarily concerned with the calculation of cross sections and the rate

coefficient for the near-resonance process, and the subsequent calculation of the rate of deactivation of CO by para-H_2. However, the dependence of the results on the rotational state of the H_2 will also be studied in some detail.

Very recently a quantum mechanical study of the near-resonance process was carried out by Bačić, Schinke, and Diercksen (1984b). These authors employed the same decoupling approximations as used in the present study, but employed the DK potential. The rate for para-H_2 agrees to within a factor of two with the experimental rate in the temperature range $100 \leq T \leq 300$K, however, although the relaxation rate for the near-resonance process is found to be large its contribution to the total para-H_2 rate is only of minor importance unlike in the study of Poulsen and Billing (1982).

2. Description of the system

In Chapter V.5 it was shown that the P potential provides a better description of rovibrational excitation of CO by H_2 than the VH potential, consequently only the P potential will be employed in these calculations. Since we now take explicit account of the rotational degree of freedom of H_2, the H_2 anisotropy terms in the interaction potential must be included in the calculations. The interaction potential may be written

$$V(\hat{r}_1, \hat{r}_2, R) = \sum_{\lambda_1 v_1} V_{\lambda_1 v_1}(r_1, \hat{r}_2, R)\, Y_{\lambda_1 v_1}(\hat{r}_1). \qquad \text{VI.2.1}$$

where $\lambda_1 = 0, 2,$ and 4

In keeping with the dynamical approximations employed in these calculations (i.e., the rotational motion of CO is treated within the IOS approximation, the rotational motion of H_2 is treated within the CS approximation), we consider only those terms with $v_1 = 0$ (Chapter II.3.3). As in the previous H_2 + CO calculations the internuclear separation of the H_2 molecule is constrained at its equilibrium value $r_{1,eq}$ where

$$r_{1,eq} = 1.4 \text{ a.u.}$$

The potential may now be written

$$V(\theta_1, \phi, \theta_2, r_2, R) = \sum_{\lambda_1} V_{\lambda_1 0}(\theta_2, r_2, R)\, Y_{\lambda_1 0}(\theta_1, \phi), \qquad \text{VI.2.2}$$

where $\phi = \phi_1 - \phi_2$.

The coordinate system is that defined by figure 1 of Chapter V.2, see Chapter V.2 for details of the P potential.

As mentioned in Chapter V.2 there is an error in the long range multipole moment interactions given in the paper of Poulsen (1982). These interactions are given by (e.g. see Flower et al. (1979), Leavitt (1980)) (cf. V.2.7)

$$\tilde{V}_{Q\mu} = -4\pi(15)^{-1/2} Q^{HH} \mu^{CO} R^{-4} \left(3 Y_{20}^{HH} Y_{10}^{CO}\right)$$

$$\tilde{V}_{QQ} = 4\pi(5)^{-1} Q^{HH} Q^{CO} R^{-5} \left(6 Y_{20}^{HH} Y_{20}^{CO}\right)$$

$$\tilde{V}_{Q4\mu} = -4\pi(27)^{-1/2} Q_4^{HH} \mu^{CO} R^{-6} \left(5 Y_{40}^{HH} Y_{10}^{CO}\right)$$

$$\tilde{V}_{Q4Q} = 4\pi(45)^{-1/2} Q_4^{HH} Q^{CO} R^{-7} \left(15 Y_{40}^{HH} Y_{20}^{CO}\right) \qquad \text{VI.2.3}$$

where Q^{HH} and Q_4^{HH} are the quadrupole and hexadecapole moments of the H_2 molecule respectively, and μ^{CO} and Q^{CO} are the dipole and quadrupole moments of the CO molecule respectively and where

$$Y^{HH}_{l,0}\, Y^{CO}_{l20} = \frac{1}{2}\left[Y_{l,0}(\theta_1,\phi_1)\,Y_{l20}(\theta_2,\phi_2) + Y_{l,0}(\theta_1,\phi_1)\,Y_{l20}(\theta_2\phi_2)\right] \qquad \text{VI.2.4}$$

In the paper of Poulsen (1982) the factor of 1/2 is omitted from VI.2.4 (Bačić, Schinke, and Diercksen (1984b)). This error was present in our computer programme, and therefore some of the cross sections presented in this chapter are in error. The effects of the above error are discussed in detail in Appendix 4 at the end of this thesis.

The vibrational basis functions of the CO were taken to be the Morse oscillator wavefunctions employed in the IOS calculations presented in Chapter V. The details of these wavefunctions are given in Chapter V.3, and their calculation is discussed in Appendix 3 at the back of this thesis.

The major object of these calculations is to evaluate cross sections and rate coefficients for the near-resonance process.

$$CO(v_2=1) + H_2(j_1=2) \rightarrow CO(v_2=0) + H_2(j_1=6) + \Delta E \qquad \text{VI.2.5}$$

The energy defect, ΔE, associated with a near-resonance process is extremely important. Small changes in ΔE can lead to significant changes in the magnitude of the

near-resonance cross sections (e.g. see Bačić, Schinke, and Diercksen (1984b)). It was therefore, considered important that ΔE was as close as possible to values quoted in the literature (e.g., Andrews and Simpson (1976), Poulsen and Billing (1982)). Bačić, Schinke, and Diercksen (1984b) (hereafter referred to as BSD2) employed a value for the defect which is roughly a factor of 2 too high, and on the opposite side of resonance. In Appendix 4, in addition to discussing the error in our potential routine we will present the results of BSD2 obtained employing the P potential. In particular it will be shown that the erroneous energy defect used by BSD2 leads to an overestimation of the cross sections for the near-resonance process by a factor of $\lesssim 2$. The values of the energy defects employed by the above authors are given in Table 1.

There are a number of sources in the literature from which one may obtain values for the vibrational eigenenergies (e.g., Herzberg (1950), Mies (1964), Mizushima (1975)) and values for the rotational eigenenergies (e.g., Herzberg (1957), Mizushima (1975), Flower and Launay (1977)). In Table 2 we present the values of the energy defect, ΔE, resulting from a number of combinations of the above vibrational and rotational energies. It was decided to employ the eigenenergies calculated using the data from Herzberg (1950), since these ensure a reasonable value for the defect. It will be recalled that in our previous study of H_2 + CO in Chapter V we employed the

TABLE 1

Values of the Energy Defect, ΔE, employed by various authors.

	$\Delta E(cm^{-1})$
Andrews and Simpson (1976)	82.0
Poulsen and Billing (1982)	83.3
Bačić, Schinke, and Diercksen (1984b)	-43.3

TABLE 2

Values of the Energy Defect, $\Delta E(cm^{-1})$, calculated using vibrational and rotational eigenenergies taken from the literature.

Eigenenergies		
Vibrational	Rotational	$\Delta E(cm^{-1})$
Herzberg	Herzberg	87.03
Mizushima	Mizushima	91.41
Mies	Herzberg	95.98
Mies	Mizushima	100.36

Morse vibrational eigenenergies given by Mies (1964). We consider that this slight inconsistency should have an insignificant effect on the 'V-T' cross sections (i.e., any comparisons that are made with the results of Chapter V should be valid). In conclusion the vibrational and rotational eigenenergies are calculated using:-

Vibrational Eigenenergies

$$\mathcal{E}_{v_2} = \omega_0 v_2 - \omega_0 x_0 v_2^2 + \omega_0 y_0 v_2^3 \qquad \text{VI.2.6}$$

where $\omega_0 = 2156.7721 \text{cm}^{-1}$, $\omega_0 x_0 = 13.4148 \text{ cm}^{-1}$, and $\omega_0 y_0 = 0.0303 \text{ cm}^{-1}$.

Rotational Eigenenergies

$$\mathcal{E}_{j_1} = B_0 j_1(j_1+1) - D_0 j_1^2 (j_1+1)^2 \qquad \text{VI.2.7}$$

where $B_0 = 59.3125 \text{ cm}^{-1}$ and $D_0 = 0.0456552 \text{ cm}^{-1}$.

The equilibrium CO internuclear separation is taken to be

$$r_{2,eq} = 2.132 \text{ a.u.}$$

The reduced masses of the CO and H_2 + CO system are taken to be $\mu_{CO} = 12499.6$ a.u., and $\mu = 3427.79$ a.u. respectively. See Chapter V.3 for more details.

3. Numerical Methods

We extend the study of the vibrational de-excitation of $CO(v_2 = 1)$ by para-$H_2(j_1 = 0)$ presented in Chapter V by performing calculations in which the rotational degree of freedom of the H_2 molecule is treated explicitly.

We are primarily interested in the calculation of cross sections for the near-resonance process (VI.2.5) and for the 'V-T' process in which $j_1 = j_1' = 2$. We note that we examine the near-resonance process in a model calculation in which only the directly relevant rotational states $j_1 = 2$ and 6 are included in the coupled equations. This is discussed in Section 4.2.1. Relaxation rate coefficients evaluated using cross sections calculated for these processes are used together with the rate coefficient evaluated in Chapter V for the 'V-T' process in which $j_1 = j_1' = 0$ to calculate the rate coefficient for the de-excitation of $CO(v_2 = 1)$ by para-H_2. The above processes are studied at six energies, E_T = 64.8322, 83.0, 129.915, 208.0, 2299.36, and 3167.14 cm^{-1}, where E_T denotes the initial kinetic energy for the collision (i.e. relative to the $v_2 = 1$ $j_1 = 2$ threshold).

In addition we study the dependence of the vibrational de-excitation of CO ($v_2 = 1$) on the rotational states of H_2. The 'V-T'($j_1 = 2$) cross sections and rates are used together with the 'V-T' calculations evaluated in Chapter V to study the dependence of the vibrational de-excitation process $v_2 = 1 \rightarrow 0$ on the initial rotational state of H_2. Also we evaluate cross sections for the $\Delta j_1 = 0$ and 2 rotational transitions in the same calculations to examine the relative magnitude of $\Delta j_1 = 2$ cross sections compared to $\Delta j_1 = 0$ cross sections, and also to examine the effect of the $\Delta j_1 = 2$ transitions on the 'V-T' results.

In this section we shall present the numerical methods required for the evaluation of the cross sections for the above processes. Where possible the numerical methods developed for the calculations presented in Chapter V will be employed.

3.1 Solution of the coupled equations at fixed orientation

In these calculations we again employ the R-matrix propagator method to solve the fixed angle coupled equations, using propagators corresponding to a constant reference potential (Chapter III.4.4). A fixed step size is employed in all of the calculations. In these calculations we shall work in terms of kinetic barycentric energies rather than total collision energies, since for two different processes the total energies may be very different, whilst the initial (and possibly final) kinetic energies are identical. For example consider the following process,

$$CO(v_2=1) + H_2(j_1) \longrightarrow CO(v_2'=0) + H_2(j_1'), \qquad \text{VI.3.1}$$

where only one rotational state is retained in the coupled equations (i.e. $j_1 = j_1'$). If we let $j_1 = 0$, and denote the initial kinetic energy by E_T, then the corresponding total energy is given by

$$E = E_T + E(v_2=1), \qquad \text{VI.3.2}$$

where $E(v_2 = 1)$ is the energy of the first excited vibrational state of CO (relative to $v_2 = 0$). If we let $j_1 = 2$ and maintain the same initial kinetic energy, E_T, then the corresponding total energy is now given by

$$E = E_T + E(v_2 = 1) + E(j_1 = 2) \qquad \text{VI.3.3}$$

where $E(j_1 = 2)$ is the energy of the second excited rotational state of H_2 above $j_1 = 0$. Although the kinetic energies of the two processes are identical, the total energies differ by $E(j_1 = 2)$. Given these simple processes, and given that the initial kinetic energies are identical, the step size, and integration range determined for the process in which $j_1 = 0$ should be adequate to study the process with $j_1 = 2$. The addition of the H_2 anisotropy terms into the potential surface should have an insignificant effect on the variation of the interaction potential as a function of R. Below we shall generalise our arguments to more complicated situations (i.e. where there is more than one rotational channel), and therefore use numerical integration parameters determined for non-rotating H_2 ($j_1 = 0$) in calculations where the rotational degree of freedom of the H_2 molecule is explicitly treated. Consequently where possible we shall use the step size and integration range determined in Chapter V.4.1.

It will be recalled that in Chapter V.4 the lower limit of the integration range, R_{min}, was determined

at the highest total collision energy, E = 6291.4021 cm^{-1} (which is also the highest translational energy). As stated in Chapter V.4 the value of R_{min} = 2 a.u. should be satisfactory at all energies $<$ 6291.4021 cm^{-1} since we are required to start the integration in the classically forbidden region where the interaction potential is much greater than the kinetic energy. It may be shown that the maximum kinetic energy in these calculations is 5310.5314 cm^{-1}, and consequently the value of R_{min} = 2 a.u. should be satisfactory for these calculations, and will be used throughout this study.

The energy (or more precisely the translational energies) only enter into the calculations in the diagonal elements of the potential matrix, therefore as stated in Chapter V.4, as these diagonal elements decrease the off diagonal elements will be become more important. Consequently the step size required to maintain accuracy may have to be decreased. However, this dependence of the step size on the energy is weak, as shown in Chapter V.4, the step size required to maintain accuracy did not vary significantly with the initial translational energy, E_T, for 233.5549 $\leq E_T \leq$ 4138.5631cm^{-1} (where E_T is relative to $v_2 = 1 j_1 = 0$). The minimum kinetic energy considered in these calculations (and therefore the minimum diagonal element in a potential matrix in any of these calculations) is 64.8322 cm^{-1}. In Table 3 we show the values of $|S_L(v_2=1, v_2'=0/\theta_2)|^2$ evaluated, retaining two vibrational channels in the coupled equations, employing several different step sizes

TABLE 3

Comparison of $|S_L(v_2, v_2'|\theta_2)|^2$ obtained using different numbers of steps over the integration range at $E_T = 64.8322\ cm^{-1}$ for the vibrational de-excitation process, $v_2 = 1$ to $v_2' = 0$, in CO.

(a) 160 steps, (b) 380 steps, (c) 760 steps, (d) 3800 steps

θ_2 =	0°	90°	180°
L			
0	(a) 0.73965840-7	0.12582501-7	0.46712753-8
	(b) 0.74905092-7	0.12724302-7	0.47296381-8
	(c) 0.75016444-7	0.12742139-7	0.47365258-8
	(d) 0.75040162-7	0.12746161-7	0.47379490-8
10	0.10910313-7	0.16531459-8	0.92584605-9
	0.11045749-7	0.16717943-8	0.93725740-9
	0.11061607-7	0.16741672-8	0.93859710-9
	0.11064945-7	0.16747069-8	0.93887056-9

$|S_L(v_2, v_2'|\theta_2)|^2$ in units of $(a.u.)^2$

$R_{min} = 2$ a.u., $R_{max} = 40$ a.u.

at E_T = 64.8322 cm^{-1} at three CO orientations (θ_2 = 0^o, 90^o, 180^o) and at L = 0, and 10. The results were obtained maintaining R_{min} = 2 a.u., and R_{max} = 40 a.u. (which, as stated in Chapter V.4, should be more than adequate to converge vibrationally inelastic cross sections). As may be seen the agreement between the results obtained employing 3800, 760, 380 and 190 steps in the range $2.0 \lesssim R \lesssim 40.0$ a.u. is extremely good at each of the values of L shown. It appears that lowering the kinetic energy from 233.5549 cm^{-1} to 64.8322 cm^{-1} has no significant effect on the convergence of the results (see Table 9, Chapter V.4). Since we found the energy dependence of the step size to be weak in our previous H_2 + CO calculations it would have been rather surprising if we had concluded otherwise. In addition we found that the step size required to maintain accuracy did not vary significantly with the partial wave parameter, L, for $L \lesssim 100$. The range of energies, E_T, considered in the present calculations is lower than that studied in Chapter V.4, however we found that the near-resonance partial cross sections decrease more slowly with L than the "V-T" results. (Indeed,we found that at E_T = 3167.14 cm^{-1}, we needed to consider $L \lesssim 80$ to converge the integral cross sections to within 1% for both the 'V-T'($j_1 = 2$) and near-resonance ($j_1 = 2$, $j_1' = 6$) processes. As mentioned above we expect that the R variation of the interaction potential will not be significantly affected by the addition of the H_2

anisotropy terms in the potential. By employing a step size which is extremely efficient for non-rotating H_2 we should be able to accommodate any changes in the R variation of the potential that are present in rotating H_2 calculations. In conclusion we will employ a step size of 0.05 a.u. (corresponding to 760 steps in Table 3) in all of our calculations, which as one will recall was used in our previous H_2 + CO calculations.

As noted in Chapter V.4 it is necessary to integrate the coupled equations sufficiently far into the asymptotic region to where the interaction potential has become negligible before the boundary condition may be fitted, also it is necessary that the boundary condition be fitted in the classically allowed region (where the solution is a linear combination of oscillatory functions). In Table 4 we show the convergence of $|S_L(v_2=1, v_2'=0|\theta_2)|^2$ as a function of the upper limit of the integration range, R_{max}, at E_T = 64.8322 cm^{-1}. The results are shown for three CO orientations (θ_2 = 0^o, 90^o, and 180^o) at L = 0, 10, and 20. These results are evaluated maintaining R_{min} = 2 a.u., a step size of 0.01 a.u. (corresponding to 3800 steps in Table 3), and retaining two vibrational channels in the coupled equations. As may be seen, at L = 20 it is impossible to maintain accuracy as we are dealing with numerical zeros. The results indicate that reducing the kinetic energy from 233.5549 cm^{-1} to 64.8322 cm^{-1} does not significantly increase the required value of R_{max}. In Table 4 a value R_{max} = 25 a.u. is

TABLE 4

Comparison of $|S_L(v_2=1 j_1=0, v_2'=0 j_1'=0|\theta_2)|^2$ obtained using different values of R_{max} (a.u.) at E_T = 64.8322 cm^{-1}.

(a) 20.0, (b) 25.0, (c) 30.0.

θ_2 =	0^o	90^o	180^o
L			
0	(a) 0.74975379-7	0.12752299-7	0.47262148-8
	(b) 0.75026976-7	0.12744359-7	0.47376643-8
	(c) 0.75021103-7	0.12745729-7	0.47376178-8
10	0.11065894-7	0.16734425-8	0.94681785-9
	0.11061700-7	0.16745149-8	0.93894562-9
	0.11060899-7	0.16747638-8	0.93890258-9
20	0.14782977-15	0.13784626-17	0.67046550-14
	0.83126358-18	0.11468204-19	0.49776530-16
	0.13198875-17	0.11565855-19	0.24848210-16

$|S_L(v_2 j_1, v_2' j_1'|\theta_2)|^2$ in units of (a.u.)^2

R_{min} maintained at 2 a.u.

Step size 0.01 a.u.

able to converge $|S_L(v_2=1, v_2'=0|\theta_2)|^2$ to within a few per cent (cf. Table 16, Chapter V.4). In conclusion the coupled equations are solved by employing ~ 460 steps (step size = 0.05 a.u.) in the range $2.0 \lesssim R \lesssim$ 25.0 a.u., as was done in our calculations in Chapter V.

3.2 Description of the H_2 molecule

In these calculations we are primarily interested in the calculation of cross sections for the near-resonance process (VI.2.5). For this calculation the rotational structure of the H_2 molecule is represented by a truncated basis set consisting of the directly relevant states $j_1 = 2$ and $j_1 = 6$. This approximation will be discussed in detail, and justified in Section 4.2.

In Chapter V we performed calculations of the vibrational deactivation of $CO(v_2 = 1)$ by H_2 constrained in its ground rotational ($j_1 = 0$) state. In doing so we explicitly neglect the effect of any coupling from other rotational channels. In order to study the dependence of the 'V-T' cross sections and rate coefficients on the rotational state of the H_2 molecule we have performed calculations in which only the $j_1 = 2$ rotational state is included in the basis and neglect all other rotational states.

We also carry out a number of calculations to study the effect of $\Delta j_1 = 2$ transitions on the $\Delta j_1 = 0$ results, and to study the magnitude of $\Delta j_1 = 2$ cross sections relative to the corresponding $\Delta j_1 = 0$ cross sections. This was in response to Schinke (private communication)

who informed us that $\Delta j_1 = 2$ transitions are important, and consequently claimed that our 'model calculation' of the near-resonance process was inadequate (Notice that the inclusion of just $j_1 = 2$ and $j_1 = 6$ in the rotational basis explicitly ignores $\Delta j_1 = 2$ transitions). This is in sharp contrast to Poulsen and Billing (1982) who find that $\Delta j_1 = 2$ transitions are insignificant (compared to the corresponding $\Delta j_1 = 0$ transitions). We study cross sections for the rotational transitions $j_1 = 0 \rightarrow 0$ $j_1 = 0 \rightarrow 2$, $j_1 = 1 \rightarrow 1$, and $j_1 = 1 \rightarrow 3$ (while the CO undergoes the vibrational transition, $v_2 = 1 \rightarrow 0$) including only the directly relevant rotational channels ($j_1 = 0$ and 2, and $j_1 = 1$ and 3 respectively) to examine the claims made by Schinke. In Section 4 we present our calculations of $\Delta j_1 = 0$ and $\Delta j_1 = 2$ cross sections and rates, and as mentioned above, discuss the validity of the rotational basis set employed to examine the near-resonance process, in the light of our calculations.

3.3 Description of the CO molecule

In the present calculations the interaction potential is more anisotropic than that employed in our previous H_2 + CO calculations. This is due entirely to the introduction of the rotational degree of freedom of the H_2 molecule, and there are no additional anisotropy terms describing the CO molecule. In addition the range of total barycentric collision energies studied in the present calculations is lower than that studied in Chapter V($E \leq 5664.76$ cm^{-1} compared with $E \leq 6291.4021$ cm^{-1}). We therefore conclude

that the treatment of the CO molecule in our previous calculations should be satisfactory, and accordingly we retain three vibrational channels in all these calculations. It will be recalled that this basis ensures that the cross sections for the vibrational de-excitation process, $v_2 = 1$ to $v_2' = 0$, are converged to within a few percent (see Table 18, Chapter V.4).

For these diatom-diatom calculations the potential matrix elements may be written (cf. II.3.22)

$$V_{v_2 j_1 \Omega_1, v_2' j_1' \Omega_1'}(R,\theta_2) = \delta_{\Omega_1,\Omega_1'} \sum_{\lambda_1} V_{\lambda_1}^{v_2 v_2'}(R,\theta_2)\, X(j_1 j_1' \Omega_1 \lambda_1), \qquad \text{VI.3.4}$$

where

$$V_{\lambda_1}^{v_2 v_2'}(R,\theta_2) = \sum_{\lambda_2} P_{\lambda_2}(\cos\theta_2) \int_0^\infty dr_2\, \phi_{v_2}(r_2)\, V_{\lambda_1\lambda_2}(R,r_2)\, \phi_{v_2'}(r_2), \qquad \text{VI.3.4a}$$

and where

$$X(j_1 j_1' \Omega_1 \lambda_1) = (-1)^{\Omega_1} [(2j_1+1)(2j_1'+1)]^{\frac{1}{2}} \begin{pmatrix} j_1 & j_1' & \lambda_1 \\ 0 & 0 & 0 \end{pmatrix} \begin{pmatrix} j_1 & j_1' & \lambda_1 \\ \Omega_1 & -\Omega_1 & 0 \end{pmatrix}. \qquad \text{IV.3.4b}$$

To evaluate cross sections for the near-resonance process one must perform three separate calculations at each CO orientation, θ_2. The coupled equations must be solved at three values of Ω_1 (i.e. $\Omega_1 \leq 2$, since $\Omega_1 \leq \min(j_1 = 2, j_1 = 6)$). The vibrational potential matrix elements, $V_{\lambda_1}^{v_2 v_2'}(R,\theta_2)$, are however independent of Ω_1, and consequently one only need evaluate the values of

$V_{\lambda_1}^{v_2 v_2'}(R,\theta_2)$ at the initial value of Ω_1, and they may be used at subsequent values of Ω_1. However it was found that there was insufficient storage available to do this, and consequently the matrix elements $V_{\lambda_1}^{v_2 v_2'}(R,\theta_2)$ had to be evaluated at each value of Ω_1.

In our previous H_2 + CO calculations we employed a 96- point Gauss Legendre quadrature to evaluate the vibrational potential matrix elements, $V_{\lambda_1}^{v_2 v_2'}(R,\theta_2)$. Employing this quadrature, and retaining the same vibrational basis it was found that the calculation of $V_{\lambda_1}^{v_2 v_2'}(R,\theta_2)$ was roughly a factor of 3 more expensive in the present calculations, due to the additional terms in the interaction potential. Since we employ an approximate potential algorithm to solve the coupled differential equations, the calculations at subsequent partial waves require no explicit reference to the potential matrix elements, however we considered the increase in computer time at the initial partial wave unacceptably high. Note that this is further increased by the addition of H_2 rotational states into the calculation, and in addition as the number of H_2 rotational states is increased we found that the advantage gained at subsequent partial waves decreases. It is worth mentioning that this is one of the major reasons for employing our model calculation to evaluate cross sections for the near-resonance process. Essentially we could not afford to retain more than two rotational channels. This is discussed in Section

4.2.1. One will recall that a 96-point quadrature ensures extremely high numerical accuracy. The agreement between the results evaluated employing 48-, 64-, and 96- point Gauss Legendre quadratures is excellent (see Table 4, Chapter V.4). It should therefore be possible to reduce the number of quadrature points used to evaluate $V_{\lambda_1}^{v_2 v_2'}(R,\theta_2)$ considerably without any significant loss of accuracy.

In Table 5 we compare the values of $|S_L(v_2 j_1 \Omega_1, v_2' j_1' \Omega_1/\theta_2)|^2$ evaluated at $E_T = 64.8322\ cm^{-1}$ and $L = 0$ employing 64- 48-, and 28- point Gauss Legendre quadratures to evaluate the vibrational potential matrix elements. Three vibrational channels, and two rotational channels ($j_1 = 2$ and 6) are retained in the coupled equations. The results are shown for $\Omega_1 = 0$ and $\theta_2 = 0^\circ$, 90°, and 180° for the transitions $v_2 = 1$ $j_1 = 2 \rightarrow v_2' = 0$ $j_1' = 2$, and $v_2 = 1$ $j_1 = 2 \rightarrow v_2' = 0$ $j_1' = 6$. At this energy, which is the lowest studied, any errors in the evaluation of the potential matrix elements should have maximum effect on the values of $|S_L(v_2 j_1 \Omega_1, v_2' j_1' \Omega_1/\theta_2)|^2$. As can be seen the agreement between the results evaluated employing 28-, 48-, and 64- point quadratures is very good, in addition it is worth noting that a 28-point quadrature results in a reduction of a factor of ~ 3 in the computer time required by a 96-point quadrature for the calculation of $V_{\lambda_1}^{v_2 v_2'}(R,\theta_2)$ for $v_2(v_2') \leq 3$. In conclusion a 28-point Gauss Legendre quadrature will be employed throughout these calculations.

TABLE 5

Comparison of $|S_L(v_2=1 j_1 \Omega_1=0, v_2'=0 j_1' \Omega_1' | \theta_2)|^2$ obtained using different N-point Gauss Legendre quadratures to evaluate the vibrational potential matrix elements at E_T = 64.8322 cm^{-1} and L = 0.

(a) N = 64, (b) N = 48, (c) N = 28.

θ_2 =		0°	90°	180°
j_1 = 2 to				
j_1' = 2	(a)	0.18974629-6	0.78139596-8	0.36535433-8
	(b)	0.18974629-6	0.78139596-8	0.36535433-8
	(c)	0.19038483-6	0.78146348-8	0.36776693-8
j_1' = 6	(a)	0.29757500-6	0.13217708-5	0.15669486-5
	(b)	0.29757500-6	0.13217708-5	0.15669486-5
	(c)	0.29867127-6	0.13201466-5	0.15660986-5

$|S_L(v_2=1 j_1 \Omega_1=0, v_2'=0 j_1' \Omega_1' | \theta_2)|^2$ in units of (a.u.)^2

3.4 Quadrature over the CO orientations

In the present study we shall be principally interested in the calculation of rotationally summed cross sections, $\sigma(v_2=1 j_1 \rightarrow v_2'=0 j_1')$, such cross sections may be employed to evaluate vibrational relaxation rate coefficients. In Chapter V.4 the quadrature over the CO orientations, θ_2 , was examined in some detail. In the energy range considered in those calculations, $E_T \leq 4138.5631\ cm^{-1}$, a 28- point Gauss Legendre quadrature was able to determine rotationally summed cross sections for the vibrational de-excitation process $v_2 = 1$ to $v_2' = 0$ to within a few per cent (see Table 25, Chapter V.4). On the other hand the convergence with respect to the number of orientations, θ_2 , included in the calculations, of the corresponding cross sections for the individual rotational transitions in CO was less satisfactory. One will recall that to evaluate cross sections for the transition $v_2 = 1\ j_1 = 0\ j_2 = 0 \rightarrow v_2' = 0\ j_1 = 0 j_2'$ one must evaluate an integral of the type (V.4.4) that involves the function $Y^*_{j_2'0}(\cos\theta_2)$ which becomes more oscillatory as a function of θ_2 as j_2' increases. In the present calculations however, we only evaluate such cross sections for the rotational transition $j_2 = 0 \rightarrow 0$ in CO. For this transition the spherical harmonic $Y^*_{j_20}(\cos\theta_2)$ is a constant, and therefore the convergence as a function of the number of θ_2 values included in the calculation of these cross sections is similar to that of the rotationally summed cross sections. However it is not identical since the

integral one must perform to evaluate $\sigma^L(v_2 j_1 \rightarrow v_2' j')$ involves $|S_L(v_2 j_1 \Omega_1, v_2' j' \Omega_1 | \theta_2)|^2$ which is a less oscillatory function of θ_2 than the real and imaginary parts of the S-matrix, included in the integrals for $\sigma^L(v_2 j_1 j_2 \rightarrow v_2' j' j_2')$. See Chapter V.4 for a more detailed discussion.

As mentioned previously in this section, the interaction potential used in the present calculations is more anisotropic than that employed in our previous H_2 + CO calculations, although as also mentioned this additional anisotropy is entirely due to the H_2 molecule, consequently a quadrature over the CO orientations, θ_2, should not be seriously affected. It was found (see Chapter V.4) that the convergence of the results as a function of the number of orientations θ_2, considered in the calculation improved with both decreasing E_T, and increasing L. Therefore in the energy range considered in these calculations, $E_T \leq 3167.14$ cm^{-1} a 28-point Gauss Legendre quadrature should be capable of evaluating rotationally summed cross sections, and individual rotational cross sections for $j_2 = 0 \rightarrow 0$ to within a few per cent. In conclusion a 28-point Gauss Legendre quadrature is employed in all these calculations.

4. Results and discussion

The results presented in this section are those evaluated employing the P potential as presented by Poulsen (1982) (i.e. the factor of 0.5 is omitted from VI.2.4). The effects of this error are discussed in detail in Appendix 4 at the back of this thesis. Essentially we

show that only the results for the near-resonance process have been seriously affected, the cross sections are overestimated by a factor of $\sim$ 4. The results for the $\Delta j_1 = 0$ and 2 transitions are changed by a few percent.

4.1 The dependence of the vibrational de-excitation of CO on the rotational state of H_2

In Chapter V we presented the results of a calculation in which we studied the rovibrational excitation of CO by non-rotating $H_2(j_1 \quad 0)$. To study the dependence of the results on the rotational state of the H_2 molecule, we have performed a number of calculations in which the H_2 was constrained in its second excited rotational state ($j_1 = 2$). In Figure 1 we show a comparison of partial cross sections, $\sigma^L(v_2 = 1,\ j_1,\ j_2 = 0 \rightarrow v_2' = 0,\ j_1,\ j_2 = 0)$ for $j_1 = 0$ and 2. The comparison is made at the same value of the initial kinetic energy E_T (i.e. the collision energies differ by the energy separation of the $j_1 = 2$, and $j_1 \quad 0$ rotational levels of H_2). Results are shown for $E_T = 667.5\ cm^{-1}$, $1535.3\ cm^{-1}$, and $2837.0\ cm^{-1}$. It is evident that at all the energies studied the variation of σ^L with respect to L is very similar for both $j_1 =$ 0 and 2. The partial cross sections are only shown for every tenth partial wave at the two lowest energies, and at every twenty partial waves at the highest energy. Hence the sharp changes in gradient that are seen in the plots.

A more 'complete' comparison would involve the comparison

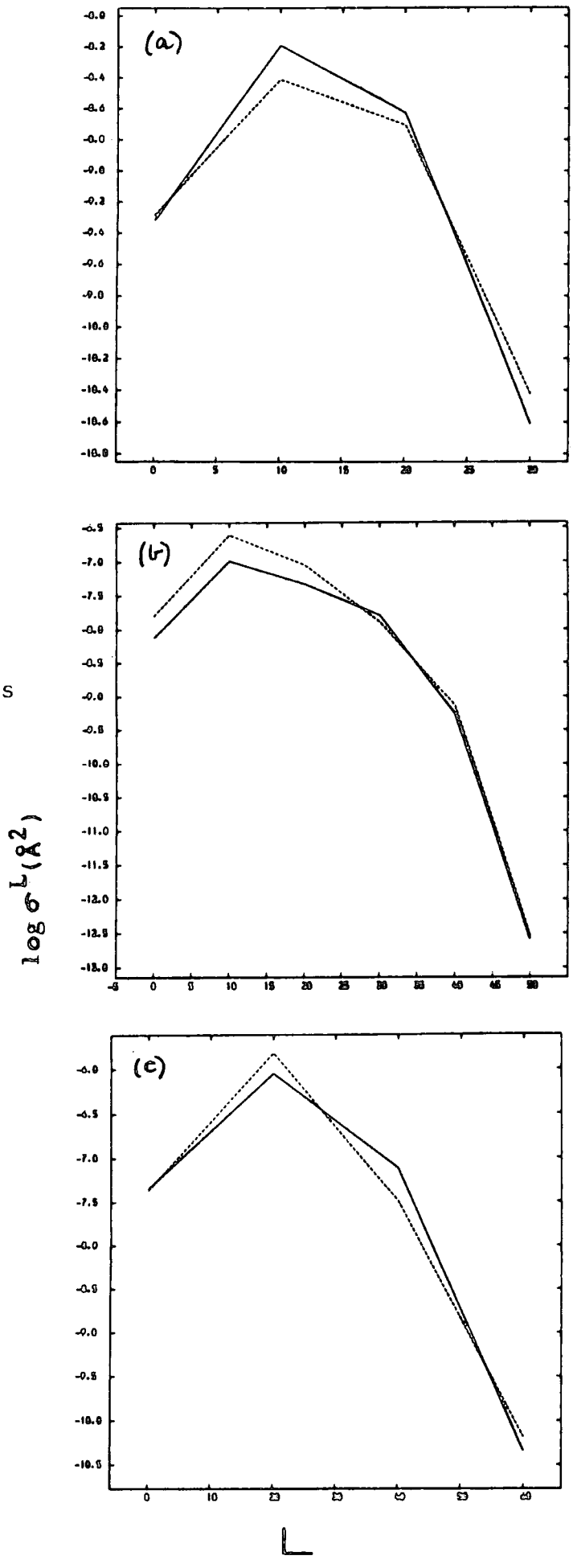

Figure 1

A comparison of partial wave cross sections, $\sigma^L(v_2=1 j_1 j_2=0 \rightarrow v_2'=0 j_1' j_2'=0)$ in $Å^2$, for j_1 = 0 (solid lines) and j_1 = 2 (dashed lines).

The initial kinetic energies are

(a) 667.5 cm^{-1},

(b) 1535.3 cm^{-1},

and

(c) 2837.0 cm^{-1}.

of the corresponding rates of vibrational relaxation. The method of calculation is summarised in Chapter V, however in the present calculation of the 'V-T' ($j_1 = 2$) rate (and also the near-resonance rate) the spline interpolation procedure was extremely prone to error in the temperature range of interest, $80 \lesssim T \lesssim 600$ K, due to the lack of results in the energy range, $208 \lesssim E_T \lesssim 2300$ cm^{-1} (see Table 11). We resolved this problem by plotting the rotationally summed cross sections versus energy, and obtaining additional data. For the 'V-T' process we plotted $\log_{10} E_T$ versus $\log_{10} \sigma$, however for the near-resonance process σ varies quite slowly with E_T, and a plot of $\log_{10} E$ versus σ was sufficient.

In Table 6, we show a comparison of the rates of vibrational relaxation, α ($v_2 = 1$ $j_1 \rightarrow v_2' = 0 j_1'$) for the 'V-T' processes in which $j_1 = j_1' = 0$ (i.e. the results presented in Chapter V.5) and in which $j_1 = j_1' = 2$. Poulsen and Billing (1982) have found that α ($v_2 = 1$ $j_1 \rightarrow v_2' = 0 j_1$) is independent of the rotational state of the H_2 molecule in the range $j_1 = 0$ to 3 within the statistical uncertainty of about 25%. The results shown in Table 6 confirm this observation, namely that the relaxation rate σ ($v_2 = 1$ $j_1 \rightarrow v_2 = 0 j_1$) is not sensitive to the value of j_1 for small j_1. BSD2 come to the same conclusion in their calculations employing the P potential and employing the DK potential.

The similarity of these 'V-T' calculations might indicate rather small $Y_{20}(\cos\theta_1)$ terms in the interaction

TABLE 6

Values of the vibrational relaxation coefficient, $\alpha(v_2=1, j_1 \rightarrow v_2'=0, j_1')$ (10^{-17} cm^3 s^{-1}), calculated for j_1 0 (Chapter V) and j_1 2.

T(K)	$\alpha(v_2 = 1, j_1 \rightarrow v_2' = 0, j_1')$	
	$j_1 = 0$	$j_1 = 2$
200	4.4	4.0
220	5.9	5.2
240	7.7	6.6
260	10.1	8.5
280	13.0	11.0
300	16.6	14.0
400	48	44
500	112	116
600	230	267

potential. One will recall that the potential matrix elements involve a weight factor X given by

$$X(j_1 j_1' \Omega_1 \lambda_1) = (-1)^{\Omega_1} [(2j_1+1)(2j_1'+1)]^{\frac{1}{2}} \begin{pmatrix} j_1 & j_1' & \lambda_1 \\ 0 & 0 & 0 \end{pmatrix} \begin{pmatrix} j_1 & j_1' & \lambda_1 \\ \Omega_1 & -\Omega_1 & 0 \end{pmatrix} \quad \text{IV.4.1}$$

Because of the triangular condition for the angular momentum coupling coefficients only the Yoo ($\cos\theta_1$) term can directly influence the $j_1 = 0 \longrightarrow 0$ cross section, however for $j_1 = 2 \longrightarrow 2$, terms with $\lambda_1 = 2$ contribute. Since the above rates are very similar one would expect the $Y_{20}(\cos\theta_1)$ potential terms to be small, in addition Poulsen and Billing (1982) find that the $\Delta j_1 = 2$ rates are insignificant compared to the corresponding $\Delta j_1 = 0$ rates.

This however, is not true, Schinke (private communication) pointed out that from intermediate to large intermolecular separations ($R \gtrsim 6$ a.u.) the $Y_{20}(\cos\theta_1)$ term is the dominant term of the P potential. This has been confirmed by our own examination of the P potential, and also in the calculation of $\Delta j_1 = 2$ cross sections. In Table 7 we show rotationally summed cross sections, $\sigma(v_2 = 1\ j_1 \rightarrow v_2 = 0 j_1')$ for $j_1 = 0$, and $j_1' = 0$ and 2 at $E_T = 233.5549$ and $1101.3346\ cm^{-1}$. These results were obtained employing a rotational basis set including $j_1 = 0$ and 2. As can be seen the $\Delta j_1 = 2$ cross sections are roughly 50% of the $\Delta j_1 = 0$ cross sections. Also shown in Table 7 are the corresponding $\Delta j_1 = 0$ cross sections

TABLE 7

Comparison of rotationally summed cross sections, $\sigma(v_2 j_1 \rightarrow v_2 j_1')$ ($Å^2$), evaluated employing different rotational basis sets: (a) $j_1 = 0$ and 2; (b) $j_1 = 0$; (c) $j_1 = 1$ and 3; (d) $j_1 = 1$.

E_T (cm^{-1})	$\Delta j_1 = 0$		$\Delta j_1 = 2$	
	$\sigma(10 \rightarrow 00)$	$\sigma(11 \rightarrow 01)$	$\sigma(10 \rightarrow 02)$	$\sigma(11 \rightarrow 03)$
233.5549	(a) 0.118-5 (b) 0.952-6	(c) 0.109-5 (d) 0.113-5	(a) 0.673-6	(c) 0.827-6
1101.3346	(a) 0.528-4 (b) 0.488-4		(a) 0.188-4	

presented in Chapter V. It is worth noting that they agree extremely well with the present $\Delta j_1 = 0$ cross sections. It appears that in the present calculations any indirect effect that the $Y_{20}(\cos\theta_1)$ term might have upon the $\Delta j_1 = 0$ cross section is averaged out in the angular integration, (see Table 5, Chapter VII).

Now for vibrational transitions for the type $v_2 = 1$ to $v_2' = 0$, terms of the potential that are independent of r_2 do not contribute to the integral VI.2.4a. The long range potential involves terms in $(r_2 - r_{2,eq})$, $(r_2 - r_{2,eq})^2$, and $(r_2 - r_{2,eq})^3$ (Section 2), however the major contribution to the integral will come from terms involving $(r_2 - r_{2,eq})$. The leading long range terms are therefore (cf. VI.2.3).

$$V'_{Q\mu} = -4\pi(15)^{\frac{1}{2}} Q^{HH}_{(0)} \mu^{CO}_{(1)} R^{-4} P_1(\cos\theta_2) \qquad \text{VI.4.2a}$$

$$V'_{QQ} = 4\pi(5)^{-1} Q^{HH}_{(0)} Q^{CO}_{(1)} R^{-5} P_2(\cos\theta_2) \qquad \text{VI.4.2b}$$

$$V'_{Q4\mu} = -4\pi(27)^{-1/2} Q^{HH}_{4(0)} \mu^{CO}_{(1)} R^{-6} P_1(\cos\theta_2) \qquad \text{VI.4.2c}$$

$$V'_{Q4Q} = 4\pi(45)^{-1/2} Q^{HH}_{4(0)} Q^{CO}_{(1)} R^{-7} P_2(\cos\theta_2) \qquad \text{VI.4.2d}$$

where $Q^{HH}_{(0)} = 0.4876$, $Q^{HH}_{4(0)} = 0.08408$, $\mu^{CO}_{(1)} = 2.4790$, and $Q^{CO}_{(1)} = 1.879$. For the discussion of $\Delta j_1 = 2$ cross sections it is only necessary to notice that $V'_{Q\mu}$ and V'_{QQ} are

large.

What is therefore, surprising is the similarity of the 'V-T' calculations for $j_1 = 0$ and 2, in view of the results shown in Table 7. One will recall that for $j_1 = 2 \rightarrow 2$ we must also consider terms with $\lambda_1 = 2$ as well as terms with $\lambda_1 = 0$. However, the weight factors involving $\lambda_1 = 2$ are rather different to those involving $\lambda_1 = 0$. In Table 8 we show the numerical values of the weight factors, X, for a number of combinations of $j_1 = j_1'$, λ_1 and Ω_1. As can be seen the weight factors for $\lambda_1 = 2$ are much smaller than for $\lambda_1 = 0$ which probably explains the similarity of the 'V-T' calculations.

In addition we have evaluated results for ortho-H_2 ($j_1 = 1,3,5---$). Rotationally summed cross sections, $\sigma(v_2 = 1\ j_1 \rightarrow v_2' = 0\ j_1')$ for $j_1 = 1$ and $j_1' = 1$ and 3 at $E_T = 233.5549\ cm^{-1}$ are also shown in Table 7. It is apparent that at a given energy (E_T) the $j_1 = 1 \rightarrow 3$ cross section is larger than the $j_1 = 0 \rightarrow 2$ cross section. It appears that $\Delta j_1 = 2$ cross sections are dependent upon the initial rotational state although all of them are induced by the same potential term, and in addition the corresponding weight factors, X, shown in Table 9 are roughly the same for combinations of j_1, j_1', Ω_1, and λ_1 considered. The difference is due to the difference of the energy defects for the two rotational transitions, i.e.

TABLE 8

Weight factors, X, for $j_1 = j_1'$

j_1	Ω_1	λ_1	X
0	0	0	1
2	0	0	1
2	0	2	0.286
2	1	2	0.143
2	2	2	0.286

TABLE 9

Weight factors, X, for $j_1' = j_1 + 2$

j_1	j_1'	Ω_1	λ_1	X
0	2	0	2	0.447
1	3	0	2	0.393
1	3	1	2	0.321

$$CO(v_2=1) + H_2(j_1=1) \rightarrow CO(v_2=0) + H_2(j_1=3) + 1556.65\,cm^{-1} \quad \text{VI.4.3a}$$

$$CO(v_2=1) + H_2(j_1=0) \rightarrow CO(v_2=0) + H_2(j_1=2) + 1789.16\,cm^{-1} \quad \text{VI.4.3b}$$

Any transition which reduces the energy defect increases the relaxation cross section, consequently the cross section for $j_1 = 1 \rightarrow 3$ is larger than that for $j_1 = 0 \rightarrow 2$.

As mentioned in Appendix 4 the above observations concerning $\Delta j_1 = 2$ transitions are in quantitative agreement with the results obtained by BSD2 in their calculations employing the P potential. However, BSD2 find that when the DK potential is used the $j_1 = 0 \rightarrow 2$ cross sections are of the same order as the $j_1 = 0 \longrightarrow 0$ cross sections, and the effect is more pronounced for $j_1 = 1$ (and for $j_1 = 2$). At large distances the $Y_{20}(\cos\theta_1)$ potential term is proportional to $\mu^{CO}_{(1)}$, the first derivative of the dipole moment of CO (i.e. VI.4.2a). In the DK potential the long range $Y_{20}(\cos\theta_1)$ interaction is included in the SCF calculation. On the SCF level $\mu^{CO}_{(1)}$ is probably overestimated by a factor of 1.5-2 (e.g. see Jaquet et al. (1980)). Hence the overestimation of $\Delta j_1 = 2$ transitions obtained with the DK potential.

It will be recalled that in Chapter V the 'V-T' relaxation rate ($j_1 = 0$) was compared with the experimental rate for ortho-H_2. In doing so we were guided by the study of Poulsen and Billing (1982). These authors found that the relaxation rate for $\Delta j_1 = 2$ transitions are much smaller than the rate for $\Delta j_1 = 0$. Therefore we

concur with BSD2 in that we consider the interpretation of the 'V-T' rate as an ortho rate is wrong. The rate, α ($v_2 = 1$ $j_1 = 0 \rightarrow v_2' = 0$, $j_1 = 0$) is roughly a factor of 2 to 3 lower than the experimental rate for ortho-H_2. BSD have shown that relaxation cross sections evaluated with the CO molecule treated within the CS approximation are roughly a factor of 1.5 larger than the corresponding IOS cross sections (Chapter V.5). We therefore argue that the P potential is capable of providing a better description of the experimental rate for ortho-H_2 than the DK potential if the rate coefficients for the $\Delta j_1 = 0$ and 2 processes are evaluated using cross sections calculated within the CS approximation. On the other hand, the $\Delta j_1 = 0$ relaxation rate calculated using IOS cross sections evaluated employing the DK potential agree well with experiment. The inclusion of the $\Delta j_1 = 2$ rate, and the use of the CS approximation would ruin this agreement. We must, of course, assume that the above ratio of CS approximation rates to IOS approximation rates for non-rotating H_2 is valid for rotating H_2. In view of the large $Y_{20}(\cos\theta_1)$ term it is not clear why Poulsen and Billing (1982) obtained such insignificant $\Delta j_1 = 2$ relaxation rates. This is probably another indication that the semiclassical approximation employed by these authors is inappropriate for the H_2 + CO system (see Chapter V.5 for a more detailed discussion).

4.2 The near-resonance process

4.2.1 Discussion of the model calculation

As stated in Section 3 when investigating the near-resonance process (VI.2.5) we include only the directly relevant rotational states of the H_2 molecule, $j_1 = 2$ and 6. This is however, contrary to the usual procedure of retaining all the channels up to and including the channels of interest, and adding extra channels (if necessary) to converge the transitions being studied. To study the near-resonance process one would need to include all the rotational channels up to $j_1 = 6$ (at least), as is done by BSD2. Our 'model calculation' explicitly neglects the $\Delta j_1 = 2$ transitions, which are significant compared to the corresponding $\Delta j_1 = 0$ cross sections.

When we performed these calculations, one of our reasons for such a model calculation was the similarity of the $\Delta j_1 = 0$ results for $j_1 = 0$ and 2. As explained in Section 4.1 one would expect the $Y_{20}(\cos \theta_1)$ terms of the interaction potential to be small, in addition Poulsen and Billing (1982) find that $\Delta j_1 = 2$ rates are insignificant compared to the corresponding $\Delta j_1 = 0$ rates, in their semi-classical study employing the P potential. However, at low temperatures, $E_T \lesssim 300$ K, where we expected the near-resonance process to be dominant (e.g. see Andrews and Simpson (1976)), as is confirmed by our calculations (see Table 11) both $\Delta j_1 = 0$ and 2 cross sections are insignificant compared to the corresponding near-resonance cross sections, even

when one accounts for the error in our programme and we believe (in the regime of thermal energies) that the numerical values of the near-resonance cross sections have not been seriously affected by the truncation of the rotational basis set. This is confirmed at E_T = 208 cm^{-1} by the calculation of BSD2 employing the P potential, and employing the j_1 = 0,2,4, and 6 rotational states of the H_2 molecule. Good agreement is found between the results of our calculation, and that of BSD2 for the near-resonance cross section as is shown in Appendix 4. It is worth mentioning that, as BSD2 conclude, such a model calculation is not feasible if one employs the DK interaction potential due to the poor description of the $Y_{20}(\cos\theta_1)$ term (and the resulting overestimated $\Delta j_1 = 2$ cross sections). In Section 4.2.2 we show that in the regime of thermal energies the cross sections for the transition $j_1 = 2 \rightarrow 4$ are larger than the corresponding near-resonance cross sections.

At the two highest energies studied in these calculations we would expect our model calculation to be unsatisfactory. At such high kinetic energies, E_T = 2299.36 cm^{-1} and 3167.14 cm^{-1}, the 'V-T' processes are dominant (see Table 11) and consequently the neglect of $\Delta j_1 = 2$ transitions will probably not be justified. However, one will recall that the magnitude of the $\Delta j_1 = 2$ cross sections relative to the corresponding $\Delta j_1 = 0$ cross sections decrease with E_T, and therefore at these high energies will not be particularly important, nevertheless they are probably

still comparable in magnitude to the corresponding near-resonance cross sections. In conclusion we would expect the near-resonance results to be overestimated at these high energies, due to the neglect of coupling to the $j_1 = 4$ and 0 rotational states, however, notice that while the description of the near-resonance process may not be completely satisfactory it will form an insignificant contribution to the rate of deactivation of CO ($v_2 = 1$) by para-H_2 at such high energies. The near-resonance process is only important in the energy range $100 \lesssim E_T \lesssim 500$ K (e.g. see Andrews and Simpson (1976)).

Another reason for employing this model calculation, is that it was the largest feasible. We did not have sufficient computer time to perform calculations including the $j_1 = 0$ and $j_1 = 4$ rotational states, and study sufficient energies to accurately evaluate vibrational relaxation rate coefficients. As mentioned in Section 3 to obtain cross sections for the near-resonance process it is necessary to solve the coupled differential equations at three values of Ω_1 ($\Omega_1 \leq 2$) at each of the 28 CO orientations. In Table 10 we give the approximate computer times required to solve the coupled differential equations at one orientation using the Cray-1 computer. Three vibrational channels are retained in all the calculations, and the equations are solved at 460 values of R. The size of rotational basis is increased as shown in Table 10. Times for the initial and subsequent partial waves are given for each value of Ω_1 that must be considered. At the initial partial

TABLE 10

The approximate computer times required to solve the fixed angle coupled equations at one orientation using the Cray-1 computer. Three vibrational channels are included in all the calculations, and the rotational channels retained are;-

(a) j_1 = 2, and 6, (b) j_1 = 0,2 and 6, (c) j_1 = 0,2,4, and 6.

Times are given for the initial and subsequent partial waves at Ω_1 = 0,1, and 2.

Ω_1 =		0	1	2
Time(s)				
Initial	(a)	3.70	3.70	3.70
Partial	(b)	5.00	"	"
Wave	(c)	6.50	5.00	5.00
Subsequent		0.50	0.50	0.50
Partial		1.00	"	"
Waves		2.00	1.00	1.00

wave including the $j_1 = 0$ and 4 rotational states results in a $\sim$ 50% increase in the computer time necessary for our model calculation, however at subsequent values of L we find that the inclusion of these states results in an increase in the time by $\sim$ 200%.

Although at subsequent partial waves there is no explicit reference to the potential matrix elements, it is necessary to perform various matrix operations (e.g., inversion, multiplication, etc.). In particular we have found that as the dimensions of the matrices increase , matrix multiplication becomes a rather costly operation, and eventually begins to form a significant percentage of the total computer time required to solve the coupled equations. For example if we retain four rotational states, it accounts for $\sim$ 30% of the total time. In conclusion as the size of the rotational basis is increased the advantage gained at subsequent partial waves decreases as is shown in Table 10.

In our HD + CO calculations (Chapter VII) this problem was alleviated by optimizing the matrix multiplication routine for the Cray-1 computer, however note that in the HD + CO system a model calculation of the type performed in these calculations is not feasible. In the present calculation we believe that our model calculation is a sufficiently accurate description of the H_2 molecule in the regime of thermal energies, where the near-resonance process is dominant.

4.2.2 Results

In Table 11 we compare rotationally summed cross sections, $\sigma(v_2 = 1\ j \rightarrow v_2' = 0\ j_1)$ for the 'V-T' process, in which $j_1 = j_1' = 2$, and for the near-resonance process, in which $j_1 = 2$ and $j_1' = 6$. It may be seen that the cross sections for the near-resonance process are almost independent of the initial kinetic energy whereas the 'V-T' cross sections increase rapidly with E_T. The energy difference between the initial and final channels becomes less important at E_T increases. Therefore the magnitude of the near-resonance cross sections relative to the $\Delta j_1 = 0$ cross sections decreases with E_T as is clearly observed in Table 11. Due to the error in the potential routine the near-resonance cross sections are roughly a factor of 4 too large, as is shown in Appendix 4. Even when the cross sections shown are reduced by a factor of ~ 4, it is evident from Table 11 that in the region of thermal energies, $E_T \simeq 300$ K, one would certainly expect the near-resonance process to significantly influence the rate of vibrational deactivation of $CO(v_2 = 1)$ by para-H_2, although as we will show later in this section the near-resonance relaxation rate is insufficient to account for the difference between the experimental rates for ortho- and para-H_2.

It is clear from Table 11 that the near-resonance cross sections rise as the $v_2 = 1\ j_1 = 2$ threshold is approached. We are unable to offer a satisfactory explanation for this unphysical behaviour. We believe

TABLE 11

A comparison of rotationally summed cross sections, $\sigma(v_2 j_1 \rightarrow v_2' j_1')(\text{Å}^2)$, for the 'V-T' ($j_1 = j_1' = 2$) and near-resonance vibrational relaxation process.

Note that 1 cm^{-1} = 1.4388K.

$E_T(cm^{-1})$	(12 → 02)	(12 → 06)
64.8322	0.359(-6)	0.596(-4)
83.0	0.389(-6)	0.556(-4)
129.915	0.534(-6)	0.515(-4)
208.0	0.914(-6)	0.503(-4)
2299.36	0.668(-3)	0.548(-4)
3167.14	0.209(-2)	0.563(-4)

Numbers in brackets are powers of 10.

that our numerical methods described in Section 4 and in Chapter V.4 are an accurate description of this system and some additional calculations have indicated that the error in our programme is not responsible for this behaviour. It is worth noting that the 'V-T' cross sections were evaluated employing identical numerical methods and since the energy variation of these cross sections appears to be satisfactory, it is probable that the truncation of the rotational basis set might be the cause of the unphysical energy variation of the near-resonance cross-sections. However at very low energies, $E_T \lesssim 100$ K, where the rise of the cross sections is most noticeable, the $j_1 = 2$ rotational level is not significantly populated, and consequently such cross sections will have an insignificant effect on the rate of vibrational relaxation of $CO(v_2 = 1)$ by para-H_2.

In Table 12 we compare the values of the near-resonance relaxation rate coefficient with the corresponding results evaluated by Poulsen and Billing (1982). It is worth repeating that both calculations employ the P potential, and use Morse oscillator wavefunctions to describe the vibrational motion of the CO molecule. The energy defects for the near-resonance process, employed in the calculations, differ by 3.73 cm^{-1} (see Table 2), this small difference is insignificant compared to the different dynamical approaches used in the calculations. If the relaxation rate from the present calculations is divided by a factor

TABLE 12

A comparison of the rate coefficient for vibrational relaxation by the near-resonance process; (a) present IOS calculation; (b) semi-classical calculation of Poulsen and Billing (1982).

T(K)	$\alpha(v_2 = 1 \quad j_1 = 2 \rightarrow v_2' = 0 \quad j_1' = 6)$	
	(a)	(b)
80	65	35
100	67	36
120	70	37
140	73	38
160	76	39
180	79	40
200	82	41
220	85	42
240	88	43
260	91	44
280	94	45
300	97	45
400	111	48
500	124	51
600	136	53

$\alpha(v_2 = 1 \quad j_1 = 2 \rightarrow v_2' = 0 \quad j_1' = 6)$ in $10^{-17} cm^3 s^{-1}$.

of $\sim$ 4 to account for the error in the potential routine, they are roughly a factor of 2 lower than the results obtained by Poulsen and Billing. It is worth repeating that when we had accounted for this error, and the 'incorrect' rotational energy levels employed by BSD2, our results were in reasonable agreement with the results obtained by BSD2 in a calculation employing the P potential, and which included the $j_1 = 0$ and 4 states in the rotational basis (see Appendix 4). The discrepancies between the present calculations and those of Poulsen and Billing (1982) is perhaps yet another indication that the SCA employed by these authors is not suitable to study the rovibrational excitation of CO by H_2.

In Figure 2 we compare the results of BSD2 for the near-resonance process evaluated in calculations employing the DK potential, and including the $j_1 = 0$ and 4 states in their rotational basis set, with the corresponding results evaluated in the present study. We recall that BSD2 employ Morse oscillator wavefunctions to describe the vibrational motion of the CO molecule. Although the magnitude of the cross sections obtained using the two potentials are somewhat different, both the P and DK potentials produce near-resonance cross sections which are slowly varying with energy. Both calculations give overestimated near-resonance cross sections. In the present calculations the cross sections are roughly a factor of 4 too large, also BSD2 overestimate the process by

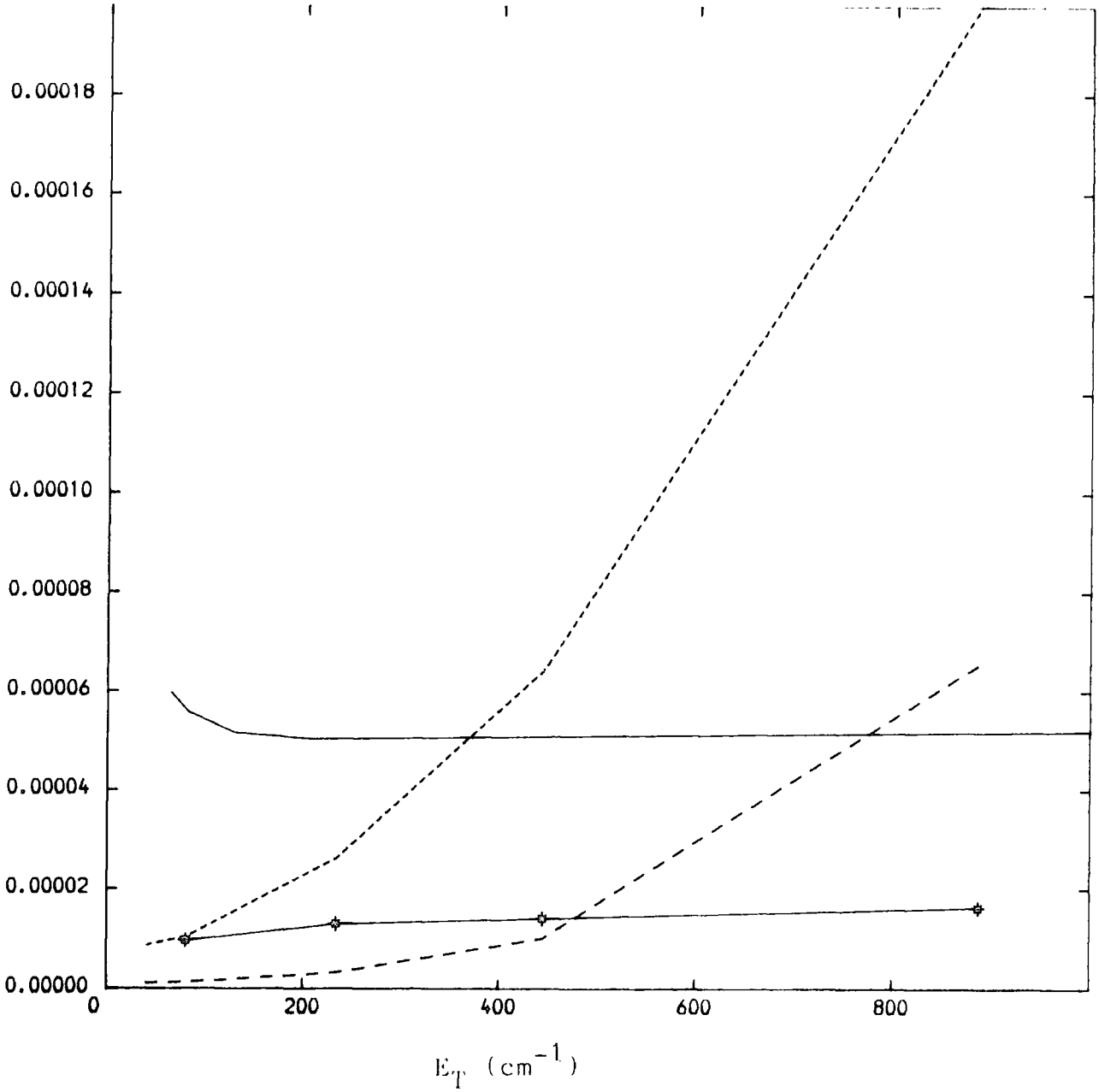

Figure 2. A comparison of rotationally summed cross sections for the near-resonance process, $\sigma(12 \rightarrow 06)$ Å^2.

(———) : Present calculations;
(—✱—✱—) : BSD2.

Also shown are the cross sections evaluated by BSD2 for the 'V-T' process in which j_i = 2 (- - -), and for the Δj_i = 2 process in whch j_i = 2, and j_i' = 4 (-------).

a factor of $\lesssim 2$. This discrepancy in the calculations of BSD2 is due to the use of inaccurate rotational energy levels, as is shown in Appendix 4.

The DK potential has no $Y_{40}(\cos \theta_1)$ term (which couples directly $\Delta j_1 = 4$ transitions). BSD2 employed the long-range $Y_{40}(\cos \theta_1)$ terms presented by Poulsen (1982) (i.e. equations VI.4.2c,d). In doing so they were guided by the observation of Poulsen and Billing (1982), these authors state that the near-resonance process is primarily determined by the long range interaction between the hexadecapole moment of H_2, and the dipole (and quadrupole) moment of CO. In view of the dependence of the near-resonance process on these interactions (Appendix 4), they are clearly very important. However, even when one accounts for the discrepancies discussed above, the DK and P potentials give different near-resonance cross sections. Clearly the long range $Y_{40}(\cos \theta_1)$ terms are not the only contributors to the near-resonance process.

In particular it is interesting to note that the so-called long range multipole moment ($Y_{40}(\cos \theta_1)$) interactions are included in both the potential surfaces at all intermolecular distances in the integration range. As mentioned above Poulsen and Billing (1982) conclude that the near-resonance process is primarily determined by the long range interactions. However, it is not obvious (at least to us) that the near-resonance process is only determined by the multipole interactions at long range. The process

may be determined (partially) by these interactions at short range ($R \lesssim 6$ a.u.). This by itself does not explain the discrepancies between the near-resonance cross sections determined by the P and DK potentials. However, it is worth noting that at short range the multipole moment interactions given by Poulsen (1982) will be inaccurate, since the forms of interactions given by VI.4.2a,b,c,d are asymptotic forms. If these interactions are important at short range, then we consider that an accurate determination of the near-resonance process would be extremely difficult, since one would require an accurate ab initio determination of the multipole moment interactions at $R \lesssim 6$ a.u.

Also shown in Figure 2 are the cross sections for the $j_1 = 2 \rightarrow 2$ and $j_1 = 2 \rightarrow 4$ transitions evaluated by BSD2. Clearly the near-resonance rate will not form a significant contribution to the rate of de-excitation of CO by para-H_2. The near-resonance cross sections are much smaller than the $\Delta j_1 = 2$ cross sections. Note that the $j_1 = 2 \rightarrow 4$ cross sections are strongly diminished by the P potential, since this potential employs the more accurate value for the dipole moment of CO. In addition the near-resonance cross sections are clearly not significantly larger than the $\Delta j_1 = 0$ cross sections at thermal energies (cf. Table 11).

In conclusion it is apparent that the P potential provides a better description of the near-resonance process

than the DK potential, also it would appear that the P potential provides a better description of the experimental results for ortho-H_2. We discussed the effect of $\Delta j_1 = 2$ transitions, and the CS approximation in Section 4.1. In view of the different determinations of the r_2 dependence of the interactions it is surprising (at least to us) that the P potential should provide a better description of the vibrational excitation of CO by H_2 (see Chapter V.5). Before the present studies, and the calculations of BSD and BSD2 had been carried out, the DK potential was considered to be the most accurate description of the H_2 + CO interaction (e.g. see Schinke et al. (1984)). Indeed the DK potential was constructed employing highly accurate SCF calculations, and Schinke et al. (1984) have shown that the DK potential provides the best overall description of rotational excitation in the D_2 + CO system.

The interaction potential is expressed in the form (VI.2.1)

$$V(\theta_1, \phi, \theta_2, \underline{r}_2, R) = \sum_{\lambda_1} V_{\lambda_1 0}(\theta_2, \underline{r}_2, R)\, Y_{\lambda_1 0}(\theta_1, \phi) \qquad \text{VI.4.4}$$

where $V_{\lambda_1 0}(\theta_2, \underline{r}_2, R) = \sum_{\lambda_2} V_{\lambda_1 \lambda_2}(\underline{r}_2, R)\, P_{\lambda_2}(\cos\theta_2)$

we may expand in a Taylor series about the equilibrium CO internuclear separation, $r_{2,eq}$, and obtain (cf. V.5.3).

$$V_{\lambda_1 0}(\theta_2, \underline{r}_2, R) = \sum_{\lambda_2} P_{\lambda_2}(\cos\theta_2) \Big[V_{\lambda_1 \lambda_2}(r_{2,eq}, R) \qquad \text{VI.4.5}$$

$$+ (r_2 - r_{2,eq}) \frac{\partial}{\partial r_2} V_{\lambda_1 \lambda_2}\Big|_{r_2 = r_{2,eq}} + \frac{1}{2}(r_2 - r_{2,eq})^2 \frac{\partial^2}{\partial r_2^2} V_{\lambda_1 \lambda_2}\Big|_{r_2 = r_{2,eq}} + \cdots \Big].$$

As noted in Chapter V, the successive terms of the expansion VI.4.5 are responsible for the transitions with $\Delta v_2 = 0,1,2---$. Therefore rotational excitation will only involve the first term (and in the calculations r_2 is constrained at its equilibrium value, $r_{2,eq}$), and therefore it cannot be considered as a sufficient examination of an interaction potential. However, calculations studying the vibrational excitation process $\Delta v_2 = 1$ will involve the second (chiefly), and higher order terms in the expansion. Such terms are more difficult to determine, and consequently vibrational excitation is a more stringent test of an interaction potential.

In order to compare with the measurements of the rate of vibrational deactivation of $CO(v_2 = 1)$ in para-H_2, the rate coefficients must be weighted by the relative populations of the H_2 rotational channels, given by a Boltzmann distribution. At low temperatures only the $j_1 = 0$ and 2 levels are significantly populated, therefore we may write:

$$\alpha(T) = \frac{\alpha_0(T) + \alpha_2(T)\frac{\omega_2}{\omega_0} e^{-\Delta E(0,2)/kT}}{1 + \frac{\omega_2}{\omega_0} e^{-\Delta E(0,2)/kT}} , \qquad \text{IV.4.6}$$

where

$$\alpha_0(T) = \alpha(v_2 = 1\ j_1 = 0 \rightarrow v_2' = 0\ j_1' = 0)$$

$$\alpha_2(T) = \alpha(v_2 = 1\ j_1 = 2 \rightarrow v_2' = 0\ j_1' = 2)$$

$$+ \alpha(v_2 = 1\ j_1 = 2 \rightarrow v_2' = 0\ j_1' = 6) ,$$

and $w_j = 2j+1$.

E(0,2) is the energy of $j_1 = 2$ level above the $j_1 = 0$ ground state of H_2, and k is Boltzmann's constants. In Figure 3 we compare the results of the present calculations with the experimental results of Andrews and Simpson (1976). Also shown are the results of Poulsen and Billing (1982) and the results of BSD2. Clearly the best agreement with experiment is obtained by BSD2, however in view of the overestimated $\Delta j_1 = 2$ transitions we consider this level of agreement accidental. The near-resonance process is overestimated in our own calculations, consequently the P potential provides a relatively poor description of the experimental results for para-H_2. Most notably, neither the P or DK potentials produce a sufficiently large near-resonance rate to account for the difference between the rates for para- and ortho-H_2. These results are in sharp contrast to the conclusion of Poulsen and Billing (1982), however in view of the discrepancies between the results of Poulsen and Billing and our own results (e.g. for $\Delta j_1 = 0$ and 2 transitions) the rate obtained for para-H_2 must be treated with a degree of caution. In the light of the present study (and also the study of BSD2 employing the P potential) we consider this good agreement with experiment accidental.

The present calculations were performed treating the CO within the IOS approximation, if the CS approximation had been employed one might expect an increase of a factor

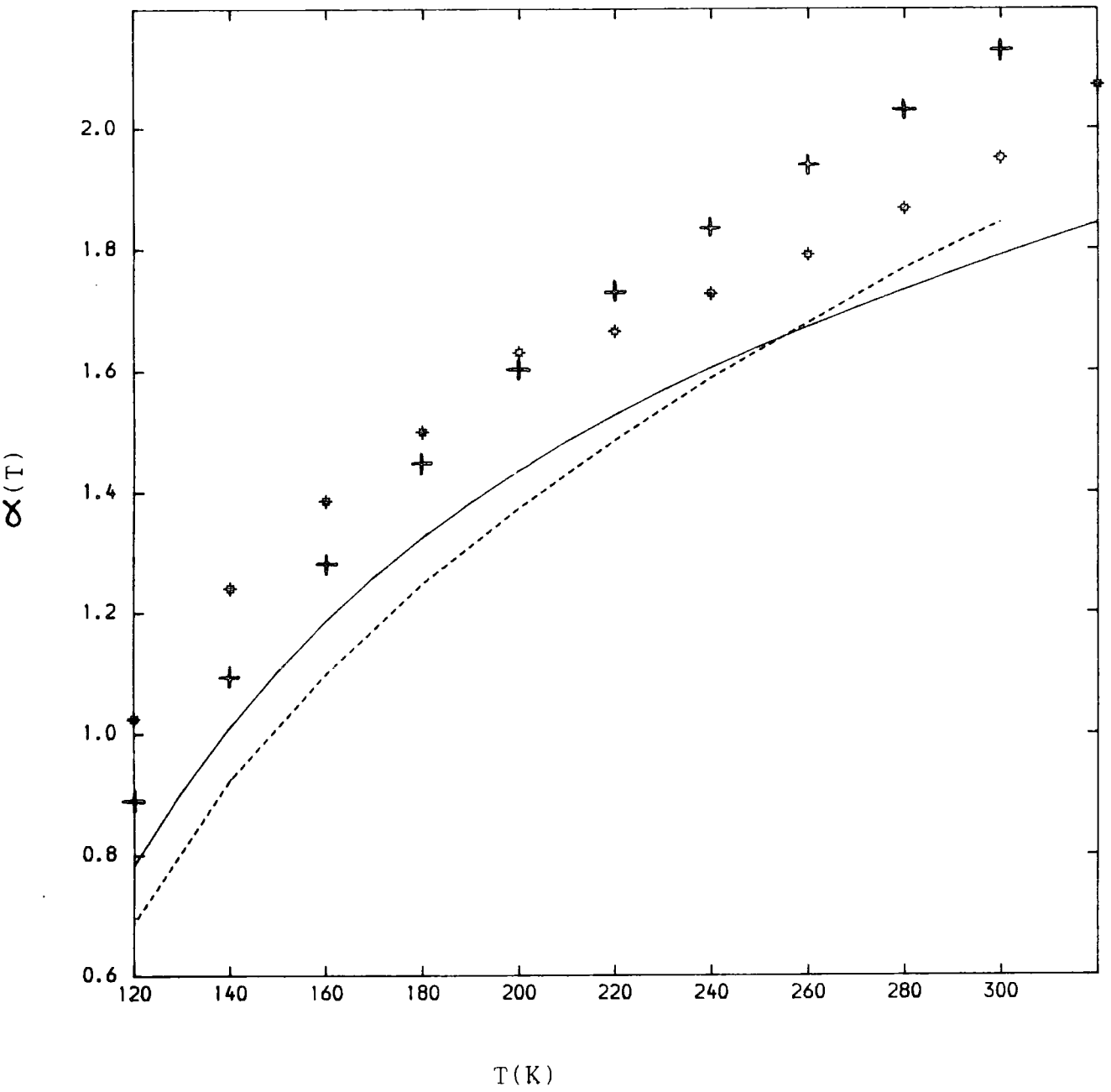

Figure 3. The variation with temperature of the vibrational relaxation coefficient, $\alpha(T)$ (in units of $10^{-17}cm^3s^{-1}$). Solid curve : present calculations : dashed curve : Poulsen and Billing (1982); + : BSD2; * : Andrews and Simpson (1976).

of ~1.5 in the relaxation rates. However even then the agreement with experiment would still be far from satisfactory. As shown in this study the magnitude of the near-resonance process is highly dependent on the long range multipole interactions, the interactions between the hexadecapole moment of H_2, $Q_{4(0)}^{HH}$, and the first derivative of the dipole moment of CO, $\mu_{(1)}^{CO}$ (chiefly) and the first derivative of the quadrupole moment of CO, $Q_{(1)}^{CO}$ (VI.4.2c,d).

$$V'_{\Phi 4\mu} = -4\pi(27)^{-1/2} Q_{4(0)}^{HH} \mu_{(1)}^{CO} R^{-6} P_1(\cos\theta_2) \quad \text{VI.4.7a}$$

$$V'_{\Phi 4Q} = 4\pi(45)^{-1/2} Q_{4(0)}^{HH} Q_{(1)}^{CO} R^{-7} P_2(\cos\theta_2) \quad \text{VI.4.7b}$$

As mentioned in Chapter V.2 Poulsen (1982) employed the most accurate multipole moment functions available in the literature. It is worth repeating that the interactions VI.4.7a,b were also employed in the DK potential. However, in view of the poor description of the difference between the experimental rates for ortho- and para-H_2, it is necessary to bring into question the accuracy of the hexadecapole moment of H_2 and the first derivative of the dipole moment of CO.

$Q_{4(0)}^{HH}$ was determined by Karl et al. (1975) who employed the electronic wavefunctions of Kolos and Wolniewicz (1965, 1975). For $r_2 < 2.2$ a.u. these authors employed the 54 term wave functions of Kolos and Wolniewicz (1965), and for larger internuclear separations, $r_2 \geq 2.2$ a.u., they used the first 44 (or 30) terms of the function

used by Kolos and Wolniewicz (1975). It is apparent from the paper of Karl et al. (1975) that above computations ensure excellent convergence, and the authors consider the value of $Q_{4(0)}^{HH}$ to be accurate to a few percent. $\mu_{(1)}^{CO}$ was determined by Chackerian (1976) by combining numerical solutions of the Schrödinger equation with absolute intensity data of vibration-rotation bands. It is evident from the paper of Chackerian (1976) that there is some doubt concerning the accuracy of $\mu_{(1)}^{CO}$. However in view of the good agreement between the results of Chackerian (1976) with the experimental determination (Weisback and Chackerian (1973)), and the theoretical determination (Tipping (1976)) of the matrix elements for vibration-rotation transitions (involving $\Delta v_2 = 1$) in CO, it is not possible that the first derivative of the dipole moment is in error by as much as a factor of $\gtrsim 2$. Indeed this is the level of error that one would have to find in both $\mu_{(1)}^{CO}$ and $Q_{4(0)}^{HH}$ to provide a satisfactory explanation for the poor description of the experimental rates for para-H_2.

It is interesting that Poulsen and Billing (1982) postulate that if the higher multipole moments of CO were treated explicitly like the dipole and the quadrupole (the interaction between the higher multipole moments of H_2 and CO are accounted for in the short range potential) that larger near-resonance cross sections might be produced. Very recently the above authors published the results of a calculation of the rate coefficient for the vibrational

de-excitation of CO(v_2 = 1) by para-H_2 employing the P potential in which the octopole and hexadecapole of the CO molecule were treated explicitly (Poulsen and Billing (1984)). They find that the rate coefficient for the near-resonance process are increased by $\sim$ 50%. However, in view of the discrepancies between the results of Poulsen and Billing (1982) and the present calculations (and also those of BSD2) we consider that the rate coefficient for the de-excitation of CO(v_2 = 1) by para-H_2 as evaluated by Poulsen and Billing (1984), which agree extremely well with the experimental results, should perhaps be treated with a degree of caution. As already discussed it is probable that the semi-classical approximation employed by Poulsen and Billing (1984) is not appropriate to study the vibrational excitation of CO by H_2, and only after a fully quantum mechanical calculation of the near-resonance process has been performed employing the new P potential (e.g. the P potential employing the explicit expressions for the octopole and hexadecapole moments of CO) can the significance of these higher multipole moments be properly assessed.

5. Summary

We have performed quantum mechanical calculations of the vibrational de-excitation of CO by H_2, where the rotational degree of freedom of the H_2 molecule has been treated explicitly within the CS approximation. The rotational degree of freedom of the CO molecule was treated

within the IOS approximation, and the vibrational motion was described using Morse oscillator wavefunctions. The interaction potential surface of Poulsen (1982) has been employed. We have been primarily interested in the calculation of cross sections and rates for the near-resonance process,

$$CO(v_2=1) + H_2(j_1=2) \rightarrow CO(v_2=0) + H_2(j_1=6),$$

although we have also studied the following processes

$$CO(v_2=1) + H_2(j_1) \rightarrow CO(v_2=0) + H_2(j_1')$$

for $j_1' = j_1$ and $j_1' = j_1 + 2$ where $j_1 \leq 2$.

The multipole moment interactions (VI.4.2) given by Poulsen (1982) are a factor of 2 too large, these errors were present in our potential routine. Only the cross sections evaluated for the near-resonance process have been seriously affected, they are a factor of ~ 4 too high.

We have found that the cross sections and rates for the 'V-T' processes in which $j_1' = j_1$ are independent of the rotational state of the H_2 molecule, for small j_1. In addition we find that the cross sections for the process in which $j_1' = j_1 + 2$ are roughly 50% of the corresponding $\Delta j_1 = 0$ cross sections for $j_1 = 0$, and that the effect is more pronounced for initial rotational state, $j_1 = 1$. Our results are in quantitative agreement with the calculations of BSD2 employing the P potential, however when the DK potential is employed by these authors, while the 'V-T' cross sections are independent of j_1

for small j_1, they are roughly a factor of 3 higher than the present results, also $\Delta j_1 = 2$ cross sections are found to be the same order as the corresponding $\Delta j_1 = 0$ cross sections for $j_1 = 0$, and the effect is more pronounced for $j_1 = 1$ and 2. The latter effect is attributed to the overestimation of the $Y_{20}(\cos \theta_1)$ term of the DK potential. Poulsen and Billing (1982) also find that the 'V-T' rate is insensitive to j_1, for small j_1, although the 'V-T' rate is roughly a factor of $\sim$2.5 greater than that found in the present calculations, and in addition these authors find that $\Delta j = 2$ rates are insignificant compared to the corresponding $\Delta j_1 = 0$ rates. It is not clear to us why they come to this conclusion since they also employ the P potential. In the light of our results, we concur with BSD2 that the interpretation of the $\Delta j_1 = 0$ rate as an ortho-H_2 rate is wrong. In addition we conclude that the P potential is capable of providing a more satisfactory description of the experimental rate for the deactivation of $CO(v_2 = 1)$ by ortho-H_2 than the DK potential if one includes the effect of $\Delta j_1 = 2$ rates, and treats the rotational degree of freedom of the CO molecule in the CS approximation.

We find that the cross sections for the near-resonance process are almost independent of the initial kinetic energy, in contrast the $\Delta j_1 = 0$ cross sections are rapidly varying with energy. At thermal energies the near-resonance process is the dominant process, however, the computed

rate is insufficient to account for the difference between the experimental rates of the de-excitation of CO by ortho- and para-H_2 as determined by Andrews and Simpson (1976). When the error in our potential routine is accounted for, the agreement with the experimental results is diminished. Our results for the near-resonance process disagree with both the results of Poulsen and Billing (1982) and of BSD2. Even when the present results are corrected to account for the error in our programme, the agreement with the above calculations is still unsatisfactory. The results of BSD2 for this process are overestimated by a factor of ~ 2 due to the use of inaccurate rotational energy levels, even when this correction is made discrepancies remain. However, given the same potential, energy defect, and rotational basis set, we find good agreement between our results and those of BSD2 for this process. In particular we conclude that the P potential provides the best description of the near-resonance process, but we are unable to offer a satisfactory explanation for the poor agreement with experiment. We consider that the discrepancies of the present calculations with those of Poulsen and Billing (1982) are probably due to the failure of the semi-classical approximation employed by these authors.

In conclusion the near-resonance process is sensitive to high order terms in the interaction potential, the energy defect, and the H_2 rotational basis set. We agree

with BSD2 in that we consider an accurate ab initio study of the near-resonance process (VI.2.5) in a complex system like H_2 + CO is not feasible at the present time.

CHAPTER VII

ROVIBRATIONAL EXCITATION OF $^{12}C^{16}O$ BY HD

1. Introduction

In this chapter we will present calculations of the rovibrational excitation of CO by HD. The motivations for such a study are three fold. There are no existing theoretical studies of this process in the literature, secondly there is a potential energy surface available, and thirdly there are experimental results with which we can compare our results.

The potential energy surface for HD + CO can be obtained from a knowledge of the H_2 + CO potential by means of a co-ordinate transformation. Within the Born-Oppenheimer (BO) approximation (see Chapter I), isotopic substitution within one of the constituent molecules merely causes a shift of the centre of mass of the molecule, leaving the nature of the intermolecular interaction unaffected. Thus within the validity of the BO approximation, the interaction potential for HD +CO expressed in coordinates about the centre of mass of the HD molecule can be extracted from a H_2 + CO interaction potential by a suitable coordinate transformation. An accurate numerical procedure for carrying out such a transformation is available in the literature (Liu et al. (1978)), and will be employed in these calculations.

The experimental data available is in the form of relaxation rate coefficients. Andrews and Simpson

(1976) have obtained the rate coefficient for the vibrational de-excitation of CO(v_2 = 1) by HD in the temperature range, $75 \leq T \leq 340$ K. Although we will compare the rate coefficient evaluated using our results with the experimental data, the main object of these calculations is to determine the effects of the isotopic substitution on different aspects of the scattering calculations. For example we will discuss its effect on the description of the collision partners, and on the parameters such as the step size and the integration range. Thus throughout the course of this study we will make numerous comparisons with results obtained for the H_2 + CO system. To facilitate these comparisons the same dynamical approximations used in our studies of the H_2 + CO system are employed in the present calculations. Thus the rotational degrees of freedom of the CO and HD molecules are treated within the IOS and CS approximations respectively. Since HD is a heavier molecule than H_2, the IOS approximation will be less valid for the CO molecule (Chapter II.3.3). The vibrational motion of the CO molecule will be treated within the close-coupling approximation.

Only the interaction potential of Poulsen (1982) is used in these calculations, the transformation of this potential is described in Section 2, in Section 3 we present the numerical details and make comparisons with the H_2 + CO system, and finally in Section 4 we

compare our results with the experimental data and draw our final conclusions regarding this system.

2. The Interaction Potential

As mentioned in Section 1, within the BO approximation, isotopic substitution does not change the nature of the interaction potential, hence for example the H_2 + CO interaction potential of Poulsen (1982) has been employed in D_2 + CO calculations without any modifications (Billing and Poulsen (1982)). However, if only one of the atoms is isotopically substituted, this causes a shift of the centre of mass of the molecule towards the heavier nucleus. Hence if one of the H atoms is replaced by a D atom, this causes the centre of mass to shift a distance δ towards the D atom, as shown in Figure 1.

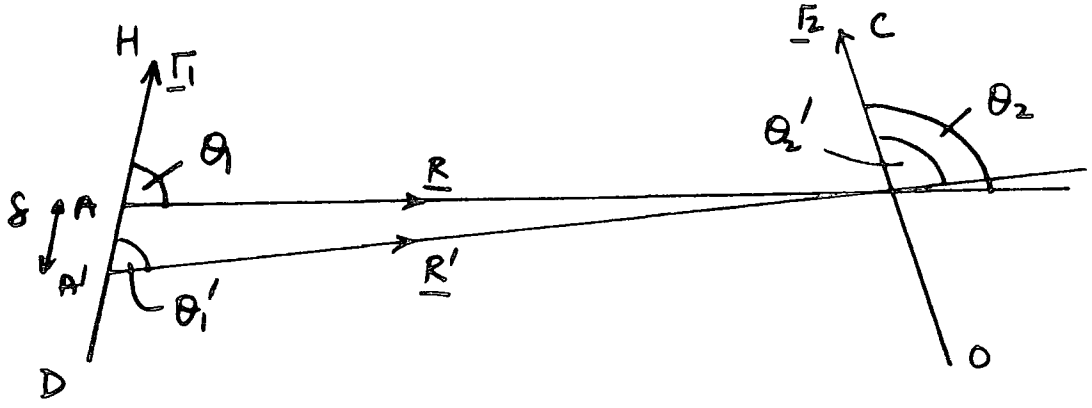

Figure 1.

The H_2 + CO interaction potential may be expressed (cf. VI.2.2).

$$V(\theta_1,\theta_2,r_2,R)=\sum_\lambda V_\lambda(\theta_2,r_2,R)P_\lambda(\cos\theta_1) \qquad \text{VII.2.1}$$

and in terms of the new coordinates ($\theta_1',\theta_2',r_2,R'$) the HD + CO interaction may be written

$$U(\theta_1',\theta_2',r_2,R')=\sum_k U_k(\theta_2',r_2,R')P_k(\cos\theta_1'), \qquad \text{VII.2.2}$$

where R, θ_1', and θ_2' are simply related to R, θ_1, and θ_2 by geometrical relations

$$R=R'(1+t^2-2t\cos\theta_1')^{\frac{1}{2}}, \qquad \text{VII.2.3a}$$

$$\cos\theta_1=(\cos\theta_1'-t)/(1+t^2-2t\cos\theta_1')^{\frac{1}{2}}, \qquad \text{VII.2.3b}$$

and $$\theta_2=\theta_2'+\theta_1-\theta_1', \qquad \text{VII.2.3c}$$

where $t=\delta/R'$.

Since as mentioned above the isotopic change does not significantly alter the potential surface, we have $V(\theta_1,\theta_2,r_2,R)=U(\theta_1',\theta_2',r_2,R)$ and using the orthogonality properties of the Legendre polynomials (e.g. see Liu et al. (1978), and Kreek and Le Roy (1975)).

$$U_k(\theta_2',r_2,R)=(k+2)\int_{-1}^{+1}d(\cos\theta_1')P_k(\cos\theta_1')V(\theta_1,\theta_2,r_2,R)$$

$$=(k+\tfrac{1}{2})\sum_{\lambda=0}^{4}\int_{-1}^{1}P_k(x')V_\lambda(\theta_2,r_2,R)P_\lambda(x)dx' \qquad \text{VII.2.4}$$

where $x = \cos\theta_1$ and $x' = \cos\theta_1'$.

The functions $U_k(\theta_2', r_2, R')$ are determined numerically from the exact H_2 + CO potential, $V(\theta_1, \theta_2, r_2, R)$ by evaluating the integral VII.2.4 using Gauss Legendre quadrature. This technique has been employed in several calculations (e.g. see Liu et al. (1978), and Buck et al. (1980)) both these authors have shown the above method to be more accurate than an analytical method for determining the U_k functions in terms of the V_λ functions, derived by Kreek and Le Roy (1975). Furthermore the method presented by Kreek and Le Roy (1975) involves much complicated algebra, and would be extremely tedious to employ, especially in view of the complex form of the P potential.

To date only atom-diatom potentials have been transformed using VII.2.4 (Liu et al. (1978), Buck et al. (1980), and Liu and McCourt (1979)). For diatom-diatom potentials relations VII.2.3a, VII.2.3b, and VII.2.4 are still valid, however one must ensure that the relative configuration of the two diatoms remains fixed as the intermolecular vector moves from A to A'. Thus one should transform from θ_2 to θ_2' using relation VII.2.3c, however in the present calculations we omitted this transformation. For an intermolecular separation of R = 3 a.u. which is the minimum in these calculations, its omission results in an error in θ_2' of $\lesssim 3^\circ$ which is unimportant when one recalls that the CO molecule

is treated within the IOS approximation which ignores some of the potential anisotropies.

To test the transformation VII.2.4 for the present calculations we evaluated the exact HD + CO potential by substituting VII.2.3a and VII.2.3b directly into VII.2.1, and compared these 'exact' results with the numerical values obtained by employing VII.2.4 and VII.2.2. Such a comparison is given in Table 1, results are shown for $\theta_1' = 0^\circ$, and $\theta_2' = 90^\circ$ at several intermolecular separations, R, and at three CO internuclear distances, r_2. The value of the shift, δ, was taken to be $0.1665\, r_{1,eq}$ (Kreek and Le Roy (1975)), where $r_{1,eq}$ is the equilibrium separation given in Chapter V. 3 , $r_{1,eq} = 1.4$ a.u. Liu et al. (1978) claim that for an integral of the type VII.2.4 an N-point Gaussian quadrature, with

$$k + \lambda \leq 2N + 1 \qquad \text{VII.2.5}$$

should be highly accurate, hence for the results presented, the 24- point Gauss Legendre quadrature employed should be satisfactory.

Table 1 clearly illustrates that as more terms are retained in the expansion VII.2.2, the results tend to the exact values. As R' increases the number of terms that must be retained to achieve a given accuracy decreases; as expected the potential is more anisotropic at close approach. For the range of R' values considered in these calculations ($3.0 \leq R' \leq 35.0$ a.u.) it is clear

TABLE 1

Comparison of $U(\theta_1', \theta_2', r_2, R')$ (a.u.) evaluated retaining different numbers of terms in the expansion VII.2.2 with the "exact" HD + CO interaction potential. $\theta_1' = 0^\circ$, $\theta_2' = 90^\circ$.

(a) 7 terms, (b) 9 terms, (c) 11 terms, (d) Exact.

R'(a.u.) =		3.0	6.0	9.0	12.0	15.0	18.0	21.0
r_2(a.u.)								
1.56	(a)	0.23954684+0	0.95137229−3	−0.34034793−4	0.36049242−5	0.33412153−5	0.16962740−5	0.86362398−6
	(b)	0.23969749+0	0.95149703−3	−0.34032951−4	0.36050263−5	0.33412266−5	0.16922692−5	0.86362437−6
	(c)	0.23970159+0	0.95149794−3	−0.34032954−4	0.36050265−5	"	"	"
	(d)	0.23970168+0	0.95149795−3	"	"	"	"	"
2.10		0.19173893+0	0.69110975−3	−0.50385332−4	−0.28349556−5	0.20662239−5	0.11890060−5	0.63125529−6
		0.19186333+0	0.69121246−3	−0.50383842−4	−0.28341305−5	0.20662331−5	0.11890084−5	0.63125562−6
		0.19186557+0	0.69121321−3	−0.50383837−4	−0.28341290−5	"	"	"
		0.19186568+0	"	"	"	"	"	"
2.64		0.13406818+0	0.26345843−3	−0.84256029−4	−0.82027613−5	−0.50595754−6	0.16781638−6	0.16364326−6
		0.13413996+0	0.26351752−3	−0.84255252−4	−0.82027183−5	−0.50595263−6	0.16781721−6	0.16364344−6
		0.13414189+0	0.26351796−3	"	"	"	"	"
		0.13414193+0	"	"	"	"	"	"

24 Gauss Legendre points used to evaluate VII.2.4

that satisfactory results may be obtained by retaining seven terms in the expansion VII.2.2.

In Table 2 we show the convergence of the results obtained using VII.2.4 with respect to the number of quadrature points used to evaluate the integral. Seven terms are retained in VII.2.2 in all these calculations. Using the empirical rule, VII.2.5, given above, with $k = 7$ and $\lambda = 4$, one finds that $N \geq 6$. This is confirmed by the results shown in Table 2, where a 6-point Gauss Legendre quadrature gives reasonable results. For $R' \geq 3$ a.u. satisfactory results may be obtained using an 8-point Gauss Legendre quadrature. It is evident that the interaction potential becomes positive in the asymptotic region (for the orientation shown), however this behaviour is present in the untransformed H_2 + CO potential. The only explanation that we are able to offer is that the analytical fit given in the paper of Poulsen (1982) is 'breaking down' as R (or R') increases, since we are satisfied that we have computed the P potential correctly. However, we note that although the potential is positive in the asymptotic region, it is tending to zero, consequently the sign of the potential should not be important at large R' values.

The resultant HD + CO system is somewhat more anisotropic than the H_2 + CO system from which it was derived largely because of the introduction of a $Y_{10}(\cos\theta_1)$ HD anisotropy term in the interaction potential. This

TABLE 2

Comparison of $U(0^o,90^o,r_2,R')$(a.u.) evaluated using different numbers of Gauss Legendre quadrature points in the integral VII.2.4.

(a) 6 points, (b) 8 points, (c) 10 points, (d) 12 points.

R'(a.u.) =		3.0	6.0	9.0	12.0	15.0	18.0	21.0
r_2(a.u.)								
1.56	(a)	0.23879365+0	0.95019497-3	-0.34060882-4	0.36029737-5	0.3340947-5	0.16962146-5	0.86361074-6
	(b)	0.23954638+0	0.95138223-3	-0.34034794-4	0.36049243-5	0.33412153-5	0.16962674-5	0.88362398-6
	(c)	0.23954684+0	0.95147229-3	-0.34034793-4	"	"	"	"
	(d)	"	"	"	"	"	"	"
2.10		0.19112257+0	0.69014215-3	-0.50406392-4	-0.28507334-5	0.20660054-5	0.11889637-5	0.63124445-6
		0.19173855+0	0.69110971-3	-0.50385332-4	-0.28349556-5	0.20662239-5	0.11890069-5	0.63125529-6
		0.19173893+0	0.69110975-3	"	"	"	"	"
		"	"	"	"	"	"	"
2.64		0.13370682+0	0.26290654-3	-0.84266924-4	-0.82035866-5	-0.50607573-6	0.16677926-6	0.16363723-6
		0.13406796+0	0.26345841-3	-0.84256029-4	-0.82027613-5	-0.50595754-6	0.16781638-6	0.16364326-6
		0.13406818+0	0.26345843-3	"	"	"	"	"
		"	"	"	"	"	"	"

Seven terms retained in the expansion VII.2.2

allows for collisional transitions between the adjacent rotational manifolds of HD (i.e. a $\Delta j_1 = \pm 1$ collisional selection rule is operative in these calculations).

As already mentioned a number of times in this thesis the long range multipolar interactions as given by Poulsen (1982) are a factor of 2 too large (Chapter VI). The effects of these errors on the present calculations are discussed in Appendix 5 at the end of this thesis. It is worth mentioning that the leading long range (multipolar) term is now the interaction between the dipole moment of HD and the derivatives (with respect to r_2) of the dipole moment of CO, which varies as R^{-3} (e.g. see Leavitt (1980)).

3. Numerical details

As stated in Section 1, one of the objects of these calculations is to make a comparison with the experimentally determined rate coefficient for the vibrational relaxation of CO ($v_2 = 1$) by HD in the temperature range, $75 \leq T \leq 340$K. Thus we are concerned with the calculation of rotationally summed cross sections, $\sigma(v_2 j_1 \rightarrow v_2' j_1')$, for the process

$$CO(v_2=1) + HD(j_1) \rightarrow CO(v_2'=0) + HD(j_1'), \qquad \text{VII.3.1}$$

in which the HD molecule undergoes the rotational transition from $j_1 = 0$ and 1 to $j_1' \leq 5$. We perform calculations at six collision energies, E = 1.03, 1.04, 1.06, 1.07, 1.09 and 1.1 $\hbar\omega$, where the unit of energy, $\hbar\omega = 0.26989$ eV.

This range of energies enables us to determine a reasonable value for the rate coefficient in the temperature range, $140 \leq T \leq 240$K. Above 240K the $j_1 = 2$ rotational state of HD is significantly populated ($>$ 20% of HD is in the $j_1 = 2$ level), to obtain the rate coefficient for $T >$ 240 K we would have to study energies at which the $v_2 = 1 j_1 = 2$ channel is open. Such calculations are not feasible with the computer time available for this study. The numerical details of the CO molecule are those given in Chapter V, the vibrational basis required in these calculations is discussed later in this section. The mass of the HD molecule is found by adding the neutron rest mass given by Weast (1975) to the mass of the H_2 molecule given in Chapter V.3, the equilibrium separation of HD is the value of $r_{1,eq}$ given for H_2 in that section. The reduced mass of the system is found to be 4975.83 a.u. a factor of ~1.5 greater than that for the H_2 + CO system. The rotational eigenenergies of the HD molecule are taken to be those calculated using the parameters given by Herzburg (1950), and are given by

$$\varepsilon_j = B_0 j_1 (j+1) - D_0 j_1^2 (j_1+1)^2$$

where $B_o = 44.6586\ cm^{-1}$ and $D_o = 0.0257873\ cm^{-1}$

As in our previous calculations the coupled equations are solved using the R-matrix propagator method employing propagators corresponding to a constant reference potential (see Chapter III). The isotopic substitution does not significantly affect the variation of the interaction

potential as a function of R', therefore the step size, X, and the starting point, R'_{min}, required to maintain accuracy should be similar to those determined for our H_2 + CO calculations (see Chapter V.4.1). We began our convergence tests with HD constrained to its ground rotational state, and found that a value of X = 0.05 a.u. is able to converge the results to within a few per cent at all the energies studied in these calculations, increasing X to 0.1 a.u. changes the results by $\sim$ 1%. In addition we found that a value of R'_{min} = 3 a.u. was satisfactory. At a given collision energy the range of partial wave parameters that must be considered to converge the integral cross sections to within 1% is roughly a factor of 1·5 higher than that required in a corresponding H_2 + CO calculation. For example, at E = 1.1 $\hbar\omega$ we required all partial cross sections with $L \leq 30$ to evaluate $\sigma(v_2=1 j_1=0 \rightarrow v_2'=0 j_1'=0)$ in our H_2 + CO calculations, in the HD + CO system we must consider all partial cross sections with $L \lesssim 45$. This is due to the higher reduced mass of the HD + CO system, which makes the interaction potential more important at a given value of L (see Chapter IV.A). Despite the higher reduced mass we found no significant increase in the upper limit of the integration range employed in our H_2 + CO calculations, a value of R'_{max} = 25 a.u. is able to maintain convergence to within a few per cent at all the collision energies studied. It is worth

noting that employing a step size of 0.1 a.u. and increasing the value of R'_{max} to 40 a.u. changes the results by $\lesssim$ 1%. As expected vibrational excitation is not important for $R' \gtrsim 25$ a.u.

In Table 3 we show the values of $|S_L(v_2=1 j_1 \Omega_1, v_2'=0 j_1' \Omega_1 / \theta_2')|^2$ evaluated at E = 1.1 eV and L= 0, 10 at $\theta_2' = 0^\circ$ using a step size of 0.1 a.u. Results are shown for $j_1 = j_1' = 0$ at two values of R'_{max}, R'_{max} = 25.0, 30.0 a.u. Also shown are the corresponding 'V-T' results evaluated for the H_2 + CO system. This comparison with the H_2 + CO results gives the first indication of the effects of the isotopic substitution on the final results. Physically since the HD molecule is heavier than H_2 it is less effective in vibrationally exciting CO than H_2 (i.e. at a given kinetic energy the HD moves at a slower speed).

When we introduced the HD rotational degree of freedom into the calculation we found that it was not possible to converge the values of $|S_L(v_2=1 j_1 \Omega_1, v_2'=0 j_1' \Omega_1 / \theta_2')|^2$ for the individual rotational processes to the same level of accuracy as shown in Table 3. As discussed later in this section we claim that this is due to the transfer of flux to and from the HD rotational states, which are closely spaced and strongly coupled by the potential. Only when we sum the values of $|S_L(v_2=1 j_1 \Omega_1, v_2'=0 j_1' \Omega_1 / \theta_2')|^2$ over the final HD rotational states, j_1', do we find reasonable agreement.

TABLE 3

Comparison of $|S_L(v_2=1, v_2'=0|\theta_2')|^2$ (a.u.)^2 evaluated using different values of R'_{max} at E = 1.1 $\hbar\omega$ and $\theta'_2 = 0^o$. Also shown are results obtained for the H_2 + CO system.

(a) R'_{max} = 25 a.u., (b) R'_{max} = 30 a.u.

L		$\lvert S_L(v_2=1, v_2'=0\rvert\theta_2')\rvert^2$	
		HD + CO	H_2 + CO
0	(a)	0.24441874-7	0.55028077-6
	(b)	0.24441238-7	0.55028163-6
10	(a)	0.10376396-7	0.18848531-6
	(b)	0.10376931-7	0.18848694-6

TABLE 4

Comparison of results obtained retaining different numbers of vibrational channels in the coupled equations at E = 1.1 $\hbar\omega$. Also shown are results for the H_2 + CO system.

(a) 2 channels, (b) 3 channels, (c) 4 channels.

θ'_2 =		0°	90°	180°
HD + CO	(a)	0.24441874-7	0.36120377-8	0.96716586-9
	(b)	0.28660642-7	0.36762079-8	0.14648386-8
	(c)	0.28662355-7	0.36762540-8	0.14649408-8
H_2 + CO		0.55028077-6	0.80104030-7	0.51323274-7
		0.59879974-6	0.80773173-7	0.62622036-7
		0.59880180-6	0.80772145-7	0.62641953-7

Values of $|S_L(v_2=1, v_2'=0|\theta_2')|^2$ (a.u.)^2 obtained at L = 0.

Due to the enhanced reduced mass of the HD + CO system the vibrational channels of CO are more strongly coupled by the potential. In Table 4 we show the convergence of $|S_L(v_2=1 j_1=0 \Omega_1, v_2'=0 j_1'=0 \Omega_1' \theta_2')|^2$ at E = 1.1 $\hbar\omega$ and L = 0, at three CO orientations, $\theta_2' = 0^\circ$, 90°, 180° for both the H_2 + CO and HD + CO systems. As one can see it is sufficient to include all the open and one closed vibrational channel to obtain satisfactory results for both systems at this collision energy, however notice that as expected the closed channels are much more important in the HD + CO system. For example at $\theta_2' = \theta_2 = 180^\circ$ the addition of the second excited vibrational state, $v_2 = 2$, changes the result by roughly 50% (even at this energy, E = 1.1 $\hbar\omega$, which is well below the $v_2 = 2$ threshold), whereas the corresponding result is changed by $\sim$ 20% in the H_2 + CO system. Even at E = 1.9 $\hbar\omega$, at $\theta_2 = 180^\circ$, the addition of $v_2 = 2$ only changes the result by $\sim$ 40% in the H_2 + CO system (see Table 18 , Chapter V). This imposes a strong restriction upon the energy range we can study, as we shall show later in this section it is necessary to include at least the first six rotational levels of HD to obtain satisfactory results, with such a large rotational basis we found that the addition of each vibrational channel increased the computer time required to solve the coupled equations by $\sim$ 50%. Evidently as the collision energy increases beyond E = 1.1 $\hbar\omega$, it will soon be necessary

to include at least two closed vibrational channels to obtain a satisfactory description of the CO molecule and such calculations are not feasible, if sufficient energies are to be studied to evaluate a reasonably accurate value for the rate coefficient. We employ a vibrational basis consisting of $v_2 \leq 2$ in all these calculations, the vibrational potential matrix elements are evaluated using a 28- point Gauss Legendre quadrature, this ensures the results are converged to within a few per cent at all the energies studied in this calculation.

Generally speaking the HD molecule was much more difficult to deal with than the CO molecule. We recall that in our H_2 + CO calculations we determined the step size and integration range required to maintain accuracy at a given initial kinetic energy, E_T, in calculations involving H_2 constrained to its ground rotational state. These parameters were then employed in calculations studying rotating H_2 at the same initial kinetic energy (see Chapter VI). In the present calculations, however, we do not take account of the initial rotational state of HD (i.e. if we study HD ($j_1 = 0$) at a total collision energy of E, we do not increase the collision energy to $E + \mathcal{E}_{j_1}$ to study HD($j_1 \neq 0$)). This appears to be a reasonable approach since the rotational energy levels of HD are very closely spaced compared with the energy spacing of the vibrational energy levels in CO (cf. $\mathcal{E}_{v_2=1} \sim 2000$ cm^{-1}, $\mathcal{E}_{j_1=1} \sim 90$ cm^{-1}, $\mathcal{E}_{j_1=5} \sim 1300$ cm^{-1}).

The slight change in the initial kinetic energy at a given collision energy should not have any significant effect upon the integration parameters.

In Table 5 we show the convergence of the results as a function of the number of rotational states included in the coupled equations for both the HD + CO and H_2 + CO systems. The results are shown for the transition $v_2 = 1\ j_1 = 0 \rightarrow v_2' = 0\ j_1' = 0$ at $E = 1.1\ \hbar\omega$ and $L = 0$ and at $\theta_2' = 180^\circ$. We were extremely surprised by the number of rotational states that had to be included in the HD + CO calculations to achieve convergence to within $\sim 5\%$, as can be seen we require at least six states. In contrast the convergence of the results in the H_2 + CO system is extremely rapid, only two channels are needed to achieve the same degree of convergence. It is worth mentioning that the same computer programme was used to study each system. The HD + CO calculations only required that trivial modifications be made to the existing routines (e.g., we must implement the potential transformation VII.2.4, which appears to be working correctly, as is shown in Section 2, and we must account for the $\Delta j_1 = 1$ collisional selection rule in HD). Although channels denoted by $v_1 = 1\ j_1$ are open only for $j_1 \leq 1$ at this energy, channels denoted by $v_2 = 0\ j_1$ are open for $j_1 \leq 6$. The only reasonable explanation we are able to offer is that these open channels (which are closely spaced, and strongly coupled by the potential)

TABLE 5

The convergence of $|S_L(v_2=1 j_1=0, v_2'=0 j_1'=0|\theta_2')|^2$ (a.u.)^2 as a function of the number of rotational states retained in the coupled equations at E = 1.1 $\hbar\omega$ and L = 0. Results are shown for both the HD + CO and H_2 + CO system at $\theta_2' = \theta_2 = 180^\circ$.

Number of Rotational states	$\lvert S_L(v_2=1 j_1=0, v_2'=0 j_1'=0\rvert\theta_2')\rvert^2$	
	HD + CO	H_2 + CO
1	0.96713045-9	0.51323744-7
2	0.70576707-8	0.60346349-7
3	0.67240391-8	0.60381697-7
4	0.11571327-8	0.60378485-7
5	0.19664733-9	
6	0.15790107-9	
7	0.15804647-9	
8	0.15773195-9	

are having a significant effect upon the convergence of the results. Notice that in the H_2 + CO system, at the same collision energy relatively few rotational channels are open, the channels that are open are more widely spaced (and the potential is less important due to the smaller reduced mass of the H_2 + CO system).

We have carried out similar numerical tests at other CO orientations at this energy, and at lower collision energies. We conclude that if we retain the first six rotational channels in the calculations, this is sufficient to converge the results for the transitions from $v_2 = 1$ $j_1 = 0$ and 1 to $v_2' = 0 j_1'$, for $j_1 \leq 4$ to within $\sim$10% at all the energies studied. However, the cross sections for transitions to $j_1' = 5$ are unsatisfactory, they are overestimated by a factor of ~ 2.

As already mentioned we found that the convergence (as a function of R'_{max}) of the results for the individual rotational transitions in HD is extremely poor, however we found reasonable agreement between the values of

$S^{\Omega_1}_{Lj_1}(v_2=1, v_2'=0/\theta_2')$ where,

$$S^{\Omega_1}_{Lj_1}(v_2=1, v_2'=0/\theta_2') = \sum_{j_1'=0}^{5} |S_L(v_2=1 j_1 \Omega_1, v_2'=0 j_1' \Omega_1/\theta_2')|^2$$

where $j_1 = 0$ and 1,

evaluated at different values of R'_{max} (for $R'_{max} \geq 25$ a.u.). In Table 6 we show the convergence of the results with respect to R'_{max} at E = 1.03 and 1.1 $\hbar\omega$, at $\Omega_1 = 0$, and $\theta_2' = 180^\circ$ for several values of the partial wave parameter L. As may be seen the agreement between the rotationally summed S-matrices, $S^{\Omega_1}_{Lj_1}(v_2=1, v_2'=0/\theta_2')$,

TABLE 6

Comparison of results evaluated for the HD + CO system using different values of R'_{max} at $\theta'_2 = 180^{\circ}$.

Values of $|S_L(v_2=1 j_1=0, v_2'=0 j_1'=0 | \theta_2')|^2$ at 25 a.u. (a) 30 a.u.(b) 35 a.u.(c)

Values of $S^{\Omega_1=0}_{L j_1=0}(v_2=1, v_2'=0)$ " (d) " (e) " (f)

L =		0	10	20	30
E(ħw)	(a)	0.309166-10	0.218707-10	0.624210-11	
	(b)	0.299687-10	0.152809-10	0.108027-10	-
	(c)	0.372277-10	0.136936-10	0.292512-11	
1.03	(d)	0.130552-8	0.180378-9	0.365532-10	
	(e)	0.115856-8	0.184097-9	0.688069-10	-
	(f)	0.116303-8	0.204528-9	0.154583-10	
		0.113764-9	0.165744-9	0.107513-10	0.436577-11
		0.898453-10	0.651079-9	0.158327-10	0.152427-11
		0.157901-9	0.335476-9	0.391858-10	0.521410-11
1.10		0.622574-8	0.252239-8	0.499629-9	0.304969-10
		0.634130-8	0.335065-8	0.217264-9	0.822254-10
		0.603609-8	0.314152-8	0.267515-9	0.468743-10

is far superior to the agreement between the S-matrices for the process $j_1 = j_1' = 0$ (given for comparison, note that the S-matrices for all the rotational processes are similar in magnitude). As L increases the agreement between the rotationally summed results does however, deteriorate, the only reasonable explanation we can offer, is that since the numerical values of the S-matrices are small, the computer code is having difficulty maintaining accuracy. The partial cross sections with these high L values (i.e. $L \geq 20$ at $E = 1.03\hbar\omega$, and $L \geq 30$ at $E = 1.1\ \hbar\omega$) do however, form a relatively small contribution to the final integral cross section.

We have carried out similar tests for the H_2 + CO system at $E = 1.1\ \hbar\omega$, and $L = 0$, 10. Again we conclude that the convergence of the results for the individual rotational process $j_1 = j_1' = 0$ is less satisfactory than for the rotationally summed results. (However, the results evaluated at $R'_{max} = 25.0$ and 30.0 a.u. for the transition $j_1 = j_1' = 0$ do agree to within $\sim$ 5%).

The only conclusion we can draw regarding the results evaluated for this system , is that the long range interactions are causing flux to be transferred from one rotational state to another, consequently we are unable to determine individual rotational transitions, but as already shown in this section vibrational excitation is not important for $R'_{max} \geq 25$ a.u., and thus we find reasonable agreement between the values of $S^{\Omega}_{v_1 j_1}(v_2 = 1, v_2' = 0 / \Omega_2')$

evaluated at R'_{max} = 25.0, 30.0 and 35.0 a.u. (indeed it is highly unlikely that the H_2 or HD could vibrationally excite the CO molecule at such large intermolecular separations). The leading long range interaction in the HD + CO interaction potential is, as mentioned in Section 2, the interaction between the dipole moment of HD, and the derivatives (with respect to r_2) of the dipole moment of CO, which varies as R'^{-3}. However this interaction should only have a significant influence on the convergence of the vibrationally elastic results (as was seen in the $H_2 + H^+$ system, Chapter IV.A). As shown in Section 2, the interaction potential is tending to zero as $R \rightarrow \infty$, in addition we are confident, in the light of our H_2 + CO calculations, that the asymptotic boundary condition is fitted correctly in our programme. One will recall that our results for H_2 + CO are in good agreement with the results of BSD2 evaluated using the P potential, as is shown in Appendix 4.

We are reasonably sure that the convergence problems seen in HD + CO are all caused by the long range multipolar interactions (as we claim above), when we employ just the short range and dispersion terms of the potential in the scattering calculations we find excellent agreement between the results for the individual rotational transitions (they agree to within $\sim$ 1%) evaluated at the values of R'_{max} given in Table 6.

We have carried out numerous tests on the potential transformation given in Section 2, in particular we are confident that the transformed multipolar interactions are sufficiently accurate to study rovibrational excitation (prior to these calculations, the transformation VII.2.4 given by Liu et al. (1978) had only been employed in calculations studying pure rotational excitation). For example, at fixed values of θ_1', and θ_2' we evaluated the ratio (employing just the multipolar interactions).

$$X = \frac{U(r_2(i)) - U(r_2(i+1))}{r_2(i) - r_2(i+1)} \qquad \text{VII.3.2}$$

where $U(r_2(i)) = U(\theta_1', \theta_2', r_2(i), R')$.
At both R'_{max} = 20.0 and 30 a.u. we find excellent agreement between the values of X (they agree to eight significant figures) for i = 1, ---, 28, as one will recall we use a 28- point Gauss Legendre quadrature to evaluate the vibrational potential matrix elements. Evidently one could include the multipolar interactions in these calculations explicitly using numerical values for the HD dipole and quadrupole moments taken from the literature, however a number of additional calculations indicate that this procedure would result in qualitatively similar results.

Since we find good agreement between the rotationally summed results, the conclusion that one should draw

is that the 'net' effect of the long range forces are unimportant, and therefore while the errors in the potential routine might change individual rotational transitions, it is questionable that the rotationally summed (vibrational) results should be seriously affected. However, as we show in Appendix 5, the errors in our potential routine have significantly affected both the cross sections for individual rotational transitions and for the vibrational transitions. As is discussed in Appendix 5, it is apparent that the long range interactions play a significant role in determining the numerical values of the vibrational de-excitation cross sections, which would appear to be in conflict with our conclusion drawn above. We have, unfortunately, no satisfactory explanation for this.

When the scattering calculations were performed we employed 320 steps of fixed length in the range $3 \leq R \leq 35$ a.u. which is more than satisfactory to obtain converged rotationally summed (vibrational) cross sections. Because of the uncertainties in the cross sections for the individual rotational transitions, in Section 4 we present only the rotationally summed cross sections, $\sigma_{j_1}(v_2=1 \rightarrow v_2=0)$, i.e.,

$$\sigma_{j_1}(v_2=1 \rightarrow v_2=0) = \sum_{j_1'=0}^{5} \sigma(v_2=1 j_1 \rightarrow v_2'=0 j_1') \qquad \text{VII.3.3}$$

where $j_1 = 0$ and 1.

Maintaining the same integration range, and step size the computer time required to solve the coupled equations, retaining the same number of vibrational states and no rotational states (i.e. just $j_1 = 0$), is roughly a factor of 5 greater than that required for the H_2 + CO system. Using equation VII.2.4 to transform the interaction potential is extremely expensive, even retaining just seven terms in the expansion VII.2.2 , and employing an 8- point Gauss Legendre quadrature to evaluate the integral. We therefore compute the potential using VII.2.4 before performing the scattering calculations and use a spline interpolation procedure to evaluate the potential at the required values of R' (the potential is 'pre-computed' at all the values of θ_2', the CO orientations, and r_2, the vibrational coordinates required). Routines written in FORTRAN IV capable of interpolating data by means of a cubic spline are available and have been used numerous times in work presented in this thesis (e.g. see Chapters V.5 and VI.4).

In Table 7 we show a comparison of the values of $S_{L_{j_1}}^{\Omega=0}(v_1=0, v_2=0/\theta_2)$ evaluated using 137-, 86-, and 69- point splines in the range $2.0 \leq R \leq 35$ a.u. The potential was computed retaining 9 terms in the expansion VII.2.2 and employing a 10- point Gauss Legendre quadrature to evaluate the integral VII.2.4. Also shown is the numerical value of the S-matrix evaluated

TABLE 7

A comparison of results obtained using different N-point splines in the range $2 \leq R \leq 35$ a.u. to generate the potential. Also shown is the result obtained in a calculation in which the potential was evaluated at each value of R in the integration range using VII.2.4.

(a) N = 69 points, (b) N = 86 points, (c) N = 137 points, (d) Result obtained using VII.2.4 at each value of R .

	$S_{Lj}^{\Omega=0}(v_2=1, v_2'=0)$ $(a.u.)^2$
(a)	0.12964002 - 8
(b)	0.11887458 - 8
(c)	0.11943994 - 8
(d)	0.11630300 - 8

Results evaluated at E = 1.03 $\hbar\omega$ and L = 0, and at $\theta_2' = 180^\circ$. $j_1 = 0$ only, $j_1' \leq 5$.

TABLE 8

The convergence of $\sigma_{j_1}^{L}$ $(v_2 = 1 \rightarrow v_2' = 0)$ with respect to the number of CO orientations, θ_2', included in the calculations at E = 1.1 $\hbar\omega$ and L = 0 .

(a) 16 orientations, (b) 20 orientations, (c) 28 orientations .

	$\sigma_{j_1}^{L}$ $(v_2 = 1 \rightarrow v_2' = 0)$ (Å^2)	
	$j_1 = 0$	$j_1 = 1$
(a)	0.20560412-8	0.17204594-8
(b)	0.20598170-8	0.16401752-8
(c)	0.20569189-8	0.16563214-8

in a calculation in which the potential is computed using the integral VII.2.4 at each step in the integration range. Results are shown for E = 1.03 $\hbar\omega$ and L = 0 at $\theta_2' = 180^\circ$ and $\Omega_1 = 0$. At this energy, which is the lowest studied in these calculations, if we employ a 137 point spline (i.e. in which the potential is pre-computed every 0.25 a.u. in the range $2.0 \leq R \leq 35.0$ a.u., recall that the coupled equations are solved in the range $3.0 \leq R \leq 35$ a.u., there is therefore no extra-polation of data), this ensures that the results are determined to within $\sim$5% at this energy. Note that as the collision energy increases, errors in the potential matrix elements should be less important. In conclusion the 137- point spline will be employed in all our cal-culations. We mention that it results in a reduction in the computer time needed to solve the coupled equations at one orientation by a factor of ~ 4 (if three vibrational and six rotational channels are included in the calculations). Even with this vast reduction in computer time at the initial partial wave, the calculations are still extremely expensive. Using the IBM 370/168 computer at NUMAC the approximate computer time required at the initial partial wave is $\sim$ 110 s (70s at $\Omega_1 = 0$ and 40s at $\Omega_1 = 1$) and at subsequent partial waves is $\sim$ 60s (40s at $\Omega_1 = 0$ and 20s at $\Omega_1 = 1$). Using the spline to generate the potential has no effect upon the computer time required at subsequent partial waves, since there is no explicit reference to the potential matrix elements. As already

mentioned (Chapter VI.4), the majority of the computer time at subsequent partial waves (when we are dealing with 'large' matrices) is accounted for by matrix multiplication. By vectorizing the matrix multiplication, and R-matrix propagator routines we are able to reduce the computer time given above for the calculations at subsequent values of L by a factor of $\sim$15 using the Cray-1 computer (rather than the more usual factor of $\sim$8). It is worth repeating that due to the enhanced reduced mass of the HD + CO system (a factor of 1.5 larger than that for H_2 + CO) we need to calculate $\sim$50% more partial waves at a given energy. Since the coupled equations are to be solved at 16 orientations we consider six rotational channels the maximum feasible.

In Table 8 we compare rotationally summed (with respect to both final CO and HD rotor states) cross sections, $\sigma^{L}_{j_1}(v_2=1, v_2'=0)$), evaluated using 16-, 20-, and 28- point Gauss Legendre quadratures at E = 1.1 $\hbar\omega$ and L = 0. We recall that the convergence of the results (as a function of the number of CO orientations included in the calculations) improves with both increasing L and decreasing E (Chapter V.4.3). As can be seen a 16-point Gauss Legendre quadrature ensures good results for both j_1 = 0 and 1. Employing this quadrature we consider that the results will be evaluated to within $\sim$5% at all the energies studied in these calculations.

4. Results and discussion

In this section we will present and discuss the

results of our calculations of the vibrational de-excitation of CO(v_2 = 1) by HD. In Table 9 we show the numerical values of the rotationally summed cross sections, $\sigma_{j_1}(v_2=1 \rightarrow v_2'=0)$ i.e.

$$\sigma_{j_1}(v_2=1 \rightarrow v_2'=0) = \sum_{J=0}^{5} \sigma(v_2=1 j_1 \rightarrow v_2'=0 j_1') \qquad \text{VII.4.1}$$

where j_1 = 0 and 1.

Both the collision energy, E, and the initial translational energy, E_T, are given in Table 9. As both the v_2 = 1 j_1 = 0 and v_2 = 1 j_1 = 1 thresholds are approached the cross sections begin to rise. We are reasonably sure that this threshold behaviour is due to orbiting resonances. The effective potential for the system, at a partial wave parameter L, is given by

$$V_{eff}^{L}(R') = \bar{V}_{int}(R') + \frac{L(L+1)}{2\mu (R')^2} \qquad \text{VII.4.2}$$

where μ is the reduced mass of the system and where $\bar{V}_{int}(R')$ is the spherically symmetric component of the HD + CO interaction potential. Resonances can occur only when the effective potential possesses an attractive well capable of supporting one or more bound states. These resonances are said to be of shape or Feshbach type according to whether they occur in an open or a closed channel (e.g. see Child (1974)).

At E = 1.03 meV we have located a Feshbach resonance in the v_2 = 1 j_1 = 1 channel. The kinetic energy of the system in this state is $-3.43\,10^{-5}$ a.u., compared with

TABLE 9

Rotationally summed cross sections,

$$\sigma_{j_1}(v_2=1 \rightarrow v_2'=0) = \sum_{j_1'=0}^{5} \sigma(v_2=1 j_1 \rightarrow v_2'=0 j_1'),$$

(in Å^2) for the vibrational relaxation processes in which $j_1 = 0$ and $j_1 = 1$. E is the total collision energy, $E_T(cm^{-1})$ is the initial kinetic energy, relative to the $v_2=1 j_1$ threshold ($j_1 = 0$ or 1).

	$j_1=0$		$j_1=1$	
E(ħw)	E_T	$\sigma_0(v_2=1 \rightarrow v_2'=0)$	E_T	$\sigma_1(v_2=1 \rightarrow v_2'=0)$
1.03	81.69	0.117-6	-	-
1.04	103.39	0.117-6	14.17	0.143-6
1.06	146.78	0.146-6	57.56	0.115-6
1.07	168.47	0.169-6	79.26	0.109-6
1.09	211.86	0.226-6	122.65	0.131-6
1.10	233.55	0.264-6	144.34	0.152-6

Note that 1 cm^{-1} = 1.4388K.

the minimum of the effective potential (at L = 0, $-2.63\ 10^{-4}$a.u., and at L = 10, $-3.78\ 10^{-5}$ a.u.). The minima of the effective potentials are at positive energies for $L > 10$. For $L \leq 10$ there is a possibility of the system becoming trapped in the potential well. In Figure 2 we show the energy dependence of $\sigma^{L}(v_2 = 1\ j_1 = 0 \rightarrow v_2' = 0\ j_1' = 0)$ at L = 0. Clearly the partial cross sections pass through a resonance at $E \simeq 1.03\ \hbar\omega$. (For obvious reasons the effects of a Feshbach resonance are observed in the open channels). We mention that we have found a shape resonance centred at $E \simeq 1.04\ \hbar\omega$ in the $v_2 = 1\ j_1 = 1$ channel. The kinetic energy of the system in this state is $6.46\ 10^{-5}$ a.u. compared with the height of the potential barrier at L = 11, $\sim 8.21\ 10^{-5}$ a.u. (the minimum is at $\sim 2.02\ 10^{-6}$ a.u.).

In Figure 3 we show the energy dependence of the integral cross section, $\sigma_{j_1=0}(v_2 = 1 \rightarrow v_2' = 0)$. Also plotted are the contributions to $\sigma_{j=0}(v_2 = 1 \rightarrow v_2' = 0)$ from partial cross sections with $L \leq 10$, and from partial cross sections with $11 \leq L \leq 20$, these we denote by A and B respectively,

$$A = \sum_{L=0}^{10} \sigma^{L}_{j_1=0}(v_2 = 1 \rightarrow v_2' = 0) \qquad \text{VII.4.3a}$$

$$B = \sum_{L=11}^{20} \sigma^{L}_{j_1=0}(v_2 = 1 \rightarrow v_2' = 0) \qquad \text{VII.4.3b}$$

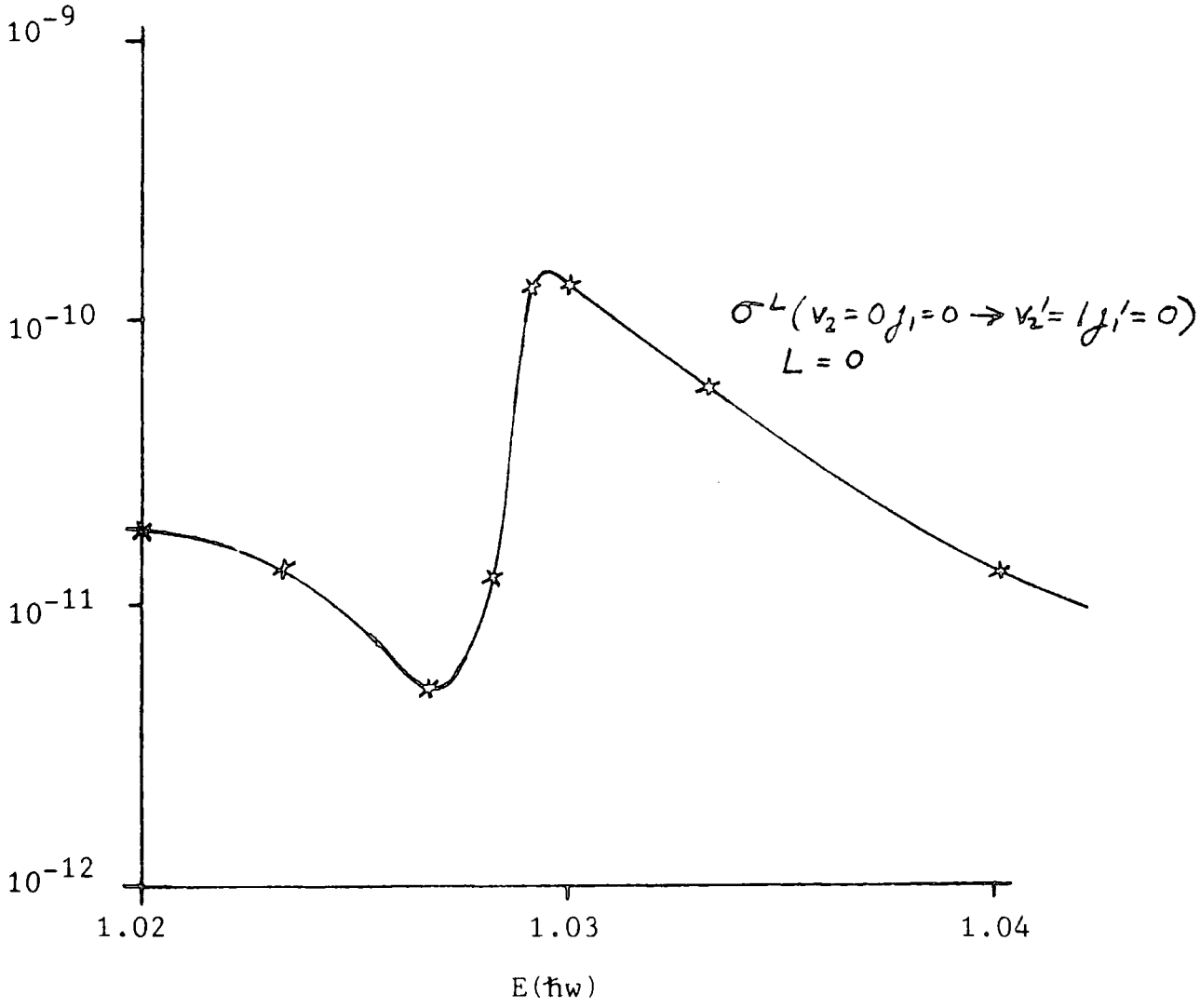

Figure 2 The energy variation of the partial cross section, $\sigma^L(v_2=1 j_1=0 \rightarrow v_2'=0 j_1'=0)$, in $Å^2$ at L = 0.

In the text we state that only the rotationally summed cross sections $\sigma_j^L(v_2=1 \rightarrow v_2'=0)$ are of interest due to the convergence problems associated with the results for the individual rotational transitions, however notice that the uncertainty in all the cross sections shown should be similar in the small energy range considered.

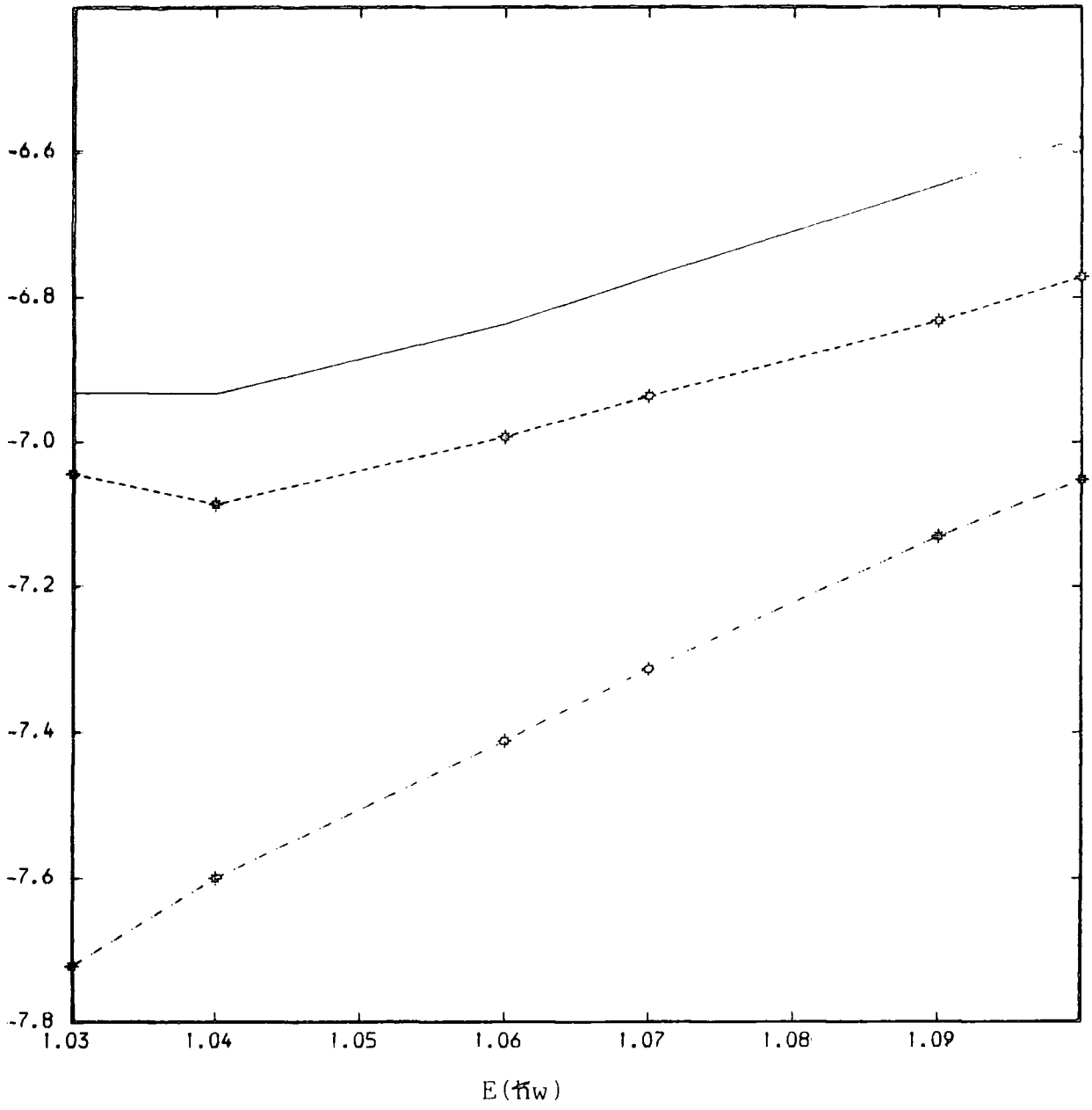

Figure 3 The variation with collision energy, E, of the rotationally summed integral cross section, $\sigma_{j_1}(v_2 = 1 \rightarrow v_2' = 0)$ ($Å^2$), for $j_1 = 0$ (————).

Also shown are the contributions to $\sigma_{j_1}(v_2=1 \rightarrow v_2'=0)$ from $L \leq 10$ (------), and $11 \leq L \leq 20$ (- - - -).

Notice that A and B are overestimated at E 1.03, and 1.04 $\hbar\omega$ respectively (where we located the resonances). If our numerical methods were deteriorating as $E \to 0$, B would probably continue to increase for $E < 1.04\ \hbar\omega$. In addition as L increases one requires a smaller step size to maintain accuracy, so for a given step size it is not consistent that we should determine B to a higher degree of accuracy than A (e.g. at $E = 1.03\ \hbar\omega$). Furthermore the contribution A is sufficient to account for the rise in the cross section at $E = 1.03\ \hbar\omega$, similar arguments can be used to explain the threshold behaviour of $\sigma_{J=1}\ (v_2=1 \to v_2'=0)$.

To determine the theoretical rate coefficient for the deactivation of CO ($v_2 = 1$) by HD, the rate coefficients evaluated using the rotationally summed cross sections, $\sigma_{j_1}\ (v_2=1 \to v_2'=0)$, which we will denote by $\alpha_0(T)$ and $\alpha_1(T)$ for $j_1 = 0$ and 1 respectively, are weighted by the relative populations of the HD rotational states, given by a Boltzmann distribution (cf. IV.4.6).

$$\alpha(T) = \frac{\alpha_0(T) + \alpha_1(T)\frac{\omega_1}{\omega_0} e^{-\Delta E(0,1)/kT}}{1 + \frac{\omega_1}{\omega_0} e^{-\Delta E(0,1)/kT}} \qquad \text{VII.4.4}$$

where E(0,1) is the energy separation of the $j_1 = 1$ and 0 rotational levels in HD (see Chapter VI.4 for definitions). As in our previous calculations the theoretical rate is obtained by means of a cubic spline interpolation procedure (Chapter V.5) , the comparison of $\alpha(T)$

with the experimentally determined rate coefficient (Andrews and Simpson (1976)) is given in Figure 4 for the temperature range, $140 \leq T \leq 240$ K. Above $T > 240$ K, the agreement with the experimental points is extremely poor, as mentioned in Section 3, we need to consider collision energies $> 1.1\,\hbar\omega$ (initial kinetic energies > 300 K) to accurately evaluate the rate coefficient for $T > 240$ K. In the temperature range shown the theoretically determined rate is a factor ~ 2-3 lower than the experimental points. In view of our previous comparisons with experiment (Chapter V,5, and Chapter VI.4) we consider this level of agreement to be satisfactory, indeed we would have been surprised if the agreement had been better. The summation over j_1', the final rotational state, in equation VII.4.1 includes $j_1' = 5$, despite the cross sections for the rotational transitions to $j_1' = 5$ being overestimated by a factor of ~ 2. As mentioned in Section 3, the six rotational states ($j_1 \leq 5$) employed in the calculations is insufficient to accurately determine the cross sections with $j_1' = 5$. At the energies we study in these calculations, $E \leq 1.1\,\hbar\omega$, the $j_1 = 6$ state is open, the cross sections with $j_1' = 5$ also account for the flux that should have gone into the $j_1 = 6$ channel.

When one accounts for the error in the potential routine the agreement with experiment will be diminished, as is discussed in Appendix 5. Indeed it appears that the resulting agreement with experiment would be extremely

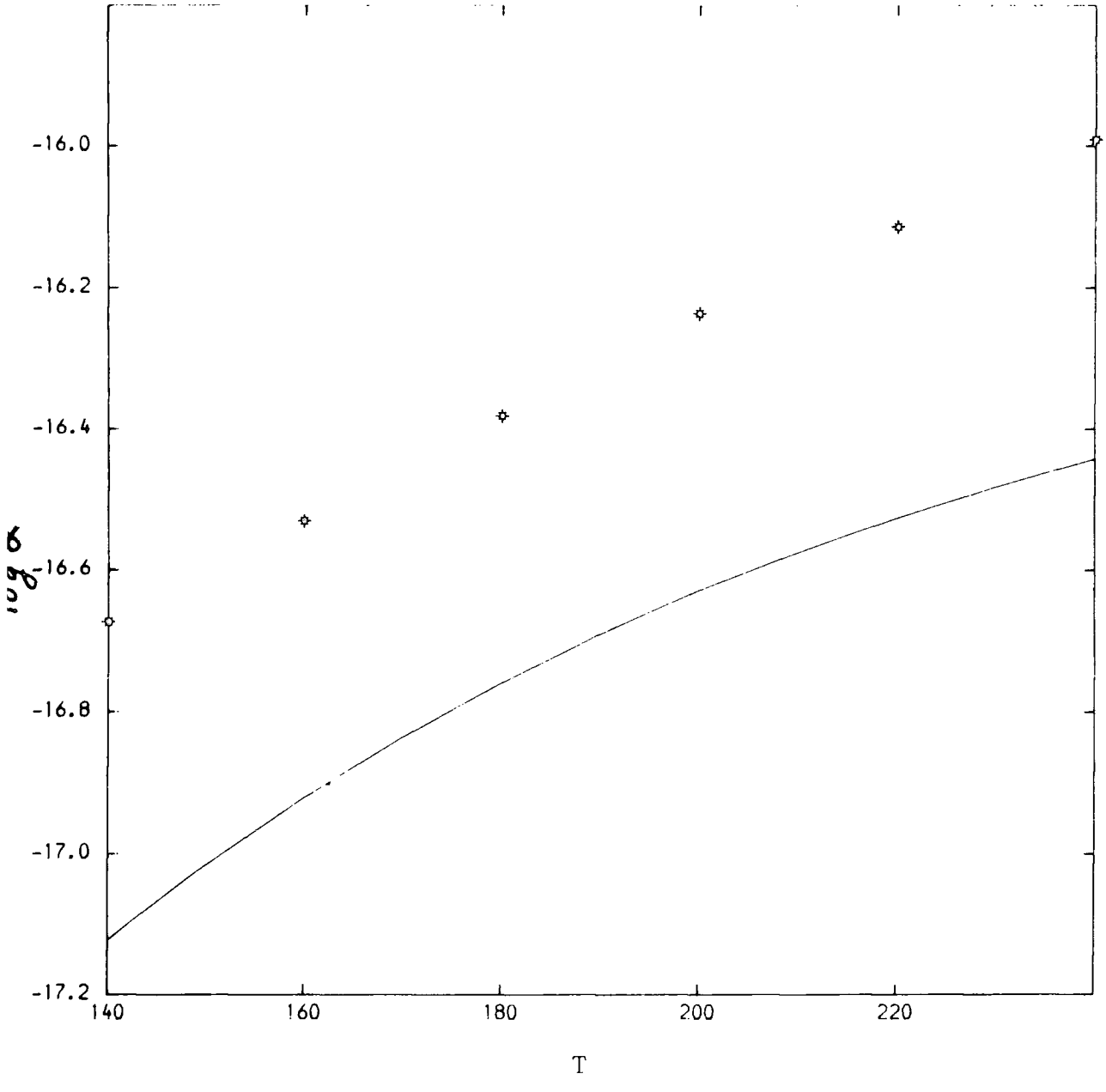

Figure 4. The variation with temperature, T(K), of the vibrational relaxation coefficient, $\alpha(T)$ (in units of $cm^3 s^{-1}$).

Solid curve : present calculations; * : experimental results of Andrews and Simpson (1976).

poor. Some improvement would result if the rotational degree of freedom of CO was treated within the CS approximation (assuming that the ratio of CS to IOS rates, as determined by BSD for $H_2(j_1 = 0) + CO$, is valid for HD ($j_1 \neq 0$) + CO). The IOS rate would be increased by a factor of $\sim$1.5, insufficient to account for the discrepancies between experiment and theory. However, in view of the expense of these IOS calculations, we consider that a similar calculation employing the CS approximation would not be feasible.

As we have mentioned already in this chapter, it is apparent from our discussion in Appendix 5 concerning the errors in the P potential, that the long range interactions play a significant role in determining the numerical values of the vibrational de-excitation cross sections. None of the transitions studied in these calculations are near-resonance, so we find it extremely difficult to understand why we arrive at the above conclusion, especially in view of the results obtained for the H_2 + CO system. One will recall that the $\Delta j_1 = 0$ and 2 cross sections were changed by only a few per cent when we accounted for the error in our potential routine (Appendix 4). In particular, it is not clear, at least to us, why the agreement with experiment is so poor.

Finally we conclude that we would have to spend a great deal more time investigating this system before we fully understand all the results presented in this chapter. However, using the present results we are

able to draw a number of conclusions regarding the effects of the isotopic substitution on the calculations, and have some indication of the level of agreement between experiment and theory.

CHAPTER VIII

CONCLUSIONS AND SUGGESTIONS FOR FUTURE WORK

The main results presented in this thesis are the calculations of the rovibrational excitation of CO by para-H_2 (Chapters V and VI). The work on H_2 + CO is essentially complete in the sense that we have a reasonable understanding of the sensitivity of the vibrational relaxation cross sections upon the potential energy surface, the dynamical approximations, numerical procedures, and parameters. The most crucial point is certainly the interaction potential, and since all the available H_2 + CO interaction potentials have now been tested (the potentials of Poulsen (1982) and van Hemert (1983) in this work, and the potential constructed from the SCF data of Diercksen and Kraemer (1984) by BSD and BSD2) it seems pointless continuing these calculations. The potential of van Hemert (1983) is unsatisfactory, of the two remaining surfaces, neither "stands out" as the best overall description of the H_2 + CO interaction. However, together the P and DK potentials probably represent the best we can do for a complex system like H_2 + CO, given present ab initio techniques.

Of special interest in this work is the near resonance-process (VI.1.1). It is evident from our research that this is an extremely complex process, and it will be some time before a satisfactory

theoretical description of this process is achieved, especially, if as postulated in Chapter VI, the multipole moment interactions are important at short range. Poulsen and Billing (1982) suggest that the cross sections for this process would be enhanced if higher multipole moments of CO were treated explicitly in the potential surface. Indeed, such a calculation has been performed (Poulsen and Billing (1984)), the P potential was employed and the octopole and hexadecapole moments of CO were treated explicitly. However, it is possible that the semi-classical approximation employed by these authors is inapplicable to the H_2 + CO system, and therefore the results presented by Poulsen and Billing (1984) should be treated with a degree of caution. Only when a quantum mechanical calculation has been performed can the importance of the higher multipoles of CO be properly assessed.

Due to the error in our potential routine,the HD + CO calculations presented in Chapter VII are seriously in error, however it is not worth repeating these calculations. The calculations are extremely expensive computationally, and the present results do at least give us a reasonable understanding of the effects of isotopic substitution. Nevertheless it is probably worth continuing work on this system to determine more precisely the role played by the long range multipolar interactions.

In Chapter IV we used the H_2 + H^+ system to examine the applicability of the asymptotic series expansions

of the type introduced by Gailitis (1976) in heavy particle scattering calculations. The results indicate that we have at our disposal an extremely powerful tool, their use may provide substantial savings in computer time in systems whose interaction potential surface contains long range interactions.

REFERENCES

Aannestad, P.A., and Field, G.B., (1973), Astrophysical Journal Letters 186, L29.

Abramowitz, M., and Stegun, I.A., (1965), Handbook of Mathematical Functions (New York : Dover).

Alexander, M.H., (1975), Chem. Phys. 8, 86.

Alexander, M.H., Dagdigian, P.J., and De Pristo, A.E., (1977), J. Chem. Phys. 66, 59 and 4126.

Alexander, M.H., and De Pristo, A.E., (1977), J. Chem. Phys. 66, 2166.

Alexander, M.H., and McGuire, P., (1976), J. Chem. Phys. 64, 452.

Allen, D.C., Price, T.J., and Simpson, C.J.S.M., (1979), Chem. Phys. 41, 449.

Amos, R.D., (1979), Chem. Phys. Lett. 68, 536.

Andres, J., Buck, U., Meyer, H., and Launay, J.M., (1982), J. Chem. Phys. 76, 1417.

Andrews, A.J., and Simpson, C.J.S.M., (1975), Chem. Phys. Lett. 36, 271.

Andrews, A.J., and Simpson, C.J.S.M., (1976), Chem. Phys. Lett. 41, 565.

Arons, J., and Max, C., (1975), Astrophysical Journal Letters 169, L77.

Bačić, Z., Schinke, R., and Diercksen, G.H.F., (1984a), to be published.

Bačić, Z., Schinke, R., and Diercksen, G.H.F., (1984b), to be published.

Balint-Kurti, G.G., (1975), International Review of Science, Vol. 1 of Physical Chemistry, Series edited by A.D. Buckingham, and C.A. Coulson (London : Butterworths).

Baushchlicher, C.W., O'Neil, S.V., Preston, R.K., Shaefer, H.F., and Bender, C.F., (1973), J. Chem. Phys. 59, 1286.

Bergeron, G., Leforestier, C., and Launay, J.M., (1978), Chem. Phys. Lett. 59, 129.

Berns, R.M., and van der Avoird, A., (1980), J. Chem. Phys. 72, 6107.

Billing, G.D., (1974), J. Chem. Phys. 61, 3340.

Billing, G.D., and Clary, D.C., (1982), Chem. Phys. Lett. 90, 27.

Billing, G.D., and Poulsen, L.L., (1982), Chem. Phys. 70, 119.

Billing, G.D., and Poulsen, L.L., (1983), Chem. Phys. Lett. 99, 368.

Black, J.H., and Dalgarno, A., (1973), Astrophysical Journal Letters 184,L101.

Black, J.H., and Dalgarno, A., (1976), Astrophysical Journal 203, 132.

Bocchetta, C.J., (1983), Ph.D. Thesis, University of Bristol.

Bowman, J.M., and Leasure, S.C., (1977), J. Chem. Phys. 66, 288.

Brandt, M.A., and Truhlar, D.G., (1973), Chem. Phys. Lett. 23, 48.

Brink, D.M., and Satchler, G.R., (1975), Angular Momentum (Oxford : Clarendon).

Buck, U., Huisken, F., Schleusener, J., and Schafer, J., (1980), J. Chem. Phys. 72, 1512.

Bunker, D.L., (1971), Methods in Computational Physics 10, 287.

Burke, P.G., and Schey, H.M., (1962), Phys. Rev. 126, 147.

Calogero, F., (1967), Variable Phase Approach to Potential Scattering (New York : Academic).

Carney, G.D., and Porter, R.N., (1974), J. Chem. Phys. 60, 4251.

Chackerian, C., (1976), J. Chem. Phys. 65, 4228.

Chase, D.M., (1956), Physical Review 104, 838.

Cheung, A.S., and Wilson, D.J., (1969), J. Chem. Phys. 51, 3448.

Child, M.S., (1974), Molecular Collision Theory (Academic : London).

Chu, S.I., and Dalgarno, A., (1975a), Proceedings of The Royal Society, A342, 191.

Chu, S.I., and Dalgarno, A., (1975b), J. Chem. Phys. 63, 2115.

Clark, A.P., (1977), J. Phys. B : At. Mol. Phys. 10, L389.

Clark, A.P., Dickinson, A.S., and Richards, D., (1977), Advances in Chemical Physics 36, 63.

Collins, L.A., and Norcross, D.W., (1978), Physical Review A18, 467.

Csizmadia, I.G., Karl, R.E., Polanyi, J.C., Roach, A.C., and Robb, M.A., (1970), J. Chem. Phys. 52, 6205.

Dalgarno, A., (1975), Atomic and Molecular Processes in Astrophysics : Course at SAAS-FEE edited by M.C.E. Huber and H. Nussbaumer.

Dalgarno, A., and McCray, R.A., (1972), Ann. Rev. Astron. Ap. 10, 375.

Danby, G., (1983), J. Phys. B : At. Mol. Phys. 16, 3393.

Depristo, A.E., and Alexander, M.H., (1975), J. Chem. Phys. 63, 3552.

Depristo, A.E., and Alexander, M.H., (1976), J. Chem. Phys. 64, 3009.

Depristo, A.E., and Alexander, M.H., (1977), J. Chem. Phys. 66, 1334.

Dickinson, A.S., (1979), Comp. Phys. Comm. 17, 51.

Diercksen, G.H.F., and Kraemer, W.P., (1984), MUNICH Molecular Programme System, Reference Manuel, Special Technical Report, Max-Planck-Institut fur Physik und Astrophysik, Garching (to be published).

Drolshagen, G., and Gianturco, F.A., (1983), Mol. Phys. 48, 673.

Drolshagen, G., and Gianturco, F.A., (1984), Mol. Phys. 51, 185.

Ducuing, J., Joffin, C., and Coffinet, J.P., (1970), Opt. Commun. 2, 245.

Flower, D.R., (1983), NATO ASI "Diffuse Matter in Galaxies", (Dordrecht : Reidel).

Flower, D.R., and Kirkpatrick, D.J., (1982), J. Phys. B : At. Mol. Phys. 15, 1701.

Flower, D.R., and Launay, J.M., (1977), J. Phys. B : At. Mol. Phys. 10, 3673.

Flower, D.R., Launay, J.M., Kochanski, E., and Prissette, J., (1979), Chem. Phys. 37, 355.

Ford, K.W., and Wheeler, J.A., (1959), Annals of Physics 7, 259.

Gailitis, M., (1976), J. Phys. B : At. Mol. Phys. 9, 843.

Gautier, T.N., Fink, U., Treffers, R.P., and Larson, H.P., (1976), Astrophysical Journal Letters 207, L129.

Gerratt, J., and Roberts, L.J., (1983), to be published.

Gianturco, F.A., (1979), The Transfer of Molecular Energy by Collisions (Springer, Heidelburg).

Gianturco, F.A., Lamanna, U.T., and Petrella, G., (1982), Chem. Phys. 64, 299.

Giese, C.F., and Gentry, W.R., (1974), Physical Review A10, 2156.

Goldflam, R., Green, S., and Kouri, D.J., (1977), J. Chem. Phys. 67, 4149.

Goldflam, R., and Kouri, D.J., (1979), J. Chem. Phys., 70 5076.

Gordon, R.G., (1969), J. Chem. Phys. 51, 14.

Gordon, R.G., and Kim, Y.S., (1972), J. Chem. Phys. 56, 3122.

Gordon, M.D., and Secrest, D., (1970), J. Chem. Phys. 52, 120.

Green, S., (1974), J. Chem. Phys. 60, 2654.

Green, S., (1976), J. Chem. Phys. 65, 68.

Green, S., (1978), Chem. Phys. 41, 425.

Heil, T.G., Green, S., and Kouri, D.J., (1978), J. Chem. Phys. 68, 2562.

Heil, T.G., and Kouri, D.J., (1976), Chem. Phys. Lett. 40, 375.

Herzberg, G., (1950), Spectra of Diatomic Molecules (Princeton, N.J. : van Nostrand).

Hooker, W.J., and Millikan, R.C., (1963), J. Chem. Phys. 38, 214.

Hollenback, D.J., and Shull, J.M., (1977), Astrophysical Journal 216, 419.

Hulbert, H.M., and Hirschfelder, J.O., (1941), J. Chem. Phys. 9, 61.

Hunter, L.W., (1975), J. Chem. Phys. 62, 2855.

Jaquet, R., Kutzelnigg, W., and Staemmler, V., (1980), Theoret. Chim. Acta (Berl.), 54, 204.

Johnson, B.R., (1973), Journal of Computational Physics 13, 445.

Johnson, B.R., and Secrest, D., (1966), J. Math. Phys. 7, 2187.

Jolicard, G., and Billing, G.D., (1984), Chem. Phys. 85, 253.

Karl, G., Poll, J.D., and Wolniewicz, L., (1975), Can. J. Phys. 53, 1781.

Khare, J., (1977), J. Chem. Phys. 67, 3897.

Khare, J., (1978), J. Chem. Phys. 68, 4631.

Kinnersley, S.R., (1979), Mol. Phys. 38, 1329.

Kirkpatrick, D.J., (1983), Ph.D. Thesis, University of Durham.

Kolos, W., and Wolniewicz, L., (1965), J. Chem. Phys. 43, 2429.

Kolos, W., and Wolniewicz, L., (1975), J. Mol. Spectrosc. 54, 303.

Kouri, D.J., Heil, T.G., and Shimoni, Y., (1976), J. Chem. Phys. 65, 1462.

Kouri, D.J., and McGuire, P., (1974), Chem. Phys. Lett. 29, 414.

Kreek, H., and Le Roy, R.J., (1975), J. Chem. Phys. 63, 338.

Kreyzig, E., (1972), Advanced Engineering Mathematics (Wiley : New York).

Launay, J.M., (1976), J. Phys. B : At. Mol. Phys. 9, 1823.

Launay, J.M., (1977), J. Phys. B : At. Mol. Phys. 10, 3665.

Leavitt, R.P., (1980), J. Chem. Phys. 72, 3472.

Lester, W.A., (1968), J. Comp. Phys. 3, 322.

Light, J.C., (1971), Methods of Computational Physics, Vol. 10, edited by B. Alder, S. Fernbach, and M. Rotenburg (New York : Academic).

Light, J.C., and Walker, R.B., (1976), J. Chem. Phys. 65, 4272.

Liu, W.-K., Grabenstetter, J.E., Le Roy, R.J., and McCourt, F.R., (1978), J. Chem. Phys. 68, 5028.

Liu, W.-K., and McCourt, F.R., (1979), Chem. Phys. 37, 75.

Marcus, R.A., (1972), J. Chem. Phys. 56, 3548.

Maricq, M.M., Gregory, E.A., Wickham-Jones, G.J., Cartwright, D.J., and Simpson, C.J.S.M., (1983), Chem. Phys. 75, 347.

McCurdy, C.W., and Miller, W.H., (1977), J. Chem. Phys. 67, 463.

McGuire, P., (1976), J. Chem. Phys. 65, 3275.

McGuire, P., and Kouri, D.J., (1974), J. Chem. Phys. 60, 2488.

Meerts, W.L., de Leeuw, F.H., and Dymanus, A., (1977), Chem. Phys. 22, 319.

Messiah, A., (1962), Quantum Mechanics vol. 2 (Amsterdam : North-Holland).

Meyer, W., (1976), Chem. Phys. 17, 27.

Meyer, W., Hariharan, P.C., and Kutzel-Nigg, W., (1980), J. Chem. Phys. 73, 1880.

Mies, F.H., (1964), J. Chem. Phys. 40, 523.

Miller, D.J., and Millikan, R.C., (1970), J. Chem. Phys. 53, 3384.

Miller, W.H., (1971), J. Chem. Phys. 54, 5386.

Miller, W.H., (1974), Advances in Chemical Physics 25, 69.

Millikan, R.C., and Osburg, L.A., (1964), J. Chem. Phys. 41, 2196.

Mizushima, M., (1975), The Theory of Rotating Diatomic Molecules (New York : Wiley).

Mulder, F., Thomas, G.F., and Meath, W.J., (1980), Mol. Phys. 41, 249.

Nelson, G.I., and Roberts, R.E., (1973), Chem. Phys. 2, 445.

Ng, K-C., Meath, W.C., and Allnatt, A.R., (1979), Mol. Phys. 37, 237.

Pack, R.T., (1974), J. Chem. Phys. 60, 633.

Pack, R.T., (1977), J. Chem. Phys. 66, 1557.

Parker, G.A., and Pack, R.T., (1976), J. Chem. Phys. 64, 2010.

Parker, G.A., and Pack, R.T., (1978), J. Chem. Phys. 68, 1585.

Percival, I.C., and Seaton, M.J., (1957), Proceedings of the Cambridge Philosophical Society 53, 654.

Percival, I.C., and Richards, D., (1970), J. Phys. B : At. Mol. Phys. 3, 1035.

Pfeffer, G.A., and Secrest, D., (1977), J. Chem. Phys. 67, 1394.

Pfeffer, G.A., and Secrest, D., (1983), J. Chem. Phys. 78, 3052.

Polanyi, J.C., and Schreiber, J.L., (1974), Physical Chemistry, edited by H. Eyring, D. Henderson, and W. Jost (New York : Academic).

Poulsen, L.L., (1982), Chem. Phys. 68, 29.

Poulsen, L.L., and Billing, G.D., (1982), Chem. Phys. 73, 313.

Poulsen, L.L., and Billing, G.D., (1984), Chem. Phys. 89, 219.

Price, R.J., Clary, D.C., and Billing, G.D., (1983), Chem. Phys. Lett. 101, 269.

Prissette, J., Kochanski, E., and Flower, D.R., (1978), Chem. Phys. 27, 373.

Rabitz, H., (1972), J. Chem. Phys. 57, 1718.

Rabitz, H., (1976), Modern Theoretical Chemistry, Part A, edited by W.H. Miller (New York : Plenum).

Ramaswamy, R., Rabitz, H., and Green, S., (1977), J. Chem. Phys. 66, 3021.

Rose, M.E., (1957), Elementary Theory of Angular Momentum (New York : Wiley).

Sams, W.N., and Kouri, D.J., (1969), J. Chem. Phys. 51, 4815.

Schaefer, H.F., (1972), The Electronic Structure of Atoms and Molecules : A Survey of Rigorous Quantum Mechanical Results (Reading, Mass : Addison-Wesley).

Schinke, R., (1977), Chem. Phys. 24, 379.

Schinke, R., (1980), J. Chem. Phys. 72, 3916.

Schinke, R., Dupuis, M., and Lester, W.A., (1980), J. Chem. Phys. 72, 3090.

Schinke, R., and McGuire, P., (1978a), Chem. Phys. 28, 129.

Schinke, R., and McGuire, P., (1978b), Chem. Phys. 31, 391.

Schinke, R., Meyer, H., Buck, U., and Diercksen, G.H.F., (1984), J. Chem. Phys. 80, 5518.

Secrest, D., (1975), J. Chem. Phys. 62, 710.

Secrest, D., (1979), Atom-Molecule Collision Theory : A Guide for the Experimentalist, edited by R.B. Bernstein (New York : Plenum).

Secrest, D., and Johnson, B.R., (1966), J. Chem. Phys. 45, 4556.

Shafer, R., and Gordon, R.G., (1973), J. Chem. Phys. 58, 5422.

Sharma, R.D., and Kern, C.W., (1971), J. Chem. Phys. 55, 1171.

Simon, M., Richini-Cohen, G., Joyee, R.R., and Simon, T., (1979), Astrophysical Journal 230, L175.

Spitzer, L., and Cochran, W.D., (1973), Astrophysical Journal Letters 186, L23.

Starr, D.F., Hancock, J.K., and Green W.H., (1974), J. Chem. Phys. 61, 5421.

Stechel, E.B., Walker, R.B., and Light, J.C., (1978), J. Chem. Phys. 69, 3518.

Stephenson, J.C., and Mosburg, J., (1974), J. Chem. Phys. 60, 3562,

Takayanagi , K., (1965), Adv. Atom. Mol. Phys. 1, 149.

Tarr, S.M., Rabitz, H., Fitz, D.E., and Marcus, R.A., (1977), J. Chem. Phys. 66, 2854.

Truhlar, D.G., (1972), Intern. J. Quantum. Chem. 6, 975.

Tipping, R.H., (1976), J. Mol. Spectrosc. 61, 272.

Toennies, J.P., (1976), Annual Review of Physical Chemistry 27, 225.

Tsien, T.P., and Pack, R.T., (1970), Chem. Phys. Lett. 6, 54.

Tsien, T.P., Parker, G.A., and Pack, R.T., (1973), J. Chem. Phys. 59, 5373.

Udseth, M., Giese, C.F., and Gentry, W.R., (1973), Physical Review A8, 2483.

van der Avoird, A., Wormer, P.E.S., and Berns, R.M., (1980), Topics in Chemistry edited by R. Zahradnik (Springer, Berlin).

van Hemert, M.C., (1981), Proceedings of the Fourteenth Jerusalem symposium in Quantum Chemistry and Biochemistry (Dordrecht : Reidel).

van Hemert, M.C., (1983), J. Chem. Phys. 78, 2345.

Watson, W.D., (1974), Atomic and Molecular Processes and the Interstellar Medium : Courses at Les Houches, edited by R. Balian, P. Encrenaz, and J. Lequeux (Amsterdam : North Holland).

Weast, R.C., (1975), Handbook of Chemistry and Physics, 56th edition.

Weisback, M.F., and Chackerian, C., (1973), J. Chem. Phys. 59, 4272.

Zarur, G., and Rabitz, H., (1973), J. Chem. Phys. 59, 943.

Zarur, G., and Rabitz, H., (1974), J. Chem. Phys. 60, 2057.

APPENDIX 1

This appendix contains the derivation and the solution of the differential equations for the asymptotic series expansions A(R) and B(R), i.e.,

$$A''(R) - 2B(R)\frac{L(L+1)}{R^3} - 2B'(R)\left(k^2 - \frac{L(L+1)}{R^2}\right) = \frac{2\mu}{\hbar^2}\frac{v_n}{R^n}A(R) \qquad \text{A1.1}$$

$$B''(R) + 2A'(R) = \frac{2\mu}{\hbar^2}\frac{v_n}{R^n}B(R) . \qquad \text{A1.2}$$

We will consider a system whose potential surface involves long range terms of the form R^{-n}, where $n \geq 3$. In the IOS approximation the asymptotic form of the coupled differential equations takes the form, if we retain the first two leading long range terms of the interaction potential (cf. III.4.30).

$$\left(\frac{d^2}{dR^2} - \frac{L(L+1)}{R^2} + k^2_{v_2'} - \frac{2\mu}{\hbar^2}\left[\frac{v_n}{R^n} + \frac{v_{n+1}}{R^{n+1}}\right]\right) G^{Lv_2}_{v_2'}(R) = 0 \qquad \text{A1.3}$$

This equation must be solved, the solution will be in terms of the asymptotic series expansions A(R) and B(R). To achieve this we first consider the asymptotic form of the coupled equations, if no interaction potential terms are retained. (cf. III.4.26).

$$\left(\frac{d^2}{dR^2} - \frac{L(L+1)}{R^2} + k^2_{v_2'}\right) f^{Lv_2}_{v_2'}(R) = 0 \qquad \text{A1.4}$$

This equation is the Riccati-Bessel equation (Abramowitz and Stegun(1965)), which has real linearly independent solutions which may be written

$$\bar{j}_L = R k_{v_2'} j_L(k_{v_2'} R) \qquad \bar{n}_L = R k_{v_2'} n_L(k_{v_2'} R) .$$

Rewriting A1.3 and A1.4 in matrix notation, we have

$$G'' + uG = 0 \qquad \text{A1.5a}$$

$$f'' + wf = 0 . \qquad \text{A1.5b}$$

We write the solution of A1.5a (or A1.3) in terms of the solutions of A1.5b (or A1.4).

So $G = Af + Bf'$

Then $G'' + uG = Pf + Qf'$

Whence $P = A'' + uA - Aw - Bw' - 2Bw$

$Q = B'' + uB - Bw + 2A$

Put $P = Q = 0$

Also put $u = w + v$

Then $A'' + wA - Aw + vA - Bw - 2Bw = 0$

$B'' + wB - Bw + vB + 2A' = 0$

As $R \to \infty$, $A \to 1$ and $B \to 0$

Therefore put $A = 1 + a$, and $B = b$

We then find

$$a'' + wa - aw - bw' - 2bw = -v(1+a) \qquad \text{A1.6a}$$

$$b'' + wb - bw + 2a = -vb \qquad \text{A1.6b}$$

At large enough R the equations are uncoupled, so we may write (cf. III.4.33a,b)

$$a'' - bw' - 2bw = -V(1+a) \qquad \text{A1.7a}$$

$$b'' + 2a = -Vb. \qquad \text{A1.7b}$$

Put $w = \mathcal{E} - \frac{C}{R^2} \quad \therefore w' = \frac{2C}{R^3}$ A1.8a

$$V = D/R^n + E/R^{n+1} \qquad \text{A1.8b}$$

$$a = \sum_{m=0}^{\infty} \alpha_m R^{-m-p} \quad p \geq 1 \qquad \text{A1.8c}$$

and $$b = \sum_{m=0}^{\infty} \beta_m R^{-m-q} \quad q \geq 1. \qquad \text{A1.8d}$$

Substituting A1.8a,b,c,d, into A1.7a,b we find

$$\sum_{m=0}^{\infty} [\alpha_m (m+p)(m+p+1) R^{-m-p-2} - 2C\beta_m R^{-m-q-3} + 2\mathcal{E}\beta_m (m+q) R^{-m-q-1} - 2C\beta_m (m+q) R^{-m-q-3}]$$
$$= -DR^{-n} - ER^{-n-1} - \sum_{m=0}^{\infty} [D\alpha_m R^{-m-p-n} + E\alpha_m R^{-m-p-n-1}] \qquad \text{A1.9a}$$

$$\sum_{m=0}^{\infty} [\beta_m (m+q)(m+q+1) R^{-m-q-2} - 2\alpha_m (m+p) R^{-m-p-1}]$$
$$= \sum_{m=0}^{\infty} [D\beta_m R^{-m-q-n} + E\beta_m R^{-m-q-n-1}]. \qquad \text{A1.9b}$$

Considering leading terms in A1.9a

By definition $\alpha_0 \neq 0, \beta_0 \neq 0$ hence

$$p = q + 1$$

Considering leading terms in A1.9b

$$q = n-1$$

$$\therefore q = n-1 \text{ and } p = n$$

from A1.9b $\quad \beta_0 q(q+1) = 2\alpha_0 p$

from 1.9a $\quad 2\varepsilon\beta q = -D$

$$\therefore \beta_0 = -D/2\varepsilon(n-1) \text{ and } \alpha_0 = -D/4\varepsilon$$

Rewriting A1.9a

$$\sum_{m=0}^{\infty} [\alpha_m (m+n)(m+n+1) r^{-m-n-2} - 2C\beta_m r^{-m-n-2} + 2\varepsilon\beta_m (m+n-1) r^{-m-n} - 2\beta_m (m+n+1) r^{-m-n-2}] = -Dr^{-n} - Er^{-n-1} - \sum_{m=0}^{\infty} [D\alpha_m r^{-m-2n} + E\alpha_m r^{-m-2n-1}]$$

A1.10a

Rewriting A1.9b

$$\sum_{m=0}^{\infty} [\beta_m (m+n-1)(m+n) r^{-m-n-1} - 2\alpha_m (m+n) r^{-m-n-1}] = \sum_{m=0}^{\infty} [D\beta_m r^{-m-2n+1} + E\beta_m r^{-m-2n}]$$

A1.10b

Consider A1.10a with m = 1

$$\beta_1 = -E/2n\varepsilon$$

If we only retain the leading long range term

$$\beta_1 = 0$$

Also one can easily verify that

$$\alpha_0 n(n+1) - 2C\beta_0 - 2C\beta_0(n-1) + 2E\beta_2(n+1) = 0$$

$$\therefore \alpha_0 n(n+1) - 2Cn\beta_0 + 2E\beta_2(n+1) = 0$$

$$\therefore \beta_2 = nD/8E^2 - nCD/2(n^2-1)E^2$$

Consider A.10b and m = n - 2 (≥ 1) on LHS:

$$\beta_{n-2}(2n-2)(2n-3) - 2\alpha_{n-2}(2n-2) = 0$$

A1.11a

From A1.10a

$$\alpha_{n-2}(2n-2)(2n-1) - 2C\beta_{n-2}$$

$$+ 2E\beta_n(2n-1) - 2\beta_{n-2}(2n-3) = -D\alpha_0$$

A1.11b

A1.11a relates β_{n-2} and α_{n-2}

then A1.11b relates β_{n-2} and β_n

e.g. if n = 3, A1.11a enables α_1 to be determined from β_1, A1.11b enables β_3 to be determined from β_1 or if n = 4, A1.11a relates α_2 to β_2 and A1.11b relates β_4 to β_2

From A1.10a:

$$\alpha_{n-1}(2n-1)2n - 2C\beta_{n-1} + 2E\beta_{n+1}2n$$

$$- 2C\beta_{n-1}(2n-2) = -D\alpha_1 - E\alpha_0$$

A1.12a

From A1.10b:

$$\beta_{n-1}(2n-1)(2n-2) - 2\alpha_{n-1}(2n-1)$$

$$= -D\beta_1 - E\beta_0$$

A1.12b

A1.12a relates β_{n-1} and α_{n-1}

A1.12b relates β_{n+1} and β_{n-1}

e.g. if n = 3, A.12a relates α_2 and β_2, A1.12b relates β_4 and β_2

or if n = 4, A1.12a relates α_3 and β_3, A1.12b relates β_5 and β_3

Proceeding this way it is trivial to show that the following recursion relations are valid.

From A1.9a:

$$\alpha_{m+n-1}(m+2n-1)(m-2n) - 2C\beta_{m+n-1} + 2\mathcal{E}\beta_{m+n+1}(m+2n) - 2C\beta_{m+n-1}(m+2n-2) = -D\alpha_{m+1} - \mathcal{E}\alpha_m$$

A1.13a

From A1.9b:

$$\beta_{m+n-1}(m+2n-2)(m+2n-1) - 2\alpha_{m+n-1}(m+2n-1) = -D\beta_{m+1} - \mathcal{E}\beta_m$$

A1.13b

Defining M = m + n + 1

Identifying the terms $\mathcal{E}$ and C

$$\mathcal{E} = k^2 \qquad C = L(L+1)$$

and retaining only the leading long-range term i.e.

$$V = \frac{D}{R^n} \qquad \therefore \; D = -\frac{2\mu v_n}{\hbar^2}$$

we then obtain III.4.35a,b given in Chapter III.

$$\alpha_{M-2}(M+n-2)(M+n-1) - 2L(L+1)\beta_{M-2}(M+n-2) + 2k^2\beta_m(M+n-1) = 2\mu\nu_n\alpha_{M-n}$$

A1.14a

$$\beta_{M-1}(M+n-2)(M+n-1) - 2\alpha_{M-1}(M+n-1) = 2\mu\nu_n\beta_{M-n-1}$$

A1.14b

In conclusion we may express the solutions of A1.4 in terms of the solutions of A1.3,

$$G = Af + Bf',$$

A1.15

where A, and B are the asymptotic series expansions, and where f is either a Riccati Bessel function of the first or second kind. For example we have the asymptotic series expansions suggested by Gailitis (1976) (cf. III.4.32).

$$\left.\begin{matrix} F(R) \\ G(R) \end{matrix}\right\} = A(R)\left\{\begin{matrix} \bar{J}_L(kR) \\ \bar{n}_L(kR) \end{matrix}\right. + B(R)\left\{\begin{matrix} \bar{J}_L'(kR) \\ \bar{n}_L'(kR) \end{matrix}\right.$$

1.16

APPENDIX 2

This Appendix contains the numerical values of the expansion coefficients, $C_{v_2 i}$ (for $v_2 = 0,6$ and $i = 0, 16$), used in the calculation of the exact Morse oscillator wavefunctions used to describe the vibrational motion of the H_2 molecule in Chapter IV.

$C_{o,i}$ (i = 0,16)	$C_{2,i}$	$C_{4,i}$	$C_{6,i}$
0.9997362659260878D+00	0.1583394438966868D-01	0.6139510526205319D-02	0.2656036581540127D-02
0.1163218693121566D-01	-0.2465783719718825D-01	-0.1830786721672439D-01	-0.8537723010813653D-02
-0.1632711228085332D-01	0.9971404974587301D+00	0.4224669726391785D-01	0.1908441486170880D-01
0.9283606618763404D-02	0.4206160538054243D-01	-0.4359423771157980D-01	-0.3650280869372990D-01
-0.5229886944491531D-02	-0.4473017090904967D-01	0.9915532665926276D+00	0.6409266634765765D-01
0.2907687528153847D-02	0.2612323842033691D-01	0.6239920152055471D-01	-0.4590420180413627D-01
-0.1588149946864447D-02	-0.1564508459341225D-01	-0.7274697264143608D-01	0.9846129028956927D+00
0.8536796589344147D-03	0.9692992486130009D-02	0.4590169716696057D-01	0.7266262675976153D-01
-0.4510430173196355D-03	-0.6070681274156869D-02	-0.2849062332945778D-01	-0.9376096688198474D-01
0.2322546831118869D-03	0.3811072950367039D-02	0.1858098759581483D-01	0.6744228818575272D-01
-0.1140924988625315D-03	-0.2397763771402680D-02	-0.1261763527967854D-01	-0.4495402499347936D-01
0.5081634879187702D-04	0.1515009501173017D-02	0.8790553884305009D-02	0.3061398134166133D-01
-0.1753718589466921D-04	-0.9634213884747982D-03	-0.6228036955740254D-02	-0.2161033119590476D-01
0.7167918984570172D-06	0.6180273146541215D-03	0.4469823615511506D-02	0.1570867081513149D-01
0.7037768472831804D-05	-0.4012297399472557D-03	-0.3246632276837806D-02	-0.1167115778381858D-01
-0.9699178545446063D-05	0.2637950492856752D-03	0.2373058080181617D-02	0.8765171643826593D-02
0.9248750177871242D-05	-0.1723811957363586D-03	-0.1694602090865761D-02	-0.6435607894539396D-02

$C_{1,i}$	$C_{3,i}$	$C_{5,i}$
-0.1076072984960761D-01	-0.9627100372992155D-02	-0.3994709109965141D-02
0.9988808379359903D+00	0.2910182401121057D-01	0.1232238151078549D-01
0.2734088298782636D-01	-0.3619791607518377D-01	-0.2742002141676815D-01
-0.3022287969969510D-01	0.9946129415004488D+00	0.5425362323932358D-01
0.1736006252188273D-01	0.5392760760226234D-01	-0.4656029217135045D-01
-0.1017369502557340D-01	-0.5919211071411326D-01	0.9881855455167308D+00
0.6030032488202816D-02	0.3564813813521364D-01	0.6804600950033184D-01
-0.3553442099165638D-02	-0.2169235427781568D-01	-0.8451026675886565D-01
0.2076457976005364D-02	0.1384565351485792D-01	0.5666162677421834D-01
-0.1204455556190046D-02	-0.9087396045196334D-02	-0.3623867277526656D-01
0.6933608302287959D-03	0.6053435380237954D-02	0.2411431619547445D-01
-0.3949578918369641D-03	-0.4076057226244762D-02	-0.1675951120247155D-01
0.2212555516904443D-03	0.2773827991300784D-02	0.1201165071656047D-01
-0.1207259551616376D-03	-0.1909993637775437D-02	-0.8782113021898967D-02
0.6332075718785274D-04	0.1333148841191492D-02	0.6513946594888396D-02
-0.3144506713019350D-04	-0.9400624918006351D-03	-0.4860002003062503D-02
0.1465358296596359D-04	0.6519347029409505D-03	0.3534265945308499D-02

APPENDIX 3

This appendix contains the details of the calculation of the Morse oscillator wavefunctions used to describe the vibrational motion of the CO molecule in Chapters V, VI and VII.

The vibrational motion of the CO molecule is approximated by Morse oscillator wavefunctions in the majority of our calculations studying the rovibrational excitation of CO (harmonic oscillator wavefunctions are employed in our BS calculations in Chapter V). The normalised Morse eigenfunctions and eigenvalues are given by (see Chapter IV.3 for details and definitions)

$$\psi^{MO}_{v_2}(r_2) = A_{v_2}\, y^{-1/2}\, W_{\Sigma/2,\,\Sigma/2-1/2-v_2}(y), \qquad \text{A3.1}$$

$$\mathcal{E}^{MO}_{v_2} = \frac{4D}{\Sigma}\left\{\left(v_2+\frac{1}{2}\right) - \frac{1}{\Sigma}\left(v_2+\frac{1}{2}\right)^2\right\}, \qquad \text{A3.2}$$

where $y = \Sigma\, e^{-\phi(r_2 - r_{2,eq})}$, $A^2_{v_2} = \dfrac{(\Sigma - 1 - 2v_2)\,\phi}{v_2!\,\Gamma(\Sigma - v_2)}$,

$\Sigma^2 = \dfrac{8\mu_{CO} D}{\phi^2}$, $D = \dfrac{\hbar\omega}{4}\Sigma$, and $r_{2,eq} = 2.132$ a.u.

Σ and $\hbar\omega$ are taken from Mies (1964):-

Σ = 261.22 (dimensionless)

$\hbar\omega$ = 0.26898 eV

μ_{CO} is the reduced mass of CO, and takes the value

μ_{CO} = 12499.6 a.u.

Using these parameters the remaining parameters D, and ϕ

are found to be D = 0.64556 a.u.

$$\phi = 0.9726472 \text{ a.u.}$$

As mentioned in Chapter V.3, ϕ is quoted to so many figures to ensure that the parameters in $\psi^{Mo}_{v_2}$ are self-consistent, and maintain the orthonormality of the wavefunctions. For CO this is extremely important since we must deal with very large and very small numbers

$$\Gamma(\mathcal{E}) \sim 10^{500} \quad , \quad \exp\left(-\tfrac{1}{2}\mathcal{E}\, e^{-(r_2 - r_{2,eq})}\right).$$

The calculation of CO Morse wavefunctions is therefore rather less straightforward than for example, the calculation of H_2 Morse wavefunction, for which $\Gamma(\mathcal{E})$ is large ($\sim 10^{38}$), but can nevertheless be handled by a computer. The Whittaker function, $W_{\mathcal{E}/2,\, \mathcal{E}/2 - 1/2 - v_2}(y)$, can be written in terms of a generalised Leguerre polynomial (Chapter IV).

$$W_{\mathcal{E}/2,\, \mathcal{E}/2 - 1/2 - v_2}(y) = e^{-\frac{1}{2}y}\, y^{\mathcal{E}/2 - v_2}\, (-1)^{v_2}\, v_2!\, L^{\mathcal{E}-2v_2-1}_{v_2}(y)$$

So the normalization actually used is

$$N_{v_2} = A_{v_2}\, v_2! \, .$$

Hence $N^2_{v_2} = (\mathcal{E} - 1 - 2v_2)\, \phi\, v_2! / \Gamma(\mathcal{E} - v_2)$,

the normalization coefficients, $N^2_{v_2}$ are evaluated recursively employing

$$N^2_{v_2+1} = \frac{(\mathcal{E} - 1 - 2(v_2+1))\,(v_2+1)\,(\mathcal{E} - (v_2+1))\, N^2_{v_2}}{(\mathcal{E} + 1 - 2(v_2+1))} \, ,$$

starting with $N_0^2 = \dfrac{\phi}{\Gamma(\mathcal{E}-1)}$.

However, as one will recall it is not possible to evaluate N_0^2 in one step due to the large value of $\Gamma(\mathcal{E}-1)$, nevertheless the calculation of the wavefunctions can be

made relatively simple by taking judicial combinations of large and small numbers.

The wavefunctions are calculated once in a scattering calculation, during the initialization of the potential. Their calculation is shared between two routines, LAGR which is called once at each value of r_2, and evaluates

$$A(y) = v_2! L_{v_2}^{\varepsilon-2v_2-1}(y) y^{\frac{\varepsilon-1}{2}} e^{-y/4} \qquad \text{A3.3}$$

for all the vibrational states considered in the scattering calculations starting with $N_o^2 = \frac{\phi}{\Gamma(\varepsilon-1)}$, and WFN which is called for each combination of v_2 and v_2' to evaluate the potential matrix elements. WFN evaluates

$$B(y) = \psi_{v_2}^{Mo} = A(y) \times \frac{e^{-y/4}(-1)^{v_2}}{y^{v_2}}. \qquad \text{A3.4}$$

Notice that A3.3 involves $e^{-y/4}$ with is manageable using the computer (while $e^{-y/2}$ is not).

The numerical value of $N_o = \frac{(1943.3674\ 10^{-18})^{\frac{1}{2}}}{10^{250}}$.

LAGR evaluates A(y) in the following manner:-

1. The quantity $P = e^{-y/4}$ is calculated.
2. A do loop is entered and the following calculation is performed ten times,
   $$P = \left(\frac{y^{[(\varepsilon-1)/20]}}{10^{25}}\right) \times P$$
3. The do loop is left.
4. LAGR evaluates $N_o = P \times (1943.3674\ 10^{-18})^{\frac{1}{2}}$.
5. LAGR then calculates A(y) for each value of $v_2(v_2')$ needed.

Although no more than three open vibrational channels are required in any of our calculations, however so that the CO molecule is properly described it is necessary to include closed vibrational channels. When these studies were begun we did not know how many channels would have to be included in the coupled equations to obtain satisfactory results. Therefore, so that the convergence of the results as a function of the size of the vibrational basis could be properly tested, we included the first six ($v_2 \leq 5$) Morse wavefunctions in our preliminary calculations studying the evaluation of the potential matrix elements (Chapter V.4.1). Some of our CO Morse oscillator wavefunctions are shown in Figure 1. Qualitatively they appear satisfactory, we mention that using our technique of evaluating N_o, outlined above, we were able to reproduce the MOEX wavefunctions employed in our $H_2 + H^+$ calculations.

In Table 1 we show the values of the overlap integral, I, for $v_2(v_2') \leq 5$, where I is given by

$$I = \int_0^\infty \psi^{MO}_{v_2}(r_2)\, \psi^{MO}_{v_2'}(r_2)\, dr_2 = \delta_{v_2 v_2'} . \qquad \text{A3.5}$$

A3.5 was evaluated using a 96-point Gauss Legendre quadrature in the range, $1.4 \leq r_2 \leq 2.8$ a.u. As expected orthonormality deteriorates with v_2' since we evaluate the integral numerically. It is worth mentioning that in Chapter V.4.1 we show that the values of the potential

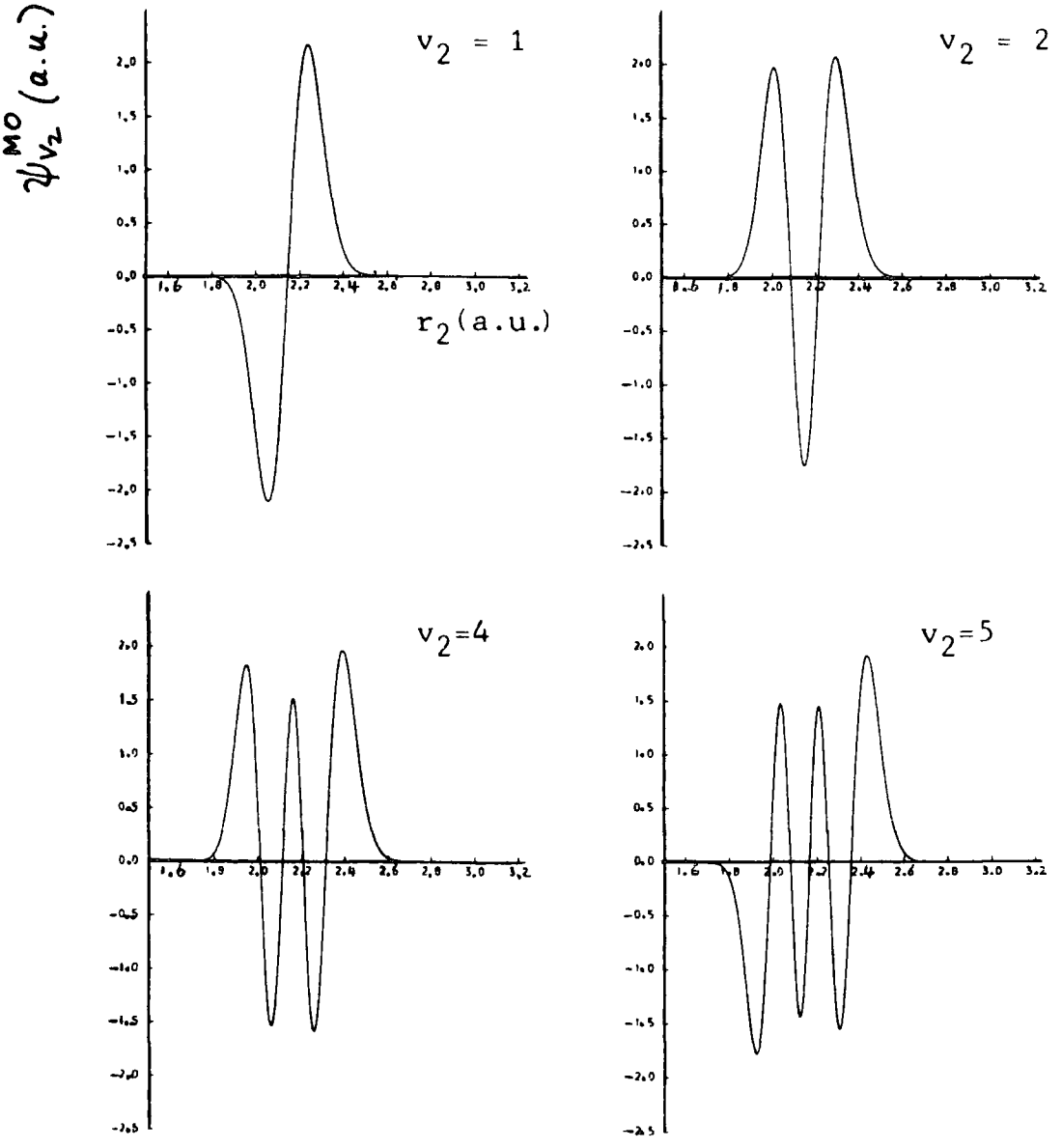

Figure 1. CO Morse oscillator wavefunctions.

TABLE 1

Values of the overlap integral, $I(v_2, v_2') = \int_0^\infty \psi^{MO}_{v_2} \psi^{MO}_{v_2'} dr_2$, for $v_2(v_2') \leq 5$.

v_2' \ v_2	0	1	2	3	4	5
0	1.0					
1	0.1408(-15)	1.0				
2	-0.3058(-14)	0.6277(-14)	1.0			
3	-0.1214(-13)	-0.1354(-12)	-0.3205(-13)	1.0		
4	0.1689(-11)	-0.9326(-12)	-0.6397(-12)	0.3891(-12)	1.0	
5	-0.2567(-11)	-0.2101(-10)	-0.2051(-10)	0.1259(-11)	0.1022(-10)	1.0

Numbers in brackets are powers of 10.

matrix elements are insensitive to changes of $\pm$ 0.2 a.u. in the values of the integration limits. In view of the results presented in Figure 1 and Table 1 we claim that our CO Morse wavefunctions are satisfactory.

APPENDIX 4

In this appendix we will discuss the effect of the error in our P potential routine on the H_2 + CO results presented in Chapter VI. In addition we will compare our calculations with the cross sections evaluated by BSD2 in a calculation employing the P potential.

N.B. BSD2 = Bačić, Schinke, and Diercksen (1984b).

As discussed in Chapter VI.2, there is an error in the long range multipole interactions given in the paper of Poulsen (1982). These interactions are given by (cf.VI.2.3).

$$\tilde{V}_{Q\mu} = -4\pi(15)^{-1/2} Q^{HH} \mu^{CO} R^{-4} (6 Y_{20}(\cos\theta_1) Y_{10}(\cos\theta_2)) \quad \text{A4.1a}$$

$$\tilde{V}_{QQ} = 4\pi(5)^{-1} Q^{HH} Q^{CO} R^{-5} (12 Y_{20}(\cos\theta_1) Y_{20}(\cos\theta_2)) \quad \text{A4.1b}$$

$$\tilde{V}_{Q_4\mu} = -4\pi(27)^{-1/2} Q_4^{HH} \mu^{CO} R^{-6} (10 Y_{40}(\cos\theta_1) Y_{10}(\cos\theta_2)) \quad \text{A4.1c}$$

$$\tilde{V}_{Q_4Q} = 4\pi(45)^{-1/2} Q_4^{HH} Q^{CO} R^{-7} (30 Y_{40}(\cos\theta_1) Y_{20}(\cos\theta_2)) \quad \text{A4.1d}$$

where Q^{HH} and Q_4^{HH} are the quadrupole and hexadecapole moments of the H_2 molecule respectively, and μ^{CO} and Q^{CO} are the dipole and quadrupole moment of the CO molecule respectively. However, the interactions given by A4.1 are a factor of 2 too large. This error was detected by BSD2, but was present in our potential routine.

We have since corrected this error in our computer programme, and have repeated the scattering calculation at an initial kinetic energy of E_T = 208 cm^{-1}. The results of these calculations for the 'V-T' process in which $j_1 = j_1' = 2$, and the near-resonance process are shown in Table 1 together with the results of our original calculations at this energy. It may be seen

	$\sigma(1j_1 \rightarrow 0j_1')$ $j_1 = j_1' = 2$	$j_1 = 2$ $j_1' = 6$
Original calculation	0.914(-6)	0.503(-4)
Calculation employing the corrected form of the multipolar interactions.	0.861(-6)	0.124(-4)
Calculation employing the H_2 rotational eigenergies of BSD2	0.861(-6)	0.214(-4)
BSD2	0.736(-6)	0.225(-4)

Table 1 Cross sections (in Å^2) for the 'V - T' process in which $j_1 = j_1' = 2$, and the near-resonance process in which $j_1 = 2$ and $j_1' = 6$. The initial kinetic energy is $E_T = 208\ \text{cm}^{-1}$. Numbers in brackets are powers of 10.

that whilst the value of the $\Delta j_1 = 0$ cross section is changed by only a few percent, the near-resonance cross section has been decreased by a factor of roughly 2^2. Poulsen and Billing (1982) conclude that the near-resonance process is primarily determined by the interaction between the hexadecapole moment of H_2 and the derivatives (with respect to r_2) of the dipole (and quadrupole) moment of CO, and this has been confirmed by BSD2. In the light of this fact, the above discrepancy is not particularly surprising. It follows that the comparison with the measurements of the vibrational relaxation of CO in para-H_2 (Andrews and Simpson (1976)) shown in Figure 3 of Chapter VI.4 will be less satisfactory.

BSD2 are primarily interested in the DK potential, however they have performed a number of calculations employing the P potential. Also shown in Table 1 are the results of BSD2 for the $\Delta j_1 = 0$ ($j_i = 2$), and near-resonance cross sections at $E_T = 208$ cm^{-1}, the agreement in the values of the 'V-T' cross sections shown in Table 1 is satisfactory, particularly in view of the differences in the rotational basis sets. In our own calculations only the $j_1 = 2$ and $j_1 = 6$ rotational states of the H_2 molecule are included, whereas BSD2 also include the states, $j_1 = 0$ and 4. As can be seen the discrepancy in the near-resonance cross section is roughly a factor of 2.

In their study, BSD2 employed the simple expression $\varepsilon_{j_1} = B j_1 (j_1+1)$ with B = 60.7 cm^{-1}, to calculate the values of the rotational energies of the H_2 molecule. This expression becomes progressively inaccurate, as j_1 increases. Consequently BSD2 find that the near-resonance process is endothermic by 43.3 cm^{-1} in their calculations, as comapred with an exothermicity of 87.03 cm^{-1} in our own calculations and of 83.3 cm^{-1} in the calculation of Poulsen and Billing (1982). It follows that the near-resonance process is artifically nearer to resonance in the calculation of BSD2, and hence they overestimate the magnitude of the near-resonance cross section in all their calculations employing the P or DK potentials.

In Table 1, we also give cross sections calculated using the same H_2 rotational eigenenergies as BSD2. Good agreement is found between the near-resonance cross sections. As already mentioned in this Appendix we neglect the j_1 = 0 and 4 rotational levels of H_2 in our calculations. The results shown in Table 1 show that our model calculation involving just the directly relevant channels j_1 =2 and 6 is sufficient to give a reasonable determination of the near-resonance process (at least at this energy). This is discussed in greater detail in Chapter VI.4.

Also presented in Chapter VI are cross sections for the process Δj_1 = 2. The importance of such transitions

was pointed out to us by Schinke (private communication), and is demonstrated by BSD2. The results for $\Delta j_1 = 2$ presented in Chapter VI.4 were evaluated using the erroneous potential, however our results for this rotational transition are in quantitative agreement with the results evaluated by BSD2 using the correct P potential. We therefore, believe that the error in the $\Delta j_1 = 2$ cross sections is similar to that in the corresponding $\Delta j_1 = 0$ cross section.

APPENDIX 5

In this appendix we examine the effects of the errors in our P potential routine (see Chapter VI) on the results for the HD + CO system. Due to the large amount of computer time required for these calculations, it was not possible to recalculate the integral cross sections at any of the energies studied. Instead we have evaluated cross sections at two partial waves using both the corrected and erroneous P potentials. The results of these calculations are shown in Table 1 for E = 1.03 $\hbar\omega$ and L = 0,10. All four calculations are performed by evaluating the interaction potential using the transformation VII.2.4 at each value of R in the integration range, $3.0 \lesssim R \lesssim 35$ a.u. Six rotational channels were retained in the calculations, as was done in our production calculations, however we could only afford to retain two vibrational channels in the coupled equations. In Chapter VII.3 we show that all the open and one closed vibrational channel must be retained to describe the CO molecule correctly, however at E = 1.03 $\hbar\omega$ we doubt that the omission of $v_2 = 2$ is particularly serious. The coupled equations were solved at sixteen Gauss Legendre orientations. Cross sections are shown both for the individual rotational transitions, $v_2 = 1 j_1$ to $v_2' = 0 j_1'$, and the rotationally summed (vibrational) process, $\sigma^{J}_{j_1}(v_2 = 1 \rightarrow v_2' = 0)$

$$\sigma^{J}_{j_1}(v_2 = 1 \rightarrow v_2' = 0) = \sum_{j_1'=0}^{5} \sigma^{J}(v_2 = 1 j_1 \rightarrow v_2' = 0 j_1') \qquad \text{A5.1}$$

TABLE 1

A comparison of results obtained for the HD + CO system at E = 1.03 $\hbar\omega$ and L = 0, and 10.

(a) Interaction potential as given by Poulsen (1982).
(b) Using corrected form of the multipolar interactions.

$\sigma^L(v_2 = 1 j_1 = 0 \rightarrow v_2' = 0 j_1')$ Å^2

L =		0	10
j_1' = 0	(a)	0.12729669-9	0.59519616-10
	(b)	0.70139206-11	0.53321374-10
1		0.27855396-9	0.16454552-8
		0.22493702-9	0.12308612-8
2		0.23209391-9	0.13000787-8
		0.79410652-10	0.76231700-9
3		0.26621255-9	0.10365287-8
		0.52604018-10	0.46122836-9
4		0.11499915-9	0.12751663-9
		0.32152667-10	0.12222946-9
5		0.52859194-9	0.29590703-8
		0.58877245-10	0.28626125-9

$\sigma^L_{j_1=0}(v_2 = 1 \rightarrow v_2' = 0) = \sum_{j_1'=0}^{5} \sigma^L(v_2 = 1 j_1 = 0 \rightarrow v_2' = 0 j_1')$

	(a)	0.15477482-8	0.71281691-8
	(b)	0.45499552-9	0.29162186-8

where $j_1 = 0$ only (at E = 1.03 eV the $v_2 = 1\, j_1 = 1$ channel is closed).

As can be seen the results obtained using the corrected potential are lower than the results evaluated using the original potential (as given in the paper of Poulsen (1982)). For some transitions the results are significantly changed (e.g. $j_1 = 0$ to $j_1' = 0$ at L = 0), while other cross sections are changed by only a few per cent (e.g. $j_1 = 0$ to $j_1' = 1$ at L= 0, 10). The rotational energy levels of HD are closely spaced, and strongly coupled by the potential. As we claim in Chapter VII.3 it is possible that the long range (multipolar) interactions cause flux to be transferred from one rotational channel to another, thus making it extremely difficult to accurately determine the cross sections for the individual rotational transitions. This would appear to be a reasonable explanation for the sensitivity of the results upon the form of the long range interactions. In Chapter VII.3 we invoke the same argument is a slightly different context, we find that it is extremely difficult to converge the results for the individual rotational transitions (i.e., we cannot obtain consistent values for $|S_L(v_2 = 1 j_1 \Omega_1 , v_2' = 0 j_1' \Omega_1 / \Theta_2)|^2$ evaluated at R'_{max} = 25.0, 30.0 and 35.0 a.u.), however when we sum the results over the final rotational states, if

$$S^{\Omega_1}_{j_1}(v_2 = 1 \rightarrow v_2' = 0) = \sum_{j_1' \neq 0}^{5} |S_L(v_2 = 1 j_1 \Omega_1, v_2' = 0 j_1' \Omega_1 / \Theta_2)|^2$$

A5.2

we do find reasonable agreement between the values of $S^{2J}_{L_{j_0}}(v_2=1 \to v_2'=0)$ evaluated at the above values of R'_{max}.

We consider this acceptable, since at these values of R'_{max} it is unlikely that the HD can affect the vibrational state of the CO (i.e., at these distances vibrational excitation should not be important). Thus we are rather surprised that the errors in the P potential have had such a significant effect upon the rotationally summed partial cross sections, $\sigma^{L}_{j_0}(v_2=1 \to v_2'=0)$. We have only studied two values of L, and from that point of view our results are inconclusive, however it appears that the results presented in Chapter VII have been seriously affected by the errors in the P potential. One will recall that the cross sections for the near-resonance process studied in our H_2 + CO calculations were overestimated by a factor of ~ 4, however the $\Delta j_1 = 0$ and 2 cross sections were changed by only a few per cent by the errors in our potential routine (Appendix 4). One can easily verify that none of the transitions studies in these calculations are near-resonance, and consequently we are very puzzled by the dependence of the cross sections, $\sigma^{L}_{j_0}(v_2=1 \to v_2'=0)$, on the form of the multipolar interactions.

As is discussed in Chapter VII.3, we are reasonably sure that the transformation VII.2.4 is sufficiently accurate to study vibrational excitation, and we are

therefore, unable to provide a satisfactory explanation for the results presented in this appendix. In particular the agreement between the experimental results of Andrews and Simpson (1976) and the theoretical rate will be diminished (Chapter VII.4), and in view of the results presented in this appendix it appears that the resulting agreement will be extremely poor.